2015

Frβ-Directed Car T Cells for Immunotherapy of Cancer

Rachel Christina Lynn
University of Pennsylvania, rlynn85@gmail.com

Frβ-Directed Car T Cells for Immunotherapy of Cancer

Abstract

T-cells expressing chimeric antigen receptors (CARs) can elicit dramatic clinical responses in CD19+ malignancies; however, therapeutic options for acute myeloid leukemia (AML) and solid tumors remain limited. Folate receptor beta (FRβ) is a myeloid-lineage antigen expressed in 70% of AML. Here, we tested the hypothesis that FRβ could be an effective new CAR T-cell target in AML. Low affinity FRβ CAR T-cells displayed specific reactivity for FRβ+ cells in vitro and delayed human AML outgrowth in mice but were unable to completely eliminate the tumor. An optimized higher affinity CAR exhibited drastically increased anti-leukemic activity in vitro and in vivo. Further, we assessed the potential for toxicity caused by recognition of non-tumor tissues, the primary concern for new CAR target antigens. As many cell-surface markers are shared between AML blasts and healthy hematopoietic stem cells (HSCs), we measured CAR recognition of FRβ on HSCs. Neither low nor high affinity CAR T-cells showed reactivity against bone marrow HSCs. However, we noted high surface FRβ on mature monocytes and found that they were lysed when cultured with high affinity CAR T-cells. To minimize the potential for toxicity, we investigated transient CAR expression via mRNA electroporation. High affinity mRNA CAR T-cells retained effective anti-tumor activity while posing a decreased risk for long-term myeloid toxicity.

In addition to AML, FRβ is also expressed on tumor associated macrophages (TAMs) in human patients and mouse models of cancer. Since TAMs help promote tumor growth and correlate with worse prognosis, we hypothesized that redirecting CAR T-cells to target FRβ+ TAMs could be an effective way to improve CAR T-cell therapy in epithelial cancers. We developed a mouse FRβ-specific CAR for use in implantable murine ovarian tumor models. Our preliminary data suggest that adoptive transfer of FRβ CAR T-cells results in destruction of FRβ+ TAMs, a mild delay in tumor growth, and systemic immune activation. However, transient toxicity and on-target depletion of macrophages in non-tumor tissues was also observed, warranting caution when translating FRβ CARs for clinical use. Our results suggest that safe application of FRβ CAR T-cells could contribute to tumor elimination in AML and solid tumors.

Degree Type

Dissertation

Degree Name

Doctor of Philosophy (PhD)

Graduate Group

Cell & Molecular Biology

First Advisor

Daniel J. Powell

Keywords

AML, Cancer Immunotherapy, CAR T cells, FRβ

Subject Categories

Allergy and Immunology | Cell Biology | Immunology and Infectious Disease | Medical Immunology

FRβ-DIRECTED CAR T CELLS FOR IMMUNOTHERAPY OF CANCER

Rachel C. Lynn

A DISSERTATION

in

Cell and Molecular Biology

Presented to the Faculties of the University of Pennsylvania

in

Partial Fulfillment of the Requirements for the

Degree of Doctor of Philosophy

2015

Supervisor of Dissertation

_____

Daniel J. Powell Jr., PhD
Research Associate Professor of Pathology and Laboratory Medicine

Graduate Group Chairperson

_____

Daniel S. Kessler, PhD
Associate Professor of Cell and Developmental Biology

Dissertation Committee

Carl H. June, MD
Professor of Pathology and Laboratory Medicine

Steven M. Albelda, MD
Professor of Medicine

Jose R. Conejo-Garcia, MD, PhD
Wistar Institute Professor of Pathology and Laboratory Medicine

Gregory L. Beatty, MD, PhD
Assistant Professor of Medicine

FRβ-DIRECTED CAR T CELLS FOR IMMUNOTHERAPY OF CANCER

ACKNOWLEDGMENTS

First and foremost, I have to thank my thesis mentor, Dr. Daniel J Powell, Jr. His enthusiasm, good nature, and positive attitude have made working with Dan for the last 5 years easy and enjoyable (even when experiments were not). I have to thank Dan for always supporting my ideas and giving me the flexibility to try new things and take the project in new directions and always creating a supportive and collaborative environment. I also need to thank Dan for somehow getting us the best view in town.

I have to acknowledge our collaborators Yang Feng and Dimiter Dimitrov at the NCI for providing the m909 and m923 scFv sequences and IgGs. Phil Low was also instrumental to the development of the CARs. Takami Matsuyama kindly provided us with CL10 scFv sequence and IgG. I also need to acknowledge the laboratory of George Coukos for sharing (literally everything) with us, Ehay Jung and Tom Garrabrant for their supportive roles in the lab. (A special thank-you to Tom for keeping the Canto alive all these years). I want to acknowledge everyone who has been a part of the Powell lab over the last 5 years, even if I don't have room to name them all. Mathilde Poussin, who has always helped me with mice and makes sure the lab stays afloat and her newer sidekick, Prannda Sharma. I have to thank Evros Lanitis and Denada Dangaj, who were essential in helping me learn everything when I first joined the lab and were also great late-night lab pals. Steve Santoro for his cell lines, reagents, protocols, helpful comments, late nights. Kasia Urbanska for not scaring me out of science. Jenessa Smith, my conference roommate, lunch buddy, and fellow grad student. I've been lucky to have you all to talk science with, have fun with, celebrate and commiserate with over the years. I want to thank Keith Schutsky for always being willing to help me bleed mice. Jessica Chacon for her positive energy and lending a helping hand. Elaine Ho, a bright and enthusiastic undergraduate student

who I was lucky to have working with me for two summers. Andrew Best at the OCRC tumor bank. Alina Boesteanu for her help with chromium. Anna Kalota for her expertise scoring CFU plates. I want to thank Steve Wang and the Albelda lab for training me in my first rotation and always being willing to provide helpful input and reagents. I am deeply indebted to the Stem Cell and Xenograft Core. Gwenn Danet-Desnoyers, Tony Secreto, Wini Trottman, and Josh Glover for their many hours of assistance in our AML and xenograft studies. Liz Browning at the SAIF. Ying Jiang at the Cancer Histology Core, for her assistance with embedding and cutting slides. Veterinary pathologists Liz Buza and Amy Durham at the Penn Veterinary Comparative Pathology Core for their rigorous and meticulous pathology assessments (and Liz, for doing her best in explaining them to me). Everyone at the HIC (and especially the donors) for making sure we always had fresh cells to work with. I want to thank the trusty (and not so trusty) FACS Canto, who, like me, is finally being replaced. I would like to acknowledge all past and present members of the OCRC and TRP/CCI. Both centers are full of amazingly helpful, collaborative people who have made our research possible. I have to acknowledge my thesis committee members for their support and guidance throughout my thesis work. I would also like to acknowledge the CAMB coordinators Meagan Schofer, Anna Kline, and Kathy O'Connor-Cooley for all their support. Finally, I need to thank my friends and family who have been wonderfully supportive not just throughout this endeavor but throughout all my life and helping me to get where I am (and for always visiting me wherever I go).

ABSTRACT

FRβ-DIRECTED CAR T CELLS FOR IMMUNOTHERAPY OF CANCER

Rachel C. Lynn

Daniel J. Powell Jr

T-cells expressing chimeric antigen receptors (CARs) can elicit dramatic clinical responses in $CD19^+$ malignancies; however, therapeutic options for acute myeloid leukemia (AML) and solid tumors remain limited. Folate receptor beta (FRβ) is a myeloid-lineage antigen expressed in 70% of AML. Here, we tested the hypothesis that FRβ could be an effective new CAR T-cell target in AML. Low affinity FRβ CAR T-cells displayed specific reactivity for $FR\beta^+$ cells *in vitro* and delayed human AML outgrowth in mice but were unable to completely eliminate the tumor. An optimized higher affinity CAR exhibited drastically increased anti-leukemic activity *in vitro* and *in vivo*. Further, we assessed the potential for toxicity caused by recognition of non-tumor tissues, the primary concern for new CAR target antigens. As many cell-surface markers are shared between AML blasts and healthy hematopoietic stem cells (HSCs), we measured CAR recognition of FRβ on HSCs. Neither low nor high affinity CAR T-cells showed reactivity against bone marrow HSCs. However, we noted high surface FRβ on mature monocytes and found that they were lysed when cultured with high affinity CAR T-cells. To minimize the potential for toxicity, we investigated transient CAR expression via mRNA electroporation. High affinity mRNA CAR T-cells retained effective anti-tumor activity while posing a decreased risk for long-term myeloid toxicity.

In addition to AML, FRβ is also expressed on tumor associated macrophages (TAMs) in human patients and mouse models of cancer. Since TAMs help promote tumor growth and correlate with worse prognosis, we hypothesized that redirecting CAR T-cells to target $FR\beta^+$ TAMs could be an

effective way to improve CAR T-cell therapy in epithelial cancers. We developed a mouse FRβ-specific CAR for use in implantable murine ovarian tumor models. Our preliminary data suggest that adoptive transfer of FRβ CAR T-cells results in destruction of $FR\beta^{+}$ TAMs, a mild delay in tumor growth, and systemic immune activation. However, transient toxicity and on-target depletion of macrophages in non-tumor tissues was also observed, warranting caution when translating FRβ CARs for clinical use. Our results suggest that safe application of FRβ CAR T-cells could contribute to tumor elimination in AML and solid tumors.

TABLE OF CONTENTS

LIST OF FIGURES

CHAPTER 1: Introduction

Cancer

Cancer is currently the second leading cause of death in the United States; a close second behind heart disease[1]. Nearly 1 in 2 men and 1 in 3 women will receive a cancer diagnosis in their lifetime. In 2015, approximately 1.6 million new cases will be diagnosed and more than 500,000 people will die from this disease[2]. The term cancer is used to encompass a large, diverse group of malignancies stemming from the uncontrolled growth of one's own cells. This unrestricted expansion results from multiple acquired genetic mutations that cooperate to overcome a cell's intrinsic checkpoints designed to regulate proliferation. Hanahan and Weinberg's now famous review from 15 years ago outlines the basic requirements needed for cancer to manifest[3].

Cancer Inflammation and the Tumor Microenvironment

In the 1860s, the German physician Rudolph Virchow, heralded by many as the father of modern pathology, noted the prevalence of white blood cell infiltration into tumors. His "chronic irritation theory" proposed that cancer was caused by inflammation at the site of the tumor[4]. While only about 15% of cancer can be directly linked to inflammatory stimuli (e.g. cigarette smoking and lung cancer, Hepatitis infections and hepatocellular carcinoma, and Crohn's disease and colorectal cancer), it is now well-established that nearly all types of cancer, particularly solid tumors, contain stroma with a large component of infiltrating immune cells. The tumor cells and associated non-tumor cells are collectively referred to as the tumor microenvironment (TME). In 1986, Harold Dvorak's review highlighted similarities between stromal compartments in tumors and those involved in normal wound healing, and first popularized the notion of tumors as "wounds that do not heal."[5] Tumors can co-opt several of the body's wound-healing capabilities

to promote tumor cell growth and metastasis: angiogenesis, remodeling of extracellular matrix, and recruitment of immune cells. The importance of inflammation in cancer is now highlighted as a major underlying factor in an updated Hanahan and Weinberg Hallmarks of Cancer review published in 2011[6].

Anti-Cancer Immunity

The adaptive immune system has evolved primarily to help protect the host from foreign pathogens including bacteria, viruses, and parasites. For this reason, T cells with T cell receptors (TCRs) specific for self-antigens are deleted in the thymus during development. Because cancers derive from normal cells, the presence of tumor-specific T cells is thought to be quite low. Escape of self-reactive T cells does happen and can contribute to the development of autoimmune diseases. However, for proper activation and proliferation, T cells must encounter antigen in the presence of "licensed" antigen presenting cells (APCs) which are activated via recognition of foreign "danger signals" in the setting of a microbial infection. Tumors generally promote an immunosuppressive environment with impaired APC function. Inducing proper T cell responses against tumor cells would require breaking central tolerance (or escape of self-reactive T cells), presentation of self-antigen within MHC molecules of activated APCs, and finally, survival within a hostile TME.

In 1893, William Coley began administering a mixture of bacterial products to patients with sarcoma after his research uncovered a connection between infections and cancer regression. "Coley's toxins" were given to patients for more than 50 years, but have largely been abandoned in modern medicine for lack of clear efficacy[7]. While bacterial infections do not cure cancer, they do produce potent immune activation, something generally missing in the steps to activation of tumor-reactive T cells. It is possible that Coley's toxins provided innate immune activation,

which led to increased ability to prime an anti-tumor T cell response. Analogous strategies are now being employed as components of cancer vaccines in preclinical and clinical use.

While the theory of adaptive cancer immunity dates back to the early twentieth century, the idea was highly controversial due to lack of appropriate model system in which to test the hypothesis. In the last two decades, seminal work from the Schreiber group was finally able to show definitive evidence for increased tumor growth in immunocompromised mice[8,9]. Either lymphocyte deficient or interferon-gamma (IFNg) receptor deficient mice were at greater susceptibility to carcinogen-induced and spontaneous tumor formation. In addition, when carcinogen-induced tumors from immunocompromised mice were transferred into immunocompetent hosts, a large percentage of mice rejected the tumor[9]. These finding suggested that the immune system can directly eliminate cancer and that tumors expanded in immunocompetent hosts are antigenically or otherwise phenotypically different from those in immunosuppressed hosts. These and other similar findings led to the "Three Es" hypothesis of cancer immunoediting[10] (Elimination -> Equilibrium -> Escape). This hypothesis posits that early during tumor formation, the immune system is alerted and cancer is eliminated. Any cells surviving the initial elimination phase enter a long equilibrium phase in which the immune system puts significant selective pressure on developing tumors, so that when tumors finally become clinically detectable (escape phase) they have evolved to avoid immune-mediated destruction.

Even though tumors in cancer patients have likely evolved over time to evade anti-tumor T cell responses, the presence of T cells does still seem to be beneficial. The presence of intratumoral T cells, particularly $CD8^+$ cytotoxic T cells (CTLs) or gene signatures associated with activated T cells, correlates with better prognostic factors or improved response to therapy in a wide array of cancer patients including melanoma[11], breast[12], ovarian[13], head and neck[14], lung[15,16], and

gallbladder[17]. This suggests that the elimination phase of anti-cancer immunity could be ongoing, with the tumor ultimately winning out. Stimulation of tumor-reactive T cells could tip the balance of cancer immunity towards elimination. However, a productive CTL response in the TME requires the T cells to survive the hostile immunosuppressive elements that help the tumor cells thrive.

Suppressive elements of the inflammatory tumor microenvironment

Myeloid cells

The innate immune compartment represents the first line of defense against invading pathogens and its activation is critical for subsequent adaptive immune responses in B and T cells. Myeloid cells, composed of monocyte/macrophages, dendritic cells (DCs), and neutrophils, are a major component of the innate immune system and play a vital role in promoting tumor growth. Macrophages are probably the most well-characterized myeloid component of the TME. Although likely oversimplified, the M1/M2 paradigm of macrophage polarization posits that macrophage phenotype is highly plastic and that the functional activity of macrophages is context dependent. This paradigm defines proinflammatory macrophages as M1 and immunosuppressive macrophages as M2[18]. Tumor associated macrophages (TAMs), largely thought to differentiate from infiltrating monocytes, can in theory mediate both tumor destruction (M1 phenotype) and promotion of tumor growth (M2 phenotype). However, the soluble chemokines and cytokines (CCL2, MCSF, IL4, IL10, and TGFβ) in the TME favor the recruitment and M2-like polarization of TAMs[19]. Macrophages at tumor sites can secrete growth factors, matrix metalloproteases, pro-angiogenic factors like VEGF, and express inhibitory ligands or immunosuppressive cytokines to directly promote tumor growth, angiogenesis, metastasis, and evasion of immune recognition. In the majority of cancer patients, the presence and density of TAMs correlates with poorer

prognoses[20]. Strategies to block myeloid recruitment[21-23] or differentiation[24], promote TAM depletion[25-27], or TAM repolarization[28-31] have shown promising results in preclinical studies.

Tumor-associated dendritic cells also show dysfunctional tumor-promoting characteristics compared to their proinflammatory counterparts. DCs function as professional antigen presenting cells (APCs) that uptake and present antigens to promote adaptive immunity[32]. For this reason, the presence of DCs within tumors is generally associated with better prognosis[33]. Upon pathogen encounter, DCs sense foreign danger signals that promote maturation and maximal functional capacity for antigen presentation. Possibly due to the lack of appropriate danger signals and other immunosuppressive cytokines in the TME, tumor localized dendritic cells tend to have a more immature phenotype with defects in antigen presentation compared to normal tissue DCs[34,35].

Although less well-studied, tumor associated neutrophils (TANs) may also display polar phenotypes affected by the TME[36]. In a mouse model, researchers recently identified the role of TGFβ in inducing a pro-tumor "N2" TAN phenotype, and show that depletion of TANs can decrease tumor growth[37].

Immature myeloid cells that heavily infiltrate tumors in both mouse models and human disease also have suppressive functions. Both monocytic and granulocytic myeloid-derived suppressor cells (MDSCs) have been described. While these compartments may contribute to the more mature TAM and TAN compartments, respectively, immature MDSCs can also secrete immunosuppressive cytokines and inhibit T cell activity through production of prostaglandin-E2 (PGE2), arginase, and iNOS[38-40].

Lymphocytes

Lymphocytes, including B and T cells, comprise the adaptive arm of the immune system. Both B and T cells are found in tumors, albeit at lower frequencies compared to myeloid cells. There are conflicting reports of the activity of B cells in the TME in various mouse models of cancer, although the majority of studies in humans generally support a favorable relationship between the presence of $CD20^+$ B cells and prognosis[41]. However, this subset is grossly understudied compared to T cells, and much remains to be discovered about the role of B cells in cancer. T cells are comprised of $CD8^+$ CTLs and $CD4^+$ helper T cells (Th). Much like myeloid cells, $CD4^+$ T cells are polarized in the TME towards an anti-inflammatory (Th2) phenotype that counteracts a productive immune response. In particular, a subset of CD25-high, $FoxP3^+$ regulatory T cells (Tregs) are commonly described in cancer. Tregs are particularly potent producers of IL10 and TGFβ and contribute to the impediment of anti-tumor immunity and are correlated with worse prognosis in cancer[42].

As noted above, activated $CD8^+$ T cells have the capacity for potent cytotoxic effects against antigen-expressing target cells, and strategies to overcome immunosuppression and stimulate tumor-reactive T cells could result in clinically beneficial anti-tumor immunity.

Tumor Immunotherapy

Cytokine therapy

Cytokines are small secreted protein messengers that bind to receptors on target cells and mediate downstream signaling changes. Cytokines are key mediators of both innate and adaptive immunity, and as discussed above, the cytokine milieu in a given microenvironment can dramatically affect the proinflammatory or immunosuppressive polarization of local immune cells. Therefore, modulation of the tumor cytokine milieu became of great interest in tumor therapy. It was reasoned that provision of proinflammatory cytokines could have direct cytotoxic

effect on tumor cells or activate a proinflammatory anti-tumor response from tumor associated myeloid cells and/or tumor-reactive T cells. Interleukin-2 (IL2) became the first cytokine therapy approved by the United States Food and Drug Administration (FDA) in 1992 for treatment of metastatic melanoma and renal cell carcinoma. Interferon-α (IFNα) is also approved for single use in high risk melanoma and some hematologic malignancies[43]. Among other cytokines, interferon-γ (IFNg) and interleukin-12 (IL12) have been broadly evaluated in preclinical models with some promising effects. Clinical application of these cytokines has not been as rewarding[44,45]. For the majority of single agent cytokines used for clinical application, including FDA approved IL2[46] and IFNα[47], systemic toxicity related to high serum cytokine levels is the limiting factor for clinical use. Paired with low to moderate anti-tumor activity[43,48], systemic toxicity of cytokine therapy has greatly limited its widespread use in the clinic. The field is developing new ways to locally deliver high concentrations of cytokines to the tumor microenvironment. These approaches[49,50] may allow for beneficial use of cytokine therapy without systemic toxicity in the future.

Tumor vaccines

Like common vaccines for infectious diseases, tumor vaccines aim to generate anti-tumor immunity by injecting the patient with tumor antigen. With the exception of a few viral tumor antigens (like E6/E7 HPV viral proteins involved in the pathogenesis of cervical cancer) the vast majority of targeted tumor antigens are self-proteins. As discussed above, tumor vaccine strategies must provide an extra "danger signal" to break central tolerance to self-antigens. GM-CSF is widely used in vaccine strategies due to its potent activation of APCs like dendritic cells and macrophages[51]. The tumor antigen component can be derived from selected tumor antigen peptides, DNA or viral vectors encoding tumor antigens, or non-selected whole tumor cell

vaccine approaches[52]. The first FDA-approved tumor vaccine, Provenge, was approved for prostate cancer in 2010. Other vaccine strategies are proving efficacious, particularly when used in combination with T cell immunomodulatory antibodies.

Immunomodulatory antibodies

Costimulation

T cells in the tumor microenvironment likely encounter multiple immunosuppressive elements. One strategy to boost anti-tumor immunity is to provide positive costimulation in the form of monoclonal antibodies (mAbs). CD28 provides the classic second signal of T cell activation in the setting of foreign antigen encounter on activated APCs. Unfortunately, provision of "superagonist" anti-CD28 mAb resulted in severe cytokine storm and related toxicity in humans[53]. Agonistic antibodies for T cell costimulatory receptors of the TNF receptor superfamily are also currently under evaluation in the clinic. Agonistic antibodies against CD137 (4-1BB)[54,55], CD134 (OX40) and CD27 have been evaluated in clinical trials. Anti-CD137 antibody therapy yielded response rates of about 6%, although hepatotoxicity did occur at higher doses[55]. Anti-OX40 therapy demonstrated evidence of immune activation in patients with advanced cancer; however, the development of human anti-mouse antibodies precluded further use[56]. New humanized OX40 antibodies are in development to reduce potential immunogenicity. Anti-CD27 therapy resulted in one complete response and stable disease in a few additional patients with hematological malignancies[57]. Agonistic antibodies for TNF receptor family members are generally well tolerated, and response rates will likely improve in combination with other immunomodulatory regimens.

Checkpoint Blockade

Like costimulatory receptors, inhibitory receptors are also present on the surface of T cells following activation to serve as a checkpoint to prevent over-activation and resulting immune pathology. T cell inhibitory receptors cytotoxic T-lymphocyte-associated protein 4 (CTLA-4) and programmed cell death protein 1 (PD-1) are important components driving the retraction phase following clearance of microbial pathogens. CTLA-4 outcompetes CD28 in binding shared ligands CD80 and CD86, effectively blocking CD28 costimulation in T cells, while also propagating inhibitory signaling upon ligation[58]. PD-1, upon binding its ligands PD-L1 or PD-L2, activates the inhibitory phosphatase SHP2, which mediates inhibition of TCR activating signals[59,60]. Tumors take advantage of these pathways and commonly upregulate expression of ligands for inhibitory receptors as a means to evade T cell-mediated destruction. The expression of PD-1 ligand PD-L1 is inversely correlated with survival in many different types of cancer[61]. Blocking the interaction of inhibitory receptors and their respective ligands is showing great promise in recent clinical trials. In 2011, ipilimumab, an antibody for CTLA-4, received FDA approval for the treatment of advanced melanoma[62], although efficacy in other types of cancer has been minimal. A second CTLA-4 antibody showed early promise but failed to show improvements over standard chemotherapy in Phase III trials. A comparison of the isotypes led to the now well-accepted hypothesis of a second means of action of ipilimumab involving depletion of CTLA-4$^+$ suppressive Tregs. The anti-PD-1 antibodies nivolumab and pembrolizumab were also recently granted FDA approval for advanced melanoma and non-small-cell lung carcinoma (NSCLC). Initial trials blocking PD-1[63,64] and PD-L1[65] have provided exciting response rates in a number of different types of cancer. A comparison of ipilimumab and nivolumab or combination provided direct evidence for the greater efficacy of PD-1 blocking antibody therapy in melanoma patients. PD-1 directed therapies have lower side effects, broad efficacy across multiple tumor types, and better efficacy as single use agents[66]. For these reasons, PD-1 blocking strategies are currently being built into a wide range of preclinical and clinical studies as single use agents or in

combination with traditional chemotherapy, radiation therapy, and other immunotherapies such as cancer vaccines and adoptive T cell therapies.

Adoptive T cell Therapy

TIL

Cytokine therapy, tumor vaccines and immunomodulatory antibodies share the common goal of inducing expansion and improving functional reactivity of tumor-specific T cells in the patient. Instead of relying on *in vivo* activation and proliferation, tumor infiltrating lymphocyte (TIL) therapy involves the isolation and *ex vivo* expansion of tumor-reactive T cells which are then re-infused into the patient. TIL can be activated non-specifically or pulsed with autologous tumor or antigen-specific peptides. TIL therapy trials have been conducted for melanoma since 1988[67]. In this time, more than 200 patients with metastatic melanoma have been treated with TIL after lymphodepleting preconditioning, and objective response rates range from 49-75% with 22% of patients achieving a complete tumor regression[68]. Response rates increased with the strength of lymphodepleting conditioning, now well accepted to increase engraftment and activity of transferred T cells[69]. This likely works through depletion of suppressive Tregs and other lymphocytes that serve as sinks for homeostatic T cell cytokines[70,71]. While the vast majority of trials have been conducted in melanoma, clinical studies in other types of cancer are currently recruiting patients. Early results using TIL for HPV-related cancers recently reported encouraging results in patients with metastatic cervical cancer[72].

A common theme from the evolution of tumor immunotherapy, particularly strategies attempting to harness the power of naturally-occurring tumor reactive T cells, is that not all patients respond and certain types of cancer are much more amenable to these therapies than others. Melanoma, for example, seems to be particularly responsive to tumor immunotherapeutic strategies. Unlike

other tumors, T cells make up a large percentage of tumor infiltrating immune cells in melanoma[73]. Incidentally, melanoma also has the highest mutation rate compared to other types of cancer[74], suggesting that it may be a particularly immunogenic tumor. This hypothesis is strengthened by recent identification of tumor mutation-specific T cell clones in the infused TIL product in some patients with positive responses to TIL therapy[75,76]. Other types of cancer with lower mutational load and lower incidence of tumor-reactive T cells may be less affected by immunomodulatory therapies.

Engineered Tumor-Specific T cells

Recent advances in DNA manipulation techniques and development of safer viral vector technology have advanced the efficiency and safety of gene transfer into lymphocytes. Instead of relying on the endogenous presence of tumor reactive T cell clones, tumor specificity can be engineered into patient T cells *ex vivo* before reinfusion into the patient. This approach has the potential to broaden the opportunity for effective T cell therapy in patients with cancer that does not naturally induce T cell immunity. One method of introducing tumor specificity is through gene transfer of tumor antigen specific TCRs. For this method, alpha and beta TCR genes are cloned from tumor-reactive clones and transferred into patient T cells using viral vectors. The first engineered TCR to enter the clinic was specific for melanoma antigen MART-1[77] and provided evidence for the safety and potential of genetically engineered lymphocytes in melanoma patients. Affinity-enhanced MART-1 TCRs improved the response rate in melanoma but also resulted in destruction of healthy melanocytic tissue[78]. The cancer testis antigen NY-ESO-1 is rarely expressed in adult tissue outside of the testes and is commonly re-expressed in a wide variety of cancers[79]. TCRs specific for NY-ESO-1 displayed *in vitro* reactivity against a panel of melanoma as well as non-melanoma cell lines of epithelial and sarcoma origin[80]. Initially tested in melanoma and synovial sarcoma, the NY-ESO-1 TCR became the first platform to

safely and successfully treat non-melanoma cancer with TCR gene-engineered cells[81]. Long-term follow-up of 38 patients revealed >50% response rate in both melanoma and synovial cell sarcoma[82]. Clinical responses using an affinity-enhanced NY-ESO TCR have also been recently reported in multiple myeloma[83].

Even when high functioning engineered TCRs can be isolated and applied to patients with many types of cancer, they are inherently restricted to use in only some subsets of the population. TCRs recognize peptide antigen within the context of specific HLA molecules. For example, both the MART-1 and NY-ESO-1 TCRs are restricted to use in patients with HLA-A0201 alleles. Even as one of the most widely represented HLA serotypes, HLA-A0201^{+} individuals only make up 20-50% of the US population[84]. Like natural tumor-reactive T cells, gene-engineered TCRs also rely on tumor cell antigen processing and presentation on surface MHC molecules. Downregulation of MHC-class I and abnormalities in antigen processing machinery are common mechanisms used by tumors to evade immune recognition[85]. Provision of exogenous α and β chains into open repertoire T cells has the potential to create autoantigen specificity by mispairing with endogenous TCR α and β chains. While this theoretical concern has not yet resulted in any observed toxicity, mispairing with endogenous TCR chains also likely leads to decreased surface bioavailability of functional transferred TCR.

CAR T cells take the driver's seat

T cells engineered to express chimeric antigen receptors (CARs) share the benefits of tumor-specific TCR engineered cells and overcome many of their limitations. With credited development by Zelig Eshhar and colleagues in 1989, CARs are chimeric proteins composed of a tumor antigen recognition domain coupled to intracellular T cell activation signaling domains[86,87] (see **Figure 1.1** for a simplified schematic representation). The tumor antigen recognition

domain is most often derived from the single-chain variable fragment (scFv) of a tumor-specific monoclonal antibody, although ligand/receptor-based chimeric immune receptors have also been developed to target the respective ligand/receptor expressed on tumor cells (ex: CD27/CD70[88], NKG2D/NKG2DL[89,90], IL13/IL-13Ra2[91], FSH/FSHR[92]). CAR T cells recognize native surface protein expressed on the tumor cell surface and do not rely on functioning tumor cell antigen processing and presentation in MHC complexes. In principle, CAR T cells can also be applied to any patient with antigen-positive tumor regardless of HLA serotype. CAR T cell constructs contain both antigen recognition and T cell activation domains, so mispairing with endogenous TCR components is not a major concern. Although the original constructs published by Eshhar utilized constant regions from the TCR α and β chains, most modern CARs utilize signaling domains from CD3ζ chain to modulate T cell activation (**Figure 1.1**).

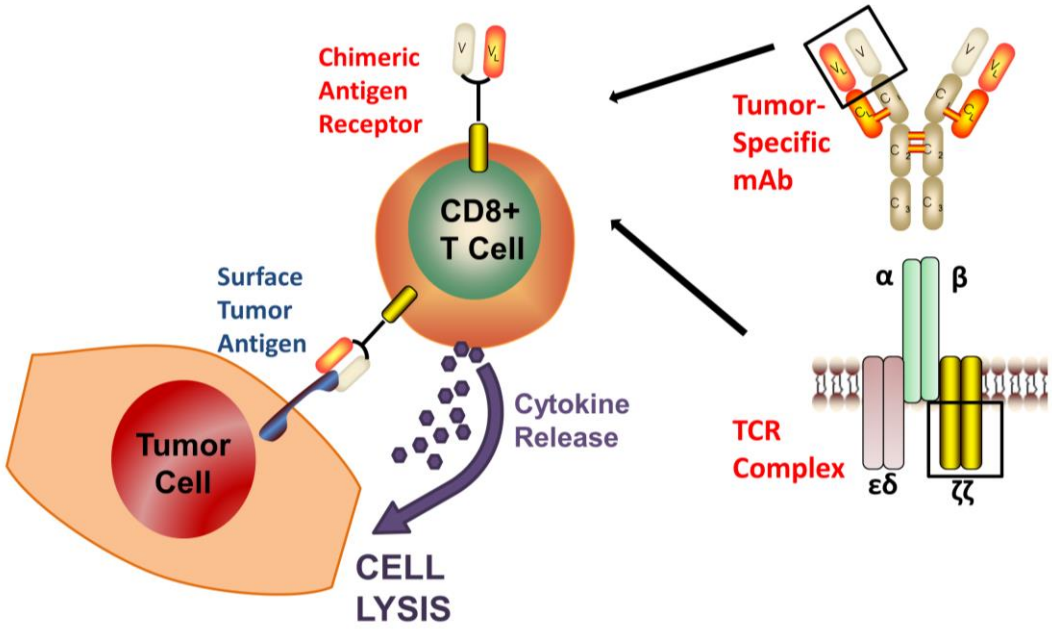

Figure 1.1 Schematic representation of CAR design and functional activity.
mAb – monoclonal antibody, V – Variable heavy chain, V_L– variable light chain, TCR – T cell receptor.

The possibility of utilizing tumor-redirected chimeric T cell receptors was quickly realized using T cells recognizing the ovarian cancer antigen FRα[93,94]. Early clinical application of FRα-specific CAR T cells was well tolerated but their efficacy was disappointing due to the poor survival of CAR T cells after infusion in patients[95]. Decreasing T cells numbers coincided with the development of inhibitory factors in the serum. Responses in other early CAR T cell trials for $CD171^+$ glioblastoma[96] and $CD20^+$ lymphoma[97] were also minimal with relatively short CAR T cell persistence. These early trials all used CAR constructs with only CD3ζ signaling. In the meantime, research in preclinical CAR T cell models suggested that inclusion of CD28 costimulatory signaling domains in CAR constructs greatly enhanced T cell cytolytic capacity, cytokine secretion, and *in vivo* efficacy[98-101]. These platforms were coined "second generation" CAR T cell constructs due to the inclusion of additional costimulatory signaling domains. Following CD28, incorporation of costimulatory domains from TNF receptor family members 4-1BB[102,103] and OX40[102,104] were incorporated into second generation and third generation CAR constructs utilizing both CD28 and TNFR costimulation[104-108]. Consensus shows that any costimulation greatly improves the *in vivo* persistence and efficacy of CAR T cells compared to CD3ζ signaling alone, and some studies suggest TNFR costimulation is particularly important for long term persistence[106,107,109,110]. The greatly improved performance of second and third generation costimulated CAR T cells in preclinical mouse models quickly led to incorporation of these domains in CARs designed for clinical protocols.

CAR T cells in the clinic

First generation "zetakine" IL13Rα2-redirected CAR T cells showed evidence of transient anti-tumor activity in 3 glioblastoma patients. T cells were well tolerated with manageable transient CNS inflammation. However, poor CAR T cell persistence and disease progression was observed in all patients. Noted decreased expression of IL13Rα2 target antigen in one patient's tumor

suggested antigen escape could be a possible concern in future patients treated with zetakine T cells[111].

Similarly, clinical use of PSMA-specific first generation CAR T cells for prostate cancer only resulted in transient anti-tumor effects which were not sustained long term[112,113]. Additional trials are underway for PSMA (NCT01140373).

First generation GD2 CAR T cells showed safety and activity in some neuroblastoma patients (3/11 patients achieved complete remission) and longer persistence was associated with clinical response[114]. A new trial using third generation CD28-OX40 costimulated CAR T cells is currently recruiting with the hopes that costimulation will improve T cell persistence and increase overall response rates in patients (NCT02107963).

Second generation 4-1BB costimulated mesothelin-specific CAR T cells have been used to treat solid tumors. For safety concerns, the first trials were conducted with RNA CAR T cells where the CAR construct was introduced via mRNA electroporation for transient CAR expression. Encouraging safety and activity of RNA mesothelin CAR T cells[115] led to the development of lentivirally transduced mesoCAR T cells (NCT02159716) and preliminary reports suggest no long term toxicity and some suggestion of anti-tumor activity[116].

12 patients with metastatic renal cell carcinoma were treated with carboxy-anhydrase-IX (CAIX) specific CAR T cells. Liver toxicity was noted in the lowest dose cohort, and biopsies confirmed expression of CAIX on bile duct epithelial cells, suggesting “on-target, off-tumor” toxicity in these patients[117].

By far the most promising clinical experience with CAR therapy has been the dramatic success of CD19-directed CAR T cells in B-cell leukemia and lymphoma patients. One of the first indications of CD19 CAR T cell efficacy was reported in 2011 when two patients with refractory

chronic lymphocytic leukemia (CLL) had a complete response following T cell transfer[118,119]. Similar results were reported in clinical trials at other institutions[120,121]. Since then, CD19 CAR therapy has been applied to other B-cell malignancies, with common reports of complete responses in heavily pretreated patients. Acute lymphoblastic leukemia (ALL) patients appear to have a particularly favorable response to CD19 CAR therapy, with response rates over 90%[122-124]. The selection of the CD19 target likely plays a role in the success of CAR therapy for these patients. CD19 is highly restricted to normal and neoplastic B cells[125], eliminating the concern for recognition of antigen in healthy organs. Normal B-cell depletion is managed through immunoglobulin replacement infusions. In addition, CD19 is expressed at high surface levels and on a high percentage of all cancerous cells, decreasing the likelihood for antigen-negative escape although this phenomenon has been reported[122]. Depletion of normal B cells could also hinder an antibody response against foreign elements in the CAR, such as the murine antibody portion, thereby increasing CAR T cell persistence and activity. The enormous clinical success in heavily pretreated ALL patients led to FDA breakthrough therapy designation to CD19 CAR therapy for relapsed/refractory ALL in 2014.

Safety concerns with CAR T cells

Clinical experience with CAR T cells in the last 10-15 years has taught the field some valuable lessons. While CAR T cells can exert potent activity against antigen-positive tumor cells, they also have the potential to target antigen on healthy tissues. One major concern is the development of "on-target, off-tumor" toxicity. Indeed, one of the most serious adverse advents in clinical CAR T cell therapy was the death of a patient treated with third generation Her2-specific CAR T cells which was attributed to recognition of low levels of Her2 antigen in the lung[126]. Evidence of on-target liver toxicity was also observed in renal cell carcinoma patients treated with carboxy-anhydrase-IX (CAIX) CAR T cells[117]. Transfer of CEA-specific TCR-transduced T cells induced

severe colitis in colorectal cancer patients due to recognition of normal colonic epithelium[127]. For this reason, trial designs are now incorporating inducible suicide genes, low dose escalation strategies, or transient CAR expression techniques to test new CAR target antigens.

Development of humoral and cellular immune responses against transferred CAR T cells have been observed in some patients[95,128,129]. The immune-mediated elimination of transferred cells will severely limit the persistence and overall efficacy of CAR T cell therapy. In addition to decreased efficacy, anaphylaxis was observed in one patient receiving mesothelin RNA CAR T cells which was likely related to IgE CAR-specific antibodies binding to foreign elements of the scFv[129].

Many groups using the CD19 CAR or other CARs have observed side effects related to cytokine release syndrome (CRS), a systemic side effect of massive CAR T cell activation in the patient. This toxicity ranges from mild to life threatening, and seems to correlate with the tumor burden at the time of T cell infusion. IFNg, presumably released from activated transferred T cells is often highly present. IFNg can induce chemokines like CXCL9 and CXCL10 also elevated in one of the first reported cases in CD19 CAR T cell treated patient[118]. IL6 is often highly expressed, and treatment of CRS using tocilizamab, an anti-IL6R antibody, has decreased CRS toxicity in CD19 CAR T cell treated patients[130]. The mechanism of CRS is still not well understood. CRS following CAR T cell therapy has many similar clinical similarities to macrophage activation syndrome (MAS), suggesting activation of macrophages may contribute to the cytokine storm in these patients. Although toxicity can be severe, the benefit of CAR T cells in heavily pre-treated patients can be lifesaving. As more patients are treated with a larger diversity of CAR platforms lessons learned in the clinic will continue to inform safer and more effective T cell therapies for a large array of cancers.

Acute Myeloid Leukemia

Acute myeloid leukemia (AML) is a type of cancer originating from poorly differentiated myeloid precursors in the bone marrow. In 2015, an estimated 20,830 new cases of AML will be diagnosed and an estimated 10,460 patients will die due to AML. The 5 year survival rate remains dismally low at only 25.9% of patients living more than 5 years beyond their diagnosis[131]. Standard treatment for AML includes induction chemotherapy, usually with cytarabine, which results in complete remission (CR) in 65-75% of patients. Many patients go on to receive consolidation and/or maintenance therapy involving more rounds of intensive chemotherapy after a CR has been achieved. Despite induction of initial CR, the vast majority of AML patients will relapse following induction chemotherapy, and patients usually go on to receive additional rounds of intensive chemotherapy, however, there is no standard of care for relapsed AML, and outgrowth of chemotherapy resistant disease is common[132]. Allogeneic hematopoietic stem cell transplant (HSCT) can produce cures in a small minority of patients following a second CR, however, long-term cures are still rare. In one trial following over 1000 patients, HSCT moderately reduced the risk of relapse, however, did not produce an overall survival advantage[133]. Therefore, newer more potent therapies are urgently needed for AML patients to improve long term survival following diagnosis.

Folate Receptors and Cancer

The folate receptor (FR) family is composed of three known members, designated FRα, FRβ, and FRγ. The cDNAs were cloned by independent groups in 1989[134-136]. The two isoforms later designated FRα and FRβ are bound to the cell surface via glycosylphosphatidylinositol (GPI) linkages, whereas the truncated isoform, FRγ, lacks a GPI signal sequence and is secreted from the cell[137]. FRα and FRβ bind and uptake folate via receptor-mediated endocytosis. Folate is an

essential dietary vitamin and its derivatives are utilized during nucleic acid synthesis and methionine production; therefore, folate is important in DNA replication and cell division[138]. It is perhaps unsurprising, then, that FR isoforms were subsequently found to be highly upregulated on cancer cells[139]. FRα is selectively expressed in epithelial tissues and is substantially increased in tumor cells of epithelial origin[139-142]. The high expression on tumor cells and the concurrent finding that folate-linked proteins could be used to selectively target FR^+ cells[143] led to the rapid exploitation of this pathway for targeted delivery of therapeutic and imaging agents to FR^+ cancer. Strategies have included directly linking folate to toxic compounds[144], folate-conjugated liposomal drug delivery[145], and immunization[146]. In addition, FRα was one of the first tumor antigens exploited for CAR T cell therapy in oncology[93,94].

FRβ expression in myeloid cancer

While FRα is selectively expressed in epithelial tissues, FRβ also shows restricted expression only in cells of the hematopoietic myeloid lineage and myeloid cancer[147,148]. In 1999, Manohar Ratnam's lab showed using immunocytochemistry that many human AML patient blasts expressed FRβ[148]. This was also the first description of FRβ co-expression with myeloid lineage antigens CD11b, CD13, and/or CD14 in normal peripheral blood and bone marrow. Using a larger patient sample size, this same group showed that 68% of all AML bone marrow specimens across different subtypes expressed FRβ[149], making the beta isoform an attractive target in myeloid leukemia. As observed with $FR\alpha^+$ tumor cells, folate-conjugated liposomal doxorubicin was able to selectively target $FR\beta^+$ AML. This group also discovered that all-*trans* retinoic acid (ATRA) specifically enhanced FRβ expression in AML[150], and pretreatment with ATRA was able to enhance FRβ-targeted drug liposomal drug delivery[149]. The FRβ-inducing activity of ATRA was independent of its role in promoting differentiation of acute promyelocytic leukemia (APL), and subsequent investigation revealed direct activity at the FRβ promoter[151], which could be

enhanced with histone deacetylase (HDAC) inhibitors[152]. ATRA was unable to induce FRβ expression in FRβ$^-$ cells. Combining FRβ-targeted therapies with antigen upregulation via ATRA is an attractive strategy for AML.

Imaging studies with labeled folic acid highlight the low expression of FR in healthy organs

Imaging experiments with radiolabeled folate conjugates were initially used to assess the safety profile of FR-targeted therapies by identifying the biodistribution of folate uptake in animal models. These studies reproducibly demonstrated strong uptake by FR$^+$ tumor cells, with little to no retention in healthy tissues outside the kidneys[153-156]. Encouragingly, results were reproducible in human subjects[157]. Of note, background uptake in the liver was also noted in mice[158] and patients[157], however, the FR-specific nature of this signal has been questioned. The favorable biodistribution profile of folate imaging agents suggests the low expression of FR$^+$ cells in healthy tissues and provides rationalization for FR-targeted cancer therapy.

FRβ expression in pathologic macrophages

In investigating the mechanism of action of methotrexate (an antifolate drug) in rheumatoid arthritis (RA), Takami Matsuyama's group demonstrated the selective high expression of FRβ in synovial macrophages from the inflamed joints of RA patients.[159] Soon after, Philip Low and colleagues described folate uptake in inflamed joints of rats with experimental adjuvant-induced arthritis[160] and later in both canine and human patients with arthritis[161]. These reports highlight the cross-species finding that activated macrophages at sites of inflammation highly express FRβ compared to healthy animals without inflammation. In addition, the imaging from both rats and dogs suggested that macrophages in the spleen and liver of arthritic (but not healthy) animals also exhibited increased folate uptake, suggesting inflammatory conditions induce activated FRβ$^+$

macrophages systemically as well as locally. Both the Matsuyama and Low groups have developed preclinical models targeting FRβ$^+$ macrophages in RA using vaccination[162] and immunotoxin strategies[163-165].

FRβ has also been described as a marker of M2 macrophages[166] and is expressed on tumor associated macrophages (TAMs) in many different kinds of cancer[166-169]. The Low group noted that TAMs from murine ovarian cancer ascites could selectively endocytose folate-conjugated liposomes[170]. In addition Matsuyama's lab used their FRβ immunotoxin to deplete FRβ$^+$ TAMs and slow tumor growth in a mouse model of glioma[171]. The general consensus from all these studies reveals high expression of FRβ in activated macrophages at sites of inflammation, including both inflammatory diseases and tumor microenvironment, with low expression in healthy tissues.

A Rationale for FRβ-directed CAR T cell Development

The tissue restriction of FRβ, broad expression in AML and pathologic macrophages, vast preclinical and clinical studies demonstrating the safety of FR-targeted therapy, and demonstrated clinical efficacy of CAR T cell therapy for cancer rationalizes the preclinical development and evaluation of FRβ-specific CAR T cells. The goals of this thesis can be summarized in two major aims:

Aim1: Create and assess the functional activity and safety of human FRβ-specific CAR T cells *in vitro* and *in vivo* to test the ***central hypothesis*** that FRβ is a promising target for CAR T cell therapy for AML.

Aim2: Create and assess the functional activity and safety of mouse FRβ-specific CAR T cells *in vitro* and *in vivo* to test the ***hypothesis*** that FRβ-directed CAR T cells could be applied for

immunotherapy of solid tumors by eliminating TAMs, a major contributor to the tumor microenvironment.

CHAPTER 2: Targeting of folate receptor-beta on acute myeloid leukemia blasts with chimeric antigen receptor expressing T cells

Summary

T cells expressing a chimeric antigen receptor (CAR) can produce dramatic results in lymphocytic leukemia patients; however, therapeutic strategies for myeloid leukemia remain limited. Folate receptor beta (FRβ) is a myeloid-lineage antigen expressed on 70% of acute myeloid leukemia (AML) patient samples. Here, we describe development and evaluation of the first CARs specific for human FRβ (m909) *in vitro* and *in vivo*. m909 CAR T cells exhibited selective activation and lytic function against engineered C30-FRβ as well as endogenous $FR\beta^+$ AML cell lines *in vitro*. In mouse models of human AML, m909 CAR T cells mediated the regression of engrafted $FR\beta^+$ THP1 AML *in vivo*. In addition, we demonstrated that treatment of AML with all-trans retinoic acid (ATRA) enhanced FRβ expression, resulting in improved immune recognition by m909 CAR T cells. As many cell-surface markers are shared between AML blasts and healthy hematopoietic stem and progenitor cells (HSCs), we evaluated FRβ expression and recognition of HSCs by CAR T cells. m909 CAR T cells were not toxic against healthy human $CD34^+$ HSCs *in vitro*. Our results indicate that FRβ is a promising target for CAR T cell therapy of AML, which may be augmented by combination with ATRA.

Introduction

Acute myeloid leukemia (AML) remains a disease with a dismal clinical prognosis. While induction chemotherapy generates remission in the vast majority of patients, nearly all of them relapse and require intense consolidation chemotherapy or hematopoietic stem cell transplant. The majority of patients will eventually die of their disease, and 5-year survival remains below 50%[172]. Therefore, development of new, more effective therapies for AML is essential.

Chimeric antigen receptor (CAR) T cell therapy is an innovative, new treatment that has recently achieved groundbreaking clinical success in treating therapy-refractory lymphocytic leukemia patients. By linking the single-chain variable fragment (scFv) of a conventional monoclonal antibody (mAb) to intracellular T cell receptor signaling domains to produce a chimeric T cell receptor with antibody-like affinity[87], a patient's own T cells are genetically redirected to target antigen-positive tumor cells. In the case of acute lymphoblastic leukemia (ALL) patients, CD19-redirected CAR T cells are generating complete remissions in as high as 90% of patients[118,120-123]. One major challenge in translating the astonishing clinical success of CAR T cells in ALL to other types of cancer including AML is finding an appropriate tumor cell target.

The folate receptor (FR) family is a group of folate-binding protein receptors comprised of four known members (α, β, γ, and δ). FRα and FRβ are bound to the cell membrane via glycosylphosphatidylinositol (GPI) linkages[136], share ~70% homology, similar affinity for folate, and a common mechanism of receptor endocytosis-mediated folate uptake. However, these receptors differ in tissue distribution: FRα is expressed on epithelial tissues, while FRβ is primarily found on myeloid-lineage hematopoietic cells[147]. Interestingly, both receptors are commonly upregulated in the setting of malignancy[139,141,148]. FRα-specific CAR T cells were developed more than 20 years[93,95,109,110], with ongoing optimization and new clinical trials

currently being designed to evaluate 4-1BB costimulated CAR T cells in ovarian cancer patients[173]. However, CAR therapy has not yet been expanded to target FRβ$^+$ malignancies. FRβ is expressed on approximately 70% of primary AML patient tumors[148,174] thus making it an attractive target for CAR T cell therapy. In addition, FRβ expression can be enhanced on AML blasts by treatment with all-trans retinoic acid (ATRA), a drug already FDA-approved for subclass M3 AML[150,151]. In preclinical models, the efficacy of folate-conjugated drug therapy for targeting FRβ$^+$ AML is improved when combined with ATRA treatment[174]. Given the presence of FRβ in AML, limited expression in normal tissues, as well as inducibility by clinically-approved drugs, we sought to develop the first CAR to target FRβ. Here, we generated and characterized fully human FRβ-specific CAR constructs containing the m909 scFv[175], previously validated for recognition of human FRβ.

Materials and Methods

CAR construction

The m909 scFv[175] was PCR-amplified using the following primers: 5′-TATTGATCAGCCGAAGTGCAGCTGGTGCAGTCTGG-3′ (BclI) and 5′-TATGCTAGCCTGGCCTAGGACGGTCAGCTTGGTC-3′ (NheI). The PCR product was digested and ligated into third generation pELNS-GFP-2A lentiviral vectors containing CD3ζ or CD28-CD3ζ signaling domains (pELNS, previously described[110,176]). Resulting constructs were designated pELNS-GFP-2A-m909-Z/28Z. Vectors encoding GFP, MOV19-Z/28Z, specific for FRα, or CD19-28Z have been previously described[110,176].

Lentiviral vector production and T cell transduction

High-titer replication-defective lentiviral vectors were produced in 293T human embryonic kidney cells. $12x10^6$ 293T cells were seeded per T150 tissue culture flask 24 hours before transfection. All plasmid DNA were purified using Endo-free Maxi prep kits (Qiagen, Valencia, CA). Cells were transfected with 7µg pMD2.G, 18µg pRSV.REV, 18µg pMDLg/p.RRE, and 15µg pELNS transfer plasmid DNA using Express In (Open Biosytems). 24 and 48h supernatants were harvested and combined. Viral particles were concentrated by ultracentrifugation for 3h at 28000 rpm with a Beckman SW32TI rotor (Beckman Coulter), titered, and stored at -80°C until use. Primary human $CD4^+$ and $CD8^+$ T cells were isolated from healthy volunteer donors after leukapheresis by negative selection and purchased from the Human Immunology Core at University of Pennsylvania. All specimens were collected under a University Institutional Review Board-approved protocol, and written informed consent was obtained from each donor in accordance with the Declaration of Helsinki. $CD4^+$ and $CD8^+$ T cells were mixed at a 1:1 ratio and activated with anti-CD3/anti-CD28 mAb–coated beads (Invitrogen, Carlsbad, CA) at a 3:1

bead:T-cell ratio. T-cells were cultured in complete media (CM) (RPMI 1640-GlutaMAX supplemented with 10% heat-inactivated FBS, 100 U/mL penicillin, 100 µg/mL streptomycin sulfate). At 20 hours after activation, lentiviral vectors were added at MOI of 5-10. T cells were expanded in CM in the presence of human recombinant IL2 (Novartis, St Louis, MO) at a final concentration of 50-100 IU/mL, maintaining a cell density of 0.5-1x10^6 cells/mL. After 2 weeks, rested T cells (cell size <300 fL) were then adjusted to equalize the frequency of transgene-expressing cells before use in functional assays.

Cell lines

293Ts were purchased from ATCC. FR-negative human ovarian cancer cell line C30[177] was kindly provided by Dr. George Coukos[178]. C30 was transduced with lentiviral vectors encoding human FRβ cDNA (Origene) to generate C30-FRβ. Human AML cell lines THP1, MV411, and HL60 were kindly provided by Dr. Gwenn Danet-Desnoyers (University of Pennsylvania). All cells were grown at 37°C in CM. C30, C30-FRβ, and THP1 were transduced with lentiviral firefly luciferase (fLuc).

T cell activation and cytokine release assays

1x10^5 CAR^+ T cells were co-cultured with 1x10^5 targets in triplicate in 200µL CM. After 24h, supernatants were assayed for the presence of interferon-γ (IFNg) by ELISA (Biolegend). IL-2, IFNg, TNF-α, and MIP1α were measured by flow cytometry with Cytometric Bead Array (BD). Cell pellets were labeled for CD3 and CD69 and assessed by flow cytometry. Live, $CD3^+$ gates were used for analysis. In some cases cell pellets were labeled for FRβ expression.

T cell proliferation

T cells were labeled with 2.5µM PKH26 (Sigma-Aldrich) according to the manufacturer's protocol. T cells were co-cultured with targets at 1:1 ratio in the absence of exogenous IL-2. After

5 days, cells were labeled for CD3 and analyzed for PKH26 dilution. Live, $CD3^+$ gates were used for analysis.

Degranulation

$1x10^5$ CAR^+ T cells were co-cultured with $1x10^5$ targets in triplicate in 200µl CM with anti-CD107a and anti-CD107b antibodies (or control IgG1) and monensin (BD). After 5-6h cells were labeled for CD3 and analyzed by flow cytometry. Live, $CD3^+$ gates were used for analysis.

Cytotoxicity

fLuc-transduced targets were plated at $1x10^4$/well in triplicate. CAR^+ T cells were added at the indicated E:T (effector: target) ratios. Co-cultures were incubated overnight in phenol-free CM. The Extended-Glow Bioluminescent Reporter Gene Assay (Applied Biosystems) was used to measure residual luciferase activity from remaining targets, and lysis was calculated as follows: Percent Lysis = 100 – [(average signal from T cell-treated wells)/(average signal from untreated target wells) x100]. Monocyte lysis was assessed after 4-hour co-culture at indicated E:T ratios plated in triplicate wells. Total cells were labeled for CD3, CD14, and 7AAD. Flow cytometry with CountBright beads (Life Technologies) was used to determine the total number of live $CD3^-$, $CD14^+$ monocytes per well (N). Lysis was calculated as follows: Percent Lysis = 100 – [(average N treated wells)/(average N untreated wells) x100].

CFU

Bone marrow $CD34^+$ HSCs were isolated from healthy donors by magnetic bead selection by the University of Pennsylvania Stem Cell and Xenograft core. 2000 $CD34^+$ cells were cultured with 2000 CAR^+ T cells in V-bottom plates. After 4h, wells were diluted in methylcellulose and plated in duplicate. After 14 days colonies were counted and scored as CFU-GEMM, GM, G, M, or BFU-E. Untreated $CD34^+$ cells were cultured in the absence of T cells.

qRT-PCR

Total RNA was extracted from $5x10^6$ viable tumor cells using RNeasy Mini kit (Qiagen). RNA quantity and quality ($A_{260/280}$ = 2.0-2.1) were verified using a Nanodrop 2000 spectrophotometer (Thermo). cDNA was generated from 1µg total RNA using the High-Capacity-RNA-to-cDNA kit (Applied Biosystems). cDNA quantity (2.05 µg/µl) and quality ($A_{260/280}$ = 1.82) were verified to be equal for all samples. Human FRβ mRNA copy number was calculated using the standard curve method and ViiA7 real time PCR system (Applied Biosystems). 200ng cDNA template was added to SYBR green PCR master mix (Applied Biosystems) and 200nM PrimeTime qPCR Primers (IDT) specific for hFOLR2 in 5 replicate wells. Known quantities of plasmid-FRβ cDNA were used to construct a 6-point standard curve. Amplification was detected in all wells. Relative mRNA copy numbers are represented as indicated.

ATRA

Pre-treatment: cells were cultured in CM with 10nM ATRA. On day 5, cells were washed then stained for FRβ surface expression by flow cytometry, processed for RNA extraction, or used in co-cultures for T cell functional assays. In ATRA co-treatment assays, cells were prepared as above (for cytokine release), and 10nM ATRA was included fresh in the culture media. 3-day supernatants were analyzed for IFNg by ELISA.

Flow cytometry

All samples for flow cytometry were labeled in 100µl FACS Buffer (PBS, 2% FBS) at 4°C . Cells were processed on a BD FACS-Canto flow cytometer, and results were analyzed with FlowJo 7.6.5. m909-IgG (prepared by Dimiter Dimitrov) was conjugated to biotin using the EZ-Link Biotinylation Kit (Thermo). For FRβ staining, $3x10^5$ cells were incubated with 10µg unlabeled human IgG (Jackson ImmunoResearch) to block nonspecific Fc receptor binding. 3-

5µg/mL m909-biotin or human-IgG-biotin was added in 100µl and cells were labeled at 4°C for 30min. Cells were washed and secondary labeling with 1:200 Streptavidin-APC (BD) was conducted for 25min. Cells were washed twice and analyzed by flow cytometry in the presence of 7AAD. For *in vivo* T cell quantification, 50µL blood was obtained from treated mice via retro-orbital bleeding and labeled for human CD45, CD3, and CD8. Cell numbers were quantified with BD TruCount tubes per manufacturer's instructions. $CD4^+$ subsets were calculated by subtracting $CD8^+$ from total $CD3^+$. m909 CAR expression was detected by biotin-labeled rabbit-anti-human IgG (H+L) (Jackson ImmunoResearch), MOV19 CAR by biotin-recombinant FRα (R&D), and CD19 CAR by biotin-proteinL (GenScript). Secondary labeling with Streptavidin-APC was used for all CARs. The following marker antibodies were used for phenotypic analysis according to manufacturer recommendations: PE-Cy7- CD3; APC-Cy7- CD3; PE- CD4; APC- CD8; PE-CD45; APC- CD34; PE- CD19; PE- CD69; PE-Cy7-CD28; PerCP-Cy5.5-CD27; BV421-PD-1; PE-CD25; APC-CD86; FITC-CD70; PE-41BBL; APC-HLA-A,B,C (Biolegend) and APC-CD33; APC- CD107a; APC- CD107b; FITC-HLA-DR,DP,DQ (BD). 7AAD (Biolegend) was used to assess viability.

Xenograft model of AML

(NOD/SCID)/γ-$chain^{-/-}$ (NSG) mice were obtained from the University of Pennsylvania Stem Cell and Xenograft core. 6-12 week old female mice were bred, treated, and maintained under pathogen-free conditions in-house under University of Pennsylvania IACUC-approved protocols. $5x10^6$ THP1-fLuc tumor cells were inoculated subcutaneously or intravenously. 5 mice per group were injected intraperitoneally or intravenously with $5x10^6$ CAR^+ T cells at indicated time points. Tumor growth was assessed by weekly imaging and/or caliper measurements. Tumor volumes were calculated using the following formula: $V=1/2(length \times width^2)$, where length is greatest longitudinal diameter and width is greatest transverse diameter.

Bioluminescence imaging

Bioluminescence imaging of $fLuc^+$ tumor cells was performed with the Xenogen IVIS imaging system and quantified with the Living Image software (Perkin Elmer). Mice were injected intraperitoneally with D-luciferin (150 mg/kg) and imaged under isoflurane anesthesia. Images were recorded until 2 consecutive images showed decreasing signal. Peak signal was determined for each mouse at each indicated time point. Pseudocolor images (scale $1x10^6$-10^8) representing light intensity were generated with Living Image.

***in vivo* combination with ATRA**

8-10 week old NSG mice were inoculated with $5x10^6$ THP1 IV via tail vein injection. 5mg/kg ATRA (or vehicle control) was injected IP daily from days 6-13 and every 2 days from days 13-41 post tumor challenge. In indicated groups, $5x10^6$ CAR^+ (or GFP^+) T cells were injected IV on day 9. Tumor progression was monitored by weekly bioluminescent imaging. Peripheral blood sampling was performed on day 26 to measure CAR T cell persistence and phenotype by flow cytometry.

Statistical analysis

The data are reported as means and standard error (SEM) unless otherwise noted. Statistical analysis was performed using unpaired 2-tail student t test. GraphPad Prism 6.0 software was used for statistical calculations. $P < .05$ was considered significant.

Results

Generation of anti-FRβ CAR

The m909 scFv[175] was cloned into previously validated lentiviral constructs containing CD8α hinge and transmembrane domains with intracellular CD3ζ alone or with the CD28 signaling domain in tandem, referred to as m909-Z and m909-28Z, respectively[110,176]. Both constructs included green fluorescent protein (GFP) separated by a viral 2A peptide to identify transduced T cells (**Figure 2.1A**). MOV19 CAR T cells with specificity for human FRα, CD19 CAR T cells with specificity for human CD19, or GFP transduced T cells were used as controls (not shown). Transduction of human T cells with m909 CAR constructs was reproducibly achieved at efficiencies of 70-80%, as measured by both GFP and surface CAR expression (**Figure 2.1B**). Transduction efficiencies of m909-Z and m909-28Z were virtually identical. Following two weeks expansion, CAR expression was maintained in both $CD4^+$ and $CD8^+$ T cells with a usual ratio of 30:70 CD4:CD8 (**Figure 2.1C**).

m909 CAR T cells exhibit antigen-specific reactivity against engineered C30-FRβ

To evaluate FRβ-specific reactivity of m909 CAR T cells, we engineered C30, a FR-negative human ovarian cancer cell line, to constitutively overexpress human FRβ (C30-FRβ; **Figure 2.2A**). After overnight co-culture of CAR T cells with C30 or C30-FRβ, supernatants were assayed for release of proinflammatory cytokines. m909-Z and m909-28Z CAR T cells selectively secreted IFNg in response to C30-FRβ (**Figure 2.2B**). m909 CAR T cells also produced TNFα, IL2, and MIP1α (**Figure 2.3**). m909 CAR^+ (GFP^+) T cells specifically upregulated surface expression of activation marker CD69 in the presence of C30-FRβ but not C30 (**Figure 2.2C**). As increased *in vivo* expansion of CAR T cells[110] and persistence of transferred T cells in melanoma patients[69] correlates with anti-tumor efficacy, we tested the

ability of m909 CAR T cells to proliferate *in vitro* in response to cell-surface FRβ. T cells were labeled with PKH26, and dye dilution by proliferating cells was measured by flow cytometry after 5 days in co-culture with the indicated targets. Both m909-Z and m909-28Z exhibited specific proliferation in response to C30-FRβ but not C30 (**Figure 2.2D**). Degranulation, as quantified by increased cell-surface CD107 expression, is an established surrogate for T cell lytic function[179]. After 6 hour co-culture, we observed specific degranulation by m909 CAR^+ (GFP^+) T cells only in the presence of C30-FRβ (**Figure 2.2F**). To evaluate true lytic capability of m909 CAR T cells, we co-cultured C30-FRβ-fLuc with CAR T cells. After overnight incubation, both m909-Z and m909-28Z CAR T cells showed high, dose-dependent lysis of C30-FRβ (**Figure 2.2E**).

m909 CAR T cells exhibit specific reactivity against endogenous FRβ on human AML

After establishing antigen-specific reactivity for cell-surface human FRβ, we next evaluated m909 CAR T cell function against physiologically relevant levels of antigen in myeloid tumor cells. We acquired three human AML cell lines with high, medium, and low (undetectable) surface expression of FRβ (THP1, MV411, and HL60, respectively). Surface protein expression was assessed by labeling with m909-IgG using flow cytometry (**Figure 2.4A**), and mRNA expression was confirmed with qRT-PCR (**Figure 2.4B**). For all AML experiments, CD19-28Z CAR T cells were used as a control as none of the AML cells expressed CD19 (**Figure 2.5**). After overnight co-culture with AML targets, IFNg secretion was measured by ELISA (**Figure 2.4C**). Because not all CAR T cell donors respond comparably, we conducted 10 independent experiments using 10 distinct T cell donors. m909 CAR T cells from most donors produced significantly higher IFNg in response to $FR\beta^+$ AML targets, compared to CD19-28Z control T cells.

To evaluate the proliferative potential of m909 CAR T cells in response to FRβ$^+$ AML, T cells were labeled with PKH26 and dye dilution was measured by flow cytometry following co-culture with targets (**Figure 2.4D**). Overlaying histograms represent PKH26 fluorescence of GFP, CD19-28Z, or m909-28Z CAR T cells before (Pre) and after 5-day exposure to the indicated targets. m909-28Z CAR T cells proliferated in response to FRβ$^+$ C30-FRβ, THP1, and MV411 but not FRβ$^-$ C30 or HL60; control T cells did not proliferate under any condition. In 3 of 4 T cell donors evaluated, response to FRβ-low MV411 was slightly greater than for FRβ-high THP1. To assess whether this could be due to different levels of non-antigen specific stimulation by target cells, we evaluated HLA and costimulatory ligand expression on the AML cell lines (**Figure 2.6**). Indeed, we found that MV411 expresses more CD86, 41BB-L, and HLA-ClassII compared to THP1.

The lytic capability of m909 CAR T cells against AML was evaluated using THP1-fLuc (**Figure 2.4E**). m909 CAR T cells exhibited specific lysis of THP1 but not C30 compared to control CD19-28Z CAR T cells. Finally, surface FRβ expression was measured on remaining THP1 following overnight co-culture (**Figure 2.4F**). Cells surviving co-culture with m909-28Z CAR T cells had significantly reduced expression as measured by both FRβ median fluorescence intensity (MFI) and percent FRβ positive, suggesting m909 CAR T cell elimination of THP1 was antigen-dependent.

To validate the applicability of m909 CAR T cells to primary AML, we co-cultured m909 CAR T cells with peripheral blood cells from 2 patients with validated FRβ expression on blasts. We observed significantly higher IFNg secretion from m909-28Z CAR T cells compared to control GFP T cells after overnight co-culture (**Figure 2.7**), suggesting m909 CAR T cells are capable of recognizing FRβ$^+$ primary patient tumor cells in addition to FRβ$^+$ AML cell lines.

Antigen upregulation by ATRA enhances m909 CAR T cell recognition of AML

We hypothesized that the level of FRβ expression by some AML cells represents a possible limitation to m909 CAR T cell recognition. ATRA has been reported to increase FRβ expression on AML[150] and improve FRβ-targeted liposomal drug delivery in vivo[174]. Therefore, we sought to determine whether ATRA-treated AML is more susceptible to targeting with m909 CAR T cells. First, elevated cell-surface FRβ expression by THP1 and MV411 AML was observed over a 5 day time course in the presence of 10nM ATRA (**Figure 2.8A**). Increased production of FRβ mRNA was confirmed after 3 and 5 days of ATRA treatment (**Figure 2.8B**). Consistent with previous reports[150,152], we observed enhanced expression in FRβ$^+$ THP1 and MV411 but not FRβ$^-$ HL60. To assess whether ATRA-induced FRβ expression on target cells sensitized them to m909 CAR T cell attack, AML cells that had been pre-treated for 5 days with ATRA were washed, plated in fresh media and co-cultured with m909 CAR or control GFP T cells. m909-Z and m909-28Z CAR T cells secreted significantly more IFNg when cultured with ATRA pre-treated THP1 but not MV411 (**Figure 2.8C**). Cytokine secretion in response to ATRA-treated HL60 was slightly increased, although receptor levels were not detectably upregulated. To assess whether ATRA-treated AML is more susceptible to CAR T cell-mediated lysis, we cultured untreated or ATRA-pretreated THP1-fLuc with m909 CAR T cells. In addition to IFNg secretion, m909 CAR T cells displayed significantly increased lytic activity against ATRA pre-treated THP1 (**Figure 2.8D**).

Numerous reports suggest direct modulatory effects of ATRA on T cells. In mice, vitamin A deficiency leads to excessive Th1 and impaired Th2 responses[180], and treatment with vitamin A *ex vivo* decreases Th1 cytokine secretion by activated PBMCs[181], suggesting a role for retinoids in negatively regulating Th1 development. Retinoic acid was also shown to impair IFNg production in human cells[182]. In contrast, others report ATRA enhancement of IL2-mediated T cell activation, proliferation, and survival[183-185]. To address the possible effects of ATRA on CAR T

cells, we co-cultured (previously untreated) targets and T cells with or without 10nM ATRA continually present in the media. Because elevated surface FRβ was not measureable until 2-3 days in treatment with ATRA (**Figure 2.8A**), 3 day co-cultures were performed. IFNg was significantly elevated in m909 CAR-treated THP1 and MV411 with ATRA compared to cultures treated without ATRA (**Figure 2.8E**), indicating maintenance of a Th1 cytokine profile. Since ATRA acts in target cells at the endogenous FRβ promoter[151], C30-FRβ (with FRβ expression driven from the EF1α promoter) is not susceptible to ATRA-induced upregulation. Accordingly, the presence of ATRA did not impact IFNg secretion from m909 CAR T cells activated by C30-FRβ, suggesting that direct effects of ATRA on CAR T cells are likely not responsible for their improved reactivity against AML .

m909-28Z CAR T cells reduce AML tumor growth *in vivo*

After confirming m909 CAR T cell reactivity against human AML *in vitro*, we investigated their anti-tumor activity *in vivo*. In previous studies, inclusion of the CD28 activation domain in CAR constructs enhanced *in vivo* performance and persistence of engineered T cells in mice as well as patients receiving CD19 CAR T cells[186,187]. Therefore, m909-28Z CAR T cells were tested for *in vivo* reactivity against THP1. GFP and CD19-28Z CAR control T cells were tested in parallel. Immunocompromised NSG mice were inoculated with $5x10^6$ THP1-fLuc subcutaneously. Bioluminescent imaging was used to confirm engraftment of tumor cells. On days 8 and 10 after tumor inoculation, mice received $5x10^6$ CAR^+ (or GFP^+) T cells via intraperitoneal injection. Tumor progression was evaluated by luminescence (**Figure 2.9A-B**) and caliper measurements (**Figure 2.9C**). Treatment with m909-28Z CAR T cells mediated tumor regression and significantly inhibited THP1 outgrowth. To investigate *in vivo* expansion/persistence of m909-28Z CAR T cells, we evaluated human $CD3^+$ cells in the peripheral blood of treated mice. Consistent with a productive anti-tumor response, mice treated with m909-28Z CAR T cells

exhibited significantly increased peripheral blood T cells, comprised of both $CD8^+$ and $CD4^+$, compared to controls at 4 weeks post T cell treatment (**Figure 2.9D**). In addition, we tracked CAR expression during treatment and showed that m909-28Z CAR^+ T cells persist long term in THP1 treated mice (**Figure 2.10**). These data suggest that m909-28Z CAR T cells expanded peripherally upon specific recognition of $FR\beta^+$ tumor *in vivo*. As AML is a disseminated systemic disease in humans, we also evaluated m909-28Z CAR T cell activity against disseminated THP1, delivered by IV injection. m909-28Z CAR T cells also significantly inhibited systemic AML tumor growth *in vivo* compared to control T cells (**Figure 2.11A-B**). To begin to assess the impact of ATRA on FRβ-directed CAR T cells *in vivo* we provided ATRA IP during the course of T cell treatment. In initial results from one study, ATRA did not impact THP1 growth in untreated or T cell treated mice (**Figure 2.11C-F**), nor did it affect T cell phenotype when assessed 17 days post transfer (**Figure 2.11H-M**).

m909 CAR T cells do not inhibit $CD34^+$ colony formation or eliminate FRβ-low healthy monocytes

Many surface markers, including others exploited for CAR therapy of AML (e.g. CD123, CD33, CD38), are shared between AML blasts and normal hematopoietic stem and progenitor cells (HSCs). One concern in the development of AML-directed CAR therapies is the potential for depletion of healthy bone marrow progenitors[188-191]. FRβ has been reported at low levels on human $CD34^+$ bone marrow HSCs although this receptor was nonfunctional and unable to bind folate[192]. To investigate whether m909 CAR T cells recognize healthy HSCs, we first assessed the binding potential of m909-IgG to normal human bone marrow $CD34^+$ cells. We were unable to detect surface FRβ protein in any of three healthy donors by flow cytometry (representative donor, **Figure 2.12A**). To test for functional reactivity of m909 CAR T cells against hematopoietic progenitors, we conducted colony forming (CFU) assays following co-culture of

$CD34^+$ HSCs and CAR T cells. After 4-hour co-incubation, each well was diluted in methylcellulose and cultured for 14 days. Colonies were counted and scored for CFU-GEMM, GM, G, M, or BFU-E. Unlike other CARs targeting AML[188-191], neither m909-Z nor m909-28Z CAR T cell pre-treatment inhibited colony formation (**Figure 2.12B**). There were no significant differences in the number of total or lineage-specific colonies compared to untreated controls. Furthermore, 5 day ATRA treatment did not induce FRβ in HSCs (2 pools representing 7 normal $CD34^+$ donors tested) (**Figure 2.13**).

We recently published a study highlighting the presence of FRβ on a subset of peripheral blood monocytes in healthy donors[193]. This was confirmed in the present study with FRβ expression from one representative donor shown (**Figure 2.12C**). 5 day ATRA treatment did not enhance FRβ expression in healthy monocytes from any of 3 donors evaluated (data not shown). To assess the potential for myeloid toxicity with FRβ-directed CAR T cells, we co-cultured m909 or control T cells with $CD14^+$ monocytes isolated from healthy donors. 4hr lysis of $CD14^+$ monocytes was assessed using flow cytometry. We did not observe any significant lysis of monocytes by m909 CAR T cells compared to controls (**Figure 2.12D**). Together, our findings suggest that FRβ can be safely pursued as a target for CAR T cell therapy of AML without harming essential healthy HSCs or normal monocytes expressing low levels of FRβ.

Discussion

Here, we describe the first CAR specific for human FRβ for the targeting of AML. m909 CAR constructs are fully human in composition, addressing the issue of transgene immunogenicity reported elsewhere with CARs using mouse scFvs[95,128,129]. Our initial data using C30 and C30-FRβ, a cell line engineered for FRβ expression, confirm the feasibility of targeting cell-surface human FRβ with CAR T cells. This model provides a robust positive control for CAR T cell specificity by providing high levels of antigen for CAR stimulation in a true negative epithelial cell line. The m909 CAR platform allows for efficient and specific targeting as demonstrated by *in vitro* co-culture assays resulting in cytokine production, activation marker upregulation, proliferation and target cell lysis when high levels of antigen are present. In the presence of human AML cells expressing endogenous levels of FRβ, m909 CAR T cells maintained specific activation in the presence of antigen. However, CAR activity decreased with lower surface levels of FRβ, as demonstrated by reduced output of IFNg and cytolysis. In addition, it was clear that m909 CAR T cells specifically eliminated THP1 target cells displaying the highest antigen expression.

Despite only moderate activity against THP1 *in vitro*, m909-28Z CAR T cells did significantly inhibit subcutaneous and disseminated THP1 tumor growth *in vivo*, suggesting that systemic delivery of m909-28Z CAR T cells to tumor-bearing mice resulted in efficient trafficking, activation, and lysis at sites of tumor growth. When m909-28Z CAR T cells were delivered to mice bearing large established subcutaneous THP1 tumors (~3 weeks post tumor injection), they were unable to control tumor growth (see chapter 3). These data suggest m909-based CARs may only be effective at overcoming small tumor burden. However, over 90% of AML patients reach remission through chemotherapy but eventually relapse due to minimal residual disease (MRD)

that is often undetectable[172]. Therefore, m909-28Z CAR T cells could be utilized as an effective treatment for patients with chemotherapy-induced remission or MRD conditions.

As m909 CAR T cells displayed decreased lysis against targets with lower FRβ expression, outgrowth of FRβ-low leukemic clones remains a potential concern for m909 CAR-based therapy. However, we and others have established that ATRA specifically upregulates FRβ expression in $FR\beta^+$ AML. Tumor cells with surface antigen expression under the threshold for m909 CAR recognition can potentially be induced to levels high enough to stimulate T cell activation. Indeed, IFNg release and lytic activity from m909 CAR T cells was increased following co-culture with ATRA pre-treated AML. We also observed small increases in IFNg secretion of control GFP T cells and m909 CAR T cells against $FR\beta^-$ HL60, suggesting that other effects of ATRA on target cells may slightly enhance T cell recognition of AML. Notably, ATRA is known to induce differentiation of THP1 and HL60[194,195] as measured by greater cytokine production and costimulatory molecule expression[196]. ATRA-mediated differentiation of AML cells may have heightened the allogeneic T cell response. However, the largest differences in reactivity were observed when m909 CAR T cells were incubated with ATRA-treated $FR\beta^+$ AML, suggesting greater antigen density played the dominant role in mediating increased m909 CAR T cell reactivity. Although a pilot experiment with the addition of ATRA *in vivo* did not provide augmentation of m909 CAR T cell performance, we also did not observe any reduction in anti-tumor response. While further optimization of dosing and treatment regimen will be necessary, these preliminary results suggest ATRA can safely be combined without adverse effects on CAR T cell function *in vivo*. In addition to ATRA alone, dual treatment with HDAC inhibitors has been shown to even further stimulate FRβ expression in AML *in vitro*[152]. Optimized combinations of ATRA and other FRβ-inducing agents present an opportunity for additional augmentation of m909 CAR T cell efficacy. Importantly, ATRA did not impact FRβ

expression in healthy HSCs or monocytes suggesting ATRA-induction of FRβ in AML could be applied without increasing the capacity for healthy tissue recognition by m909 CAR T cells.

Of note, neither ATRA, HDAC inhibition, or combination is capable of inducing FRβ in non-expressing cells of either myeloid origin (like HL60) or epithelial origin (like 293)[152] suggesting their effects are not potent enough to overcome the genetic program responsible for maintaining tissue specificity. Therefore, de novo induction of FRβ expression in negative tissues is not a major concern. Similarly, AML patients would need to be pre-screened for FRβ as ATRA will not induce FRβ without baseline expression present. While previous studies have identified FRβ on all classes of AML, incidence does increase with myeloid/monocytic distinctions (M4 and M5)[174], and these patients may benefit the most from FRβ-directed CAR therapy. Generally, new cancer therapeutics are moving towards a more personalized approach and need not necessarily be applicable to all patients across one broad and complex disease indication in order to be clinically beneficial.

Beyond pharmacological upregulation of FRβ antigen, the modest activity of m909 CAR T cells against FRβ-low AML targets may also be overcome by CAR platform optimization. For example, Hudecek and colleagues were able to greatly increase activity of a ROR1-specific CAR by modifying the hinge length and improving the scFv affinity[197]. It remains possible that the monovalent affinity of the m909 scFv (K_D=57 nM) may be suboptimal for interaction with FRβ expressed at low levels. We anticipate that modifying the FRβ CAR T cell platform by introducing higher affinity scFvs could improve overall anti-tumor efficacy. However, higher affinity activity could result in increased toxicity against normal cells expressing low levels of FRβ. Further toxicology and other preclinical evaluation of m909 and variants could help identify platforms with optimal affinity for tumor cell destruction while sparing normal tissues.

In addition to leukemia, FRβ expression is also reported on some normal myeloid lineage cells and can be induced upon macrophage activation[198]. Although we did not observe lysis of peripheral blood monocytes with m909 CAR T cells, healthy myeloid tissues remain a potential target for off-tumor toxicity by FRβ specific CAR T cells. Recent innovations in the field have the potential to mitigate these risks by restricting CAR T cell persistence via transient expression through RNA electroporation[199] or combining CAR delivery with an inducible suicide gene[200]. $CD34^+$ HSCs continuously give rise to peripheral myeloid lineage immune cells. Despite previous reports of FRβ expression in HSCs, we did not observe any toxicity against $CD34^+$ bone marrow progenitors, suggesting m909 CAR T cells may be applied with reduced risk to HSCs. Therefore, by providing transient expression of the m909 CAR platform, as described above, CAR T cell elimination following tumor clearance could allow for restoration of affected healthy myeloid populations from normal HSCs.

A successful FRβ CAR T cell platform has the potential for therapeutic benefit in a wide variety of diseases beyond AML. FRβ has also been described on chronic myelogenous leukemia (CML)[139,147,148]. In addition to leukemia, FRβ is increased on the surface of macrophages associated with various pathological conditions. Tumor associated macrophages (TAMs) display high levels of FRβ in solid tumors from diverse tissue origins[166]. Since TAMs correlate with worse prognosis across multiple types of cancer[20], FRβ CAR T cells could potentially be used to improve the treatment of solid tumors by eliminating immunosuppressive, pro-tumorigenic macrophages. FRβ is also highly expressed on macrophages at sites of ongoing inflammation[159] and has been effectively exploited for imaging and targeting of pathologic macrophages in rheumatoid arthritis[160] and atherosclerosis[201]. FRβ-specific immunotoxins have successfully depleted macrophages in mouse models of glioma[171], atherosclerosis[202], collagen-induced arthritis[164], and fibrosis[203]. Given their potent effector function and ability to persist after infusion,

FRβ-specific CAR T cells have the potential to improve upon antibody-directed toxicity and may present an exciting new way to expand the use of CAR T cells to inflammatory diseases as well as cancer.

Figure 2.1

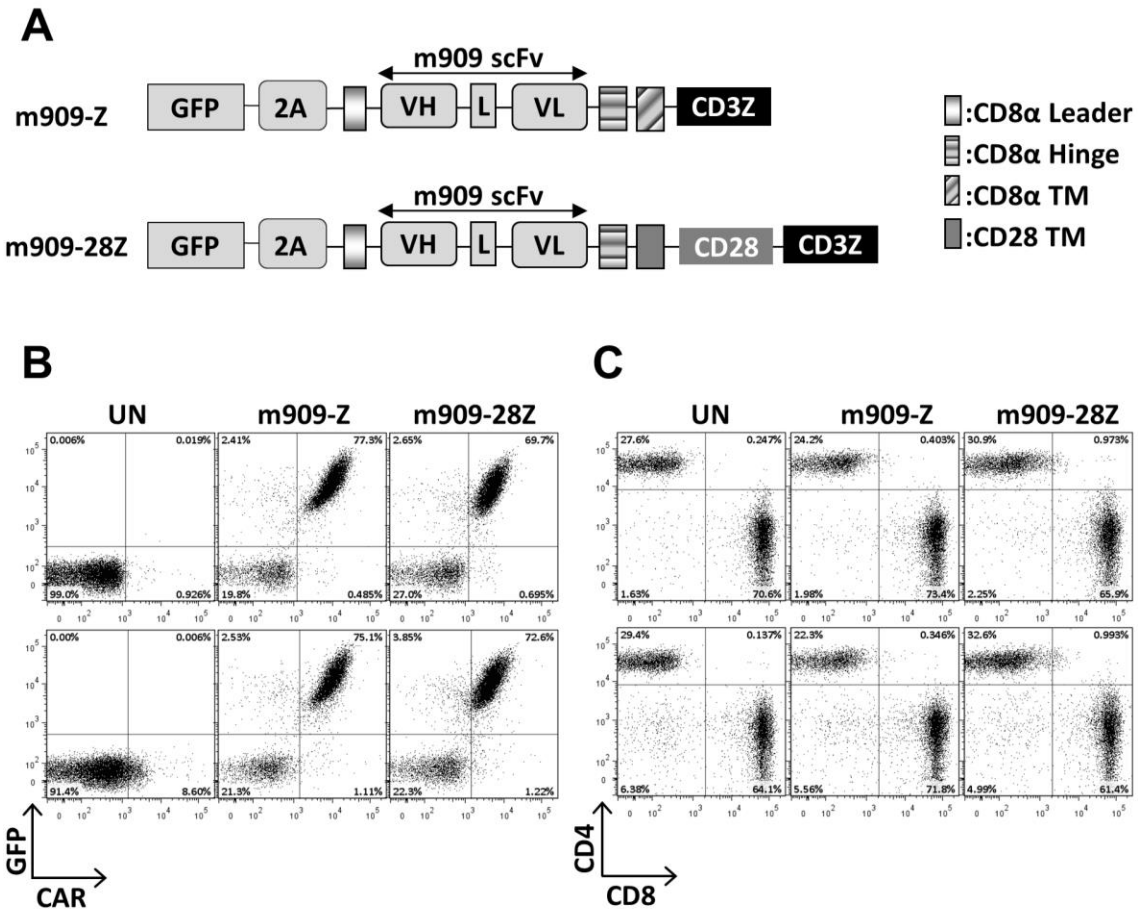

Figure 2.1 FRβ CAR construction and expression in primary human T cells.

(A) Schematic of lentiviral CAR expression vectors containing the anti-human FRβ scFv m909 linked to either intracellular signaling domains from CD3-ζ alone (m909-Z) or CD28 and CD3-ζ in tandem (m909-28Z). Both constructs also encode GFP separated by a viral T2A (2A) ribosomal skipping peptide. **(B)** CAR expression in primary human T cells. Expression of m909 CAR in primary human T cells was confirmed by GFP, and surface expression was confirmed by labeling with a rabbit anti-human IgG antibody that binds the human m909 scFv portion of the CAR. **(C)** After 13 days expansion, m909 CAR transduced T cell populations are comprised of approximately 70% $CD8^+$ and 30% $CD4^+$. Upper and lower panels show results from two representative donors. VH – variable heavy chain, VL – variable light chain. L – linker, TM-transmembrane domain. UN – represents untransduced T cells.

Figure 2.2

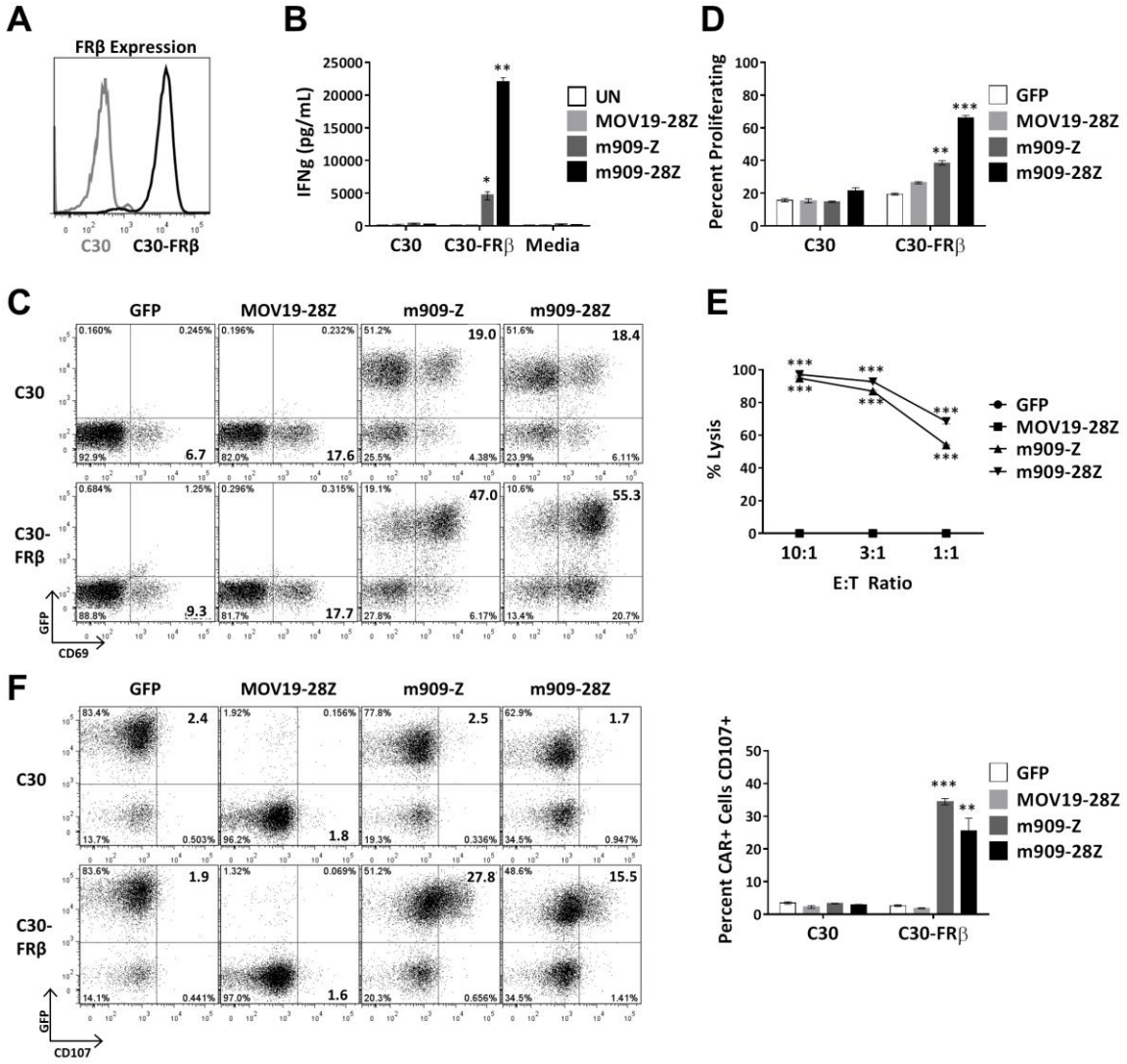

Figure 2.2 m909 CAR T cells are reactive against cell-surface FRβ on engineered C30-FRβ cell line.

To first test the functionality of m909 CARs, the antigen-negative ovarian cancer cell line C30 was transduced to stably overexpress human FRβ cDNA. Co-cultures were performed at a 1:1 E:T ratio unless otherwise noted. Control MOV19-28Z CAR T cells are specific for FRα and do not express GFP. Control GFP T cells only express GFP. Error bars represent mean ± SEM. **(A)** FRβ expression on engineered C30-FRβ was detected by flow cytometry using biotinylated m909-IgG (black histogram). For comparison, the unmodified parental C30 cells were used as a control (gray histogram). **(B)** Antigen-specific IFNg production by m909 CAR T cells as detected by ELISA from 24hr co-culture supernatants. **(C)** m909 CAR^+ T cells upregulate surface CD69

expression upon 24hr exposure to C30-FRβ. The m909 CAR^+ cells are identified by GFP expression (y axis). **(D)** m909-Z and m909-28Z CAR T cells proliferate in response to C30-FRβ. PKH26 dilution in labeled T cells was measured by flow cytometry after 5 days in co-culture. Percent of $CD3^+$ cells proliferating (diluted PKH26 compared to d0) is quantified. P values represent significant differences compared to MOV19-28Z CAR T cells. **(E)** m909-Z and m909-28Z exhibit specific lysis of C30-FRβ. Target cells were transduced to express firefly luciferase and co-cultured with CAR T cells at E:T ratios of 10:1, 3:1, or 1:1. Residual luciferase signal was determined after 18hrs. Percent lysis was determined by luminescence comparison to untreated target wells. **(F)** m909-Z and m909-28Z exhibit degranulation upon co-culture with C30-FRβ. CD107a/b surface expression was measured after 5 hours co-culture. CAR^+ cells are identified by GFP expression (y axis). Percent of CAR^+ cells with positive staining for CD107a/b is quantified to the right. P values represent significant increases compared to MOV19-28Z control T cells. (* $P < .05$, ** $P < .01$, *** $P < .001$)

Figure 2.3

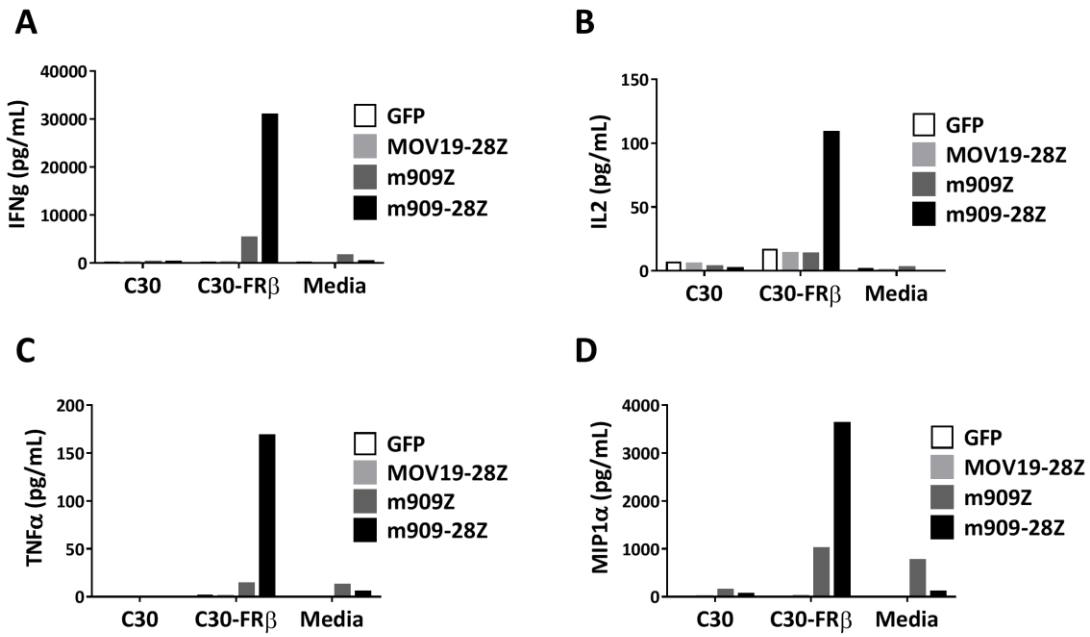

Figure 2.3 m909 CAR T cells secrete proinflammatory Th1 cytokines *in vitro*.

T cells were co-cultured overnight with C30 or C30-FRβ target cells or in media alone. Co-cultures were set up at 1:1 E:T ratio. Culture supernatants were analyzed for cytokine secretion by CBA. Levels of **(A)** IFNg, **(B)** IL2, **(C)** TNFα and **(D)** MIP1α are shown. E:T –Effector:Target, CBA – cytokine bead array.

Figure 2.4

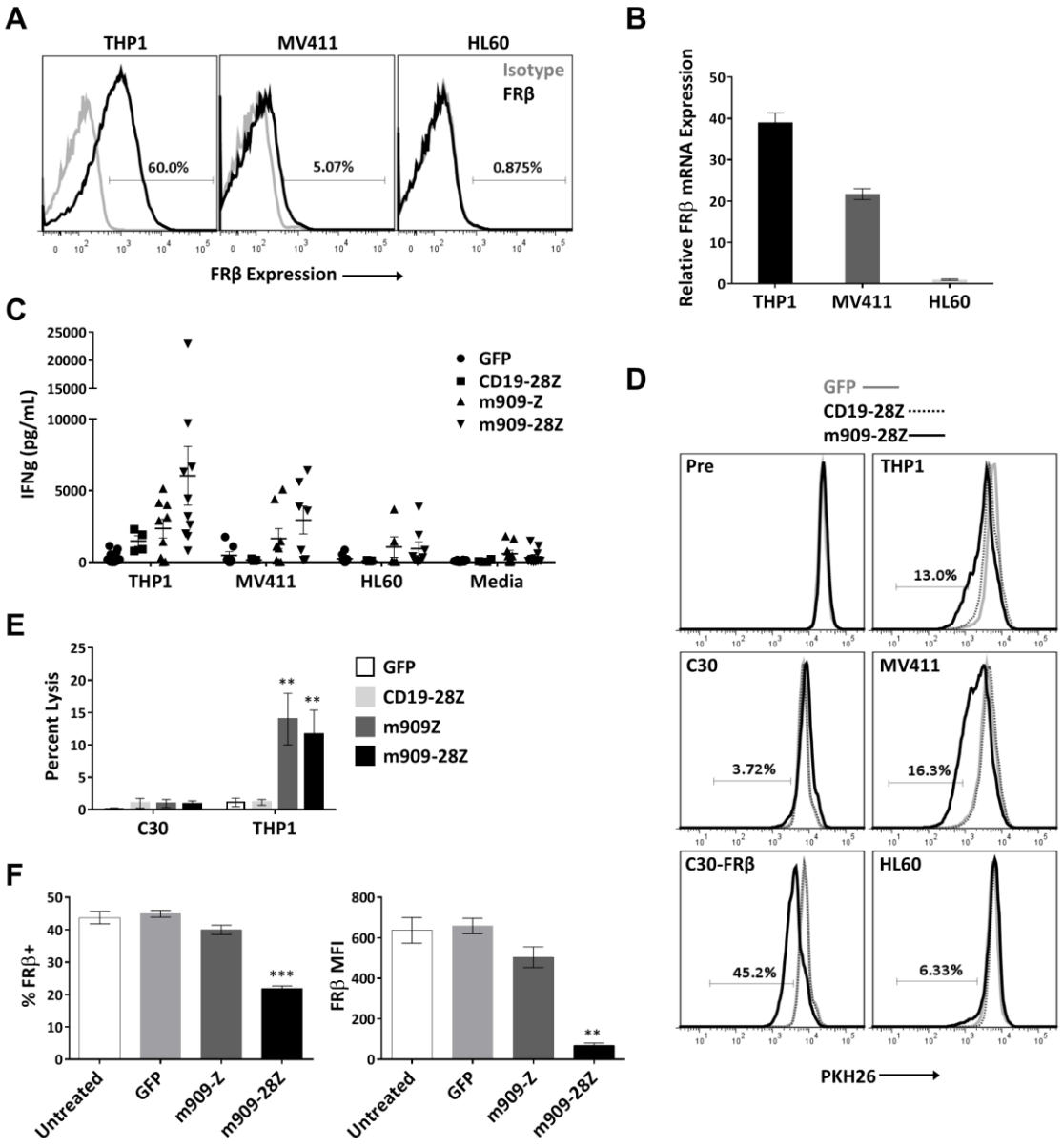

Figure 2.4 m909-28Z CAR T cells are reactive against endogenous FRβ on human AML cell lines *in vitro*.

To test m909 CAR T cell reactivity against clinically-relevant targets, we acquired three human AML cell lines with varying levels of FRβ expression. Co-cultures were performed at a 1:1 E:T ratio unless otherwise noted. Control CD19-28Z CAR T cells are

specific for human CD19 and do not express GFP. In Media controls, T cells were plated without target cells. Error bars represent mean ± SEM. **(A)** Surface expression of FRβ on AML cell lines THP1, MV411, and HL60 was determined by flow cytometry using m909-IgG (black) and human IgG isotype control (gray). Percentages represent the proportion of cells with a positive fluorescent signal compared to isotype. **(B)** Relative FRβ mRNA expression was confirmed using qRT-PCR. Indicated mRNA expression is shown relative to HL60. **(C)** Antigen-specific IFNg secretion was quantified by ELISA after overnight co-culture. Each data point represents the mean value of triplicate wells from independent experiments. n=10 different normal T cell donors are represented. **(D)** m909-28Z CAR T cells proliferate in response to THP1 and MV411, but not HL60, compared to control T cells. PKH26 dilution was measured via flow cytometry after 5 days in co-culture. Overlaying histograms display d5 PKH26 fluorescence in GFP (gray), CD19-28Z (dotted), and m909-28Z (black solid) T cell co-cultures with the indicated cell targets. A live, $CD3^+$ gate was used. Percentages represent the proportion of m909-28Z T cells with diluted PKH26 compared to CD19-28Z CAR T cells. **(E)** m909 CAR T cells exhibit specific lysis of THP1. Luciferase-expressing target cells were co-cultured with CAR T cells at 1:1 E:T ratio. Residual luciferase signal was determined after 24hrs. Percent lysis was determined by luminescence comparison to untreated target wells. Data shown are mean and SEM of n=9 independent T cell donors. P values are calculated compared to CD19-28Z control treated wells. **(F)** Decreased FRβ expression on THP1 cells surviving overnight co-culture with m909 CAR T cells. FRβ surface expression was determined by flow cytometry using m909-IgG and human IgG isotype control. A live, $CD3^-$ gate was used to distinguish surviving THP1 cells. The percent of cells showing positive FRβ staining compared to isotype (left) and the FRβ MFI (right) were determined for triplicate wells (n=3). P values were determined compared to control GFP T cell treated wells. (* $P < .05$, ** $P < .01$, *** $P < .001$, ns $P > .05$). MFI – median fluorescence intensity.

Figure 2.5

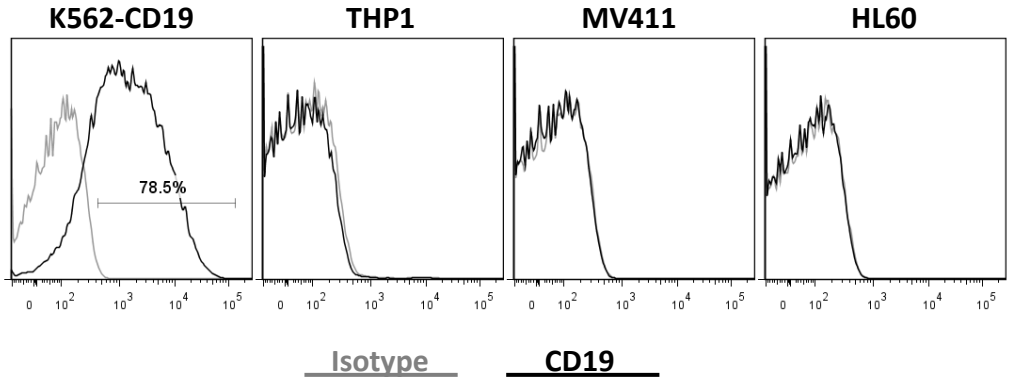

Figure 2.5 AML target cell lines do not express CD19.

Target AML cell lines THP1, MV411 and HL60 were analyzed for surface expression of human CD19 by flow cytometry. Overlaying histograms represent anti-CD19 (black) or isotype control (gray) stained cells. K562 cells engineered to overexpress CD19 were used as a positive control. AML – acute myeloid leukemia.

Figure 2.6

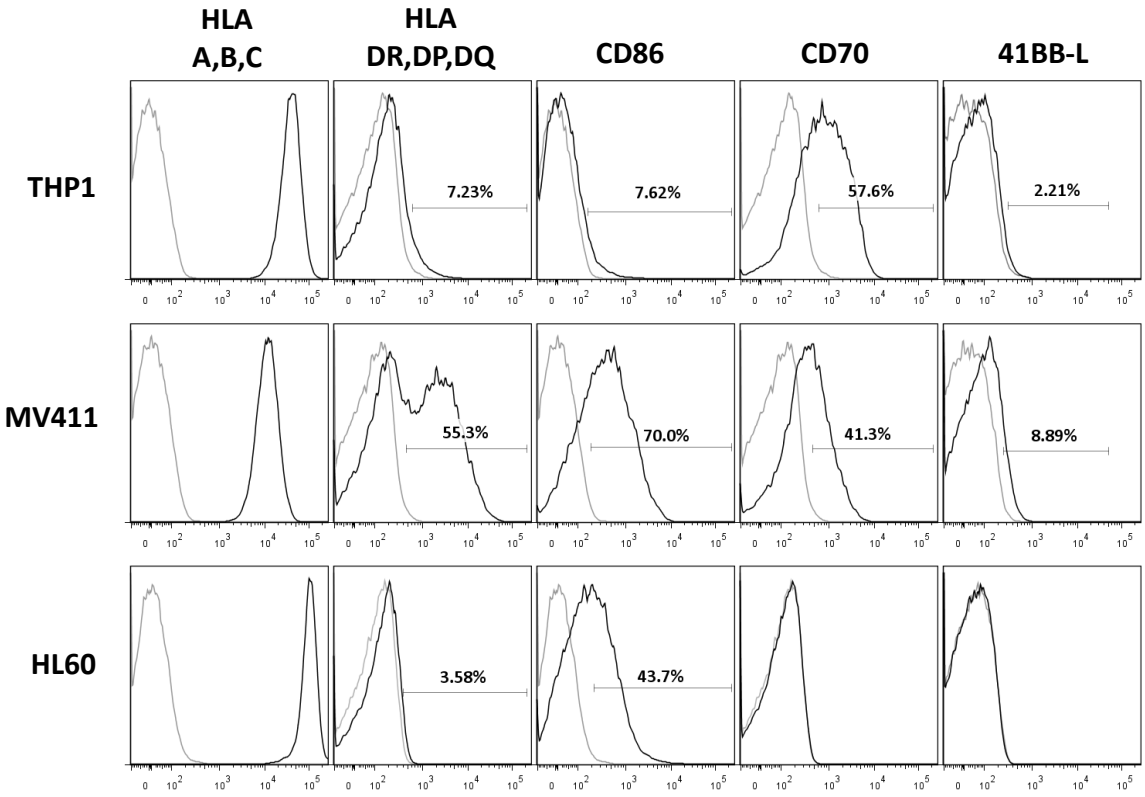

Figure 2.6 HLA and costimulatory ligand expression in human AML cell lines.

Surface expression of HLA class I and class II as well as T cell costimulatory ligands CD86, CD70, and 41BB-L was assessed on target human AML cell lines THP1, MV411, and HL60 and is represented by black lines in the above histograms. Respective isotype staining for each cell line is represented by the gray line. Percentages represent the percent of cells with a positive shift compared to isotype. (HLA- human leukocyte antigen).

Figure 2.7

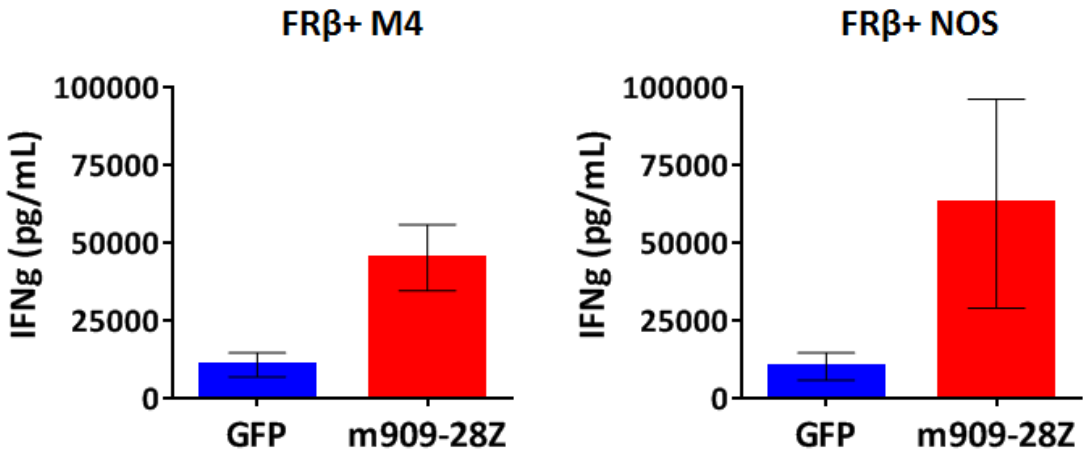

Figure 2.7 m909-28Z CAR T cells specifically recognize primary human AML.

To validate the applicability of m909 CAR T cells to primary AML, we co-cultured $1x10^5$ m909-28Z CAR^+ T cells (or GFP^+ control T cells) with $1x10^5$ peripheral blood cells isolated from 2 different patients with validated FRβ expression on blasts. IFNg secretion after overnight co-culture was assessed by ELISA. Results incorporate independent experiments using 5 T cell donors. Error bars represent mean ± SEM. (M4-myelomonocytic AML classification, NOS-not otherwise specified AML classification).

Figure 2.8

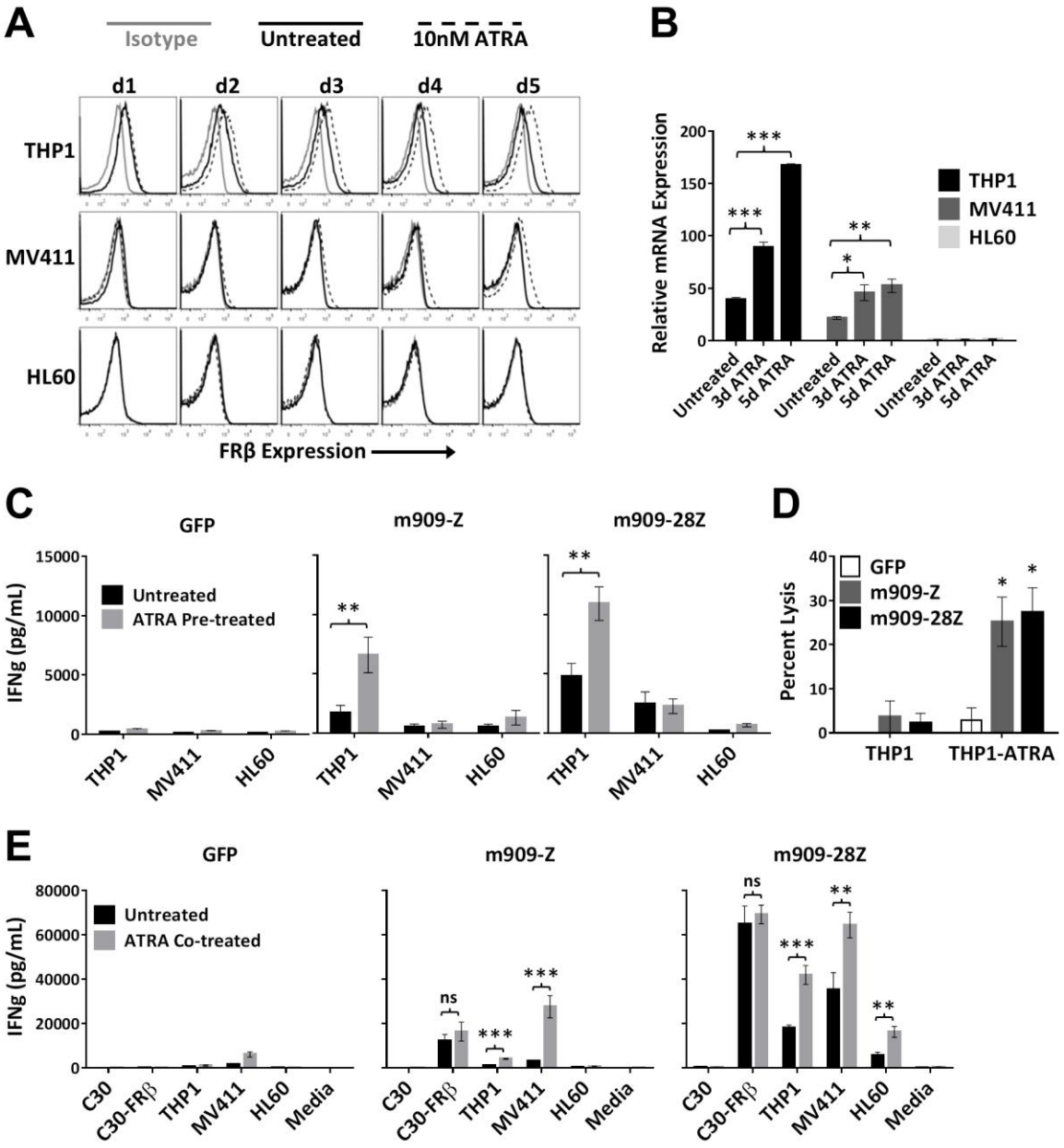

Figure 2.8 ATRA increases FRβ expression and m909 CAR T cell recognition of AML cell lines.

(A) AML cell lines were treated with (dotted black line) and without (solid black line) 10nM ATRA for 5 days. Surface FRβ expression was determined each day by flow cytometry with m909-IgG (black) or human IgG isotype control (gray). **(B)** FRβ mRNA expression was determined before (untreated) and after 3 days and 5 days of 10nM ATRA treatment. Relative mRNA is shown compared to untreated HL60. Bars represent mean ± SEM of n=5 replicate wells. P values were calculated for each cell line compared to untreated controls. **(C)** m909 CAR T cells secrete higher IFNg in response to THP1 cells pre-treated for 5 days with 10nM ATRA (gray bars) compared to untreated cells (black bars) in overnight co-cultures. **(D)** THP1-fLuc cells were pre-treated with (THP1-ATRA) or without (THP1) 10nM ATRA for 5 days before co-culture with m909 CAR or GFP control T cells at 1:1 E:T ratio. Percent lysis was determined by residual luciferase activity after overnight co-culture. **(E)** m909 CAR T cells secrete higher IFNg after 3 days co-culture in the presence of 10nM ATRA (gray bars) and AML target cell lines compared to cultures without ATRA (black bars). No significant differences in IFNg secretion were observed for m909 T cells activated in the presence of C30-FRβ with or without ATRA. In panels C-E, graphs represent mean ± SEM from n=3 independent experiments using 3 distinct T cell donors. P values were calculated for each T cell subset to compare between untreated and ATRA-treated cell lines. (* $P < .05$, ** $P < .01$, *** $P < .001$, ns $P > .05$).

Figure 2.9

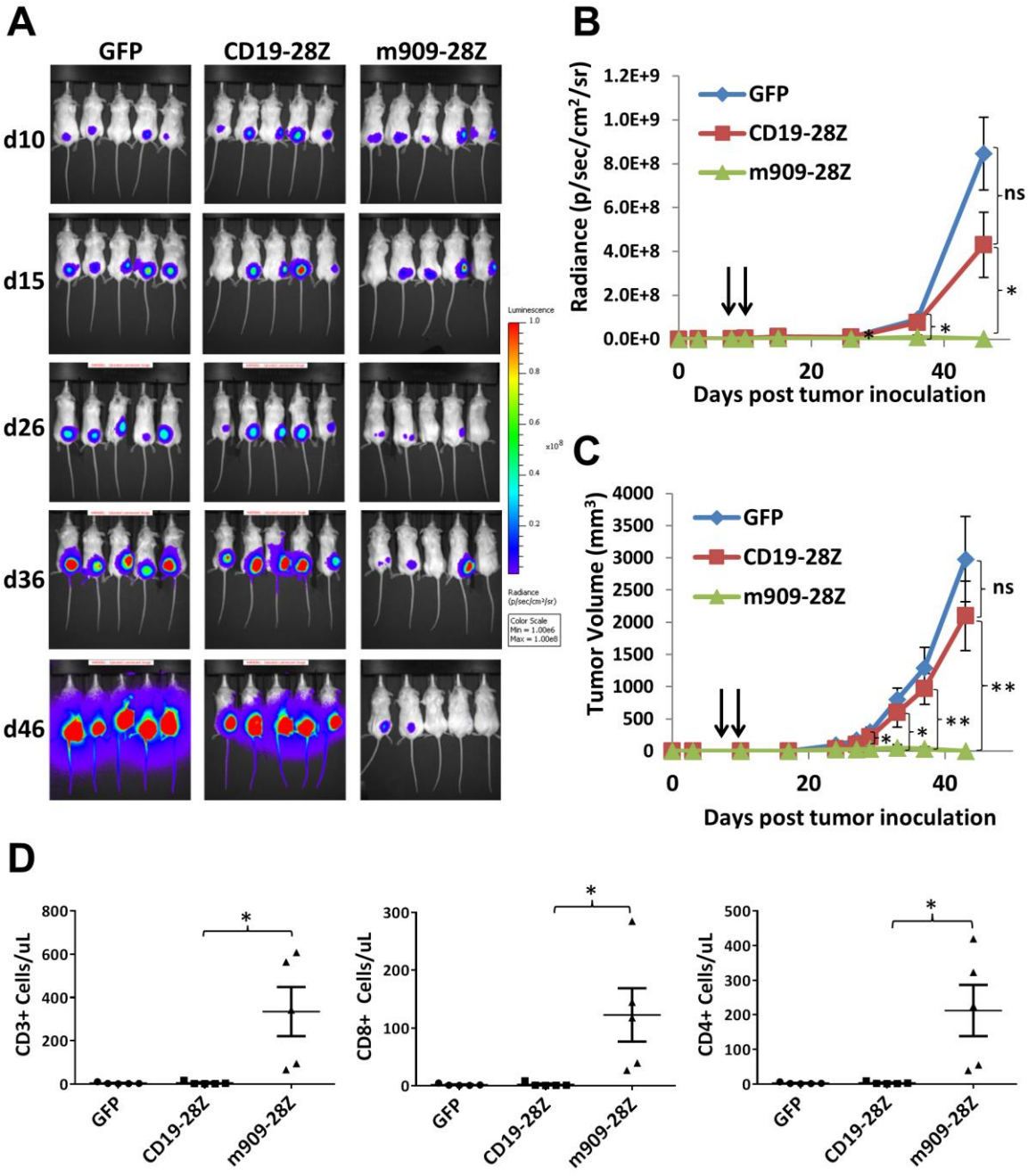

Figure 2.9 m909-28Z CAR T cells prevent THP1 AML tumor growth *in vivo.*

$5x10^6$ THP1-fLuc cells were injected into NSG mice subcutaneously on day 0. $5x10^6$ CAR^+ T cells were given intraperitoneally on days 8 and 10. Tumor growth was monitored by luminescence **(A-B)** and caliper measurement **(C)**. Graphs represent mean ± SEM of n=5 mice per experiment. P values were calculated compared to CD19-28Z treated control mice Differences between GFP and CD19-28Z groups did not reach statistical significance at any time point. **(D)** Preferential expansion and survival of peripheral human T cells in m909-28Z treated mice compared to control T cells. Peripheral blood was collected on day 38 (4 weeks post T cell injection) and absolute numbers of human $CD3^+$ (left), $CD8^+$ (middle), and $CD4^+$ (right) T cells were quantified by flow cytometry and are reported in total cells/µl blood. . (* $P < .05$, ** $P < .01$, *** $P < .001$, ns $P > .05$). NSG- NOD/SCID/γ-$chain^{-/-}$.

Figure 2.10

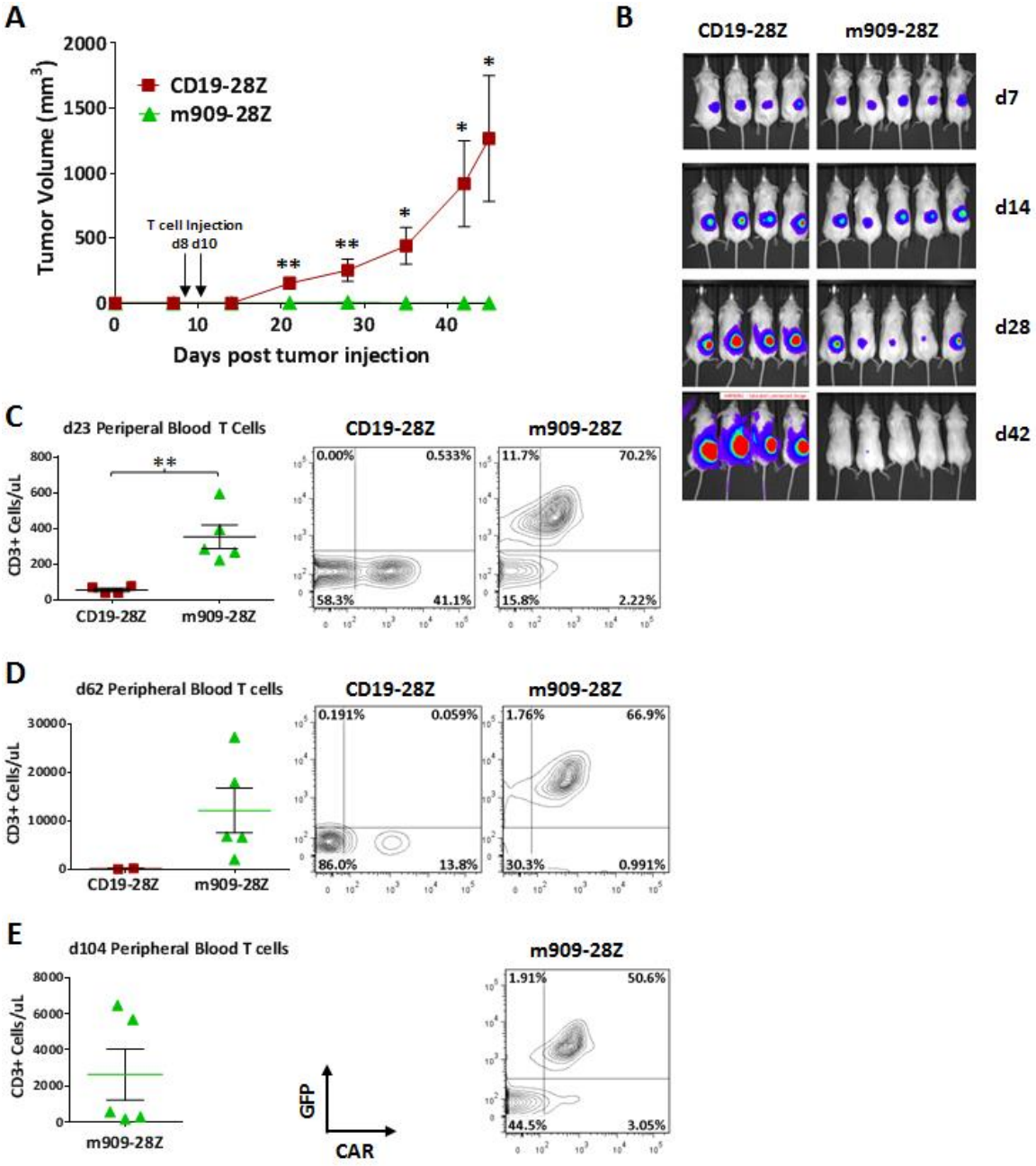

Figure 2.10 Long-term persistence of CAR$^+$ m909-28Z T cells in NSG mice bearing THP1 tumor.

NSG mice were inoculated subcutaneously with 5x10^6 THP1-fLuc on day 0. On days 8 and 10 following tumor injection, 5x10^6 CD19-28Z or m909-28Z CAR$^+$ T cells were injected IP. Tumor growth was monitored by caliper measurement **(A)** and bioluminescence **(B)**. (This is a repeat of the experiment outlined in Figure 2.9 using a different donor for CAR T cell production). Peripheral blood sampling was conducted on days 23 **(C)**, 62 **(D)**, and 104 **(E)** following tumor injection, and 50µl blood was used to quantify total CD3+ T cells/µL peripheral blood at each time point (left). Remaining blood was pooled for each group, red blood cells lysed, and stained for CAR expression by flow cytometry (right). m909-28Z CAR T cells are GFP/CAR double positive. CD19-28Z CAR T cells do not express GFP. It should be noted that the injected T cells were 54% CAR$^+$. Error bars represent mean ± SEM of n=5 mice per group. (* $P < .05$, ** $P < .01$, *** $P < .001$, ns $P > .05$). NSG- NOD/SCID/γ-chain$^{-/-}$.

Figure 2.11

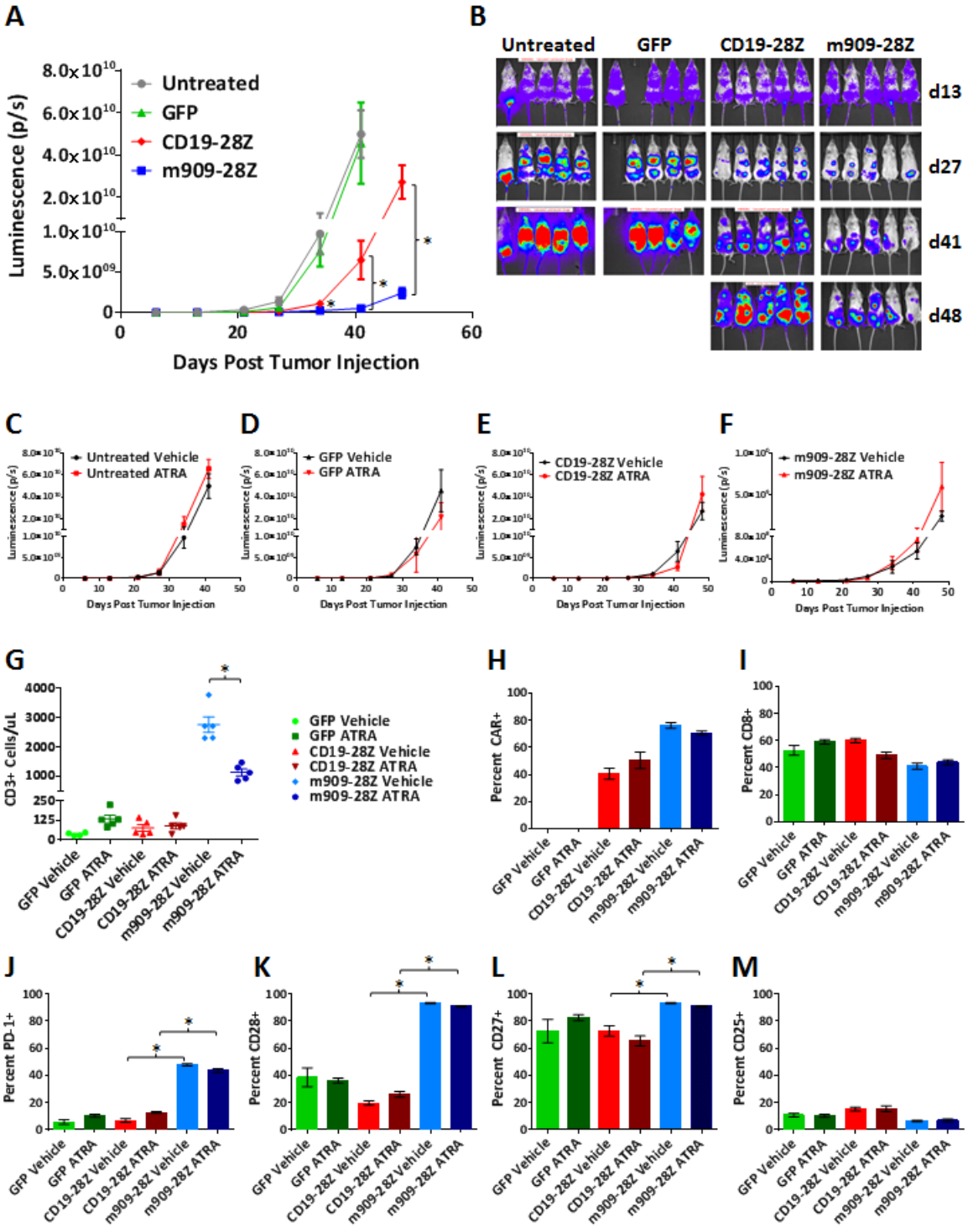

Figure 2.11 m909-28Z CAR T cells significantly delay growth of disseminated human AML.

NSG mice were inoculated with $5x10^6$ THP1-fLuc via IV injection on day 0. On day 9 following tumor injection, $5x10^6$ GFP, CD19-28Z, or m909-28Z CAR^+ T cells were injected IV. Untreated mice did not receive T cells. Tumor growth was monitored by bioluminescence **(A-B)**. To measure the impact of ATRA co-treatment on CAR T cell function *in vivo*, 5mg/kg ATRA or vehicle control was provided IP daily from d6-d13 and every other day d13-d41 following tumor inoculation. The provision of ATRA did not impact tumor growth in **(C)** Untreated, **(D)** GFP T cell, **(E)** CD19-28Z CAR T cell, or **(F)** m909-28Z CAR T cell treated mice. To measure the impact of ATRA on T cell phenotype *in vivo*, peripheral blood sampling was performed on day 26 following tumor inoculation. **(G)** Total $CD3^+$ cells/µl blood was quantified by flow cytometry using Trucount assay. $CD3^+$ T cells were also labeled with antibodies to detect **(H)** CAR**, (I)** CD8, **(J)** PD-1, **(K)** CD28, **(L)** CD27, and **(M)** CD25. In panels H-M, marker prevalence as a percentage of total $CD3^+$ cells is displayed. Error bars represent mean ± SEM for n=5 mice per group. (* $P < .05$). Although m909-28Z CAR T cells display elevated PD-1, CD28, and CD27 compared to CD19-28Z CAR T cells, there were no significant phenotypic differences between vehicle and ATRA treated groups.

Figure 2.12

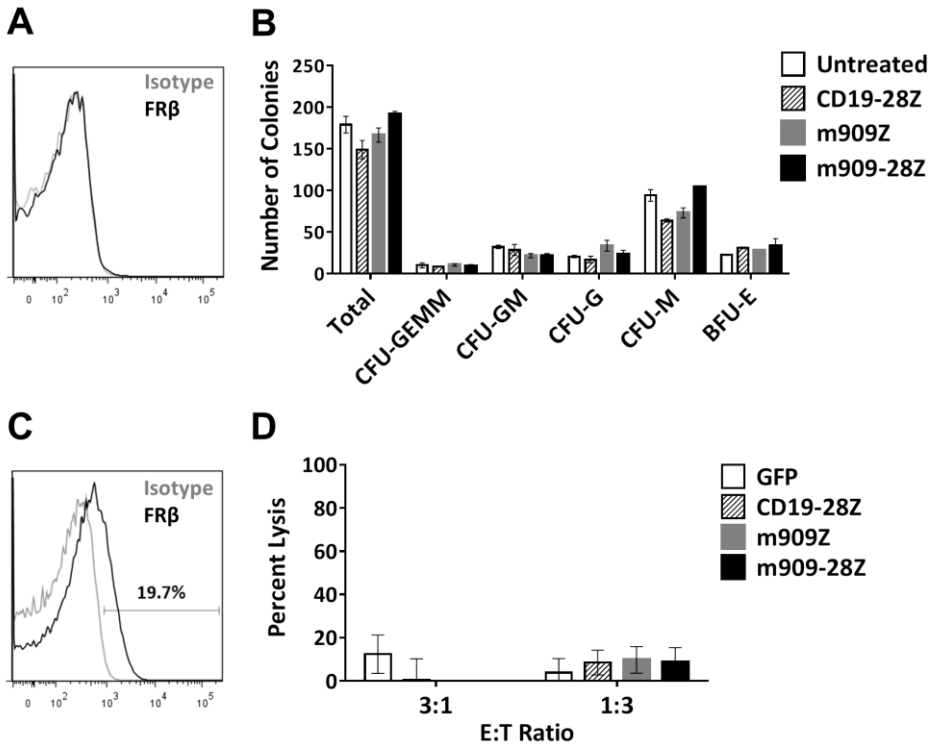

Figure 2.12 m909 CAR T cells do not inhibit CD34$^+$ HSC colony formation or eliminate FRβ-low healthy monocytes *in vitro*.

Healthy adult human bone marrow CD34$^+$ HSCs were isolated and **(A)** stained for FRβ expression using m909-IgG (black line) or human IgG isotype control (gray line). One representative donor shown. **(B)** CD34$^+$ HSCs were co-cultured with CAR T cells at 1:1 E:T ratio for 4 hours. Wells were diluted in methylcellulose and cultured for 14 days. Total colonies were counted and scored for CFU-GEMM, CFU-GM, CFU-G, CFU-M, and BFU-E. There were no significant differences between total or lineage-specific colonies for any of the treated groups compared to untreated CD34+ HSCs. Bar graphs represent mean ± SD for n=2 wells per condition. Results are representative of 4 independent experiments and 3 normal bone marrow donors. CFU- colony forming unit, GEMM-granulocyte/erythrocyte/monocyte/megakaryocyte, GM-granulocyte/monocyte, G-granulocyte, M-monocyte, BFU-E – erythroid blast forming unit. **(C)** Low surface expression of FRβ on normal human monocytes detected by flow cytometry using m909-IgG (black line) or human IgG isotype control (gray line). One representative of 7 normal donors shown. **(D)** CD14$^+$ human monocytes were co-cultured with indicated engineered T cells at a 3:1 and 1:3 effector to target cell ratio for 4 hours, after which total number of live CD3$^-$, CD14$^+$ monocytes per well was quantified by bead-based flow cytometry. Percent Lysis was calculated as (average counts for treated wells)/(average counts for

untreated wells) x100. Data incorporates results using 3 different CAR T cell donors and 4 different monocyte donors as target cells.

Figure 2.13

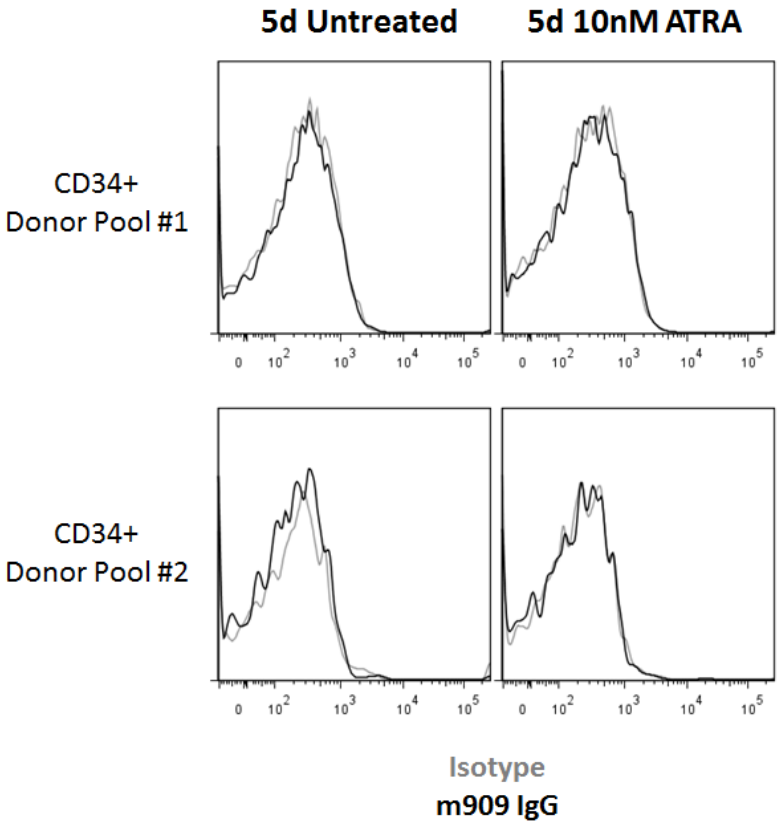

Figure 2.13 ATRA does not induce FRβ in normal HSCs.

Healthy $CD34^+$ cells isolated from normal donor bone marrow were cultured for 5 days in IMDM with 20% BIT9500 serum substitute with or without 10nM ATRA. **(A)** FRβ expression was assessed after 5 days by flow cytometry using m909 IgG (black lines) and human IgG isotype (gray lines). Live, $CD34^+$ gates were used for FRβ analysis. In contrast to THP1, we were still unable to detect FRβ expression on $CD34^+$ HSCs following 5 days ATRA treatment. Two independent samples containing pooled $CD34^+$ cells from 7 total normal donors were tested.

CHAPTER 3: High affinity FRβ-specific CAR T cells eradicate AML and normal myeloid lineage without HSC toxicity.

Summary

On-target, off-tumor recognition of antigen in healthy tissues is a major concern in developing new chimeric antigen receptor (CAR) T-cell therapies for cancer. Careful assessment of protein expression by flow cytometry or IHC can provide helpful data for prediction of potential toxicity. However, high affinity reagents should be carefully chosen in order to assure the most accurate detection of target antigen levels, which may be low in normal tissues. In optimizing our FRβ-directed CAR T-cell platform for targeting acute myeloid leukemia (AML), we isolated a high affinity scFv (m923, 2.48nM KD) for production of CAR. m923 CAR T-cells exhibited greatly enhanced reactivity against FRβ+ AML in vitro and in vivo compared to low affinity CAR (m909, 54.3nM KD). To most accurately predict m923 CAR T-cell toxicity, high affinity m923-IgG was used for analysis of FRβ expression in normal hematopoietic tissues by flow cytometry. We were able to detect previously unrecognized levels of antigen compared to analyses with lower affinity m909. CD34+ bone marrow (BM) hematopoietic stem cells (HSCs) displayed very low expression of FRβ and m923 CAR T-cells did not inhibit HSC colony formation. Upon co-culture, m923 CAR T-cells eliminated FRβ+ BM myeloid cells while sparing neighboring FRβ-negative cells. Due to the potential for myeloid toxicity, we investigated transient CAR expression via mRNA electroporation. mRNA-m923 CAR T-cells retained effective anti-tumor activity in vitro and in vivo. Our results highlight the importance of antibody affinity for assessment of target protein during CAR development. In addition, we report a highly potent FRβ-specific CAR T-cell platform that, when delivered transiently, retains anti-tumor activity while providing a decreased risk for long-term myeloid toxicity.

Introduction

Acute myeloid leukemia (AML) remains a disease with poor prognosis[131,132]. Currently, the most effective therapy, allogeneic bone marrow transplant, is not feasible in all patients, may not fully eliminate tumor cells, and carries a substantial risk of GVHD-associated toxicity[204-206]. Therefore, newer more potent therapy is needed for AML. Chimeric antigen receptor (CAR) T-cell therapy has recently produced dramatic clinical success in $CD19^+$ acute and chronic lymphoblastic/lymphocytic leukemia (ALL and CLL) with reports of up to 90% complete response rates[122-124]. CAR T-cells are genetically modified to eliminate tumor cells by linking an extracellular tumor antigen-recognition domain (most commonly antibody-derived single-chain variable fragments (scFvs)) to intracellular T-cell receptor signaling moieties[87] (usually CD3ζ with or without additional T-cell costimulatory signaling domains). Numerous target antigens are currently being explored in hopes of expanding the clinical efficacy of CD19-directed CAR therapy to many additional types of cancer. The success of CAR therapy in other malignancies depends foremost on the identification of appropriate cell-surface tumor antigens. Due to the potency of cytolytic CAR T-cells, the largest concern for development of new targets must be off-tumor expression of the target protein in healthy tissues.

The high expression of many AML surface antigens on healthy hematopoietic stem cells (HSCs) remains a prominent challenge for developing safe and effective CAR targets for AML[189-191,207,208]. We have previously established that folate receptor beta (FRβ)-specific CAR T-cells can target AML without HSC toxicity[209]. However, these CAR T-cells were functionally limited. Modifying CAR platforms with high affinity scFvs can result in improved anti-tumor activity[197,210]. However, higher affinity CARs could result in heightened activity against normal tissues with low levels of antigen and may present a greater risk for off-tumor toxicity in patients.

Indeed, toxicity related to off-tumor recognition has led to patient morbidity in clinical trials using Her2[126] and CAIX[211] CAR T-cells.

Awareness of target tumor antigen expression in normal tissues is exceedingly important for prediction of possible off-tumor toxicity. Because many target antigens for T-cell therapy are self-antigens, with overexpression on tumor cells, low levels of antigen are often expressed on normal tissues[212]. Antibodies are commonly used to assess protein expression in target cells by flow cytometry or IHC. The detection method should be carefully considered as antibodies with lower affinity for the target protein could be unable to bind low levels of antigen and produce false-negative results.

We hypothesized that our previously described FRβ-specific scFv, m909, may not be the ideal reagent for optimal interaction with FRβ, either in a CAR platform or as a labeling reagent. Therefore, in this study, we sought to develop high affinity reagents for CAR platform optimization as well as sensitive protein detection in normal bone marrow to best characterize potential toxicity related to targeting FRβ in AML.

Materials and Methods

Antibody selection by phage display

Purified recombinant human folate receptor beta protein (rFRβ) was used for panning of a human naïve Fab phage library according to the protocol described[213]. Three hundred colonies were picked from the last two rounds of panning and rescued with helper phage for screening. The best clone was selected for further affinity improvement by light chain shuffling. Briefly, the heavy chain sequence (NcoI and SpeI fragment) of the clone was gel purified and ligated with the light chain repertoire of the Fab library. The sub-library was then further screened with rFRβ for three rounds. The clone with the best affinity, m909, and m923, were converted into scFv and IgG1. The scFv fragment and IgG1 were prepared from E. coli HB2151 cells and 293Free Style cells, respectively. The recombinant scFvs have Flag tag on the C-terminus.

Surface plasmon resonance analysis

Binding of m909 Fab to human rFRβ was assayed using BiacoreX100 instrument. Purified rFRβ was diluted in 10 mM sodium acetate buffer, pH 5.0, and immobilized on a CM5 sensor chip with an amine coupling kit. The reference flow cell was treated with the amine coupling reagent without exposure to rFRβ. The running buffer was HBS-EP (10 mM HEPES, pH 7.4, 150 mM NaCl, 3 mM EDTA, 0.05% surfactant P20). m909 or m923 scFv, diluted with the running buffer to 0.04, 0.4, 4, 40, and 400 nM, was allowed to flow through the cells. The chip was regenerated with 10 mM glycine pH 2.5, 1 M NaCl. The sensorgram was analyzed with BiaEvaluation software, and data were fitted to a 1:1 binding model.

ELISA binding assay

rFRβ diluted in PBS (2 μg/ml) was coated on a 96 well plate at 100 ng/well overnight at 4°C. Wells were blocked with 100 μl of 4% nonfat dry milk/PBS (MPBS) for 1 hour at 37°C. Antibodies were diluted at indicated concentrations, and each concentration was tested with duplicates wells at 50 μl/well. After 2 hour incubation at 37°C, the wells were washed four times with PBST (0.05% Tween 20 in PBS). For direct ELISA with IgG1, a goat anti-human Fc IgG (Jackson Immunoresearch) conjugated with HRP was used at 1:1000 (1 hour x 37°C). Wells were washed again with PBST, the substrate ABTS is added (50 μl/well), and the absorbance was read at 405 nm. For competition ELISA of m909-IgG1 with m923 scFv, 20 nM of m909 IgG was constantly present in the dilutions of m923 scFv. Binding of m923 scFv was detected with anti-Flag-mAb-HRP (Sigma). For competition of m923 IgG with m909 scFv, the two antibodies switched places.

Construction of m923 and CL10-28Z CAR

The m923 scFv was amplified by PCR using the primers Fwd 5'-TATTGATCAGCCGAAGTGCAGCTGGTGCAGTCTGG-3' (BclI underlined) and Rev 5'-TATGCTAGCCTGGCCTAGGACGGTCAGCTTGGTC-3' (NheI underlined), digested with the relevant enzymes (NEB) and ligated into previously described pELNS lentiviral vectors containing CD3ζ or CD28-CD3ζ to create m923Z and m923-28Z CAR constructs. pELNs lentiviral constructs encoding GFP, CD19Z, CD19-28Z, m909Z, and m909-28Z CAR have been previously described[106,209]. The CL10 scFv specific for mouse FRβ was kindly provided by Takami Matsuyama. The CL10 scFv was PCR amplified using the following primers Fwd 5'-TAT GGA TCC GAC ATT GTG ATG ACC CAA TCT CCA TCC TCT CTG-3' (BamHI) and Rev 5'- TAT GCT AGC TGA GGA GAC AGT GAC TGA AGC TCC TTG AC-3' (NheI). The PCR product was digested with BamHI and NheI and ligated into previously described lentiviral

pELNS CAR vectors containing intracellular CD28 and CD3ζ signaling domains to produce the CL10-28Z CAR construct.

Lentiviral CAR Production

Third generation lentiviral vector was produced in 293T (ATCC) as previously described[176,209]. 10-15x10^6 293Ts were plated in T150 tissue culture flasks and transfected 24hr later with 18μg pRSV-Rev, 18μg pMDLg/pRRE, 7μg pMD2.G and 15μg pELNS CAR plasmid DNA. 24hr and 48hr supernatants were collected, filtered through .45um syringe filters, combined, and concentrated using high-speed ultracentrifugation (Beckman Coulter SW32-TI rotor). Lentiviral vectors were titered in 293Ts and stored at -80°C in individual use aliquots until use.

Cells

All cells were cultured in complete media (CM, RPMI-1640-GlutaMAX, 10% FBS, 100U/mL penicillin, 100μg/mL streptomycin) at 37°C. C30[177] was provided by George Coukos. C30-FRβ was created as described[209]. Human AML cell lines THP1, MV411, and HL60 were provided by Gwenn Danet-Desnoyers. Healthy adult bone marrow (BM), $CD34^+$ HSCs and primary human AML were purchased from the University of Pennsylvania Stem Cell and Xenograft Core (SCXC). Peripheral blood was collected by apheresis from volunteer donors by the University of Pennsylvania Human Immunology Core (HIC) with informed consent according to the Declaration of Helsinki. Whole blood, $CD14^+$ monocytes, $CD4^+$ and $CD8^+$ T-cells were purchased from HIC. T-cells were activated, transduced, and expanded as previously described[176,209]. Briefly, 1:1 CD4:CD8 were activated with αCD3/αCD28 beads (Life Technologies) and transduced with lentiviral vectors at MOI=10 20hr later. T-cells were expanded in CM with 50IU/mL IL2 (Novartis) for 10-14 days. Rested T-cells (<300fL volume)

were used for functional assays *in vitro* or *in vivo*. Transduction frequencies were normalized using untransduced T-cells before each experiment.

Flow Cytometry

Up to $1x10^6$ total cells were labeled in 100µL staining buffer (2% FBS in PBS) for 30min at 4°C containing relevant antibodies. For assessment of FRβ expression, m909 and m923 scFv and IgG were prepared as described and biotinylated (Sulfo-NHS-LC-biotin, Thermo) in vitro. 0.5µg IgG or 1µg scFv was used for primary labeling, and 1:200 Streptavidin (SA)-APC (BD) for secondary detection. Washed samples were assessed by flow cytometry using a BD FACSCantoII flow cytometer in the presence of 7AAD. Surface CAR expression was labeled using 0.3µg rabbit-anti-human IgG(H+L)-biotin (m909, m923, or CL10) or 0.3µg goat-anti-mouse IgG (H+L)-biotin (CD19) (Jackson Immunoresearch) and secondary SA-APC or PE. The following antibodies were used in this study: CD3-PECy7, CD8-APC, CD45-PE, CD4-PE, CD69-PE, CD107a-APC, CD107b-APC, CD34-APC, CD123-BV421, CD14-FITC, CD19-APCCy7, CD11b-PacBlue, CD38-PECy7 (Biolegend) and CD33-APC (BD Biosciences) at the manufacturer's recommended concentrations.

CAR binding to rFRβ

GFP-2A-CAR constructs were used to evaluate binding to rFRβ by flow cytometry. rFRβ (R&D) was biotinylated (Sulfo-NHS-LC-biotin). $2x10^5$ T-cells were incubated with 200ng, 500ng, or 1µg rFRβ-biotin and secondary SA-APC. For CAR T-cell reactivity against rFRβ, 250 or 500ng rFRβ was coated on 96-well plates overnight at 4°C. $1x10^5$ CAR^+ T-cells/well were cultured overnight in 200µL CM. IFNγ secretion was assessed by ELISA (Biolegend).

Cytokine Release and CD69

$1x10^5$ targets and $1x10^5$ CAR^+ T-cells were plated in 200 µL CM. After overnight (18-24hr) co-culture, supernatants were analyzed for IFNγ release by ELISA. In addition, IFNγ, IL2, MIP1α, TNFα, IL4, and IL10 were assessed using cytokine bead array (BD). In some cases, cell pellets were washed and labeled for CD3, CAR, and CD69 by flow cytometry following co-culture.

m923 and m909 IgG blocking CAR co-culture

For IgG blocking of m909 and m923 CAR activity (Figure 3.7), $1x10^5$ C30-FRβ target cells were pre-incubated with control human IgG, m909-IgG, or m923-IgG at 5000, 1000, 200, 40, 8, 1.6, or 0 ng IgG/well in 100µl CM in 96-well tissue culture plates. After 40 min pre-incubation at 37°C, $1x10^5$ CAR^+ T cells were added in 100µl CM to each well. m909-28Z, m923-28Z, or CD19-28Z control CAR T cells were used. Each condition was plated in triplicate wells. After overnight (18hr) co-culture at 37°C, supernatants were collected and IFNγ was assessed by ELISA.

Cell Lysis

Target cell lines C30, C30-FRβ, THP1, MV411, and HL60 were stably transduced with GFP-2A-firefly luciferase (fLuc) lentiviral vector. GFP was used to sort 100% positive lines if necessary. $2x10^4$ $fLuc^+$ target cells were plated in white 96-well plates (Gibco) and CAR^+ T-cells were added at 5:1, 1:1, or 1:5 E:T ratios in triplicate. After overnight co-culture, residual luciferase activity was measured using the Extended-Glow Luciferase Reporter Gene Assay System (Life Technologies). Percent lysis was calculated as follows [100- ((Average Signal T-cell Treated Wells)/(Average Signal Untreated Target Wells)x100)].

Degranulation

$1x10^5$ targets and $1x10^5$ CAR^+ T-cells were plated together in 200µL CM with monensin (BD) and 5µL /well CD107a-APC and CD107b-APC (BD) in triplicate. After 6hr co-culture, total cells

were labeled for CD3, CAR and 7AAD by flow cytometry. Live, $CD3^+$ CAR^+ gates were used to assess CD107 expression.

CFU Assay

2000 healthy adult BM $CD34^+$ HSCs were cultured with 2000 CAR^+ T-cells in V-bottom plates. After 4hr, wells were diluted in methylcellulose and plated in duplicate. After 14 days colonies were counted and scored as CFU-GEMM, GM, G, M, or BFU-E.

BM Lysis Assay

$1x10^5$ $CD34^-$ BM cells and $1x10^5$ CAR^+ T-cells were plated in 200µL CM. After 5hr, cells were washed and labeled for CD3, CD33, CD19, FRβ and 7AAD. The phenotype of cells surviving co-culture is indicated in represented flow cytometry plots.

Monocyte Lysis

$2x10^5$ normal donor $CD14^+$ monocytes were labeled with Cr^{51}, washed, and plated with CAR^+ T-cells at 25:1, 5:1, or 1:1 E:T ratios in 6 replicate wells per condition. Monocyte lysis was assessed after 4hr by Cr^{51} release. Spontaneous Release was assessed in untreated target wells. Lysis was induced with 10% SDS to determine Max Release. Percent Lysis = [(Release in T-cell-treated wells) – (Spontaneous Release))/((Max Release) – (Spontaneous Release))x100].

Mice

Nod/SCID/$\gamma chain^{-/-}$ (NSG) and NSGs mice were purchased from, treated and maintained under pathogen-free conditions by the SCXC under protocols approved by the University of Pennsylvania IACUC. We injected $5x10^6$ fLuc-THP1 tumor cells subcutaneously (sc) or intravenously (IV) and T-cells intraperitoneally (IP) or IV as indicated in the figure legends.

Tumor growth was monitored by caliper measurement (sc models) and bioluminescent imaging as described[209]. Peak luminescence is displayed as p/s (IV tumor) or p/s/cm^2 (sc tumor). Peripheral blood sampling was conducted via retro-orbital blood collection under isoflurane anesthesia. 50µl blood was labeled for indicated cell markers and quantified by TRUCount (BD) per manufacturer's instruction.

Humanized (NSGs-HIS) Mice

NSGs mice (Nod/SCID/γchain$^{-/-}$ with transgenic human SF, GM-CSF, and IL3) were reconstituted with 1x10^5 adult BM CD34$^+$ HSCs via intra-femur injection following sublethal irradiation by the SCXC. Engraftment was confirmed by peripheral human CD45$^+$ presence at 2 weeks post-inoculation. Mice were treated with 5x10^6 CD19Z or m923Z CAR$^+$ T-cells via IV injection. Peripheral blood collection was performed on day 8 and mice were euthanized on day 15 post T-cell treatment. BM from the injected femur was collected for further analysis.

mRNA CAR

pELNS lentiviral CAR plasmids were digested and ligated into PDA mRNA expression plasmids. mRNA was produced as described. Briefly, PDA-CAR plasmid DNA was linearized and mRNA was transcribed *in vitro* using the T7 mScript Standard mRNA kit (Cellscript). T-cells were electroporated with 10µg mRNA/10x10^6 cells using an ECM 830 BTX electroporator (Harvard Apparatus) using the following settings: unipulse, 500V, 700µs. "Mock" T-cells were electroporated without mRNA. mRNA-CAR expression and functional activity were assessed at the indicated time points following electroporation.

Statistical Analysis

Data was analyzed for significance using student's T test (GraphPad Prism 6). $P < .05$ was considered significant. All error bars represent mean and standard error (SEM) unless otherwise noted in figure legends.

Results

m923 exhibits superior affinity for FRβ compared to m909.

The m923-scFv was isolated from our phage-display library as previously described for m909. We utilized Biacore X100 (**Figure 3.1A**) to define monovalent affinities of 54nM and 2.1nM for m909 and m923, respectively. Consistent with higher affinity, m923-IgG bound better to rFRβ by ELISA (**Figure 3.1B**) and cell-surface FRβ by flow cytometry (**Figure 3.1C**). $FR\beta^+$ engineered cell line C30-FRβ and $FR\beta^+$ AML lines THP1 and MV411 all displayed higher MFI with m923-IgG than m909-IgG. m923-scFv also bound THP1 and MV411, albeit at lower levels compared to the full bivalent IgG. m909-scFv could not be visualized by flow cytometry (**Figure 3.2**). Although the epitopes recognized by m909 and m923 are unknown, blocking ELISAs demonstrated the ability of m909 and m923 to inhibit association of the other to rFRβ (**Figure 3.3**), suggesting binding at nearby locations.

High affinity m923 CAR T-cells bind rFRβ with greater affinity than m909.

m923-scFv was cloned into previously validated lentiviral vectors containing CD3ζ alone or CD28-CD3ζ intracellular signaling domains to create m923Z and m923-28Z CAR constructs (**Figure 3.1D and 3.4A**). Human T-cells were transduced with lentiviral CAR constructs, and transduction efficiency was determined by labeling for surface CAR expression. Control T-cells were transduced with GFP, CD19-28Z CAR, or CL10-28Z CAR (specific for mouse FRβ). High transduction efficiencies were reproducibly achieved at 70-80% (**Figure 3.4B)**. GFP-2A-m909 and m923 CAR T-cells were labeled with rFRβ, and binding of cell-surface CAR to recombinant antigen was determined by flow cytometry. m923 CAR T-cells highly associated with rFRβ, whereas this interaction could barely be visualized with m909 CAR (**Figure 3.1E)**. Accordingly,

high affinity m923 CAR T-cells also produced more IFNγ in response to immobilized rFRβ (**Figure 3.1F**).

High affinity m923 CAR T-cells are highly reactive against cell-surface FRβ.

Next we assessed the relative functional reactivity of m909 and m923 CAR T-cells against cell-surface FRβ by measuring T-cell cytokine secretion, CD69 expression, and lytic activity against FRβ$^+$ cell lines. Compared to m909, m923 CAR T-cells secreted dramatically increased IFNγ in the presence of FRβ$^+$ C30-FRβ, THP1 and MV411 without activity against negative lines C30 and HL60 (**Figure 3.5A**). m923 CAR T-cells also produced high levels of IL2 and MIP1α, and moderate to low TNFα, IL4, and IL10 (**Figure 3.6**). >90% of m909 and m923 CAR$^+$ T-cells upregulated CD69 in the presence of high density FRβ (C30-FRβ). However, when encountering endogenous FRβ on AML cell lines THP1 and MV411, only ~40% of m909 CAR$^+$ T-cells expressed CD69, whereas nearly all m923 CAR$^+$ T-cells expressed CD69 (**Figure 3.5B**). Like CD69, both m909 and m923 were highly lytic against C30-FRβ (**Figure 3.5C**). However, only m923 CAR T-cells efficiently lysed THP1 and MV411 AML with endogenous FRβ.

To determine whether soluble m909 or m923-IgG could block CAR T-cell activity, we measured IFNγ secretion in response to C30-FRβ in the presence of m909 or m923-IgG. High concentrations (>40ng/1x10^5 target cells) of m923-IgG completely blocked m909 CAR T-cell IFNγ secretion (**Figure 3.7**). Interestingly, neither m909 nor m923-IgG was able to block activity from m923 CAR T-cells.

m923 CAR T-cells demonstrate dramatic anti-tumor activity against FRβ$^+$ AML *in vivo*.

To determine whether high activity of m923 CAR T-cells against AML could be recapitulated in a mouse model of human disease, we inoculated immunocompromised NSG mice with FRβ$^+$ fLuc-THP1 human AML. Previously, in mice treated with T-cells at days 8 and 10 of tumor

growth, both m909 and m923 CAR T-cells led to long-term tumor-free survival[209] (and Figure 3E). Here we evaluated FRβ CAR T-cells in mice with large, palpable AML tumors. m923Z and m923-28Z CAR T-cells produced rapid and enduring complete tumor destruction (**Figure 3.8A-C**). Low affinity m909-28Z CAR T-cells were ineffective. Consistent with robust *in vivo* activation, m923 CAR T-cells were significantly elevated in peripheral blood 2 weeks post treatment whereas m909-28Z CAR T-cell numbers were not different from controls (**Figure 3.8D**). However, when analyzed at day 42, m909-28Z CAR T-cells were >5000 cells/μL (**Figure 3.8D**) suggesting activation in the presence of $FR\beta^+$ tumor *in vivo* led to robust expansion, however, likely due to low affinity, could not effectively control large tumor burden.

High affinity m923 CAR T-cell treatment resulted in expansion then contraction of peripheral T-cell numbers following tumor clearance. m923Z and m923-28Z CAR T-cells were still detectable at day 92 (**Figure 3.9**), suggesting the potential for long-lasting tumor protection. To directly assess this hypothesis, we re-challenged mice that had previously eradicated a primary tumor (m923-28Z) or previously untreated (naïve) mice with $5x10^6$ THP1 on the opposite flank. Previous treatment led to complete protection against tumor re-challenge (**Figure 3.8E**). In addition to subcutaneous tumor, m923 CAR T-cells also efficiently eliminated disseminated THP1, which more closely resembles clinical disease (**Figure 3.14C-D**).

High affinity m923 CAR T-cells are reactive against primary human AML.

Importantly, m923 CAR T-cells also recognized primary human AML. Previous reports found that 70% of AML patients express FRβ[148,149]. Using m923-IgG we confirmed expression in 15/16 specimens by flow cytometry. Four samples with varying FRβ expression (**Figure 3.10A**) were used to assess CAR function. For these experiments CL10-28Z control CAR T-cells were used because of CD19 presence in patient blood samples. Both m923Z and m923-28Z CAR T-cells

secreted significantly more IFNγ compared to control T-cells in response to all four patient samples (**Figure 3.10B**). For 3/4 primary AML, m923 IFNγ secretion was comparable to THP1, suggesting robust activity against patient tumor. The viability of cryopreserved patient samples was low, and standard lysis assays were not possible. Instead we evaluated CD107 expression on CAR^+ T-cells as a well-accepted surrogate for lytic function[179]. Significantly larger frequencies of m923-28Z CAR^+ T-cells expressed CD107 following 6hr culture with primary AML (**Figure 3.10C**) compared to control T-cells. These data confirm the potential for clinical responses in AML patients using high affinity m923 CAR T-cells.

m923-IgG reveals increasing expression of FRβ along myeloid differentiation in healthy hematopoietic cells.

We next evaluated the potential for off-tumor recognition of FRβ in healthy tissues. Although previously reported[192] we did not detect FRβ in HSCs with m909-IgG. The affinity of m909 may not be sensitive enough to detect low levels of FRβ described elsewhere. Therefore, we used m923-IgG to investigate FRβ expression in $CD34^+$ BM HSCs isolated from 5 healthy adults. In contrast to m909-IgG, we were able to detect FRβ on the surface of HSCs from most donors, albeit at very low levels (**Figure 3.11A**). FRβ expression has been previously described in mature myeloid cells[147,159,193], however, expression in BM progenitors has not been well characterized. Using myeloid markers (CD123, CD33, CD14), we found increasing FRβ expression during myeloid differentiation, with highest levels in mature $CD14^+$ monocytes (**Figure 3.11B**). Other BM lineages were FRβ-negative (data not shown). Analysis of FRβ in peripheral blood using m909-IgG has revealed expression in monocytes[193,209]. To more carefully assess possible toxicity of m923-based CAR T-cells, we repeated peripheral blood analysis of FRβ using m923-IgG. In agreement with previous results, we confirmed lack of expression in peripheral blood T-cells, B cells, NK cells, and granulocytes (**Figure 3.11C**). Peripheral blood FRβ expression was limited to

$CD14^+$ monocytes, however, m923-IgG revealed >70% of peripheral blood monocytes express FRβ, whereas m909-IgG detection suggested <40% (**Figure 3.11D**).

m923 CAR T-cells specifically eliminate $FR\beta^+$ myeloid lineage cells without toxicity against HSCs.

To assess HSC toxicity we conducted colony-forming (CFU) assays following co-culture with CAR T-cells. We did not observe inhibition in total or lineage-specific colonies formed by HSCs under any condition (**Figure 3.12A**) suggesting the very low levels of FRβ observed in some $CD34^+$ donors were insufficient to activate m923 CAR T-cells. However, surface FRβ expression increases along BM myeloid differentiation which could activate m923 CAR T-cells. We co-cultured whole $CD34^-$ BM cells with CAR T-cells and assessed the phenotype of surviving cells after 5hr (**Figure 3.12B**). Encouragingly, we did not observe extensive loss of viable myeloid-lineage ($CD33^+$) target cells, however, m923 CAR T-cells clearly eliminated $FR\beta^+$ $CD33^+$ myeloid cells (**Figure 3.12C**). These results suggest that toxicity may be limited to $FR\beta^+$ BM resident cells, while sparing neighboring $FR\beta^-$ myeloid and alternative lineage cells. m923-28Z CAR T-cells also exhibited specific lysis of peripheral $CD14^+$ monocytes compared to control CD19-28Z T-cells *in vitro* whereas m909-28Z CAR T-cells again did not lyse this population (**Figure 3.12D**).

To assess the impact of targeting FRβ in the native BM microenvironment we treated NSGs mice reconstituted with human adult BM $CD34^+$ HSCs with m923 or CD19 control CAR T cells derived from autologous BM T-cells (**Figure 3.13A-B**). Similar to our *in vitro* experiments, we did not see targeting of BM HSCs or myeloid progenitor cells after treatment with m923, however, CD19 CAR T-cell treated mice had decreased $CD19^+$ lymphoid progenitor and mature $CD19^+$ BM cells (**Figure 3.13D-G**). Total $CD14^+$ monocytes were not depleted by m923 CAR T-

cells in this model (**Figure 3.13C and H**), however it was noted that FRβ expression in CD14+ cells was lower than usually observed in fresh PB monocytes **(Figure 3.13I)**. Despite lower overall expression, m923 CAR T-cells still depleted $FR\beta^{hi}$ monocytes compared to control CD19 CAR T-cell treated mice (**Figure 3.13I**).

Transient mRNA-m923 CAR T-cells retain effective anti-tumor activity *in vitro* and *in vivo*.

High affinity m923 CAR T-cells exhibit the potential to eliminate both $FR\beta^{+}$ tumor and healthy myeloid cells. Importantly, $CD34^{+}$ BM HSCs are not targets for m923 CAR T-cell recognition. We reasoned that transient CAR expression could allow for tumor cell destruction in the short term, following which healthy myeloid cells could be repopulated from normal HSCs. Thus, we developed transient expression of the m923 CAR platform via mRNA electroporation of T-cells. 24hr (d1) post-electroporation, both m923Z and m923-28Z CAR was highly expressed on the T-cell surface. Expression gradually decreased over time (**Figure 3.14A**), coinciding with a similar reduction in THP1 lysis (**Figure 3.14B**). mRNA and lentiviral m923 CAR T-cells displayed similar *in vitro* functional reactivity (**Figure 3.15**). We chose m923Z mRNA for *in vivo* T-cell evaluation as we reproducibility observed greater stability of m923Z mRNA expression and never discerned additional benefits with CD28 in lentiviral m932 CAR. The activity of m923Z and CD19Z lentiviral and mRNA CAR T-cells was assessed against disseminated THP1 delivered IV. Although not as robust as lentiviral CAR, m923Z mRNA CAR T-cells significantly delayed disseminated THP1 tumor growth compared to CD19Z mRNA T-cells (**Figure 3.14C**). These results suggest that mRNA delivery of the m923 CAR platform could be used transiently to eliminate $FR\beta^{+}$ tumor cells.

Discussion

Introducing a higher affinity scFv significantly enhanced our platform for targeting FRβ^{+} AML *in vitro* and *in vivo*. m923 CAR T-cells reproducibly out-performed lower affinity m909 CAR T-cells as demonstrated by improved *in vitro* cytokine secretion, CD69 expression, cell lysis, and *in vivo* anti-tumor activity. m923 CAR T-cells demonstrated recognition of primary AML patient samples in addition to AML cell lines.

Utilizing m923-IgG allowed sensitive detection of even very low levels of FRβ in hematopoietic cells not detectable by m909. Our results highlight the importance of antibody affinity when evaluating normal tissue expression for preclinical evaluation of new CAR targets. In addition, the field may find it useful to employ the scFv of the CAR for antibody-based analysis of tissue expression as this may best correlate with CAR recognition. For example, we found cells that did not bind m909-IgG (like MV411 or BM progenitors) were not substantially targeted by m909 CAR T-cells.

The scFv affinity is considered critically important to CAR T-cell function, with a general consensus that higher affinity leads to increased CAR T-cell activation at lower levels of antigen present. However, this aspect of CAR T-cell design is historically under-studied, especially compared to the plethora of literature comparing intracellular signaling domains. Chmielewski and colleagues developed CARs targeting hErbb2 with scFv affinities ranging from 10^{-7} to 10^{-11} K_D, and established a threshold of 10^{-8} below which CAR T-cells responded similarly to all levels of antigen, and above which CAR T-cells only responded to high levels of antigen[210]. In addition, Hudecek and colleagues observed increased anti-tumor efficacy from ROR1-directed CAR T-cells with $5.6x10^{-10}$ K_D compared to $6.5x10^{-8}$ K_D scFvs[197]. Our experience with m909 and m923 is in agreement with these findings. m909 (K_D=$5.4x10^{-8}$) CAR T-cells show strong *in vitro* function only in response to high levels of antigen in C30-FRβ with reduced *in vitro* reactivity for lower

FRβ expression in THP1 and MV411. m923 (K_D=2.1x10^{-9}) CAR T-cells displayed strong reactivity against C30-FRβ, THP1, and MV411 without large differences in cytokine secretion in response to different levels of FRβ. It has been hypothesized that "too high" scFv affinity could result in prolonged T-cell activation and antigen-induced cell death (AICD). Of note, we do see evidence for either AICD or antigen-induced CAR internalization in co-cultures with m923 CAR T-cells and C30-FRβ, especially for m923Z (data not shown). However, we only observed this effect in the context of supraphysiological antigen density in C30-FRβ and not with endogenous high expression in THP1, suggesting this effect would not be clinically relevant.

We hypothesize that the remarkable difference in m909 and m923 CAR T-cell function is related to affinity, however, it is formally possible that they recognize different epitopes of FRβ. For other CAR platforms, recognition of epitopes more distal or more proximal to the cell surface can drastically alter CAR performance[214,215]. Blocking studies with m909 and m923 partially addressed this possibility. m909 and m923 can inhibit the binding capability and/or CAR function of the other platform suggesting a nearby region is recognized. In addition, m909 and m923 share the same variable heavy chain, and only13 amino acids are different in the light chain. This represents an overall 95% scFv sequence homology. The highly similar sequence further suggests these two scFvs do not recognize dissimilar epitopes. Therefore, we believe affinity is the major difference driving CAR function although the precise epitopes remain to be determined.

It is generally believed that the addition of costimulatory domains provides functional improvement beyond first generation CAR platforms. Notably, the only instance where we observed functional differences in m923Z and m923-28Z was increased cytokine secretion with 28Z in the context of C30-FRβ. Because there were no significant differences in *in vitro* activity of m923Z vs m923-28Z in response to AML, we used both constructs *in vivo* to determine

whether second generation CARs displayed increased persistence and anti-tumor activity (as reported for many other CARs[107,109,176,186,187]). Both m923Z and m923-28Z resulted in complete tumor regression. There were also no significant differences in CAR T-cell persistence in treated mice. It is possible that costimulation through TNFR family members (4-1BB, CD27, or OX40) could further increase the persistence of m923 CAR T-cells beyond Z or 28Z (as reported elsewhere[106,107,110]). However, as discussed below, long term persistence is likely not desirable for high affinity FRβ-specific CAR T-cells, and robust anti-tumor activity was already evident even with first generation m923Z CAR T-cells.

Encouragingly, even with high affinity m923 CAR, we failed to see evidence of $CD34^+$ HSC destruction even though very low levels of FRβ were detectable with m923-IgG. We hypothesize that the very low surface expression on a minority of $CD34^+$ HSCs was not substantial enough to cause robust activation of m923 CAR T-cells. We also evaluated FRβ in normal adult BM hematopoietic cells and have demonstrated increasing expression along myeloid lineage differentiation with a distinctly later phase of expression in hematopoietic differentiation compared to other AML tumor antigens like CD123 and CD33. This could be important as reports of gross BM toxicity have been described using CD123 and CD33 CAR T-cells[191,208]. Our *in vitro* assays targeting whole BM and *in vivo* experiments with humanized NSG mice indicate m923 CAR T-cells specifically eliminate $FR\beta^+$ cells while sparing neighboring $FR\beta^-$ myeloid lineage cells. We also observed high expression of FRβ in mature monocytes from PB, and accordingly observed depletion of $CD14^+$ monocytes *in vitro*.

Our *in vivo* model targeting autologous human BM implanted into NSGs mice resulted in decreased expression of FRβ in $CD14^+$ monocytes after m923 CAR treatment, but not decreased frequency of total $CD14^+$ monocytes. We believe this is due to the lower levels of FRβ expressed by the monocytes in this model (Figure 3.13) compared to normal donors (Figure 3.11). It has

been reported that FRβ expression is promoted by MCSF and inhibited by GMCSF during myeloid differentiation[166]. It is possible that the cytokine milieu (particularly the high levels of human GMCSF in the NSGs mice) may have contributed to the lower FRβ expression observed. However, m923 CAR T cells were still able to deplete $FR\beta^{HI}$ monocytes *in vivo* without affecting $FR\beta^{-}$ cells.

While ongoing depletion of healthy B cells in patients treated with lentiviral CD19 CAR is managed through IgG replacement therapy, an analogous therapy regimen to cope with lifelong myeloid depletion is not available. As such, long-term persistence of m923 CAR T-cells is highly undesirable. Therefore, we translated m923 CAR constructs to mRNA expression vectors for transient expression in T-cells. Multiple doses of transient mRNA CAR T-cells significantly delayed THP1 growth *in vivo*. The m923 CAR sequence is fully human derived, which decreases the propensity for transgene immunogenicity which has led to anaphylaxis after repeated administration of murine-derived CAR T-cells[129]. While m923 mRNA CAR T cells did not produce complete tumor destruction of disseminated THP1 like was observed when for lentiviral m923 CAR T cells, it is possible that a suicide gene or inducible CAR approach could be used in combination with lentiviral m923 CAR to obtain complete tumor destruction before CAR T cell depletion. Our results suggest transient treatment with m923 CAR T-cells could be a promising therapy for $FR\beta^{+}$ AML while decreasing the risk for long-term myeloid toxicity.

Figure 3.1

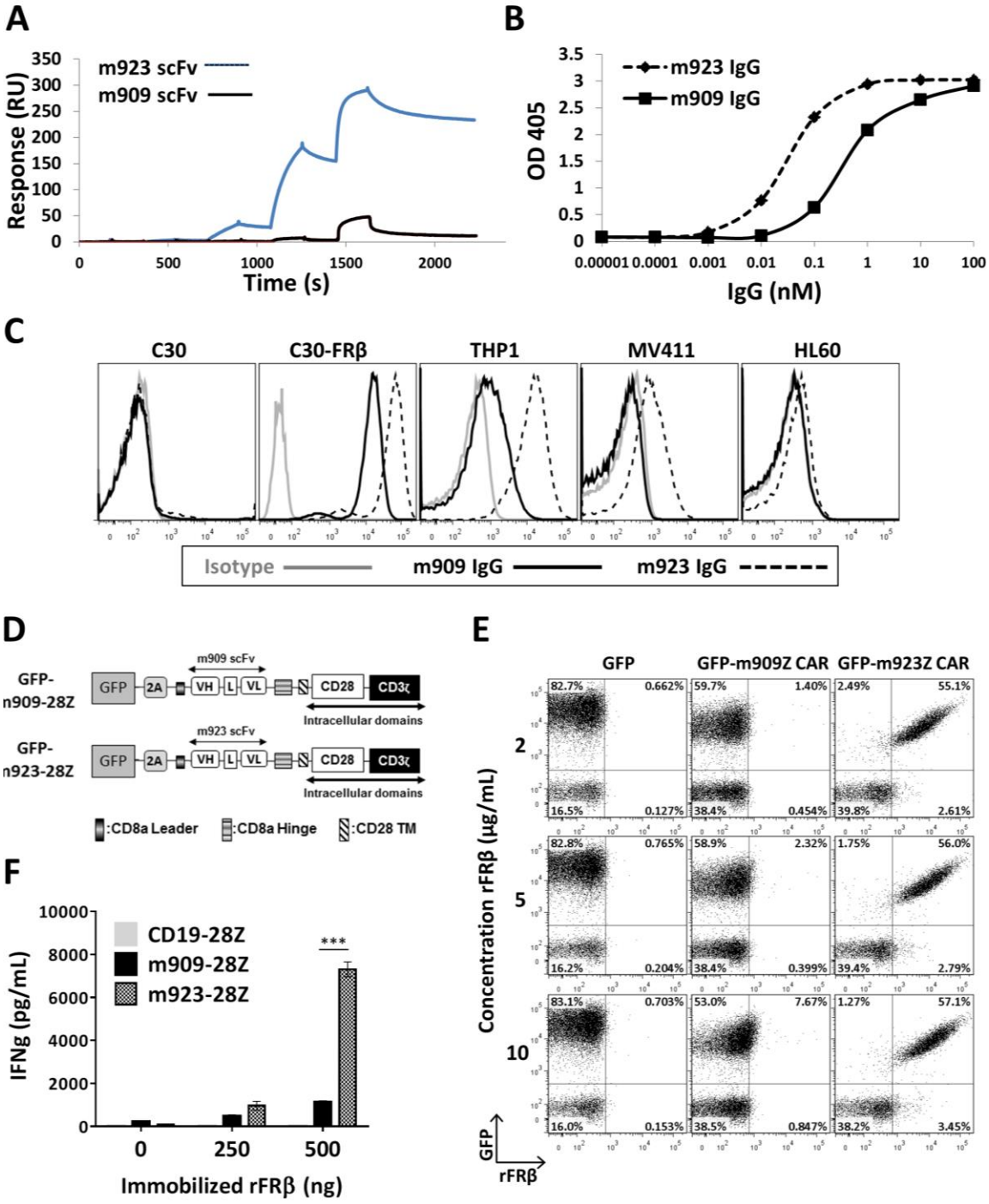

Figure 3.1 m923 exhibits superior affinity for FRβ compared to m909.

(A) Increasing concentrations (0.04, 0.4, 4, 40, and 400 nM) of soluble m909 or m923 scFv were applied to human FRβ-coated chip and affinity was measured by plasmon resonance with BiacoreX100. Binding of m909 and m923 IgG to **(B)** immobilized rFRβ measured by ELISA or **(C)** cell-surface FRβ measured by flow cytometry in the indicated cell lines. **(D)** Representative schematics of lentiviral CAR constructs (full list in Figure S3A). **(E)** Binding of m909 and m923 CAR^+ (GFP^+) T cells to soluble rFRβ. **(F)** IFNγ secretion following 24hr culture of m909 and m923-28Z CAR T cells on rFRβ-coated tissue culture plates. CD19-28Z CAR T cells were used as negative control. Error bars represent mean ± SD of triplicate wells. scFv – single chain variable fragment, VH – variable heavy chain, L – linker, VL – variable light chain, TM – transmembrane domain. (* $P < .05$, ** $P < .01$, *** $P < .001$)

Figure 3.2

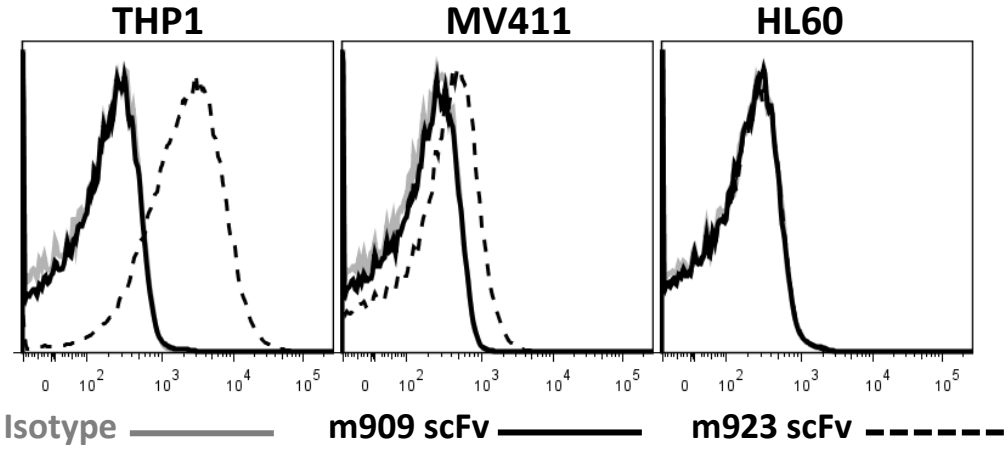

Figure 3.2 Labeling of human AML cell lines with m909 and m923 scFv.

Human AML cell lines THP1, MV411, and HL60 were labeled with 1μg biotin-conjugated scFv/3x10^5 cells for 30 minutes at 4°C, washed, and subsequently labeled with streptavidin-APC. High affinity m923 scFv can be visualized by flow cytometry whereas m909 binding is not discernable by flow.

Figure 3.3

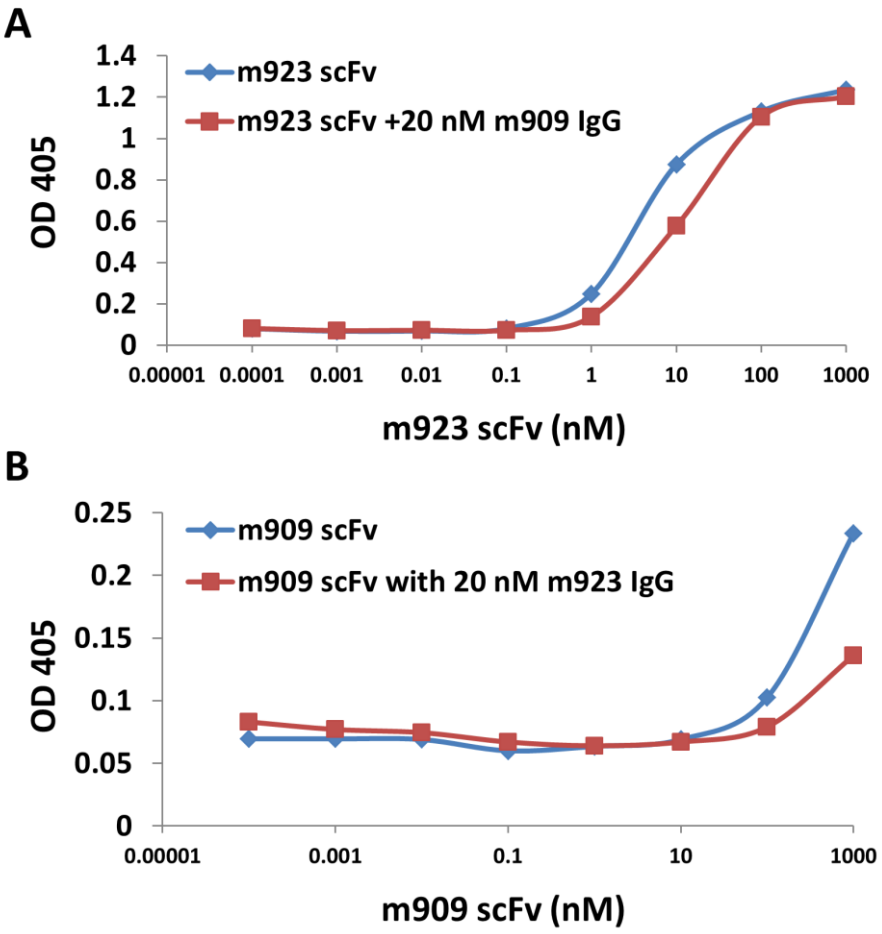

Figure 3.3 m909 and m923 IgG block binding of m923 and m909 scFv to immobilized rFRβ.

Plates were coated with recombinant human FRβ. Binding of increasing concentrations of m923 **(A)** or m909 **(B)** scFv was measured by ELISA with (red) or without (blue) the presence of 20nM respective blocking IgG.

Figure 3.4

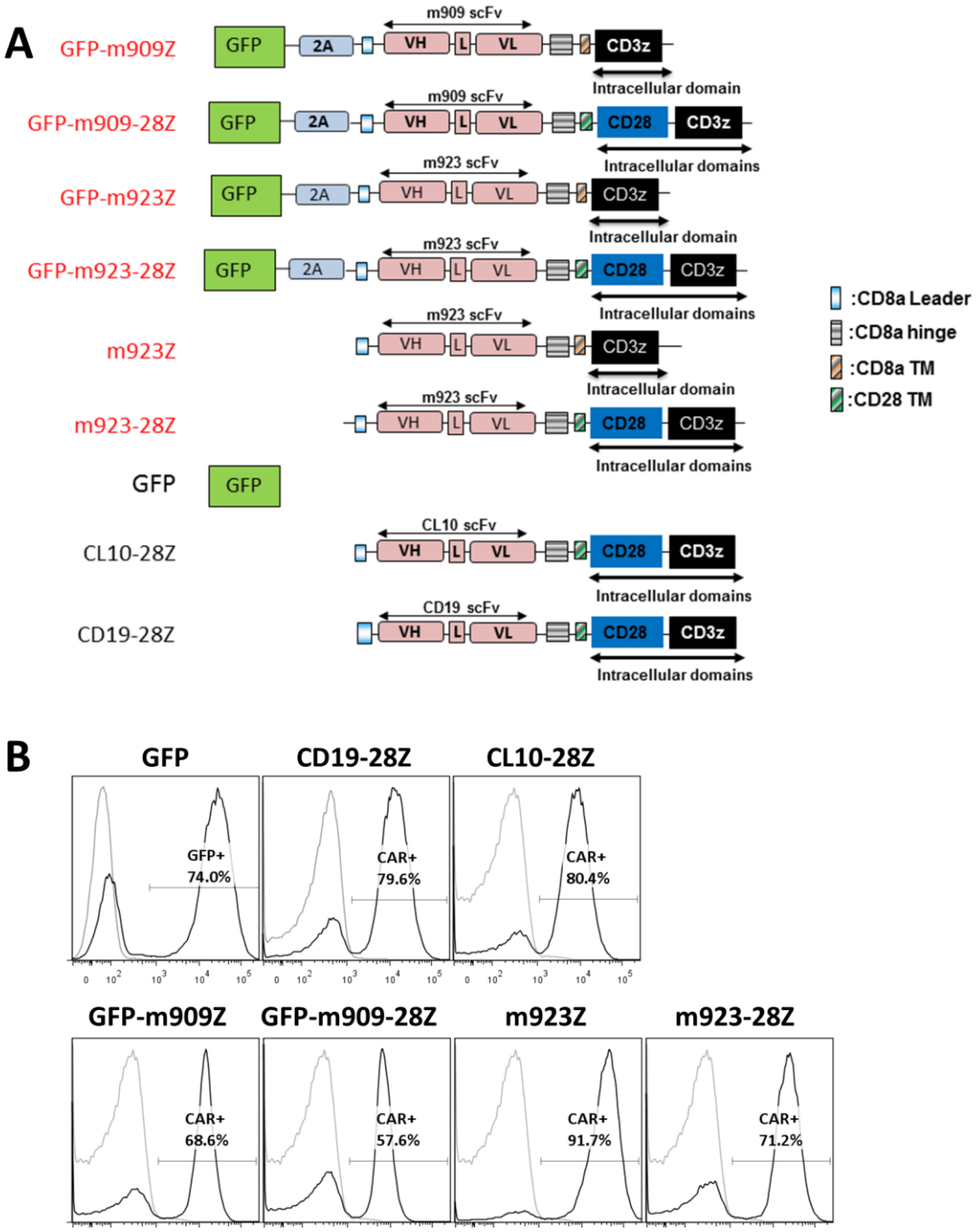

Figure 3.4 Lentiviral CAR constructs and expression in primary human T cells.

(A) Schematic representation of lentiviral CAR constructs used in this study. **(B)** Representative transduction efficiencies and surface CAR expression in primary human T cells. One representative donor shown. CAR expression is visualized with rabbit anti-human IgG(H+L)-biotin for m909, m923, or CL10 CAR and goat anti-mouse IgG (H+L)-biotin for CD19. GFP fluorescence was used to indicate transduction in GFP control T cells. Gray histograms represent labeling of untransduced T cells. scFv – single chain variable fragment, VH – variable heavy chain, L – linker, VL – variable light chain, TM – transmembrane domain.

Figure 3.5

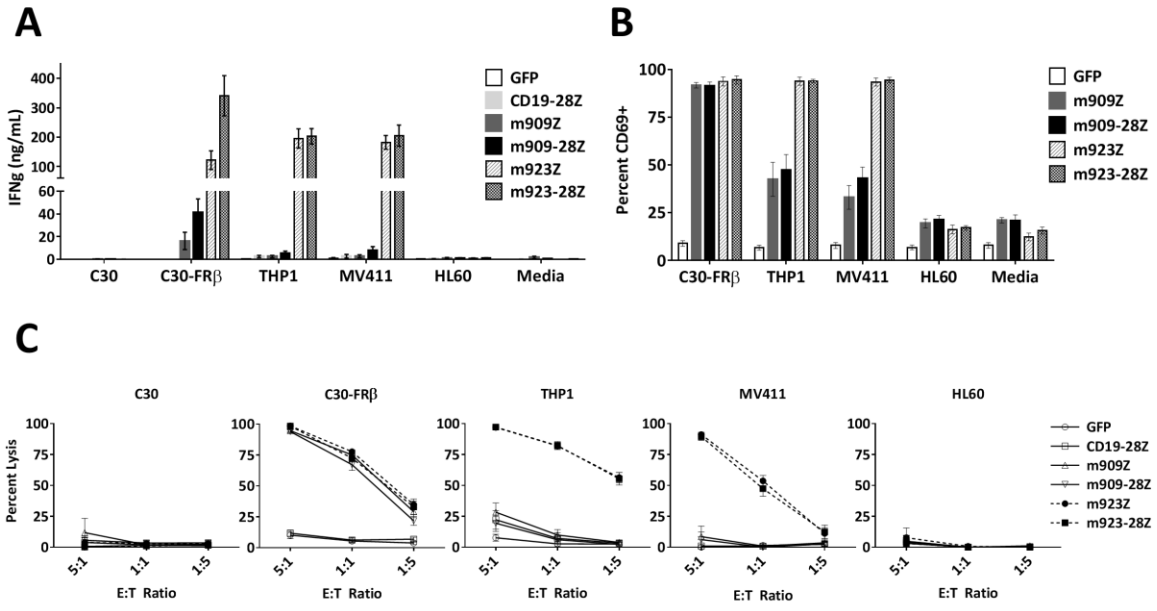

Figure 3.5 High affinity m923 CAR T cells demonstrate greater *in vitro* reactivity against FRβ$^+$ cell lines compared to m909 CAR T cells.

(A) IFNγ secretion following overnight co-culture of m909 or m923 CAR T cells with the indicated cell lines. Error bars represent mean ± SEM of n ≥5 independent experiments. **(B)** CD69 expression on CAR T cells following overnight co-culture with the indicated target cells. Live, CD3$^+$ CAR$^+$ flow cytometry gates were used to assess percent CD69$^+$ CAR T cells. Error bars represent mean ± SEM of n=4 independent experiments. (Note: unstimulated CAR$^+$ T-cells have 20% CD69$^+$ cells at baseline as revealed in the Media control). **(C)** High lytic activity from m923 CAR T cells against FRβ$^+$ cell lines compared to m909. T cells and fLuc$^+$ target cells were co-cultured at the indicated E:T ratios. Percent lysis was assessed by residual target cell luminescence following overnight culture. Error bars represent mean ± SEM of n ≥5 independent experiments. Media indicates T cells cultured without target cells. GFP and/or CD19-28Z CAR T cells were used as controls. SEM – standard error, fLuc – firefly luciferase. (* P < .05, ** P < .01, *** P < .001)

Figure 3.6

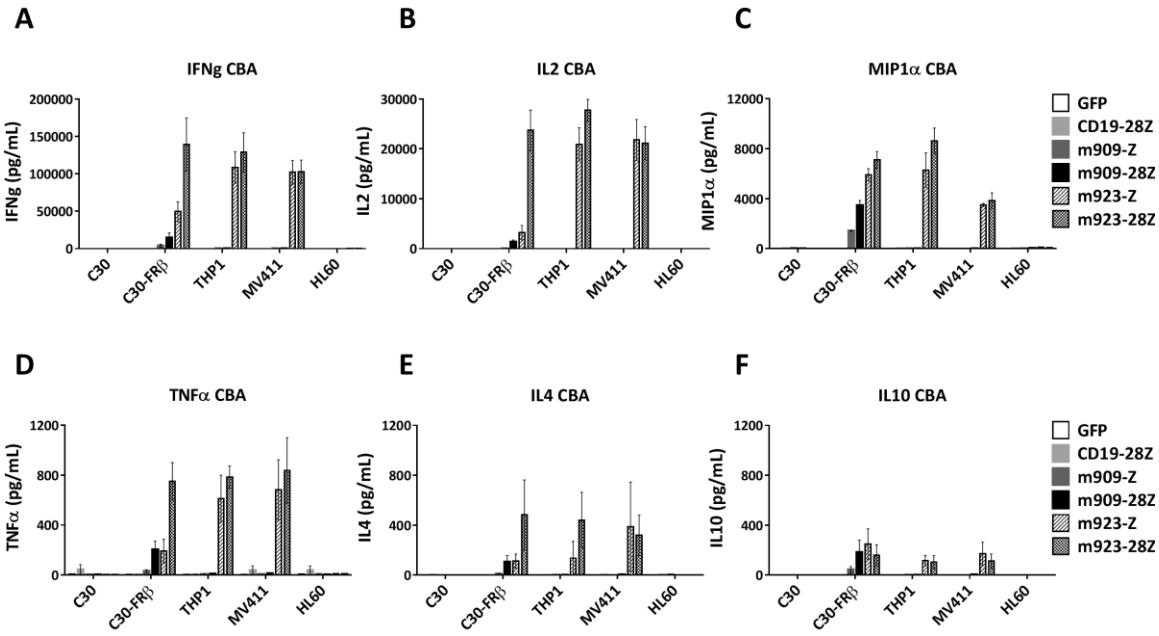

Figure 3.6 m923 CAR T cells secrete numerous proinflammatory cytokines in response to FRβ^{+} cell lines.

Supernatant was collected after overnight co-culture of 1x10^{5} CAR^{+} T cells and 1x10^{5} tumor target cells. Concentrations of **(A)** IFNγ, **(B**) IL2, **(C)** MIP1α, **(D)** TNFα, **(E)** IL4, and **(F)** IL10 were quantified by CBA. Error bars represent mean ± SEM for n=3 independent experiments using 3 distinct T cell donors.

Figure 3.7

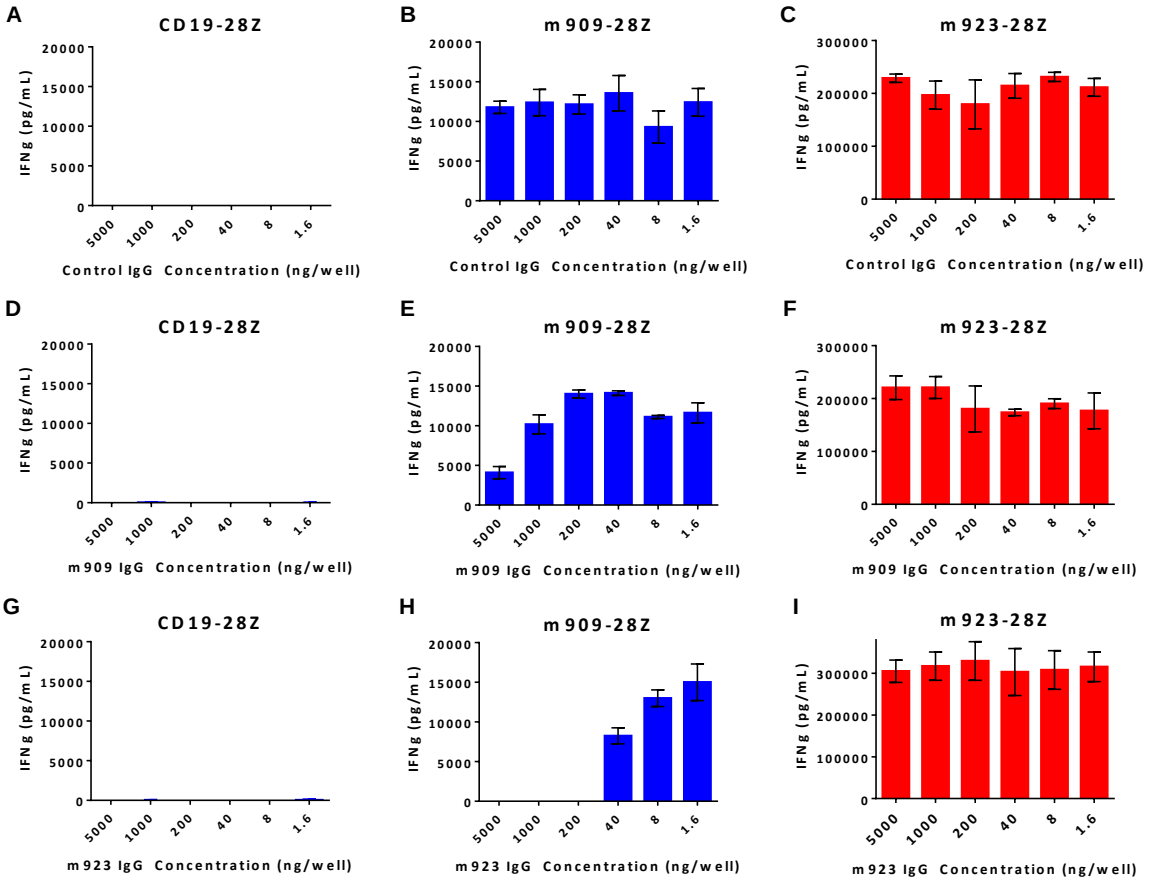

Figure 3.7 Soluble m923 IgG blocks activity of m909-28Z CAR T cells.

$1x10^5$ C30-FRβ target cells and $1x10^5$ CAR^+ T cells (CD19-28Z **(A, D, and G)**, m909-28Z **(B, E, and H)**, or m923-28Z (**C, F, and I**) were co-cultured overnight at 37°C in 200µl CM containing the indicated concentrations of control human IgG **(A-C)**, m909 IgG **(D-F)**, or m923 IgG **(G-I)**. IFNγ secretion was assessed by ELISA. Error bars represent mean ± SD of triplicate wells.

Figure 3.8

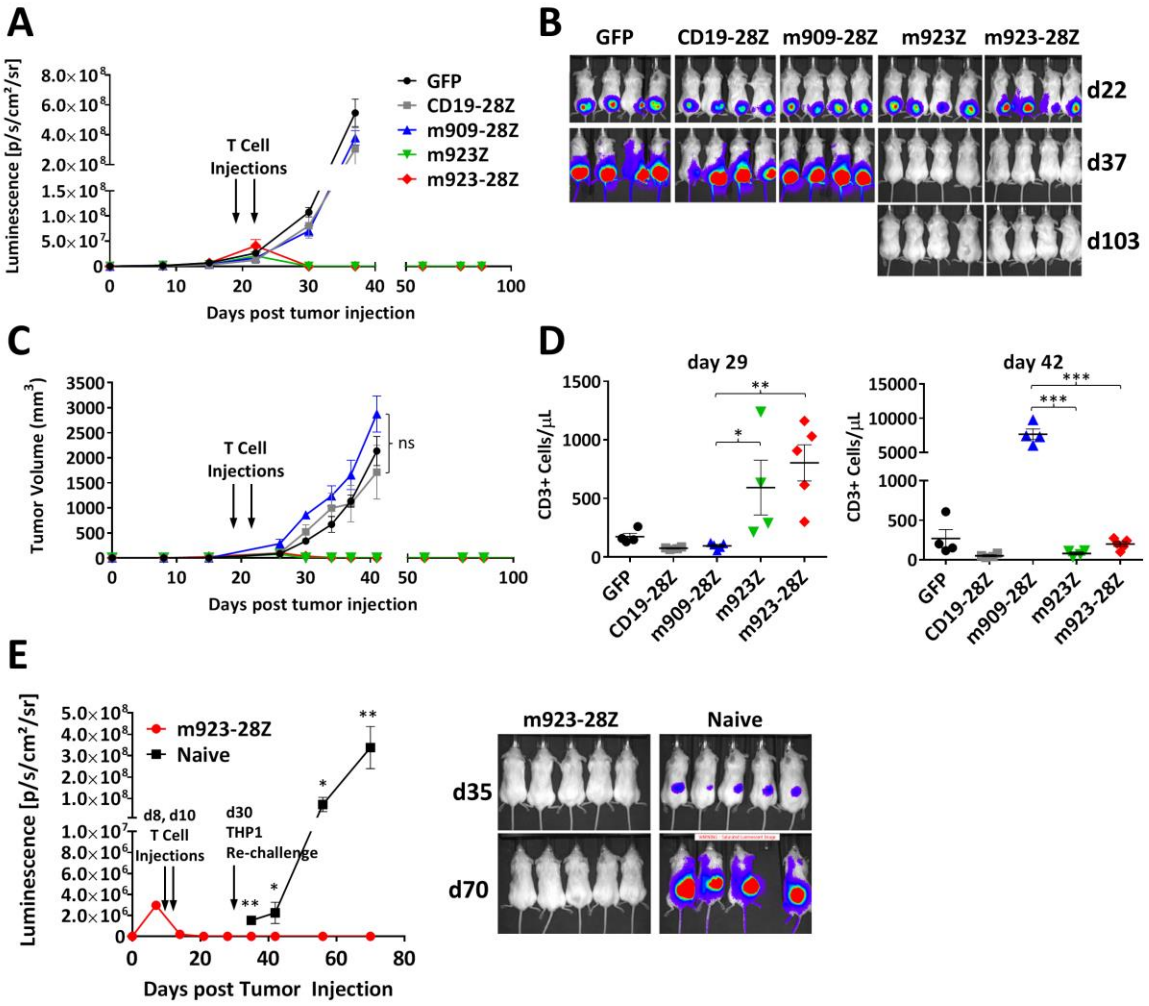

Figure 3.8 High affinity m923 CAR T cells display exceptional anti-tumor activity *in vivo*.

In panels A-D, $5x10^6$ fLuc-THP1 cells were injected sc into flanks of NSG mice. $5x10^6$ CAR^+ (or GFP^+) T cells were injected IP on days 19 and 22 post tumor inoculation. Tumor growth was monitored by tumor luminescence **(A-B)** and tumor volume **(C)**. **(D)** Peripheral blood T cell quantification on days 29 and 42 post tumor inoculation. Error bars represent mean ± SEM of n=4 mice per group. Differences in tumor growth between CD19-28Z and m909-28Z were not significant at any time point. In panel E, mice were injected with $5x10^6$ m923-28Z CAR T cells on days 8 and 10. Following tumor clearance on day 30, m923-28Z mice were re-challenged and previously untreated (naïve) mice were challenged with $5x10^6$ fLuc-THP1. Tumor growth was monitored by bioluminescence **(E)**. Error bars represent mean ± SEM of n=5 mice per group. fLuc –

firefly luciferase, NSG – Nod/SCID/γchain$^{-/-}$, sc– subcutaneous, IP – intraperitoneal, SEM – standard error. (ns – P >.05, * P < .05, ** P < .01, *** P < .001)

Figure 3.9

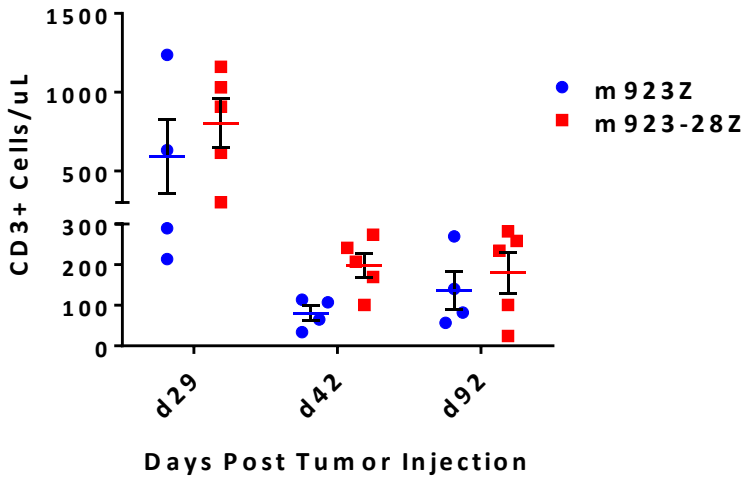

Figure 3.9. Long term persistence of m923 CAR T cells following THP1 tumor clearance.

Peripheral blood human T cell ($CD45^+$, $CD3^+$) counts from m923Z and m923-28Z CAR T cell treated mice from the experiment outlined in Figure 3.8A-D on days 29, 42, and 92 post tumor injection. Error bars represent mean ± SEM of n=4 or 5 mice per group.

Figure 3.10

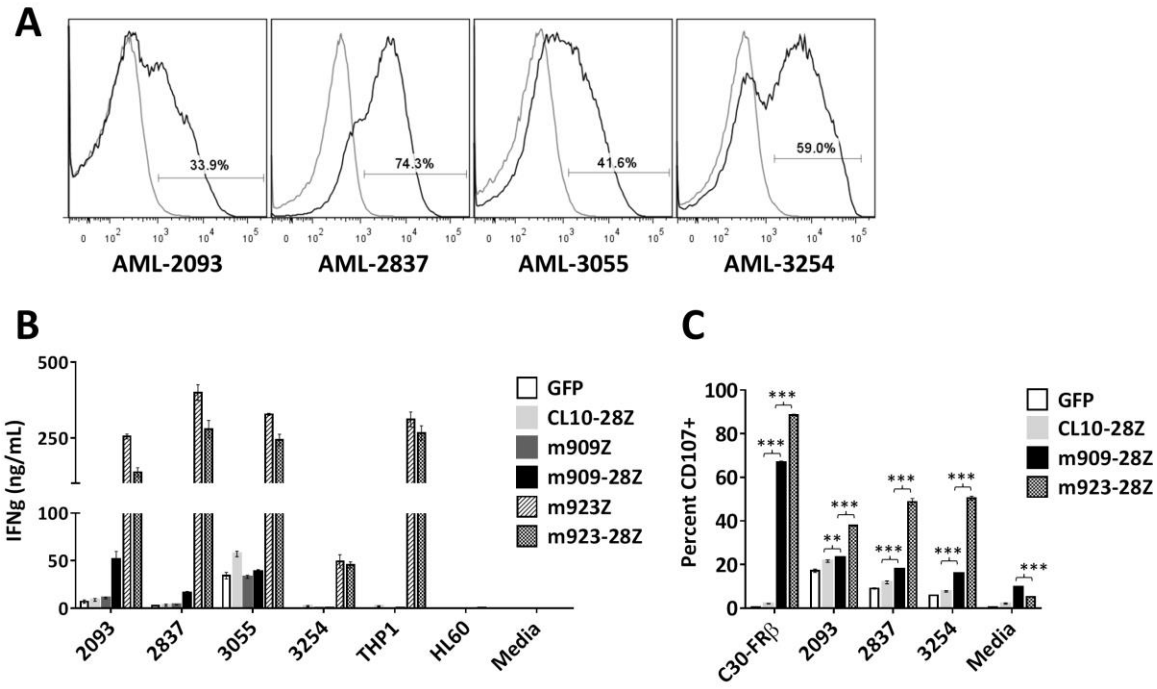

Figure 3.10 High affinity m923 CAR T cells are reactive against primary human AML.

(A) FRβ expression in primary human peripheral blood cells isolated from AML patients. Live, $CD33^+$ gates were used to assess FRβ expression by flow cytometry. (gray histogram– isotype, black histogram – m923 IgG). **(B)** IFNγ secretion after overnight co-culture of indicated primary AML samples with CAR T cells. Error bars represent mean ± SD of triplicate wells. One representative experiment shown. **(C)** CD107 upregulation on CAR^+ T cells following 6hr co-culture with primary AML patient cells. Live, $CD3^+$, CAR^+ gates were used to assess percent $CD107^+$. Error bars represent mean ± SD of triplicate wells. One representative experiment shown. SD– standard deviation. (* P < .05, ** P < .01, *** P < .001)

Figure 3.11

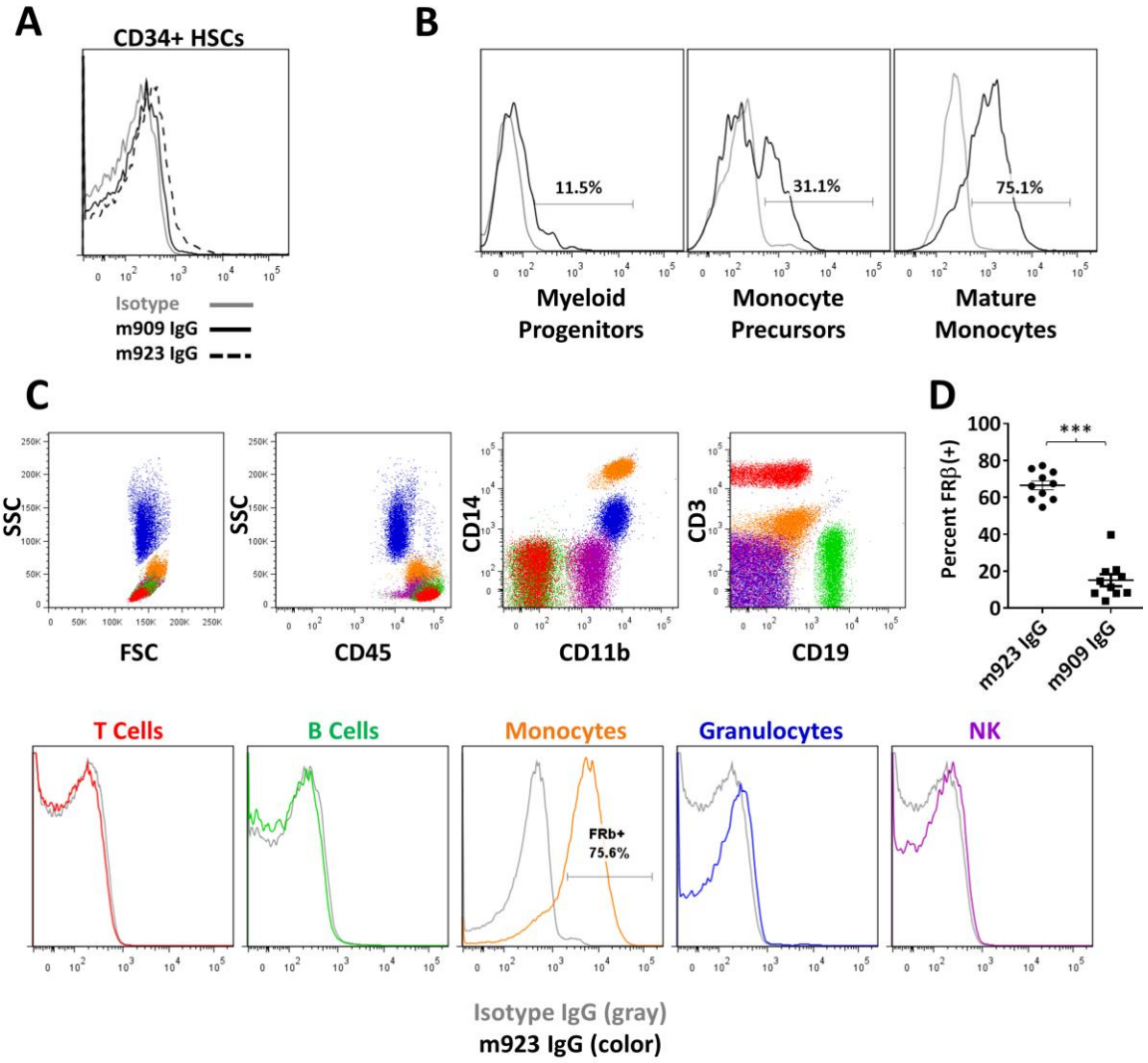

Figure 3.11 m923-IgG reveals increasing expression of FRβ along myeloid differentiation in healthy hematopoietic cells.

(A) FRβ expression in healthy adult BM $CD34^+$ HSCs. (gray histogram– isotype, black solid histogram – m909 IgG, black dashed histogram – m923 IgG). One representative donor shown. (Mean 6.3% $FR\beta^+$ using m923 IgG and n=5 donors). **(B)** FRβ expression in healthy adult BM myeloid lineage cells. Myeloid progenitors–$CD123^{HI}CD33^{(-)}CD14^{(-)}$, Monocyte precursors – ($CD123^{low}$, $CD33^+$, $CD14^{low}$), Mature monocytes ($CD123^{(-)}$, $CD33^+$, $CD14^{HI}$). (gray histogram– isotype, black histogram – m923 IgG). One representative donor shown. **(C)** FRβ expression in peripheral blood cells. Upper panels – gating strategy to identify subsets. Lower panels – FRβ expression in indicated subsets.

(gray histogram– isotype, color histograms – m923 IgG) Red – T cells, Green – B cells, Orange – monocytes, Blue – granulocytes, Purple – NK cells. One representative donor shown. **(D)** Percent FRβ expression detected in peripheral blood monocytes (n=10) using m923 IgG (mean=66.6%) or m909 IgG (15.2%) for flow cytometry. Error bars represent mean ± SEM. BM – bone marrow, HSCs – hematopoietic stem cells, SSC – side scatter, FSC – forward scatter. (* P < .05, ** P < .01, *** P < .001)

Figure 3.12

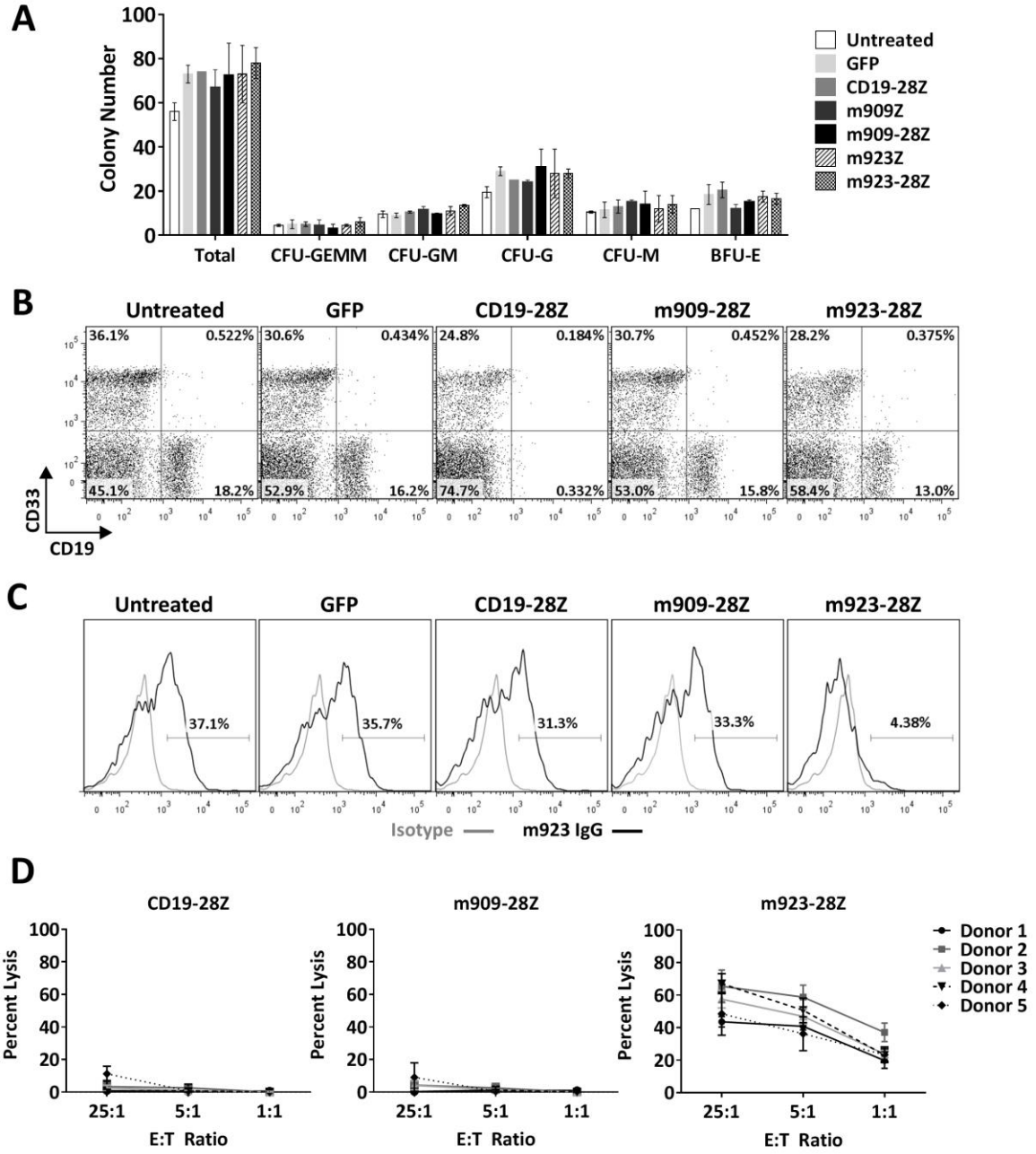

Figure 3.12 m923 CAR T-cells specifically eliminate FRβ^{+} myeloid lineage cells without toxicity against HSCs.

(A) Number of total and lineage specific colonies from CFU assay following 4hr co-culture of 2000 CD34^{+} and 2000 CAR^{+} T cells. Error bars represent mean ± SD of duplicate wells. Representative experiment shown of 4 independent assays. **(B-C)** Phenotype of CD34$^{(-)}$ adult BM following 5hr co-culture with CAR T cells. Untreated samples were cultured in the absence of T cells. **(B)** Frequency of CD33 and CD19 expression in total live, CD3$^{(-)}$ cells surviving co-culture with indicated T cells. **(C)** FRβ expression in total live, CD3$^{(-)}$CD33^{+} myeloid lineage BM cells following co-culture with indicated T cells. (gray histogram– isotype, black histogram – m923 IgG). One representative of 3 experiments is shown. **(D)** Percent lysis of CD14^{+} peripheral blood monocytes isolated from healthy donors following 4hr co-culture with CAR T cells at 25:1, 5:1, or 1:1 E:T ratios. Error bars represent mean ± SD of six replicate wells. 5 different monocyte donors were assessed. CFU– colony forming unit, GEMM–granulocyte/erythrocyte/monocyte/megakaryocyte, GM–granulocyte/monocyte, G–granulocyte, M–monocyte, BFU-E– erythroid blast forming unit, BM– bone marrow, NSG-HIS– Nod/SCID/γchain$^{-/-}$-human immune system , IV– intravenous, SD– standard deviation, SEM– standard error. (* P < .05, ** P < .01, *** P < .001)

Figure 3.13

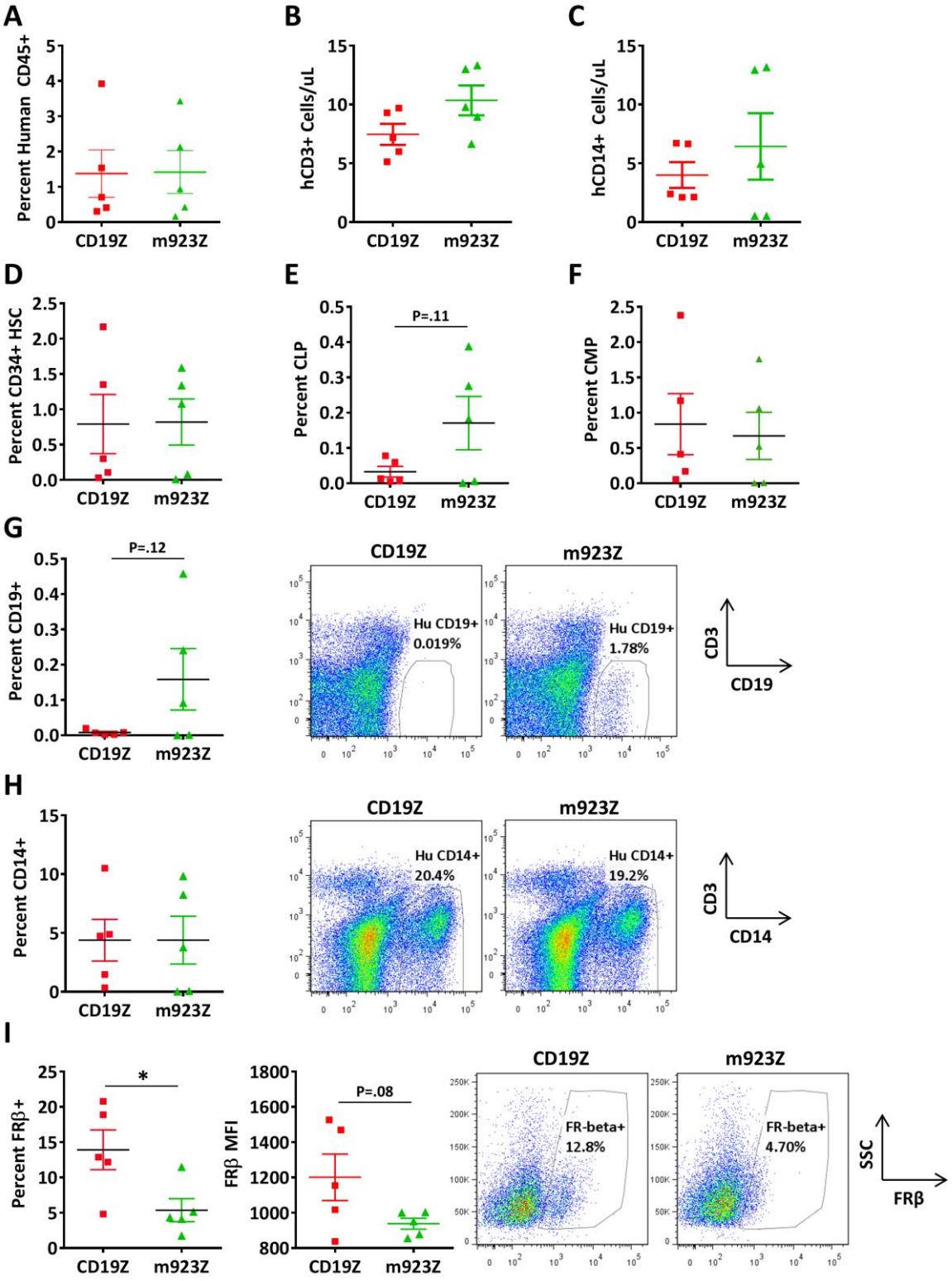

Figure 3.13 m923 CAR T cells deplete FRβ^{+} monocytes *in vivo* without HSC toxicity.

NSGs mice (Nod/SCID/γchain$^{-/-}$ with transgenic human SF, GM-CSF, and IL3) were reconstituted with 1x10^{5} adult BM CD34^{+} HSCs via intra-femur injection. **(A)** Engraftment was confirmed by measuring the frequency of human CD45^{+} in peripheral blood at 2 weeks post-inoculation. 5 mice per group were treated with 5x10^{6} autologous CD19Z or m923Z CAR^{+} T-cells via IV injection. Peripheral blood collection was performed on day 8 to evaluate T cell engraftment **(B)** and peripheral human monocytes **(C)** by TRUcount assay. Mice were euthanized on day 15 post T-cell treatment. BM from the injected femur was collected and assessed for frequency of **(D)** CD34^{+}CD38^{+} HSCs, **(E)** CD45$^{(-)}$, CD38^{+}, CD19^{+} CLPs, **(F)** CD45$^{(-)}$CD38^{+}CD123^{+} CMPs, **(G)** CD45^{+}CD19^{+} B cells, and **(H)** CD45^{+}CD14^{+} monocytes. In **D-H**, frequencies represent the percentage of total, live, BM cells. In **G-H** representative flow cytometry plots are shown for one mouse per group and the frequencies indicate percentage of live, human CD45^{+} cells. **(I)** FRβ expression in BM CD14^{+} monocytes. Left – frequency of FRβ^{+} monocytes and Right – MFI of FRβ in FRβ^{+} monocytes. Representative flow cytometry plots show FRβ in live, CD45^{+}, CD14^{+} BM monocytes. Error bars represent mean ± SEM for n=5 mice per group. (* P < .05). P values coming close to significance are indicated. It should be noted that CD19 expression is very low in NSGs mice as the transgenic factors promote differentiation of myeloid lineage. As such, mice with low total engraftment did not have any CD19 expression. If low engrafters (<0.5% initial engraftment) are removed from analysis (2 mice removed per group), the depletion of CD19^{+} CLP and B cells in E and G becomes statistically significant. CAR – chimeric antigen receptor, HSC – hematopoietic stem cell, BM – bone marrow, CLP – common lymphoid progenitor, CMP – common myeloid progenitor, MFI – median fluorescence intensity, SEM – standard error, SSC – side scatter.

Figure 3.14

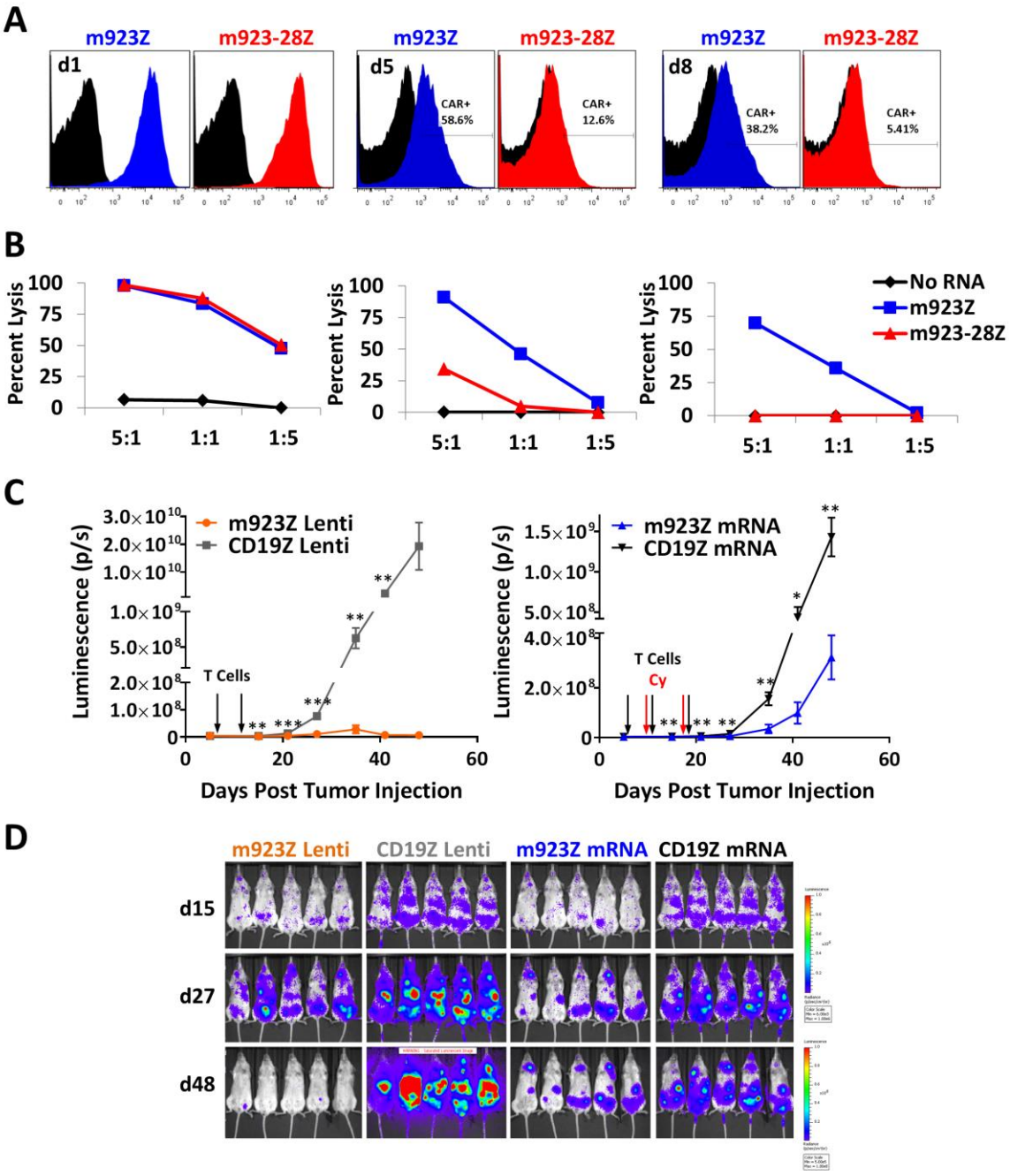

Figure 3.14 Transient m923 mRNA CAR T cells retain anti-tumor activity against disseminated AML.

m923Z and m923-28Z CAR mRNA was introduced into resting T cells by electroporation. CAR expression **(A)** and THP1 lysis **(B)** was measured on day 1 (left panels), day 5 (middle panels), and day 8 (right panels) following electroporation. "No RNA" (black) represents T cells electroporated in the absence of mRNA. **(C-D)** Bioluminescence of disseminated THP1 tumor growth in mice treated with mRNA or lentiviral (Lenti) CAR T cells. Mice were inoculated with $5x10^6$ fLuc-THP1 via IV injection. Mice received $5x10^6$ m923Z or CD19Z Lenti CAR T cells on days 6 and 11, or $10x10e^6$ m923Z or CD19Z mRNA CAR T cells on days 6, 11, and 18 post tumor injection via IV delivery. mRNA CAR T cells were injected 18hr post-electroporation. Mice receiving mRNA CAR T cells also received 60mg/kg Cyclophosphamide (Cy) IP between T cell doses (days 10 and 17) to eliminate CAR-negative T cells between doses. Error bars represent mean ± SEM of n=5 mice per group. IV– intravenous, IP– intraperitoneal, SEM– standard error. (* $P < .05$, ** $P < .01$, *** $P < .001$)

Figure 3.15

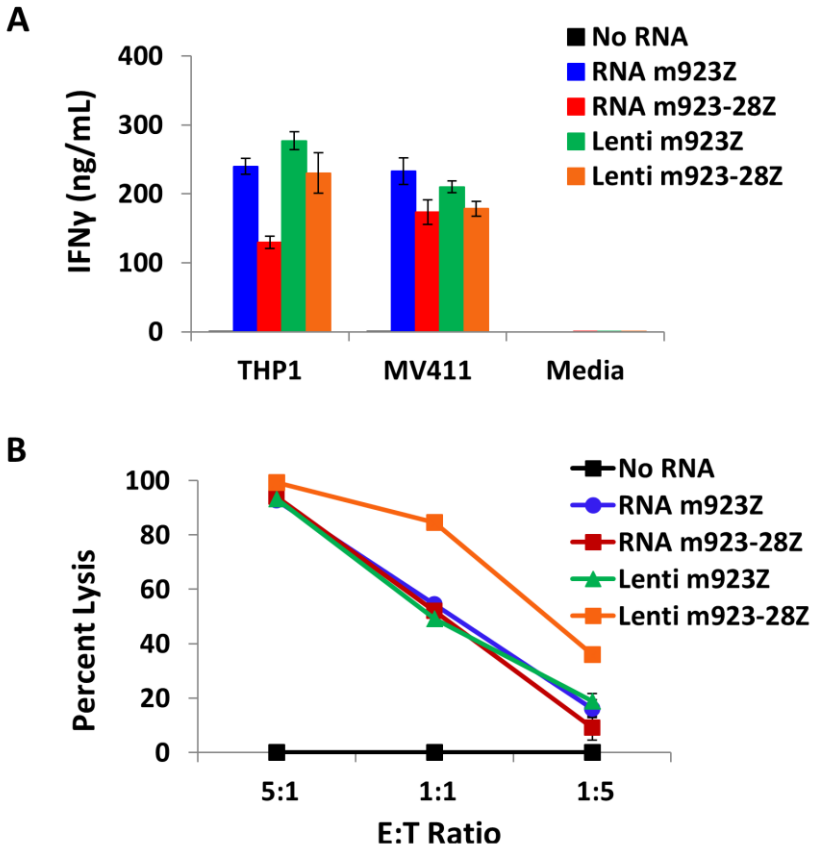

Figure 3.15 m923 mRNA CAR T cells have comparable *in vitro* function to lentiviral m923 CAR T cells.

On day 14 post activation mRNA was introduced into untransduced T cells via electroporation. On day 15, $1x10^5$ lentiviral CAR^+ T cells (Lenti) or mRNA CAR^+ T cells (RNA) were co-cultured overnight with THP1 and MV411 for assessment of IFNγ secretion **(A)** or with fLuc-THP1 at indicated E:T ratios for assessment of lytic activity **(B)**. Error bars represent mean ± SD of triplicate wells. "No RNA" T cells were electroporated in the absence of mRNA.

CHAPTER 4: Safety and efficacy of FRβ CAR T cells targeting TAMs in a mouse model of ovarian cancer.

Summary

Tumor associated macrophages (TAMs) have been identified as key pro-tumor players in the microenvironment. Reported functions of TAMs include improving tumor vascularization, matrix remodeling, and immunosuppression. Clinically, TAM density generally correlates with worse overall prognosis in most types of solid cancer. We have previously developed high affinity chimeric antigen receptor (CAR) T cells to target human FRβ for the treatment of acute myeloid leukemia (AML). FRβ is also expressed on mature macrophages and is significantly upregulated at sites of inflammation, including in the tumor microenvironment. The goals of the following studies were: 1) To test the hypothesis that elimination of TAMs with CAR T cells may be a novel mechanism to disrupt the tumor microenvironment and inhibit tumor progression and 2) To evaluate safety in a preclinical mouse model of FRβ-directed CAR T cell therapy.

We established the feasibility of targeting FRβ on human TAMs using human FRβ-specific (m923) CAR T cells *in vitro*. To model the effect of targeting TAMs in a dynamic tumor microenvironment, we developed a mouse FRβ-specific CAR platform (CL10) for use in a fully immunocompetent, syngeneic mouse tumor model. Due to the poor persistence of mouse CAR T cells compared to human T cells, *in vivo* models required some initial optimization to achieve TAM elimination. Using a single dose strategy of CAR T cells at day 5 of *ex vivo* expansion, we were able to discern a phenotype attributed to FRβ targeting. Encouragingly, CL10 CAR T cells produced a mild anti-tumor effect that required lymphodepleting preconditioning and IL2.

Interestingly, we learned that targeting FRβ with CAR T cells *in vivo* resulted in mild to severe transient toxicity in treated mice, concomitant with marked systemic monocytosis, granulocytosis and elevated serum cytokines and chemokines associated with myeloid activation. These effects were most extensive when lymphodepletion and IL2 were provided. This phenotype was specific to FRβ-directed CAR T cell therapy since preconditioning and IL2 with either control CAR T cells or tumor antigen-specific CAR T cells did not reproduce the phenotype observed with CL10.

The observed signs of toxicity (rapid weight loss, ruffled fur, distended abdomens, and lethargic behavior) after pre-conditioning and CL10 CAR T cell treatment were not dependent on the presence of tumor, suggesting an on-target, off-TAM effect. We investigated FRβ protein expression in healthy mice and noted high surface levels in liver Kupffer cells and cardiac macrophages. Preliminary histological evaluation in the liver revealed depletion of $F4/80^{+}$ macrophages in pre-conditioned CL10 CAR T cell treated mice and areas of hepatocyte necrosis. The most obvious and severe pathological finding was the presence of marked, coalescing extramedullary myelopoiesis (EMM) throughout the livers from this treatment group, which was consistent with the peripheral increases in myeloid cell numbers.

These data provide the first description of CAR T cell targeting of macrophages. Although encouraging, the small anti-tumor effects highlight several potential challenges that must be addressed for successful evaluation and application of this strategy. The transient nature of mouse CAR T cell persistence paired with ongoing repopulation of TAMs from peripheral blood monocytes made the ultimate goal of eliminating TAMs throughout tumor progression largely unfeasible. All mice showed tumor outgrowth with poor persistence of CAR T cells and resolution of early inflammation at late stages of tumor growth. Future work in this area will need to address at least one of these two confounding factors to model long term CAR-mediated

elimination of TAMs in mouse models.

We have developed a model with a reproducible phenotype in which many questions could be applied to further understand the mechanisms driving myeloid activation following CAR T cell-macrophage interactions. It may be that proinflammatory macrophage destruction activates signaling pathways to promote increased myeloid output. While we have some preliminary indication of soluble factors that may be involved, it will be of great importance to fully dissect these pathways and the players involved. Finally, this work improves our understanding of potential complications that could result when translating FRβ CAR therapy into the clinic.

Introduction

Chimeric antigen receptor (CAR) T cell therapy has shown dramatic clinical success in $CD19^+$ leukemia and lymphoma patients. However, CAR T cell therapy for solid tumors has been less successful. Developing effective CAR T cell therapies for other types of cancer may involve overcoming several obstacles associated with solid tumors. Poor blood supply and dense stromal components can hinder access of CAR T cells to tumor cells. In addition, immunosuppressive elements in the tumor microenvironment may suppress T cell functional activity. Engineering CAR T cells to combat various components of the tumor microenvironment has shown potential in preclinical models. CAR T cells engineered to recognize VEGFR2 overexpressed in tumor vasculature inhibited the growth of 5 different types of tumors in mice[216]. Multiple groups developing CARs directed against FAP on cancer associated fibroblasts observed beneficial effects in xenograft[217] and syngeneic[218] tumor models. Importantly both of these stromal targets synergized with tumor-specific CAR T cells[217,219]. Recently Caruana and colleagues showed that CAR T cells engineered to express heparanase efficiently degraded components of the extracellular matrix and exhibited increased tumor infiltration and antitumor activity[220]. Therefore, engineered CAR T cells designed to interfere with non-tumor cell components of the tumor microenvironment show great promise for enhancing CAR T cell therapy in solid tumors.

Tumor associated macrophages (TAMs) are one of the most well-described components of a tumor promoting microenvironment. Tumors co-opt macrophage function by promoting "M2" functions of macrophages associated with wound healing. M2 polarized macrophages can secrete soluble factors to enhance tumor growth, promote angiogenesis, degrade the matrix to promote metastasis, and aid in fostering an immunosuppressive environment[19]. Indeed, the presence of TAMs correlates with worse overall prognosis in many types of cancer[20]. Ovarian cancer has a particularly poor prognosis. The majority of patients are not diagnosed until the cancer has

metastasized, and 5-year survival remains below 50%[131]. Like other malignancies, the presence of TAMs has been reported to correlate with higher stage[221], higher grade[221,222], and shorter survival[223] in ovarian cancer patients. In particular, an M2 macrophage phenotype denotes worse prognosis. One report found that a high M1/M2 macrophage ratio[224] is associated with improved 5-year survival. Another identified an M2-associated gene signature[225] that was predictive of worse progression-free survival. Lan et al found that high expression of M2 marker CD163 predicted poor survival while pan-macrophage marker CD68 was not predictive[226]. These findings suggest that both TAM presence and TAM polarization could be important targets in treating ovarian cancer.

Different strategies for inhibiting TAM function have proven effective in various preclinical tumor models and include blocking recruitment of new myeloid cells[21-23], direct depletion of TAMs[25-27], and repolarization of TAMs to an anti-tumor (M1) phenotype[28-31]. We hypothesized that utilizing the power of CAR T cells to target TAMs could be an effective way to improve CAR T cell therapy in epithelial cancer.

Folate receptor-beta (FRβ) has been described as a marker of M2 macrophages[166] and is expressed on TAMs from tumors of various tissue origins[166-169]. FRβ$^+$ TAMs is correlated with higher vessel density, incidence of metastasis, and worse prognosis in pancreatic cancer[167]. Turk and colleagues demonstrated that TAMs from murine ovarian cancer ascites could be preferentially targeted with labeled folate-conjugated liposomes[170], presumably through uptake by surface FRβ. Furthermore, elimination of FRβ$^+$ TAMs with an immunotoxin reduced vessel density and inhibited tumor growth in a rat glioma model[171]. The results of these studies led us to hypothesize that CAR T cells directed against FRβ could represent a novel mechanism to deplete TAMs and delay tumor growth.

FRβ CAR T cells targeting human AML have proven efficacious in preclinical models. While *in vitro* safety studies can be done to assess the potential impact on cells isolated from healthy human donors, the real impact of targeting many tumor antigens is only clarified once patients have been treated. Researchers have developed CARs targeting the mouse homologs of some CAR targets including VEGFRII[216], FAP[217,218,227], CD19[228-231], NKG2DL[232-234], EGFRVIII[235] or evaluated CAR T cells in transgenic mice expressing the human homolog like Her2[236,237] and CEA[238]. These models can provide important preclinical safety data before moving into the clinical setting. Therefore, a second aim of this study was to assess safety in mouse models of FRβ-directed CAR T cell therapy.

Materials and Methods

Cells

All cells were grown in complete media (CM, RPMI1640-GlutaMAX with 100μg/mL streptomycin, 10μg/mL penicillin, and 10% FBS) unless otherwise noted. Human AML cell lines THP1 and HL60 were cultured in CM as described in Chapter 3. The SKOV3 human ovarian cancer cell line was obtained from ATCC and transduced with lentiviral firefly luciferase (fLuc). The ID8 murine ovarian carcinoma cell line was kindly provided by George Coukos. The ID8 line was stably transduced with a lentiviral construct containing mCherry (RFP) and fLuc separated by a viral T2A ribosomal skipping element (RFP-2A-fLuc) to create ID8-RFP-fLuc. ID8-RFP-fLuc cell line was then stably transduced with lentiviral constructs encoding murine FRβ cDNA (Origene) or human mesothelin cDNA (kindly provided by Steven Albelda) to produce ID8-mFRβ and ID8-Meso, respectively.

Human Monocyte-Derived Macrophages

Healthy donor peripheral blood monocytes were obtained from the University of Pennsylvania Human Immunology Core and differentiated in CM with 10ng/mL human MCSF (Peprotech) for 7 days. Macrophages were further cultured with MCSF only (M0), 10ng/mL LPS and IFNg (M1 polarized), or 10ng/mL IL4 and IL10 (M2 polarized).

Human T cells

Human T cells were activated, lentivirally transduced, and expanded as described in Chapter 3. Untransduced, GFP, CD19-28Z, P4Z, P4-28Z, m923-28Z, and CL10-28Z CAR^+ T cells were used for *in vitro* or *in vivo* assays on days 12-15 post activation when cells had rested to ~300fL size.

Macrophage Lysis

Human M2 polarized macrophages were plated together in CM with human CAR^+ T cells at 3:1, 1:1, or 1:3 E:T ratios. After overnight co-culture, total cells were collected and labeled for expression of CD3 and CD14 and 7AAD. Total number of live, $CD3^-CD14^+$ cells (N) was determined using count-bright beads (Invitrogen) by flow cytometry and lysis was calculated as follows: Percent Lysis = 100 – [(average N treated wells)/(average N untreated wells) x100].

SKOV3 Bystander Lysis

$fLuc^+$SKOV3 tumor cells were plated at a 1:1 ratio with human M2 polarized macrophages (SKOV3/MACS) or C30 ovarian tumor cells (SKOV3/Control). C30 is a slow growing antigen-negative cell line that serves as a negative control for macrophages. Human CAR^+ T cells were provided at 10:1, 3:1, or 1:1 E:T ratio of CAR^+ T cells: SKOV3 tumor cells. After overnight co-culture, SKOV3 lysis was determined using the Extended-GLO luciferase reporter assay (Life Technologies) and calculated as follows: Percent Lysis = 100 – [(average fLuc signal from T cell treated wells)/(average fLuc signal from untreated wells) x100].

Primary Ovarian Cancer Patient Samples

Ascites and solid tumor samples from ovarian cancer patients were obtained from the University of Pennsylvania Ovarian Cancer Research Center tumor bank. Written informed consent was obtained from each patient. Single cell suspensions from either liquid tumor ascites or digested solid tumor were labeled with antibodies and analyzed by flow cytometry, co-cultured with human CAR T cells for cytokine release, or labeled with anti-CD11b microbeads for magnetic isolation of tumor associated myeloid cells.

CD11b Magnetic Bead Isolation

Total cells from human ovarian cancer patient or mouse ID8 tumor ascites were labeled with CD11b MicroBeads (mouse/ human) (Miltenyi Biotec) and isolated with LS MACS separation columns according to the manufacturer's instructions. $CD11b^+$ and $CD11b^-$ fractions were analyzed by flow cytometry or co-cultured with CAR T cells for cytokine release and/or lytic assays as described below.

Ovarian Cancer TAM Lysis

Human ovarian cancer patient CD11b-isolated cells were plated together in CM with human CAR^+ T cells at a 1:1 E:T ratio in 6 replicate wells. After overnight co-culture, total cells were collected and labeled with α-CD14 antibody and 7AAD. Total number of live, $CD14^+$ cells (N) was determined by flow cytometry using count-bright beads (Invitrogen) and lysis was calculated as follows: Percent Lysis = 100 – [(average N treated wells)/(average N untreated wells) x100].

Mouse CAR Construction

MSGV1 retroviral plasmid DNA encoding the DC101 CAR with murine CD8α hinge and CD28 transmembrane followed by murine CD28, 41BB, and CD3ζ intracellular signaling domains was provided by Steve Rosenberg[216]. eGFP-T2A sequence and P4 scFv (specific for human mesothelin[176]) was added by Steve Santoro to create MSGV-GFP-2A-P4-m28BBZ. Plasmid DNA containing the CL10 scFv, specific for mouse FRβ, was kindly provided by Takami Matsuyama. The CL10 scFv was amplified using 2-step PCR first with primers A-Fwd and B-Rev, and second with primers C-Fwd and B-Rev to add on sequence encoding the DC101 leader sequence from the DC101 vector and restriction sites for NcoI and NotI. The purified PCR product and MSGV-GFP-2A-P4-m28BBZ plasmid DNA (Steve Santoro) were digested with the relevant enzymes (NEB), gel purified, and ligated at a 3:1 insert:vector ratio using the Rapid DNA Ligation kit (Roche) to create MSGV-GFP-2A-CL10-m28BBZ. MSGV-GFP-2A-CD19-

m28BBZ was created using an analogous strategy and primers D-Fwd, E-Rev, and F-Fwd to amplify the FMC26 scFv specific for human CD19. DNA sequencing was used to confirm the expected sequence. Hi-Speed MIDI or MAXI DNA prep kits (Qiagen) were used to produce high quality DNA.

A-Fwd 5'-agcaactgcaactggagtacattcagacattgtgatgacccaatctccatcctctctgg-3'

B-Rev 5'-tatgcggccgctgaggagacagtgactgaagctccttgaccccaggcatccataatatcg-3'

C-Fwd 5'-tatccatgggatggtcatgtatcatccttttctggtagcaactgcaactggagtacattc-3'

D-Fwd 5'-agcaactgcaactggagtacattca gacatccagatgacacagactacatcctccctgtctg -3'

E-Rev 5'-tatgcggccgc tgaggagacggtgactgaggttccttggccccagtagtccatagcatag -3'

F-Fwd 5'-tatccatgggatggtcatgtatcatccttttctggtagcaactgcaactggagtacattc-3'

Retroviral Production

The retroviral packaging cell line PlatE with ecotropic envelope was kindly provided by George Coukos. $6x10^6$ PlatE cells in log phase growth were plated in T150 tissue culture flasks in 27mL CM. 24hr later, each flask was transduced with 20µg MSGV1 retroviral transfer plasmid DNA using 3mL Optimem (Gibco) and Lipfectamine2000 (Invitrogen) at a 3:1 Lipofectamine:DNA ratio. 30mL CM was replaced at 24hr and 48hr. Supernatants from 48hr and 72hr post transfection were collected, .45um filtered, and frozen at -80C until use.

Mouse T cell Expansion

Mouse T cells were activated, transduced, and expanded in mouse T cell media (CM with 50uM beta-mercaptoethanol, 100mM sodium pyruvate, 1X GlutaMAX, and 50IU/mL murine IL2 (Peprotech)). Spleens were isolated from C57BL/6 mice after humane euthanasia according to

protocols approved by the University of Pennsylvania IACUC. Splenocytes were dissociated and pushed through a 70um cell strainer. Red blood cells were lysed using ACK lysis buffer (Gibco) and cell number was determined. $3x10^6$ total splenocytes/mL/well were activated with anti-mouse CD3/CD28 antibody coated beads (Dynabeads, Invitrogen) at a 1.33:1 bead:cell ratio in 24well plates. Splenocytes were transduced with retroviral vectors on day 1 and day 2 post activation. T cell media was added daily to maintain ~$1x10^6$ cells/mL. Beads were removed on day 4. By day 4 post activation, >97% of live cells were $CD3^+$ T cells, with a usual ratio of about 85:15 $CD8^+$:$CD4^+$. T cells were used for *in vitro* or *in vivo* assays on day 5-7 as indicated.

Retroviral Transduction

0.5mL RetroNectin (Takara) diluted to 25μg/mL in sterile PBS was immobilized overnight at 4°C in 24well non-tissue-culture-treated plates. After overnight incubation, wells were washed with PBS and blocked for 10min with 2% BSA/PBS. 3mL 48hr retroviral supernatant was added per well and plates were centrifuged at 2000xg for 1.5hr at room temperature. Supernatant was removed and 0.5mL ($1.5x10^6$) day 1 activated splenocytes were added per well. Cells were centrifuged for an additional 10min at 1000xg and returned to 37°C . Transduction was repeated on day 2 post activation using 72hr retroviral supernatant. For untransduced T cells, CM was used in place of retroviral supernatant.

Surface CAR Expression

Presence of surface CAR expression was measured in transduced T cells on day 5 post-activation by flow cytometry. P4 and CL10 CAR were measured using biotinylated rabbit anti-human IgG (H+L) and CD19 CAR was measured using biotinylated goat anti-mouse IgG (H+L) (Jackson Immunoresearch). Binding of P4 and CL10 CAR to biotinylated recombinant protein antigen was also evaluated. Recombinant murine FRβ was purchased from R&D. Recombinant human

mesothelin was produced in yeast as described. Recombinant proteins were biotinylated in-house using EZ-link-Sulfo-NHS-LC-biotin (Thermo) and purified with dialysis using Tube-O-Dialyzer Medi (G-Biosciences). T cells were labeled with 300ng biotinylated antibody or 500ng biotinylated recombinant protein for 30 minutes at 4°C . Cells were washed and secondary labeling with Streptavidin-APC was conducted for 25min at 4°C . Co-expression of GFP and APC was used to determine surface CAR expression in transduced T cells.

Cytokine Release

$1x10^5$ target cells and $1x10^5$ CAR^+ T cells were added in 200µl CM. After overnight (18-24hr) incubation at 37°C , cell-free supernatant was removed and stored at -20C until assessment. For assessment of IFNg production in response to immobilized protein antigen, 1:2 dilutions of recombinant murine FRβ (R&D) in 100µl PBS were plated in 96-well ELISA plates in triplicate wells per condition (range 31-1000 ng/well). After overnight coating at 4°C , wells were washed with PBS and $1x10^5$ CAR^+ T cells were added in 200µl CM. After 18hr culture, cell-free supernatant was removed and stored at -20C until assessment. Human and mouse IFNg release were measured using respective ELISA kits (Biolegend).

Cell Lysis

Cell lines: $1x10^4$ $fLuc^+$ target cells were plated in white 96-well plates. CAR^+ T cells were added at 5:1, 1:1, or 1:5 E:T ratios in triplicate wells and co-cultured at 37°C . After 4hr or overnight incubation, residual luciferase activity was measured using the Extended-GLO luciferase reporter assay (Life Technologies) and calculated as follows: Percent Lysis = 100 – [(average fLuc signal from T cell treated wells)/(average fLuc signal from untreated wells) x100].

***in vivo* Tumor Models**

6-8 week old female C57BL/6 mice were purchased from Charles River, housed and treated under University of Pennsylvania IACUC approved protocols. Mice were inoculated intraperitoneally (IP) with $5x10^6$ ID8-RFP-fLuc, ID8-mFRβ, or ID8-Meso tumor cells. T cells were injected IP in 200µl PBS at the doses and schedules outlined in the figure legends. In some cases 150mg/kg cyclophosphamide (Cy) was injected IV one day before T cell transfer and human IL2 was provided at 15µg/dose in 100µl IP for 3 consecutive days following T cell transfer (CyIL2 conditioning). Clodronate or PBS liposomes (clodronateliposomes.com) were provided at the manufacturer's recommended dose (100µl per 10g mouse weight) IV or IP as described. Tumor growth was monitored by bioluminescent imaging and/or weight gain. Mice were euthanized when they had gained >70% of initial body weight (tumor ascites formation) or lost >20% of pre-treatment body weight (toxicity).

Bioluminescent Imaging

Mice were injected IP with 3mg/kg D-Luciferin and imaged under isoflurane anesthesia using an IVIS Spectrum imaging system (Perkin Elmer). 5 consecutive images were collected 15-21 minutes following Luciferin injection. Peak luminescence was determined for each individual mouse using Living Image software and is displayed in photons/second (p/s). Images were generated with Living Image software using identical luminescent scales for each group.

Tissue Collection and Analysis

Mice were euthanized at the indicated time points following T cell delivery and whole tumor ascites was isolated by peritoneal wash. 10mL PBS was injected IP and total cells in the wash were collected. Red blood cells were lysed using ACK lysis buffer. $1\text{-}2x10^6$ total cells were stained and analyzed by flow cytometry as described below. Liver, lung, and/or hearts were collected, formalin fixed, and paraffin embedded by the University of Pennsylvania Cancer

Histology Core or the CHOP Pathology Core Laboratory at Children's Hospital of Philadelphia. For some mice, sections were H&E stained and evaluated for pathology. Peripheral blood was collected via retro-orbital blood collection under isoflurane anesthesia. 50µl per sample were labeled for CD45, CD11b, Ly6G, Ly6C, CD3, and CD8 and cell counts per µl blood were calculated using Trucount tubes (BD Biosciences). The remaining blood was centrifuged at 4000RPM for 10 minutes at 4°C . Clear serum was removed and stored at -80C until analysis. Serum alanine aminotransferase (ALT) and aspartate aminotransferase (AST) levels were measured by the University of Pennsylvania Mouse Phenotyping, Physiology, & Metabolism Core at the Penn Diabetes Research Center. Luminex was performed by the University of Pennsylvania Human Immunology Core using the mouse 32-plex cytokine/chemokine magnetic bead panel (EMD Millipore).

Pathology Scoring

H&E stained liver sections were evaluated by board-certified veterinary pathologists at the University of Pennsylvania School of Veterinary Medicine Comparative Pathology Core. Individual pathological indications were given a score of 0-10 to grade the pathological severity (0=not present, 2=rare/minimal, 4=mild, 6=moderate, 8=severe, 10=marked).

Flow Cytometry

Up to $2x10^6$ cells were labeled per tube in staining buffer (2% FBS/PBS). Human FRβ expression in human *in vitro* polarized macrophages and primary ovarian cancer TAMs was evaluated using biotinylated m923-IgG and Streptavidin-PE as described in Chapter 3. The following marker antibodies were used in parallel: human CD45-PerCP-Cy5.5, human CD14-APC-Cy7, human CD14-FITC, human CD206-APC, mouse/human CD11b-PacBlue, human HLA-DR/DP/DQ-FITC (Biolegend), human CD163-BV421, human CD33-APC (BD Biosciences). Human

mesothelin expression in ID8-Meso was evaluated using the K1 antibody (Santa Cruz) and secondary F(ab)2 donkey anti-mouse IgG-APC (eBioscience). Mouse FRβ expression was evaluated using CL10 IgG (kindly provided by Takami Matsuyama). Cells were preincubated with 10μg unlabeled mouse IgG (Jackson Immunoresearch) to block Fc receptors, followed by labeling with CL10 IgG or rat IgG2a isotype (Biolegend) for 30min at 4°C , washed, blocked with 10μg unlabeled goat IgG (Jackson), labeled with goat anti-rat IgG-APC (Biolegend), washed, blocked with 5μg rat IgG (Jackson), and labeled with fluorescently labeled mouse marker antibodies. The following antibodies were using in this study: mouse CD45-FITC, mouse CD45-PE, mouse CD45-PacBlue, mouse CD3-PE-Cy7, mouse CD8α-APC, mouse CD4-PE, mouse/human CD11b-PacBlue, mouse Ly6G-PerCP-Cy5.5, mouse Ly6C-APC-Cy7, mouse F4/80-PE-Cy7 (Biolegend), mouse CD204-PE (Miltenyi). The respective isotypes were also purchased from Biolegend. eFluor-506 fixable viability dye (eBioscience) was used to assess viable cells.

FRβ Expression in Healthy Tissue Macrophages

The following organs were collected from healthy 8-12 week old female C57BL/6 mice: peripheral blood, bone marrow, spleen, peritoneal wash, liver, lung, heart, kidney, brain, and GI tract. At least 3 mice were analyzed per tissue. Peripheral blood was collected via cardiac puncture. Bone marrow was flushed from isolated femurs. Peritoneal cells were collected by IP wash as described above. Spleens were dissociated by squishing and washing through a 70um cell strainer. All other organs were minced into small pieces and incubated at 37°C for 2 hours with shaking in the presence of Collagenase IV and DNAseI to gently digest tissues. Single cell suspensions were generated by washing tissue digests through 70μm cell strainers, and red blood cells were lysed using ACK lysis buffer. Single cell suspensions were labeled for FRβ using CL10 IgG and myeloid markers CD45, CD11b, Ly6G, Ly6C, F4/80, and CD204 by flow

cytometry as described above. $CD45^{+}CD11b^{+}Ly6G^{-}$ cells were gated to analyze expression of F4/80 and CD204 macrophage markers. The F4/80-CD204 gates used to evaluate FRβ expression in each tissue are indicated in the figure. (Not all tissue macrophages express F4/80 or CD204.)

F4/80 IHC

Immunohistochemistry (IHC) for F4/80 was performed in formalin-fixed, paraffin-embedded tissue sections. Sections were baked at 57C overnight before deparaffinization according to standard IHC protocols. Antigen retrieval was performed using pH6 Citrate buffer (Thermo) and the pressure cooker method. Serial blocking steps were performed to block endogenous peroxidases (Dako), Avidin/Biotin (Vector Labs), and protein block (Dako). 1:100 rat anti-mouse F4/80 antibody (Life Technologies) was incubated for 2 hours at room temperature. Secondary biotin anti-rat antibody, Vectastain Elite ABC kit, and Immpact DAB (Vector Labs) were used according to the manufacturer's instructions. Slides were counterstained with hematoxylin, dehydrated and mounted. One tissue slide was stained per mouse. 10-12 random 20X fields per slide were captured on a NikonXMZ microscope in a non-biased blinded manner. We imported the images into ImageJ and counted the total number of positive cells per field. The mean of 10-12 fields per sample was calculated.

Results

Human M2 polarized macrophages highly express FRβ

First we measured the expression of FRβ in human monocyte derived macrophages with m923-IgG by flow cytometry. As previously reported, MCSF induced high levels of FRβ expression in differentiated macrophages (M0) compared to monocytes pre-culture (**Figure 4.1A**). Further polarization with M2 cytokines IL4 and IL10 resulted in slightly increased expression, while M1 polarization with IFNg and LPS slightly decreased FRβ expression (**Figure 4.1A**). MCSF-M2 polarized macrophages also highly co-expressed FRβ and classic M2 markers CD206 (**Figure 4.1B**) and CD163 (**Figure 4.1C**). To test the hypothesis that FRβ-specific CAR T cells could be used to eliminate M2-polarized macrophages, we co-cultured MCSF-M2 polarized macrophages and m923 or control CD19 CAR T cells. m923 CAR T cells produced high levels of IFNg (**Figure 4.1D**) and dose-dependent lysis (**Figure 4.1E**) of M2 macrophages after overnight co-culture. To create a basic model of TAMs within a tumor microenvironment we co-cultured SKOV3 ovarian cancer cells with M2 polarized macrophages and CAR T cells in tissue culture wells. While m923 CAR T cells do not directly lyse SKOV3 alone, when co-cultured in the presence of M2 macrophages significant bystander lysis of SKOV3 was observed (**Figure 4.1F**). P4 CAR T cells, specific for the human ovarian cancer antigen mesothelin, were used as a positive control for SKOV3 lysis. These findings suggest that targeting TAMs in the tumor microenvironment with CAR T cells could lead to both indirect and direct anti-tumor effects.

TAMs from ovarian cancer patients highly express FRβ

To confirm the presence of $FR\beta^+$ TAMs in ovarian cancer, we measured FRβ expression by flow cytometry in primary ovarian cancer patient samples (**Figure 4.2A-B**). $CD11b^+CD14^+$ TAMs

from ovarian cancer patients exhibited high surface expression of FRβ. Data represents 4 individual patients and TAMs from both liquid tumor ascites and solid tumor digests. In addition, m923 CAR T cells produced high levels of IFNg in the presence of primary ovarian cancer ascites (**Figure 4.2C**) and specific lysis of CD11b-bead isolated TAMs from ovarian cancer patients (**Figure 4.2D**).

Development and validation of a mouse FRβ-specific CAR T cell platform

While these data confirm the clinical relevance and feasibility of targeting $FR\beta^+$ TAMs with CAR T cells, to model CAR-mediated destruction of TAMs *in vivo* in a fully immunocompetent, dynamic tumor microenvironment, we developed a mouse FRβ-specific CAR T cell platform. We cloned the CL10 rat anti-mouse FRβ scFv into previously validated MSGV retroviral CAR constructs containing murine CD28, 41BB, and CD3ζ intracellular signaling domains. The CAR constructs also contained GFP in trans to serve as a marker for transduced cells. Constructs containing the P4 scFv, specific for human mesothelin, and FMC26 scFv, specific for human CD19, were created in parallel to serve as controls (**Figure 4.3A**). After αCD3/CD28 bead activation of total C57BL/6 mouse splenocytes, retroviral transduction, and expansion with IL2 (**Figure 4.3B**), cultures contained >98% $CD3^+$ T cells with a usual ratio of 85:15 $CD8^+$:$CD4^+$ (**Figure 4.3C**). Surface CAR expression was confirmed in GFP^+ cells by labeling with recombinant protein antigen (murine FRβ and human mesothelin to detect CL10 and P4, respectively) or antibodies that recognize the scFv portion of the CAR by flow cytometry (**Figure 4.3D**). CAR transduction was reproducibly achieved at 70-80% GFP^+ cells (**Figure 4.3E**). We next confirmed specific reactivity of CL10 mouse T cells by establishing dose-dependent IFNg production in the presence of increasing concentrations of immobilized recombinant FRβ (**Figure 4.3F**).

Mouse CL10 CAR T cells display potent reactivity against ID8-mFRβ *in vitro* and *in vivo*

To create a model of CAR-targetable murine ovarian cancer we engineered the C57BL/6-syngeneic ovarian cancer cell line ID8 to stably express CL10 and P4 CAR target antigens murine FRβ (ID8-mFRβ) and human mesothelin (ID8-Meso) (**Figure 4.4A**). Mouse CL10 and P4 CAR T cells produced IFNg (**Figure 4.4B**) and specifically lysed ID8 target cells containing their respective CAR target antigen (**Figure 4.4C**). Multiple doses of CL10 mouse CAR T cells (injected at day 6-7 of T cell expansion) significantly delayed tumor progression in mice implanted IP with $fLuc^+$ ID8-mFRβ compared to control P4 CAR T cells as measured by tumor ascites formation (weight gain) (**Figure 4.5B**), tumor bioluminescence (**Figure 4.5C**), and increased long-term survival (**Figure 4.5D**). Bioluminescent images from 4 representative mice per group are shown to illustrate tumor progression (**Figure 4.5E**). These data confirmed high activity of CL10 CAR T cells *in vivo* against antigen-positive target cells.

CL10 CAR T cells display *in vitro* reactivity against TAMs isolated from ID8 tumor-bearing mice

We next asked whether the TAMs in our ID8 tumor model expressed FRβ. We collected total cells by peritoneal wash from mice with large ID8 tumor ascites. Using CL10-IgG, we observed high expression of FRβ in ~50% of $CD11b^+F4/80^+CD204^+$ TAMs by flow cytometry (**Figure 4.6A-B**). Non-myeloid lineage ($CD45^+CD11b^-$) immune cells were reproducibly negative for FRβ expression. High reactivity of CL10 CAR T cells against ID8 TAMs was verified using CD11b-microbead isolation of all $CD11b^+$ TAMs. CL10 CAR T cells produced high levels of IFNg only when cultured with $CD11b^+$ but not $CD11b^-$ ascites containing tumor cells and non-myeloid immune cells (**Figure 4.6C**). P4 control CAR T cells did not produce IFNg in either condition.

Multiple doses of CL10 CAR T cells did not influence ID8 tumor growth

We next tested the hypothesis that elimination of FRβ$^+$ TAMs using CL10 CAR T cells would inhibit tumor growth *in vivo*. We implanted mice with fLuc+ ID8 tumor cells (not expressing CAR target antigens) and treated mice with an identical dosing schedule to our previous ID8-mFRβ tumor model (**Figure 4.6D**). Multiple doses of CL10 CAR T cells (at day 6-7 of T cell expansion) did not significantly change tumor progression compared to mice treated with control P4 CAR T cells as measured by tumor ascites formation (weight gain) (**Figure 4.6E**), tumor bioluminescence (**Figure 4.6F**), and survival (**Figure 4.6G**). Bioluminescent images from 4 representative mice per group are shown to illustrate tumor progression (**Figure 4.6H**).

ID8-tumor bearing mice treated with multiple doses of CL10 CAR T cells display poor survival of CAR T cells and no depletion of FRβ$^+$ TAMs

To investigate whether CL10 CAR T cells led to the depletion of TAMs in ID8 tumor-bearing mice, we euthanized 5 mice per group on day 33 (2 days following the fourth T cell injection) in the experiment outlined in Figure 4.6. Tumor ascites from both CL10 and P4 control CAR T cell treated mice contained a very high percentage of CD45$^+$ immune cells (95% and 96% of total ascites). However, there were no significant differences in the frequency of infiltrating total CD11b$^+$ myeloid cells (**Figure 4.7A**), CD11b$^+$F4/80$^+$ TAMs (**Figure 4.7B**), total CD3$^+$ T cells (**Figure 4.7C**), or total CD3$^+$CD8$^+$ T cells (**Figure 4.7D**). In addition, FRβ$^+$ TAMs had not been specifically depleted in CL10 CAR T cell treated mice as FRβ expression was not significantly different from control treated mice (**Figure 4.7E**). To assess whether the failure of CL10 CAR T cells to deplete FRβ$^+$ TAMs could be due to poor engraftment or survival of CAR T cells we measured the frequency of CAR$^+$ T cells in total CD3$^+$CD8$^+$ cells by GFP expression. CL10 CAR T cells were detectable at a very low frequency (**Figure 4.7F**) suggesting poor survival of CAR T cells following transfer.

One large dose of CL10 CAR T cells leads to increased systemic innate immune cells and depletion of FRβ$^+$ TAMs

The very low frequency of CL10 CAR$^+$ T cells just two days post transfer led us to modify our CAR T cell dosing strategy. Instead of 4-5 multiple weekly doses of 5x10^6 day 6-7 CAR T cells, we tested delivery of one larger dose (8x10^6) on day 5 of T cell expansion in mice with 4 week established ID8 tumor (**Figure 4.8A**). We hypothesized that the larger dose at day 5 of T cell expansion would allow for greater *in vivo* persistence. In addition, if multiple CAR T cell doses resulted in an immune response boosted by the subsequent deliveries, an anti-CAR adaptive immune response could have caused the rapid depletion we observed in our previous experiment following the fourth CAR T cell dose. We rationalized that one large dose may lead to longer survival of transferred cells.

On day 28 following tumor injection mice were injected IP with 8x10^6 day 5 CAR$^+$ T cells. Mice were euthanized on day 34 (6 days following T cell transfer) to assess CAR T cell survival and impact on peripheral and tumor-localized myeloid cell populations. We noted a mild and transient weight loss in CL10 treated mice compared to controls (**Figure 4.8B**). Mice otherwise appeared healthy. On day 6 post T cell treatment, no differences in peripheral blood CD8$^+$ or CD4$^+$ T cell counts were observed (**Figure 4.8C**). At this time point, no CAR$^+$ (GFP$^+$) T cells were detected in the peripheral blood of either group (data not shown). However, we did observe significant increases in Ly6G$^+$ granulocytes at day 3 (data not shown) and day 6 (**Figure 4.8C)** and Ly6C^{HI} monocyte counts at day 6 (**Figure 4.8C**) in peripheral blood of CL10 CAR T cell treated mice. These data suggested that CL10 CAR T cell treatment led to systemic activation of the innate immune system with higher peripheral levels of activated neutrophils and myeloid precursors.

Tumor ascites was collected by peritoneal wash and tumor immune cell infiltrates were analyzed by flow cytometry (**Figure 4.8D-H**). CL10 CAR T cell treatment induced a significantly increased immune cell infiltrate compared to P4 control treated mice (**Figure 4.8D**). As a frequency of total live ascites cells, the percentage of total $CD45^+$, total $CD11b^+$, $CD11b^+Ly6G^+$ granulocytes, $CD11b^+Ly6C^{HI}$ monocytes, $CD3^+CD8^+$ T cells, and $CD3^+CD4^+$ T cells were all significantly increased in CL10 compared to P4 CAR T cell treated mice (**Figure 4.8D**). The frequency of CAR^+ (GFP^+) $CD8^+$ T cells was ~60% for both P4 and CL10 groups (**Figure 4.8E**) signifying a large increase in CAR T cell survival compared to our previous ID8 experiment (**Figure 4.7F**). Depletion of $FR\beta^+$ TAMs was also clearly evident in CL10 treated mice (<1% of $F4/80^+CD204^+$ TAMs (**Figure 4.8G**) expressed FRβ compared to ~50% expression in P4 treated mice) (**Figure 4.8F**). We also noted significant differences in the phenotype of $CD11b^+$ myeloid cells between P4 and CL10 CAR T cell treated mice. Plotting Ly6C vs CD204 (**Figure 4.8H**) revealed that in P4 treated mice nearly all myeloid cells were Ly6C negative, with 2 populations of $CD204^+$ or $CD204^-$ TAMs. However, CL10 treated mice had significant populations in all four quadrants with a continuous transition between different quadrants (**Figure 4.8H**). We believe this finding reveals a static picture of ongoing dynamic recruitment and differentiation of new monocytes to the tumor microenvironment. We hypothesize that elimination of $FR\beta^+$ TAMs resulted in increased recruitment of new ($Ly6C^{HI}$) monocytes to replace the depleted mature ($Ly6C^-F4/80^+CD204^{+/-}$) macrophages.

Cyclophosphamide and IL2 conditioning increases CL10 CAR T cell persistence and toxicity in ID8 tumor-bearing mice

Previous research in mouse models as well as clinical application of adoptive T cell therapy have found that non myeloablative preconditioning either with cyclophosphamide or sublethal irradiation in combination with high dose IL2 can greatly improve adoptive T cell engraftment

and anti-tumor efficacy. As another means to enhance CL10 CAR T cell persistence we added 150mg/kg cyclophosphamide treatment on day 27 (one day before T cell transfer) and 15μg IL2 on days 28, 29, and 30 to the one-dose CAR T cell ID8 mouse model (CyIL2) (**Figure 4.9A**). Mice were euthanized on day 34 (6 days post T cell transfer) to assess peripheral and tumor myeloid cell phenotype. The addition of CyIL2 greatly enhanced the mild weight loss seen in non-conditioned (NC) mice. CyIL2 and CL10 CAR T cells resulted in progressive weight loss in 80% of treated mice with some mice losing >15% total body weight within 6 days post T cell transfer (**Figure 4.9B**). In addition, visible signs of decreased grooming (ruffled fur) and lethargy occurred in CyIL2 CL10 CAR T cell treated mice. Phenotypic changes in peripheral and tumor myeloid cells in CyIL2 CL10 treated mice were similar to those observed in NC CL10 CAR T cell treated mice. However, CyIL2 conditioning elicited a greater magnitude in the observed response. On day 6 post T cell treatment, 3/5 CyIL2 CL10 treated mice had very high levels of $Ly6C^{HI}$ monocytes and $Ly6G^{+}$ granulocytes compared to the P4 group with 3/5 mice exhibiting >7000 $Ly6G^{+}$ cells/μl blood. In peritoneal tumor ascites, >95% of total cells were $CD45^{+}$ immune cells in CyIL2 CL10 treated mice (**Figure 4.9D**) including a large component of $CD11b^{+}$ myeloid cells (**Figure 4.9D**). $Ly6G^{+}$ neutrophils alone made up 25-30% of total ascites cells compared to < 2% of total cells in control mice (**Figure 4.9D**). The frequency of $Ly6C^{HI}$ myeloid cells was also significantly increased in CL10 mice (**Figure 4.9D**). In addition, the frequency of CAR^{+} (GFP^{+}) $CD8^{+}$ T cells was significantly higher in CL10 treated mice compared to P4 (**Figure 4.9E**). In one mouse >50% of total ascites cells were CAR^{+} $CD8^{+}$ T cells, and this high level of CAR T cells correlated with increased toxicity in this mouse.

$FR\beta^{+}$ TAMs were also significantly depleted in CyIL2 CL10 compared to P4 to a similar degree as NC CL10 mice (**Figure 4.9F**). In CyIL2 CL10 treated mice, $Ly6G^{-}$ myeloid cells exhibited

almost a completely Ly6C^{HI} phenotype whereas the majority of these cells in P4 group were Ly6C^{-} (Figure **4.9H**).

Tumor-specific CAR T cells do not recapitulate the myeloid activation and toxicity observed in CL10 CAR T cell treated mice.

To address whether our findings with CL10 CAR T cells could possibly be due to a general CAR T cell activation phenotype and not specifically related to elimination of FRβ^{+} macrophages, we repeated the CyIL2 ID8 tumor model using ID8-Meso tumor cells. In these experiments, P4 control CAR T cells served as a positive control for T cell activation in the tumor microenvironment and CD19 CAR T cells served as the negative control CAR. A treatment schedule identical to the ID8 CyIL2 model was used (**Figure 4.10A**). Again, only CL10 CAR T cell treatment led to significant weight loss and signs of toxicity in mice (**Figure 4.10B**). Although mild changes in immune cell frequencies were observed between P4 tumor-specific CAR T cells and CD19 control CAR T cells, myeloid cell phenotypes were mostly identical between these two groups in the peripheral blood (**Figure 4.10C**) and peritoneal ascites (**Figure 4.10D, F-I**) on day 7 post T cell transfer. The massive increase in peripheral blood and peritoneal ascites Ly6G^{+} granulocytic and Ly6C^{HI} monocytic myeloid cells with CL10 CAR T cells was highly reproducible in the ID8-Meso tumor model. P4 tumor-specific CAR T cells did not elicit this same dramatic myeloid cell infiltration. These experiments led us to hypothesize that innate immune cell activation and toxicity in CL10 CAR T cell treated mice is driven by FRβ-targeted CAR T cell immunopathology.

Clodronate liposome treatment produced a similar phenotype to CL10 CAR T cells in ID8 tumor-bearing mice

As a positive control for macrophage depletion we added clodronate liposomes in addition to CAR T cell treatment in the ID8 tumor model. Clodronate or control PBS liposomes were injected IV 2 days before and IP one day before a single dose of $8x10^6$ CL10 or P4 control CAR T cells on day 28 of ID8 tumor growth **(Figure 4.11A)**. Similar to CL10 CAR T cell treatment alone, addition of clodronate to control P4 CAR T cells resulted in transient, recoverable weight loss. However, addition of clodronate to CL10 CAR T cells resulted in enhanced weight loss with 2/4 mice requiring euthanasia at day 4 following T cell treatment due to deteriorating condition **(Figure 4.11B)**. We evaluated peripheral blood phenotype 3 days post T cell transfer (**Figure 4.11C**). Addition of clodronate to P4 control CAR T cells significantly elevated both T cell ($CD4^+$ and $CD8^+$) and myeloid cell ($Ly6G^+$ and $Ly6C^{HI}$) counts. Addition of clodronate to CL10 CAR T cells produced an additive effect on $Ly6G^+$ granulocytes and $Ly6C^{HI}$ monocytes.

Long term tumor growth is promoted in NC but inhibited in CyIL2 CL10 CAR T cell treated mice

To assess the impact of macrophage depletion by CL10 CAR T cells on tumor growth, we evaluated long term tumor progression in NC and CyIL2 conditioned ID8-Meso tumor bearing mice. Mice were treated with a single dose of $8x10^6$ CD19, P4, or CL10 CAR^+ T cells on day 28 following tumor inoculation (**Figure 4.12A**). One group of mice received a mixed dose of $4x10^6$ P4 and $4x10^6$ CL10 CAR T cells (P4/CL10). We monitored tumor progression by progressive weight gain in NC (**Figure 4.12B**) and CyIL2 conditioned (**Figure 4.12C**) mice and bioluminescence in NC (**Figure 4.12D**) and CyIL2 conditioned (**Figure 4.12E**) mice. The weight loss and signs of toxicity in CL10 CAR T cell treated mice recovered within 10 days of T cell treatment. We observed a trend for more rapid outgrowth of NC CL10 CAR T cell treated mice compared to controls (**Figure 4.12 B, D**) and significantly decreased tumor growth in CyIL2 conditioned CL10 CAR T cell treated mice (**Figure 4.12C, E**). To evaluate ongoing systemic

inflammation and CAR T cell persistence we measured peripheral blood cell counts on day 31 after T cell treatment. One month following T cell transfer, the inflammation observed in the first week following CL10 CAR T cell transfer (Figures 4.8-10) was completely resolved. Peripheral blood T cell and myeloid cell counts were not significantly different from controls in NC (**Figure 4.12F**) or CyIL2 conditioned (**Figure 4.12G**) mice. CAR^+ (GFP^+) T cells were nearly undetectable in all groups (range 0-0.3% of peripheral blood $CD8^+$ T cells, data not shown). Survival curves of NC mice were not different (**Figure 4.12H**). However, survival of CyIL2 conditioned P4, CL10, and P4/CL10 CAR T cell groups were all significantly enhanced compared to CD19 control treated mice (**Figure 4.12I**).

CL10 CAR T cells with CyIL2 conditioning produce toxicity in non-tumor bearing mice.

To ask whether the signs of toxicity revealed by the addition of CyIL2 were dependent on the presence of tumor, we treated non-tumor bearing C57BL/6 mice according to the same treatment protocol (CyIL2 and single dose $8x10^6$ CAR^+ T cells). We observed a similar loss in weight and ruffling/lethargy in CyIL2 CL10 treated non-tumor bearing mice (**Figure 4.13A**). These results suggested that on-target elimination of non-TAM $FR\beta^+$ cells could be responsible for the transient toxicity of CL10 CAR T cells.

FRβ is highly expressed in healthy liver Kupffer cells

Unlike in humans, FRβ is not expressed in bone marrow myeloid progenitors (data not shown) or peripheral blood monocytes (**Figure 4.14**) in C57BL/6 mice. The FRβ literature in rodents has generally described low expression of FRβ in resting macrophages, with higher expression induced upon macrophage activation and in inflammatory environments[160,198]. Nagai and colleagues used IHC to determine co-expression of FRβ and macrophage marker CD68 in a large array of healthy mouse tissues. Their findings revealed low-moderate expression in spleen,

peritoneal, liver, heart and colon macrophages[171]. To determine whether CL10 CAR T cell-mediated toxicity could be due to recognition of macrophages in these normal healthy tissues we examined FRβ in $CD11b^{+}F4/80^{+}CD204^{+/-}$ macrophage populations in C57BL/6 bone marrow, spleen, peritoneal cavity, liver, lung, heart, kidney, brain, and GI tract using CL10-IgG and flow cytometry. Our analyses revealed that most tissue macrophages do not express FRβ, with the exception of low levels in resting peritoneal macrophages and high expression in liver macrophages (Kupffer cells) and cardiac macrophages in the heart (**Figure 4.14A**). Representative F4/80 vs CD204 expression plots and gates (**Figure 4.14B**) and FRβ expression histograms (**Figure 4.14C**) are shown for each tissue.

$F4/80^{+}$ Kupffer cells are depleted in the livers of CyIL2 CL10 CAR T cell treated mice

To assess whether liver Kupffer cells were impacted by CL10 CAR T cell treatment, we evaluated F4/80 expression in fixed liver samples by IHC. Preliminary data suggest the CyIL2 conditioned CL10 CAR T cell treated mice showed depletion of $F4/80^{+}$ cells in the liver when analyzed 6-7 days post T cell transfer (**Figure 4.15**). Interestingly, NC CL10 CAR T cell treated mice show evidence of increased F4/80 expression, possibly suggesting activation or recovery but not depletion of Kupffer cells at this time point.

CL10 CAR T cell treatment with CyIL2 conditioning results in liver inflammation and necrosis

Due to the high expression of FRβ in and evidence for depletion of liver Kupffer cells, we reasoned that liver-directed tissue pathology could account for toxicity observed in CL10 CAR T cell treated mice. Liver samples collected 6-7 days post T cell transfer from NC or CyIL2 conditioned mice from experiments outlined in Figures 4.8, 4.9, and 4.10 were analyzed by board

certified veterinary anatomic pathologists. Representative H&E images are shown for each group (**Figure 4.16A**).

While low levels of extramedullary hematopoiesis (EMH) is common in the liver, CL10 CAR T cell treated mice displayed drastically increased EMH with an unusually strong skewing towards the myeloid lineage, referred to as extramedullary myelopoiesis (EMM). The severity of EMM was most notable in CyIL2 conditioned CL10 treated mice (see **Figure 4.16F** for scoring) with numerous foci throughout the liver (**Figure 4.16D**), which is consistent with the increased $Ly6G^+$ and $Ly6C^+$ cells detected by flow cytometry in the peripheral blood and peritoneal cavity. Liver assessment also revealed increases in circulating and liver infiltrating neutrophils and myeloid precursor cells in CyIL2 CL10 treated mice. Histologically, these mice also had notably increased numbers of megakaryocytes throughout the hepatic parenchyma.

Livers from all the groups had multifocal aggregates of neoplastic cells on the peritoneal surface that occasionally extended into the underlying hepatic parenchyma. Peritoneal spread of injected carcinoma cells (ID8 tumor cells), termed carcinomatosis, resulted in varying levels of surrounding hepatocellular necrosis and myeloid cell infiltrate. Histologically in the CyIL2 and CL10 treated mice the foci of carcinomatosis contained large areas of necrosis with fewer tumor cells (see **Figure 4.16B**) as compared to the other groups. Increased tumor cell necrosis in CyIL2 CL10 treated mice supports the finding of delayed tumor progression in this treatment group (Figure 4.12). There were also increased areas of hepatocyte necrosis (**Figure 4.16C**). Given the increased amount of hepatic tissue damage in these mice, there was also prominent hepatocellular regeneration characterized by increased numbers of mitotic figures (**Figure 4.16E**).

Hepatocellular necrosis results in the release of liver-specific aminotransferase enzymes into the bloodstream of affected animals. We evaluated serum alanine aminotransferase (ALT) (**Figure**

4.16G) and aspartate aminotransferase (AST) (**Figure 4.16H**) in NC or CyIL2 CAR T cell treated mice. Serum ALT and AST were within the normal range for all mice on day 6-7 (Figure 4.11G-H) and day 3 (data not shown) post T cell transfer, and there were no significant differences between any of the groups. It is possible that the moderate hepatocyte necrosis noted during liver assessment was not extensive enough to cause significant changes in serum enzyme levels.

Luminex analysis reveals increased serum cytokine and chemokine levels in CyIL2 conditioned CAR T cell treated mice

To assess potential correlates of systemic inflammation and toxicity in CL10 CAR T cell treated mice, we analyzed peripheral blood levels of 32 chemokines and cytokines on day 3 following T cell transfer. Many chemokines and cytokines were highly increased in CyIL2 conditioned CL10 CAR T cell treated mice (**Figure 4.17**). Neutrophil growth and activation factor G-CSF was particularly dramatically increased. Also of substantial note, cytokines IFNg and IL6 and chemokines IP-10 (CXCL10), MIG (CXCL9), KC (CXCL1), and MCP-1 (CCL2) were considerably elevated in CyIL2 CL10 groups. Another group of cytokines and chemokines were also statistically significantly but only moderately increased **(Figure 4.18**). These included GM-CSF, RANTES, TNFα, IL-3, IL-7, IL-10, IL-13, IL-15, MIP-1β, LIF, MIP-1α, MIP-2, and VEGF. The group of unchanged cytokines (**Figure 4.19**) included IL-1α, IL-1β, IL-2, IL-4, IL-9, IL-12, LIX, IL-17, and M-CSF. NC CL10 CAR T cell treated mice and P4 tumor-specific CAR T cell treated mice generally did not show elevations in most cytokines evaluated.

Discussion and Future Directions

To our knowledge this is the first reported study describing CAR T cells directed against macrophages. We established that targeting human FRβ^{+} macrophages is feasible using human CAR T cells and confirmed that FRβ could be a clinically relevant target in primary ovarian cancer TAMs. After some optimization of *in vivo* application of mouse FRβ-specific CAR T cells, we did observe a mild delay in tumor progression in CyIL2 conditioned CL10 CAR T cell treated mice compared to control T cells. Conversely, application of CL10 CAR T cells in non-conditioned mice may have mildly increased tumor progression. While the mechanisms responsible are unknown, it is possible that the increased engraftment of T cells and exacerbated inflammation (highlighted by increased signs of toxicity, granulo/monocytosis, and elevated serum cytokines) in CyIL2 pre-conditioned mice produced a more inhospitable environment for tumor growth and survival. CAR T cell activation could have even caused bystander lysis of neighboring tumor cells (analogous to what we demonstrated using human tumor/macrophage co-cultures *in vitro*). A proinflammatory environment could also have resulted in direct tumor cell lysis by soluble factors or activated proinflammatory (M1) macrophages and infiltrating cytotoxic neutrophils. CL10 CAR T cell application in NC mice, however, led to decreased engraftment and less systemic inflammation. It is possible that the mild induction of tumor infiltrating myeloid cells in this low inflammatory setting actually helped to promote tumor growth by increasing a source for rapid TAM repopulation. This hypothesis is partially supported by comparing the myeloid cell phenotype in NC CL10 (Figure 4.8H) and CyIL2 conditioned CL10 mice (Figure 4.9H) 6 days post T cell transfer. Whereas myeloid cells in CyIL2 conditioned CL10 mice show almost an exclusively Ly6C^{HI} phenotype, in NC mice ongoing differentiation is evident with increases in Ly6C^{low} monocytes. Future studies to determine the kinetics and phenotype of

macrophage differentiation and/or repolarization in the tumor microenvironment following CL10 CAR T cell treatment will be necessary to clarify these hypotheses.

Both NC and CyIL2 conditioned mice ultimately resolved signs of peripheral inflammation, coinciding with loss of CAR T cells at late stages of tumor progression. It is possible that more robust effects on tumor growth would have been noted in the setting of long term CAR T cell persistence and activity. Unfortunately, our earlier mouse model suggested that multiple doses of CAR T cells led to rapid depletion of T cells following later doses (Figure 4.7) decreasing the chance that repeat infusions would result in long term persistence. Since the CL10 scFv is derived from rat[171] and the P4 scFv is derived from human[176], foreign epitopes in these regions may have elicited an immune response against the surface CAR. Reports of neutralizing factors directed against mouse-derived scFvs have been described in CAR T cell treated patients[95,128], and may have been exacerbated by multiple CAR T cell infusions[129]. Therefore we think it is likely that antibody-mediated CAR T cell elimination could be partially responsible for poor CAR T cell persistence. The CD19 control CAR T cells (derived from a mouse scFv) seemed to persist slightly better than P4 and CL10 in NC (Mean = 0.20% CD19 CAR^+ $CD8^+$ vs 0.01% CL10 (P =.006) and .06% P4 (P=.03)) and CyIL2 conditioned (Mean = 0.18% CD19 CAR^+ $CD8^+$ vs 0.01% CL10 (P =.01) and .03% P4 (P=.03)) mice on day 31 post T cell transfer in ID8-Meso tumor-bearing mice. While activation induced T cell death could also account for lower persistence of CL10 and P4, lower immunogenicity of mouse-derived CD19 CAR T cells could account for the slightly increased persistence.

Even if immunogenicity could be avoided and long term CAR T cell persistence achieved, CL10 CAR T cells would likely still have to fight an up-hill battle against constant replenishment of TAMs from infiltrating $Ly6C^{HI}$ monocytes, especially in light of the increased infiltration of these cells following CL10 CAR T cell treatment. An alternative approach to enhance CL10 CAR T

cell efficacy could be to combine CL10 CAR T cells with therapeutic elimination of or blocking monocyte recruitment into the tumor. Strategies targeting CCL2/CCR2 axis could block recruitment or MCSF/CD115 axis could hamper differentiation thereby giving CL10 CAR T cells a moderate advantage in this fight.

Lymphodepleting preconditioning and IL2 drastically increased the signs of toxicity and systemic inflammation in CL10 CAR T cell treated mice. We believe the major mechanism behind these observations is the well-described phenomena of improved T cell engraftment and functional activity following lymphodepletion[70,231,235]. CD19 control CAR T cells and P4 tumor-specific CAR T cells did not reproduce the phenotype observed in CL10 treated mice, suggesting the conditioning regimen alone is not responsible. However, it is possible that cyclophosphamide has an unappreciated effect on FRβ^{+} target cells that could be driving some of the increased toxicity. We did evaluate FRβ expression in peritoneal, spleen, and liver macrophages following cyclophosphamide treatment of non-tumor bearing mice and did not see any changes in surface expression (data not shown). These findings support our original hypothesis that increased T cell function was largely responsible for the increased toxicity observed in CyIL2 conditioned mice.

The striking systemic activation of monocyte and granulocyte output was by far the most conspicuous observation coinciding with signs of toxicity in CyIL2 conditioned CL10 CAR T cell treated mice. We noted peripheral increases in Ly6C^{HI} monocytes and Ly6G^{+} granulocytes in peripheral blood and peritoneal cavity, as well as marked extramedullary myelopoiesis (EMM) in the liver. Liver EMM was correlated with on-target depletion of FRβ^{+} liver Kupffer cells. It is unknown whether local destruction of nearby cells induced EMM directly or whether spikes in peripheral cytokines led to induction of EMM in the liver. Systemic cytokine activation would likely have also induced myelopoietic output from the bone marrow and potentially the spleen, another common site for extramedullary hematopoiesis. Future studies should evaluate myeloid

output from these organs in order to determine whether abnormal EMM from the liver was solely responsible for the systemic surge in myeloid production.

The elevated levels of certain myeloid inducing cytokines in serum from CyIL2 conditioned CL10 CAR T cell treated mice highly suggests that systemic cytokine levels likely played a major role in inducing the observed monocytosis and granulocytosis. In particular, exceedingly high serum concentrations of granulocyte colony stimulating factor (G-CSF) were noted. G-CSF is considered the master regulator of granulocyte production and release from the bone marrow. G-CSF mediates rapid release of neutrophils from the bone marrow through enhancing expression of surface CXCR4 (Reviewed in ([239])). G-CSF can also promote release of other bone marrow populations, and is used clinically to mobilize HSCs before transplant[240]. Cells of the monocyte/macrophage lineage are the major producers of G-CSF although mesenchymal and endothelial cell expression has also been observed[241]. Many inflammatory stimuli including TNFα and LPS can induce G-CSF production from macrophages during inflammation. In addition to G-CSF, chemokines IP-10 (CXCL10), MIG (CXCL9), KC (CXCL1), and MCP1 (CCL2) are significantly elevated in CL10 CAR T cell treated mice. Production of IP-10[242] and MIG is induced by IFNg in a variety of cell types. IP-10 and MIG are particularly chemotactic for activated lymphocytes[243]. Although T cell numbers were not drastically impacted in our mouse models, these chemokines could have contributed to lymphocyte trafficking in CL10 CAR T cell treated mice. MCP1 is the classic chemokine driving recruitment of $CCR2^{+}$ peripheral blood monocytes into sites of inflammation[244] and tumor growth[245,246]. Therefore, elevated MCP1 likely influenced the greatly elevated numbers of $Ly6C^{HI}$ monocytes in CyIL2 CL10 CAR T cell treated mice.

We believe the high serum concentrations of IFNg are likely produced from the activated CL10 CAR T cells. Indeed we observed extraordinarily high production of IFNg upon CL10 CAR

activation *in vitro*. However, many of the other chemokines and cytokines elevated in serum from mice could be derived from either CAR T cells or a variety of other cells including the targeted macrophages themselves. Evaluating a larger array of cytokines produced using *in vitro* co-culture systems of CAR T cells and TAMs as well as other components of the peritoneal ascites will be helpful in the future to unravel the sources of cytokine production.

Of note, many of the elevated cytokines in our model have also been described in CD19 CAR T cell treated patients experiencing cytokine storm following T cell transfer (including IFNg, IL6, CXCL9, CXCL10, and TNFα)[118,121,123]. Many parallels have been drawn between the cytokine release syndrome observed in CAR patients and symptoms of macrophage activation syndrome (MAS)[247,248]. The prominent role of IL6 in both scenarios, highlighted by the effective use of IL6R inhibitor tocilizumab to control cytokine storm in CD19 CAR patients[122], suggests that macrophage activation following CAR T cell transfer could be a prominent factor driving toxicity of CAR T cell therapy in the clinic. One preclinical study using ErbB-targeted CAR T cells confirmed macrophage derived IL6 as a correlate of toxicity in mice[249]. Interestingly, this study also showed reduced IFNg production by CAR T cells *in vivo* when macrophages were depleted, possibly suggesting a feedback system between CAR T cells and activated macrophages. Our model directly targeting macrophages with CL10 CAR T cells also confirms these similarities and may be of use to further future understanding of the role of macrophages in CAR therapy.

Of note, we did not observe many significant increases in serum cytokines in P4 CAR T cell treated ID8-Meso tumor bearing mice. It is technically possible that CL10 is a "better" CAR and produces higher levels of T cell activation upon target recognition *in vivo*. Future experiments directly comparing P4 and CL10 CAR T cell efficacy against ID8-Meso and ID8-mFRβ could more directly address these potential functional differences. However, we believe that the cells targeted by CL10 (macrophages) vs P4 (tumor cells) is likely responsible for the major

phenotypic differences elicited in CL10 CAR T cell treated mice. This hypothesis is supported by the finding that clodronate liposome-mediated macrophage elimination also produced increased hematopoietic output visualized by increased peripheral blood cell counts. Like with NC CL10 mice, clodronate caused transient recoverable weight loss in combination with control T cells. However, combination of CL10 CAR and clodronate synergistically enhanced systemic myeloid activation and toxicity. We initially hypothesized that clodronate pretreatment would decrease CL10 CAR T cell toxicity by eliminating FRβ^{+} target cells before CAR T cell delivery. Instead we observed additive effects from the two treatments which ultimately produced lethal toxicity in 50% of mice. Several factors could account for these observations. Clodronate may not have eliminated all FRβ^{+} macrophages before CL10 CAR T cell transfer. The kinetics of clodronate and CL10 CAR mediated macrophage depletion will need to be clarified in the future. It is also possible that FRβ is expressed in a population of cells not targeted by clodronate. Non-macrophage FRβ expression will need to be investigated further to address this possibility. Future studies comparing the effects of clodronate and CL10 CAR T cell-mediated macrophage depletion will help untangle the phenotype of "clean" macrophage depletion to proinflammatory macrophage depletion in the setting of CAR T cells. For example, evaluating serum cytokine secretion from clodronate treated mice will be helpful in untangling whether the cytokine release observed following CL10 CAR T cell treatment was more dependent on T cell activation or macrophage destruction.

In light of high expression of FRβ in cardiac macrophages, it will be of great interest in the future to determine whether cardiac macrophages are depleted similarly to liver Kupffer cells in CyIL2 conditioned CL10 treated C57BL/6 mice and whether any evidence of cardiac pathology is present. In all of our experiments we injected CAR T cells directly IP. This could have allowed for more direct access to the liver compared to other organs like the heart. In addition, the

frequency of CAR T cells in the peripheral blood was usually low, especially compared to the frequency in peritoneal wash, suggesting CAR T cells do not efficiently or rapidly exit the peritoneal cavity. Future experiments comparing IV delivery of CL10 CAR T cells to IP delivery are warranted to investigate whether route of delivery impacts the ensuing site and severity of tissue pathology and overall degree of toxicity.

While our analyses highlighted liver and cardiac macrophage as candidate target cells for CL10 CAR T cell targeting, tissue macrophage FRβ expression was measured in healthy mice. Models of experimental inflammation have been reported to increase FRβ expression in macrophages at sites of inflammation and systemically[160]. It is unknown whether the systemic inflammation observed in CL10 CAR T cell treated mice could have induced FRβ to higher levels on tissue macrophages than those observed in healthy mice. In theory, this scenario could create a self-perpetuating model of (CAR T cell activation → systemic inflammation → higher FRβ expression in previously low/negative macrophages → increased CAR T cell activation and toxicity).

A recent report of lethal toxicity in mice treated with chimeric NKG2D CAR T cells reported strain-specific differences in the degree of toxicity with BALBc mice experiencing drastically increased lethality compared to C57BL/6[234]. Although this could be due to differential expression of NKG2D target ligands in BALBc vs C57BL/6 mice, their findings raise an important question about the variability of CAR T cell therapy in a genetically diverse population. Future experiments are warranted to evaluate whether FRβ expression is changed and whether CL10 CAR T cells produce similar toxicity in genetically divergent strains of mice.

In summary, we have developed the first model targeting macrophages with CAR T cells. It appears that CAR T cell-mediated macrophage destruction activates signaling pathways to

promote increased myeloid output. We have evaluated many of the soluble factors that are likely involved, but future studies with in vitro systems and genetic knockouts will be necessary to fully untangle the pathways and cellular mediators of these effects. Encouragingly, elimination of TAMs with CAR T cells produced a mild anti-tumor effect in our model. However, several obstacles will need to be overcome to improve CAR T cell persistence and ongoing myeloid depletion in order to fully evaluate the merits of this approach. Finally, our evaluation of on-target toxicity in healthy tissue macrophages will help educate future development of FRβ-directed CAR T cells for AML.

Figure 4.1

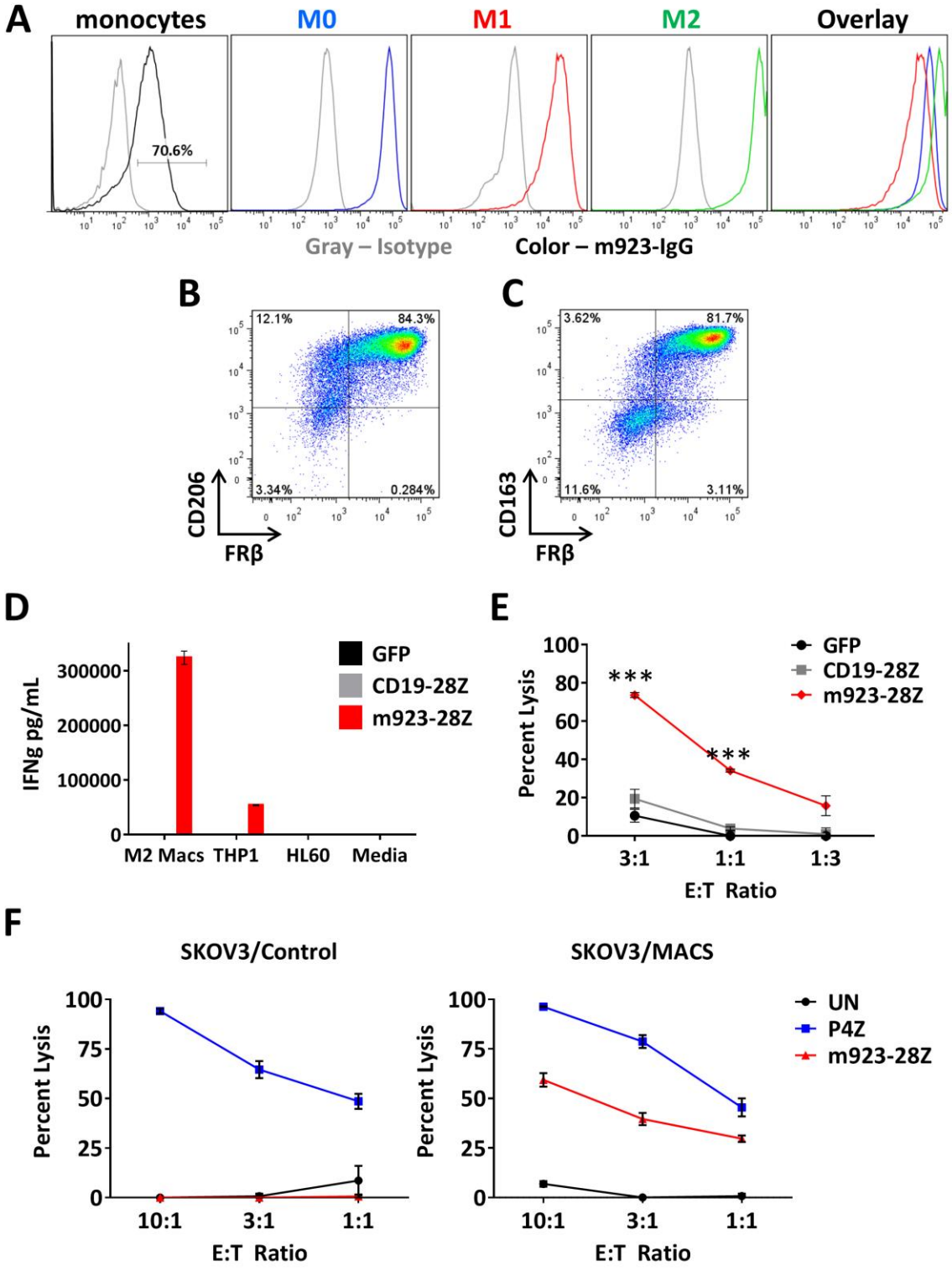

Figure 4.1 Human M2 polarized macrophages highly express FRβ and are efficiently targeted my m923 CAR T cells

(A) FRβ expression in human monocytes (pre-culture), MCSF-differentiated macrophages (M0, blue), M1 polarized (red), and M2 polarized (green) MCSF-differentiated macrophages. **(B)** M2 macrophages co-express FRβ and CD206. **(C)** M2 macrophages co-express FRβ and CD163. **(D)** IFNg secretion in supernatants from overnight co-culture of M2 macrophages and CAR T cells. Error bars represent mean ± SD of triplicate wells. Representative experiment shown. **(E)** Specific lysis of M2 macrophages after overnight co-culture with CAR T cells at 3:1, 1:1, or 1:3 E:T ratios. Lysis was measured by quantitative flow cytometry examination of live target cells following co-culture. Error bars represent mean ± SD of triplicate wells. One representative experiment shown. **(F)** Specific lysis of SKOV3 ovarian carcinoma by Untransduced (UN), P4, or m923 CAR T cells with (right, SKOV3/MACS) or without (left, SKOV3/Control) the presence of M2 macrophages present in the culture. SKOV3 and M2 Macrophages were cultured at a 1:1 ratio. Error bars represent mean ± SD of triplicate wells. One representative experiment shown. Results were repeated 3 times with similar results. SD – standard deviation. (*** $P < .001$)

Figure 4.2

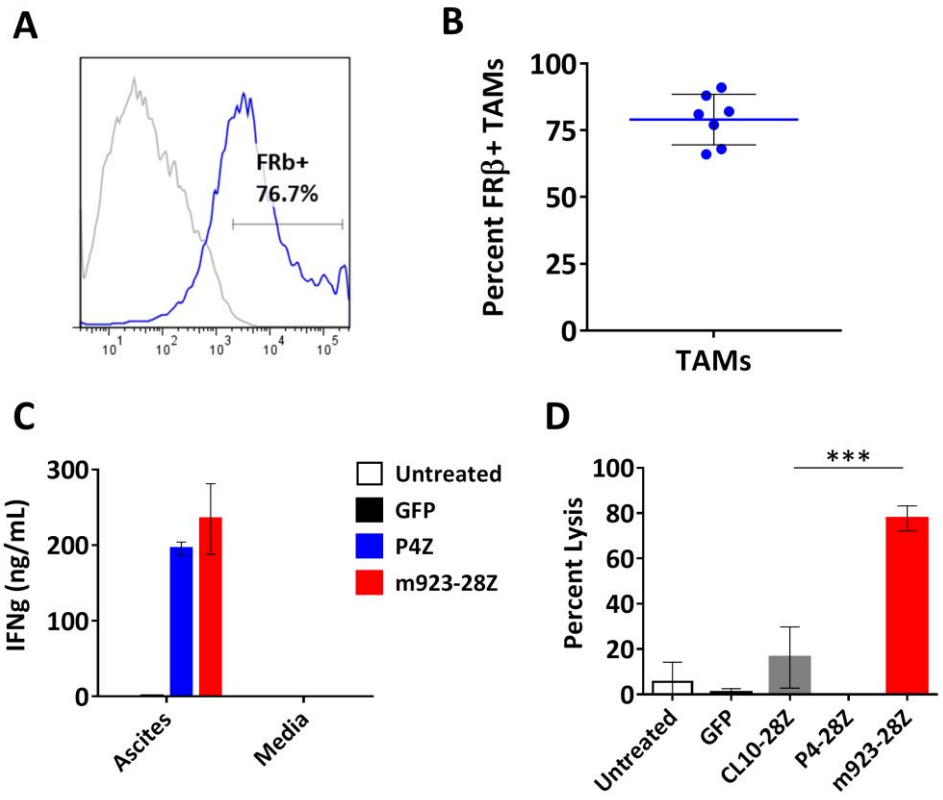

Figure 4.2 Ovarian cancer TAMs highly express FRβ and are targeted by m923 CAR T cells

(A-B) Flow cytometry assessment of FRβ in TAMs from primary ovarian cancer patients. Whole ascites or tumor digests were washed, labeled, and gated on live, $CD45^+CD11b^+CD14^+$ TAMs for assessment of FRβ. m923-IgG (blue) and isotype (gray) staining was used to determine frequency of $FR\beta^+$ TAMs. One representative sample shown **(A)**. Average frequency in 7 samples is indicated **(B)**. 4 different patients are represented. TAMs from liquid ascites and solid tumor digests were evaluated. **(C)** IFNg secretion from overnight co-culture of CAR T cells with whole ovarian cancer ascites tumor. Untreated tumor ascites was cultured in the absence of T cells. Media control wells contained T cells alone. Error bars represent mean ± SD of triplicate wells. **(D)** Percent lysis of primary ovarian cancer TAMs by m923 CAR T cells. Whole $CD11b^+$ tumor associated myeloid wells were isolated by CD11b magnetic microbeads from ovarian patient tumor ascites. After overnight culture at 1:1 E:T, quantitative flow cytometry was used to assess live $CD14^+$ TAMs following culture. Error bars represent mean ± SD of 6 replicate wells. Untreated wells were cultured in the absence of T cells. CL10 control CAR T cells are specific for mouse FRβ. SD – standard deviation. (*** $P < .001$)

Figure 4.3

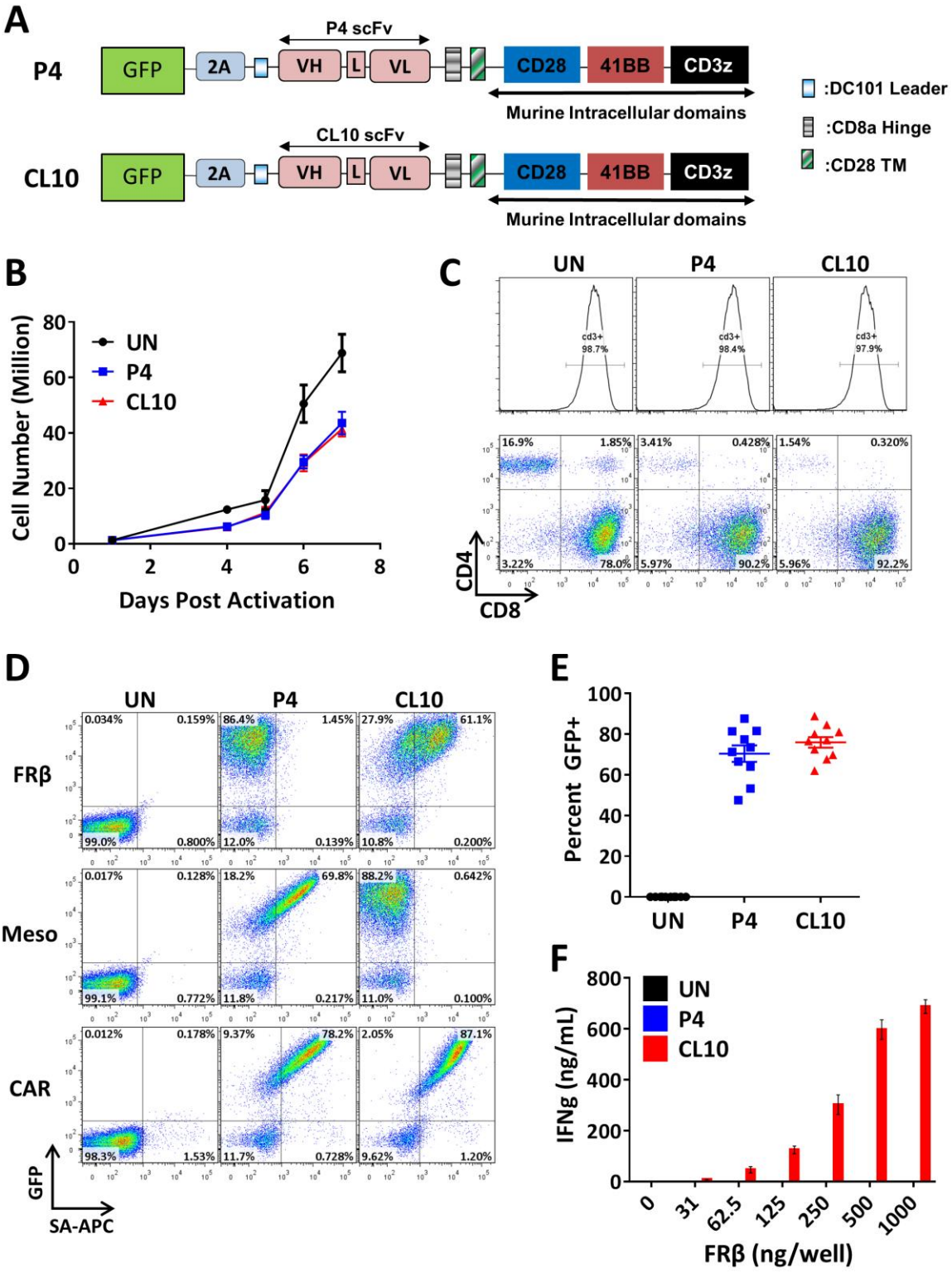

Figure 4.3 Development of a FRβ-specific mouse CAR T cell platform

(A) Schematic representation of MSGV CAR retroviral constructs. **(B)** T cell expansion of untransduced (UN), P4 and CL10 mouse CAR T cells. 10 independent experiments incorporated. Error bars represent mean ± SEM. **(C)** On day 5 of expansion cultures contained >98% CD3+ (upper) with 80-90% CD8+ (lower) T cells. **(D)** Surface CAR expression in GFP^+ cells. T cells were labeled with biotinylated recombinant murine FRβ (FRβ), human mesothelin (Meso), or α-human (H+L) antibody (CAR) and secondary streptavidin APC (SA-APC). **(E)** CAR T cell transduction efficiency across 10 independent experiments as measured by GFP expression on day 4-5 of culture. Error bars represent mean ± SEM. **(F)** IFNg production from mouse CAR T cells cultured overnight in 96-well plates coated with recombinant FRβ. Error bars represent mean ± SEM. GFP – green fluorescent protein, VH – variable heavy change, L – linker, VL – variable light chain, TM – transmembrane, SEM – standard error.

Figure 4.4

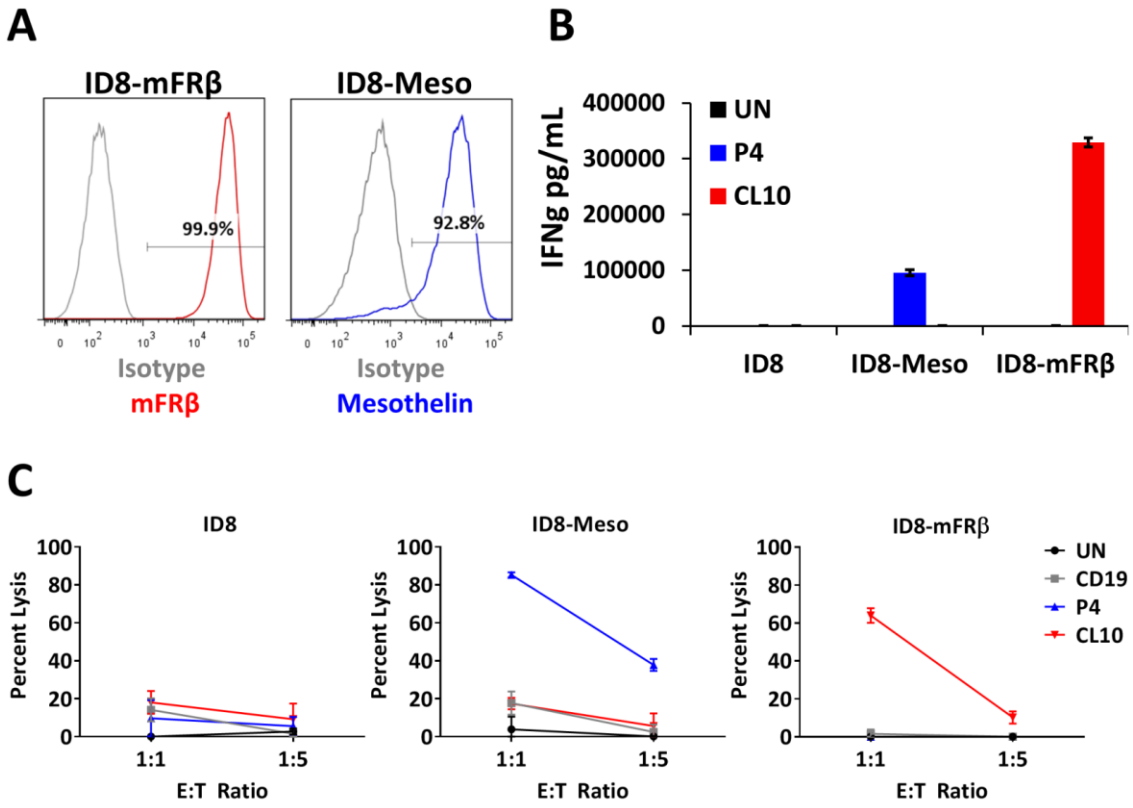

Figure 4.4 CL10 mouse CAR T cells display potent reactivity against ID8-mFRβ *in vitro*

(A) Expression of mouse FRβ (left, red) and human mesothelin (right, blue) in engineered cell lines ID8-mFRβ and ID8-Meso, respectively. Isotype staining is shown in gray histograms. **(B)** IFNg secretion following overnight co-culture of mouse CAR T cells and ID8 cell lines. Error bars represent mean ± SD of three replicate wells. Representative experiment shown. **(C)** Specific lysis of fLuc+ ID8 cell lines after 5hr co-culture with CAR T cells. Error bars represent mean ± SD of 3 replicate wells. One representative experiment is shown. UN – unstransduced, E:T – effector: target.

Figure 4.5

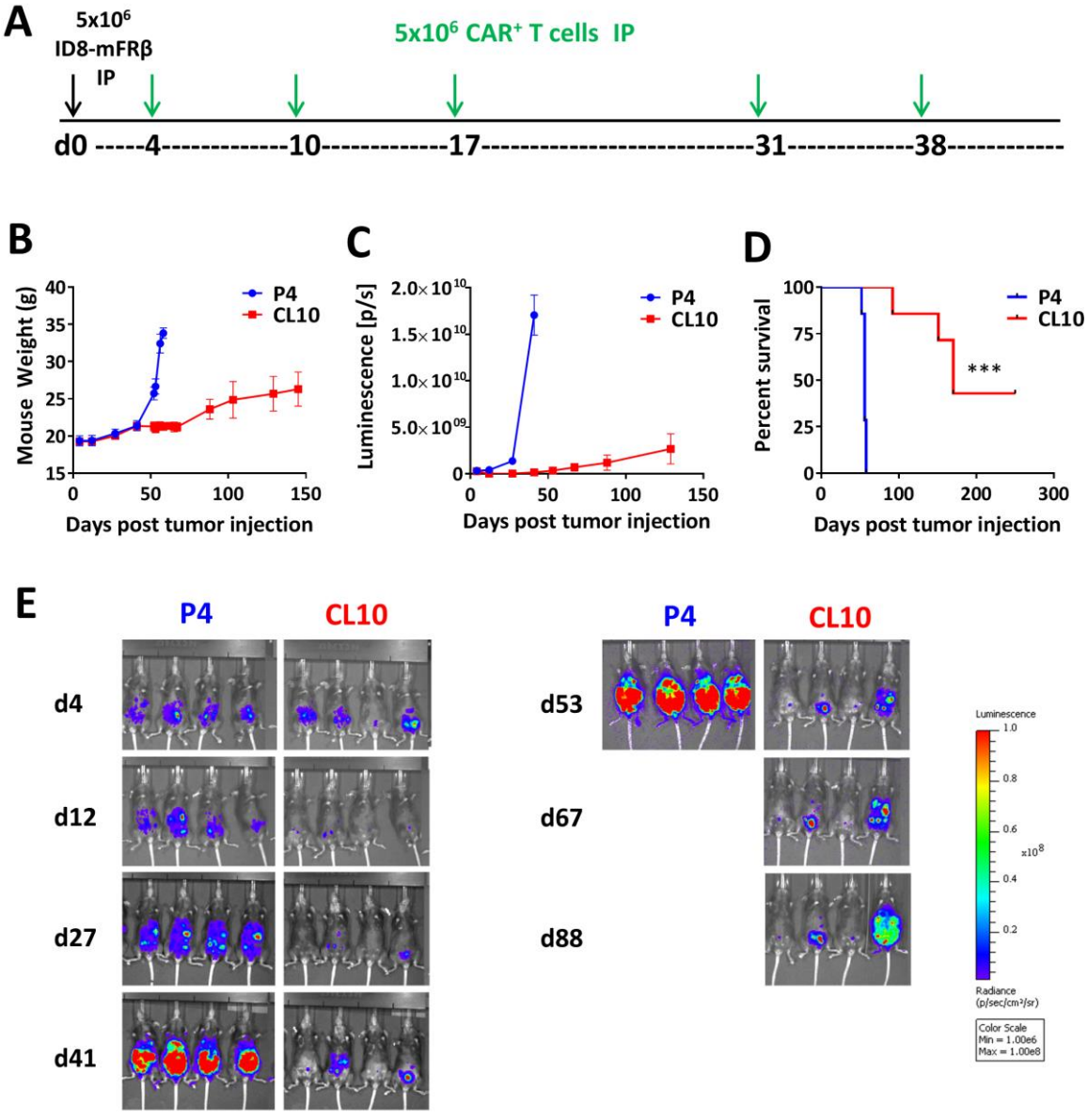

Figure 4.5 CL10 mouse CAR T cells significantly inhibit ID8-mFRβ tumor growth *in vivo*

(A) Treatment schedule of C57BL/6 mice implanted IP with $5x10^6$ fLuc+ ID8-mFRβ tumor cells with $5x10^6$ P4 or CL10 CAR^+ T cells on days 4, 10, 17, 31, and 38 following tumor injection. n=8 mice per group. Tumor progression was monitored by **(B)** progressive weight gain and **(C)** bioluminescent imaging. **(D)** Survival. (*** $P < .001$, log-rank (Mantel-Cox) test). **(E)** Representative bioluminescent images of 4 mice per group. Error bars represent mean ± SEM. IP – intraperitoneal. fLuc – firefly luciferase.

Figure 4.6

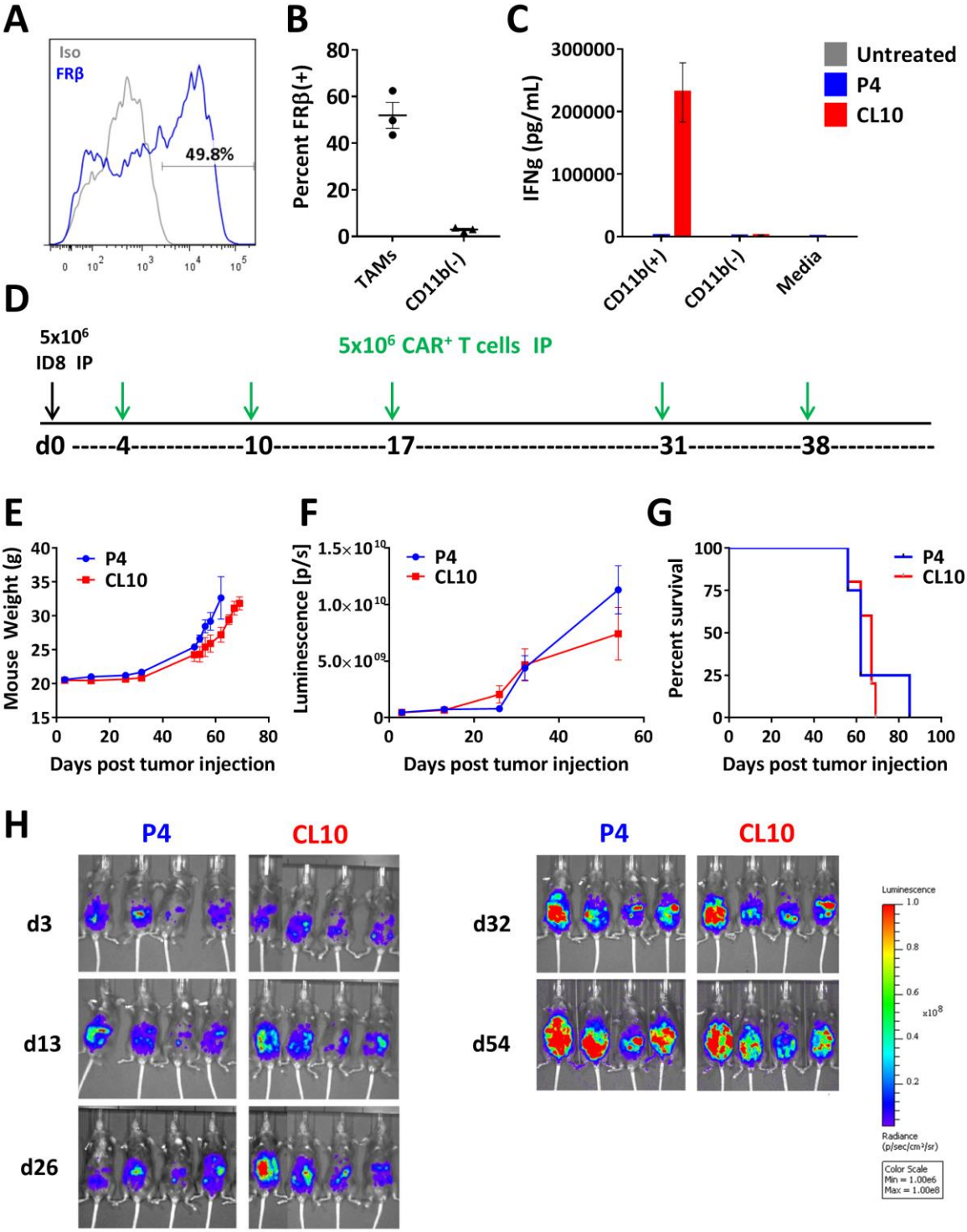

Figure 4.6 CL10 CAR T cells display *in vitro* reactivity against ID8 TAMs but fail to impact ID8 tumor growth *in vivo*

(A-B) FRβ expression in $CD45^+CD11b^+F4/80^+CD204^+$ TAMs in mice bearing large ID8 tumor ascites. **(A)** Representative histogram. Blue – CL10 IgG. Gray – rat IgG2a isotype. **(B)** Expression across n=3 mice. $CD45^+CD11b^-$ immune cells do not express FRβ. **(C)** IFNg production following overnight co-culture of CAR T cells and ID8 ascites CD11b+ or CD11b- magnetic bead-isolated fractions. **(D)** Treatment schedule of C57BL/6 mice implanted IP with $5x10^6$ $fLuc^+$ ID8 tumor cells and $5x10^6$ P4 or CL10 CAR^+ T cells on days 4, 10, 17, 31, and 38 following tumor injection. 10 mice per group (5mice per group were euthanized on d33). Tumor progression was monitored by **(E)** progressive weight gain and **(F)** bioluminescent imaging. **(G)** Survival. **(H)** Representative bioluminescent images of 4 mice per group. Error bars represent mean ± SEM. IP – intraperitoneal. fLuc – firefly luciferase.

Figure 4.7

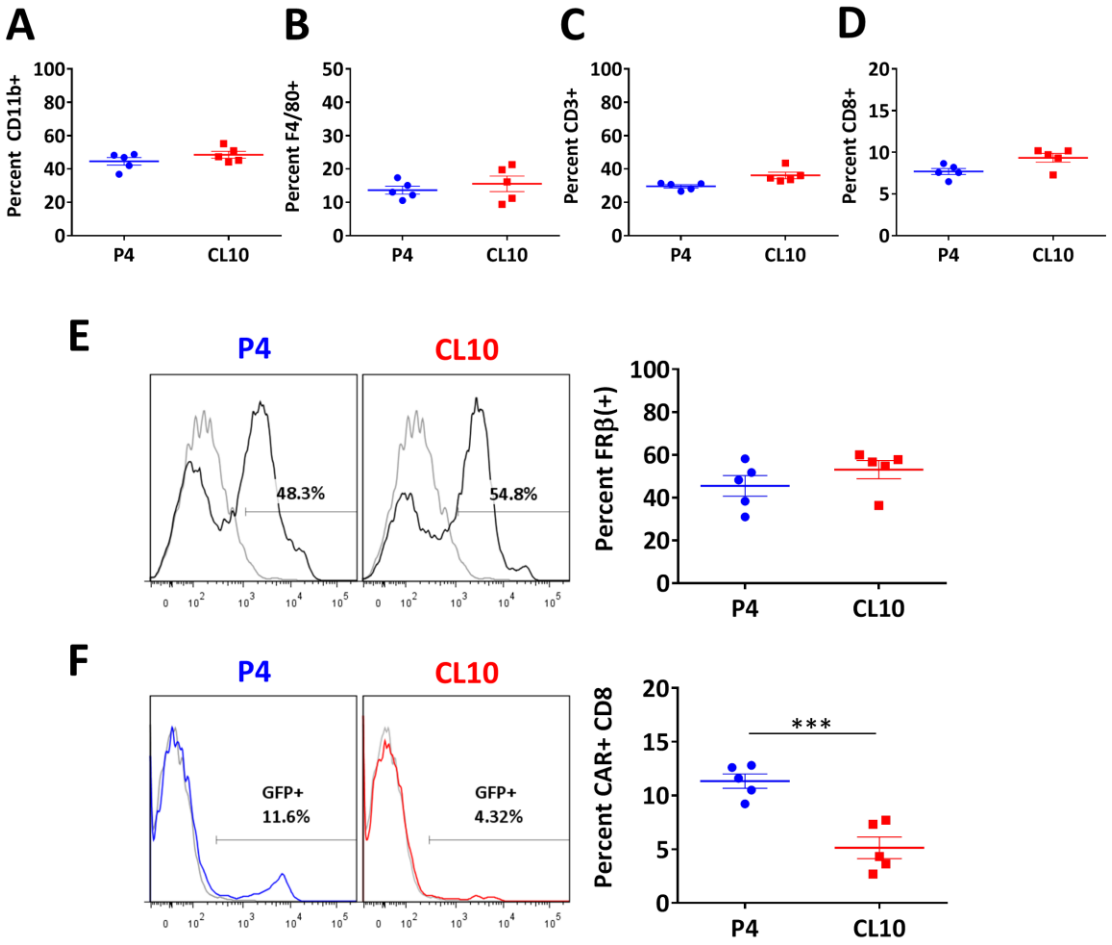

Figure 4.7 ID8-tumor bearing mice treated with multiple doses of CL10 CAR T cells display poor survival of CAR T cells and no depletion of FRβ$^+$ TAMs

5 mice/group treated in the experiment outlined in Figure 4.6 were euthanized on day 33. Tumor ascites was collected by peritoneal wash and analyzed by flow cytometry. The relative frequency of **(A)** CD45$^+$CD11b$^+$ cells, **(B)** CD45$^+$CD11b$^+$ F4/80$^+$ TAMs, **(C)** CD3$^+$ and **(D)** CD3$^+$CD8$^+$ T cells was determined. **(E)** FRβ expression in CD45$^+$CD11b$^+$ F4/80$^+$ TAMs. Black histogram – CL10 IgG. Gray histogram – rat IgG2a isotype. Representative FRβ plots are shown for one mouse per group. Total results are quantified to the right (n=5). Error bars represent mean ± SEM. **(F)** Survival of CAR$^+$ T cells on d33 (2 days following the fourth T cell injection) as measured by GFP expression in CD3$^+$CD8$^+$ T cells. One representative histogram per group. Total expression for n=5 mice per group is shown to the right. Error bars represent mean ± SEM. (*** P < .001)

Figure 4.8

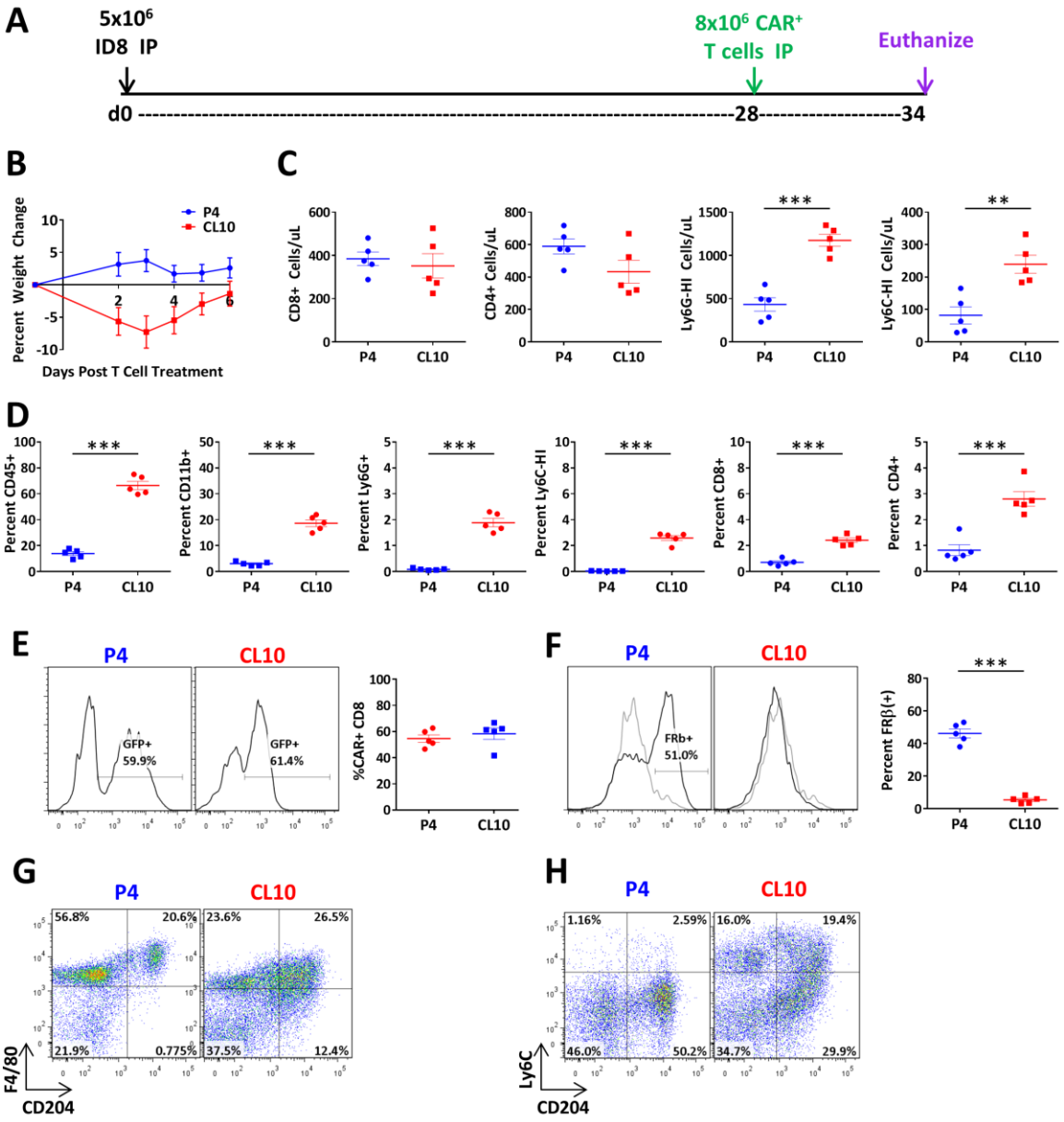

Figure 4.8 One large dose of CL10 CAR T cells leads to increased systemic innate immune cells and depletion of FRβ$^+$ TAMs

(A) Treatment schedule of C57BL/6 mice implanted IP with 5x10^6 fLuc$^+$ ID8 and 8x10^6 CAR$^+$ T cells on day 28 following tumor injection. Mice were euthanized for analysis 6 days later. n=5 mice per group. **(B)** Transient weight loss in CL10 CAR T cell treated mice. Weight change is indicated as a percentage of pre-treatment (day (-1)) body weight. **(C)** Peripheral blood cell counts at time of euthanasia (day 6 post T cell treatment). CD3$^+$CD8$^+$ T cells, CD3$^+$CD8$^-$ (CD4) T cells, CD11b$^+$Ly6G^{HI} and CD11b$^+$Ly6C^{HI} myeloid cells. **(D)** Relative frequency of indicated immune cell populations as a percentage of total live ascites cells. From left to right: Total CD45$^+$, CD45$^+$CD11b$^+$, CD45$^+$CD11b$^+$Ly6G$^+$, CD45$^+$CD11b$^+$Ly6G$^-$Ly6C^{HI}, CD45$^+$CD3$^+$CD8$^+$, and CD45$^+$CD3$^+$CD4$^+$. **(E)** Survival of CAR$^+$ T cells in peritoneal cavity on day 6 post T cell treatment as measured by GFP expression in CD3$^+$CD8$^+$ T cells. One representative GFP fluorescence histogram per group. Total expression for n=5 mice per group is shown to the right. **(F)** FRβ expression in F4/80$^+$CD204$^+$ ascites TAMs. One representative FRβ expression histogram per group. Black – CL10 IgG. Gray – rat IgG2a isotype. Total expression for n=5 mice per group is shown to the right. **(G)** Representative flow cytometry plots to indicate F480 and CD204 populations in CL10 or control P4 CAR T cell treated mice. Gated on CD45$^+$CD11b$^+$Ly6G$^-$ cells. **(H)** Representative flow cytometry plots to highlight different Ly6C and CD204 populations in CL10 or control P4 CAR T cell treated mice. Gated on CD45$^+$CD11b$^+$Ly6G$^-$ cells. All error bars represent mean ± SEM of n=5 mice per group. (* P < .05, ** P < .01, *** P < .001) IP – intraperitoneal, fLuc – firefly luciferase.

Figure 4.9

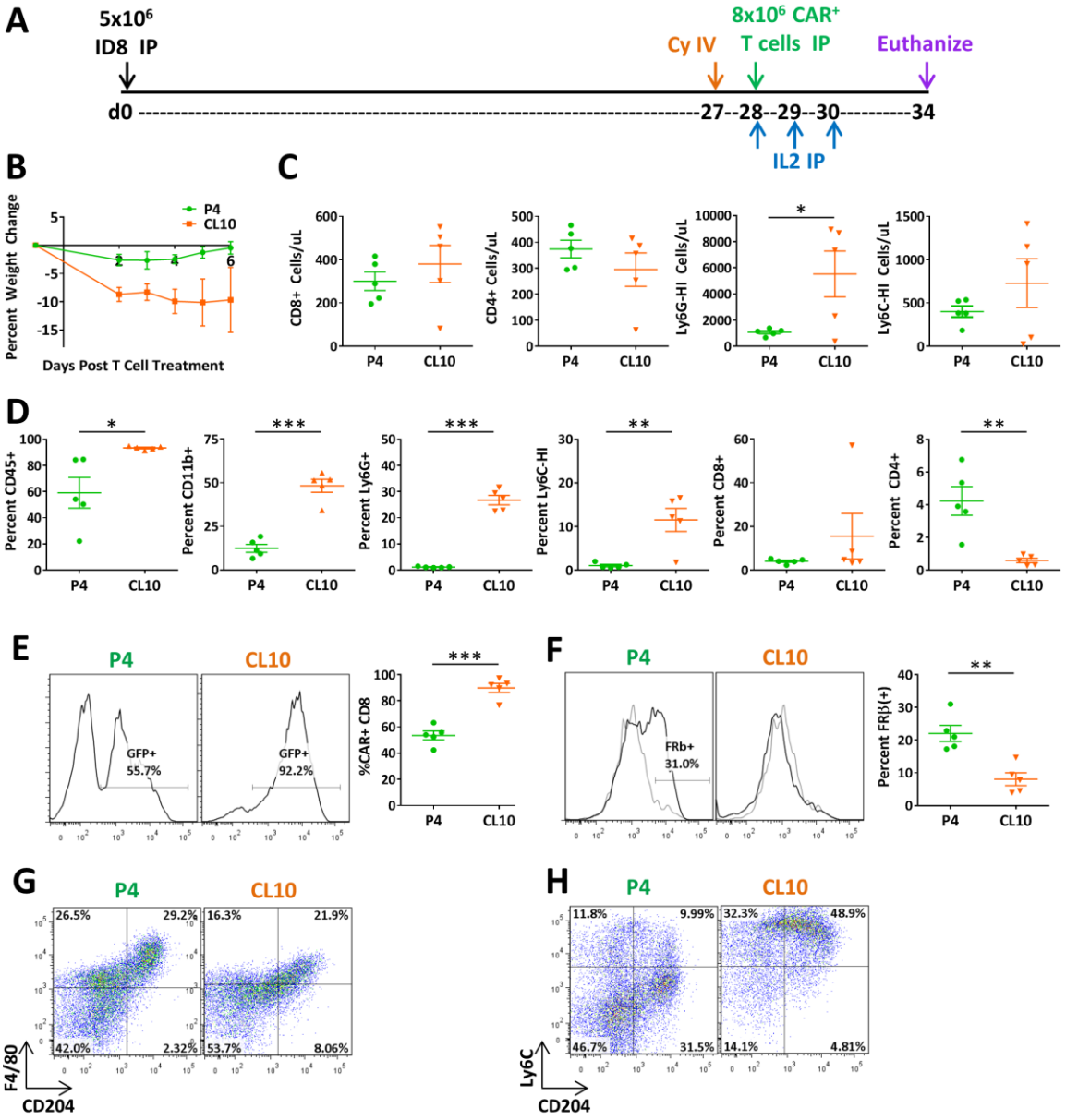

Figure 4.9 Cyclophosphamide and IL2 conditioning increases CL10 CAR T cell persistence and toxicity in ID8 tumor-bearing mice

(A) Treatment schedule of C57BL/6 mice implanted IP with $5x10^6$ $fLuc^+$ ID8 and $8x10^6$ CAR^+ T cells on day 28 following tumor injection. 150mg/kg cyclophosphamide (Cy) was given IV on day 27. 15µg IL2 was given IP on days 28, 29, and 30. (CyIL2 conditioning). Mice were euthanized for analysis 6 days later. n= 5 mice per group. **(B)** Progressive weight loss in CL10 CAR T cell treated mice. Weight change is indicated as a percentage of pre-treatment (day (-1)) body weight. **(C)** Peripheral blood cell counts at time of euthanasia (day 6 post T cell treatment). $CD3^+CD8^+$ T cells, $CD3^+CD8^-$ (CD4) T cells, $CD11b^+Ly6G^{HI}$ and $CD11b^+Ly6C^{HI}$ myeloid cells. **(D)** Relative frequency of indicated immune cell populations as a percentage of total live ascites cells. From left to right: Total $CD45^+$, $CD45^+CD11b^+$, $CD45^+CD11b^+Ly6G^+$, $CD45^+CD11b^+Ly6G^-Ly6C^{HI}$, $CD45^+CD3^+CD8^+$, and $CD45^+CD3^+CD4^+$. **(E)** Frequency of CAR^+ T cells in peritoneal cavity on day 6 post T cell treatment as measured by GFP expression in $CD3^+CD8^+$ T cells. One representative GFP fluorescence histogram per group. Total expression for n=5 mice per group is shown to the right. **(F)** FRβ expression in $F4/80^+CD204^+$ ascites TAMs. One representative FRβ expression histogram per group. Black – CL10 IgG. Gray – rat IgG2a isotype. Total expression for n=5 mice per group is shown to the right. **(G)** Representative flow cytometry plots to indicate F480 and CD204 populations in CL10 or control P4 CAR T cell treated mice. Gated on $CD45^+CD11b^+Ly6G^-$ cells. **(H)** Representative flow cytometry plots to highlight different Ly6C and CD204 populations in CL10 or control P4 CAR T cell treated mice. Gated on $CD45^+CD11b^+Ly6G^-$ cells. All error bars represent mean ± SEM of n=5 mice per group. (* $P < .05$, ** $P < .01$, *** $P < .001$) IP – intraperitoneal, IV – intravenous, fLuc – firefly luciferase.

Figure 4.10

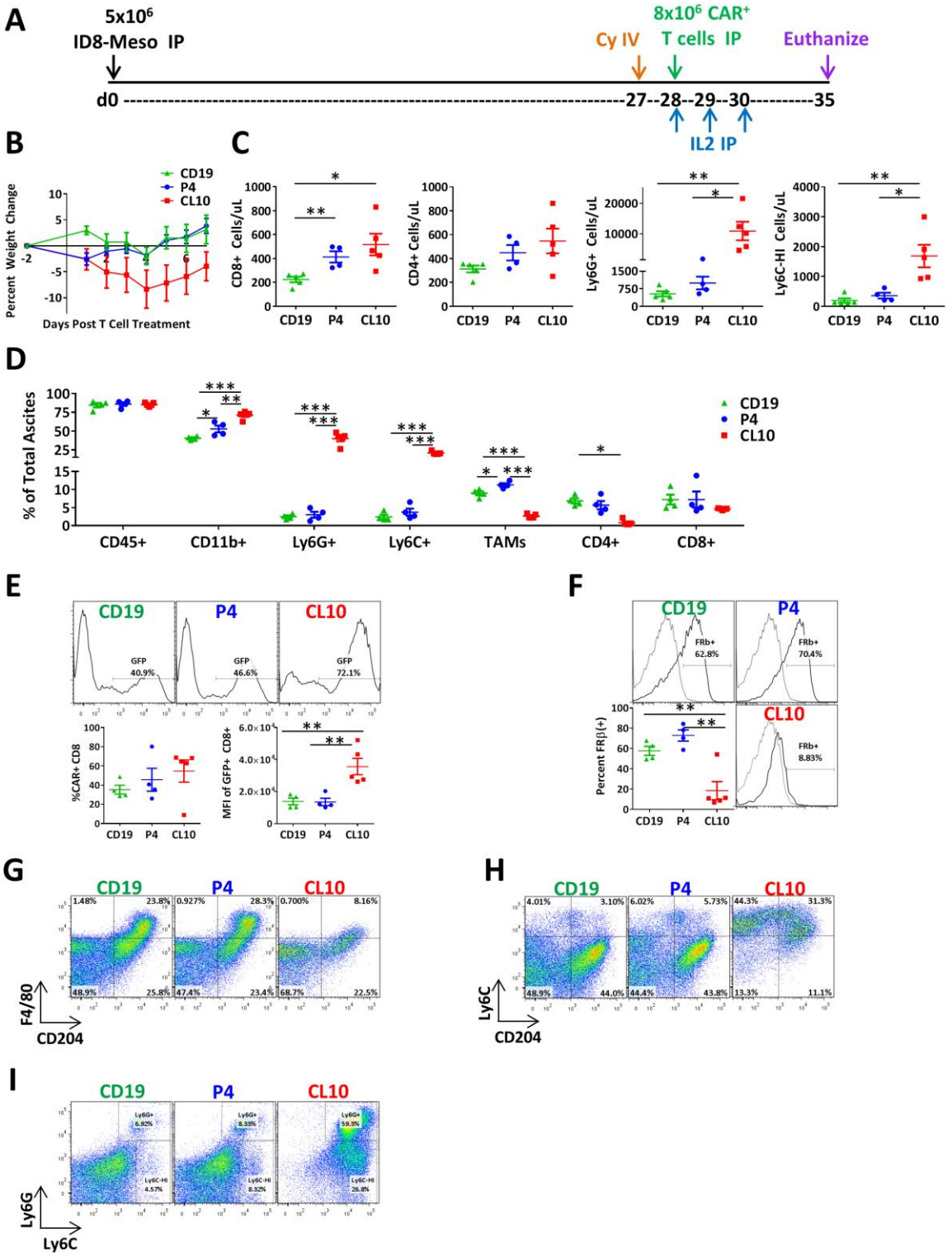

Figure 4.10 Tumor-specific CAR T cells do not recapitulate the immune cell activation and toxicity observed in CL10 CAR T cell treated mice

(A) Treatment schedule of C57BL/6 mice implanted IP with $5x10^6$ $fLuc^+$ ID8-Meso and $8x10^6$ CAR^+ T cells on day 28 following tumor injection. P4 CAR T cells are specific for ID8-Meso and serve as a positive control for T cell activation, and CD19 CAR T cells serve as a negative control. 150mg/kg cyclophosphamide (Cy) was given IV on day 27. 15μg IL2 was given IP on days 28, 29, and 30 (CyIL2 conditioning). Mice were euthanized for analysis 7 days later. n= 4 or 5 mice per group. **(B)** Progressive weight loss only in CL10 CAR T cell treated mice. Weight change is indicated as a percentage of pre-treatment (day (-2)) body weight. **(C)** Peripheral blood cell counts at time of euthanasia (day 7 post T cell treatment). $CD3^+CD8^+$ T cells, $CD3^+CD8^-$ (CD4) T cells, $CD11b^+Ly6G^+$ and $CD11b^+Ly6C^{HI}$ myeloid cells. **(D)** Relative frequency of indicated immune cell populations as a percentage of total live ascites cells. From left to right: Total $CD45^+$, $CD45^+CD11b^+$, $CD45^+CD11b^+Ly6G^+$, $CD45^+CD11b^+Ly6G^-Ly6C^+$, $CD45^+CD11b^+Ly6G^-F4/80^+CD204^+$ TAMs, $CD45^+CD3^+CD4^+$, and $CD45^+CD3^+CD8^+$. **(E)** Frequency of CAR^+ T cells in peritoneal cavity on day 7 post T cell treatment as measured by GFP expression in $CD3^+CD8^+$ T cells. One representative GFP fluorescence histogram per group. Total GFP expression (left) and GFP MFI (right) for n=4 or 5 mice per group is shown below. **(F)** FRβ expression in $F4/80^+CD204^+$ ascites TAMs. One representative FRβ expression histogram per group. Black – CL10 IgG. Gray – rat IgG2a isotype. Total expression for n=4 or 5 mice per group is shown to the left. **(G)** Representative flow cytometry plots to indicate F4/80 and CD204 populations in CL10, P4, or CD19 control CAR T cell treated mice. Gated on $CD45^+CD11b^+Ly6G^-$ cells. **(H)** Representative flow cytometry plots to highlight different Ly6C and CD204 populations in CL10, P4, or CD19 control CAR T cell treated mice. Gated on $CD45^+CD11b^+Ly6G^-$ cells. **(I)** Representative flow cytometry plots to highlight the large frequency of infiltrating $Ly6G^+$ neutrophils only in CL10 treated mice. Gated on $CD45^+CD11b^+$ cells. All error bars represent mean ± SEM of n=4 or 5 mice per group. (* $P < .05$, ** $P < .01$, *** $P < .001$) IP – intraperitoneal, IV – intravenous, fLuc – firefly luciferase, MFI – median fluorescence intensity.

Figure 4.11

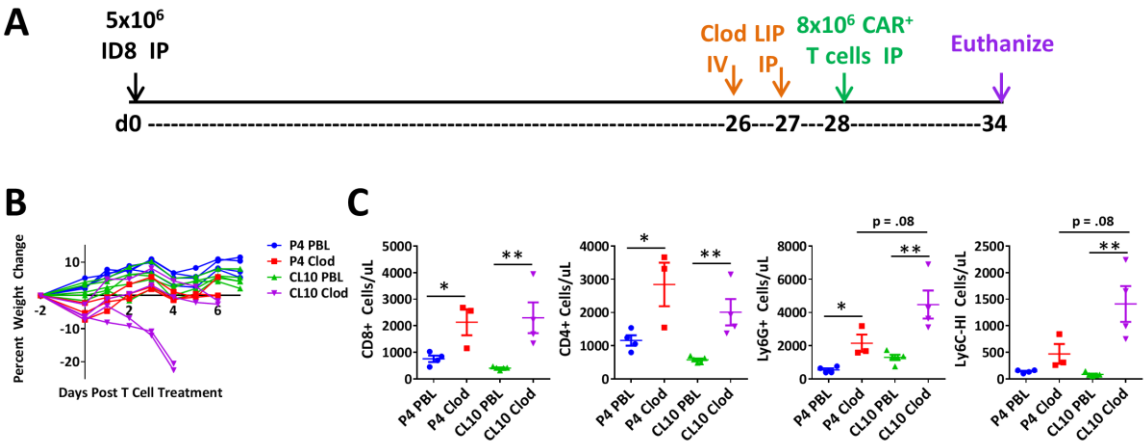

Figure 4.11 Clodronate liposome-mediated macrophage depletion causes a similar increase in myelopoiesis and synergizes with CL10 CAR T cells

(A) Treatment schedule of C57BL/6 mice implanted IP with $5x10^6$ $fLuc^+$ ID8 and $8x10^6$ CAR^+ T cells on day 28 following tumor injection. Clodronate liposomes (Clod) or PBS control liposomes (PBL) were provided IV on day 26 and IP on day 27. Mice were euthanized for analysis 6 days later. n=5 mice per group. **(B)** Rapid weight loss in 50% of CL10-clodronate treated mice. Weight change is indicated as a percentage of pre-treatment (day (-2)) body weight. Each line represents one mouse. **(C)** Peripheral blood cell counts at day 3 post T cell treatment. $CD3^+CD8^+$ T cells, $CD3^+CD8^-$ (CD4) T cells, $CD11b^+Ly6G^+$ granulocytes and $CD11b^+Ly6C^{HI}$ monocytes. Error bars represent mean ± SEM of n=3 to 5 mice per group. (* P < .05, ** P < .01) IP – intraperitoneal, IV – intravenous.

Figure 4.12

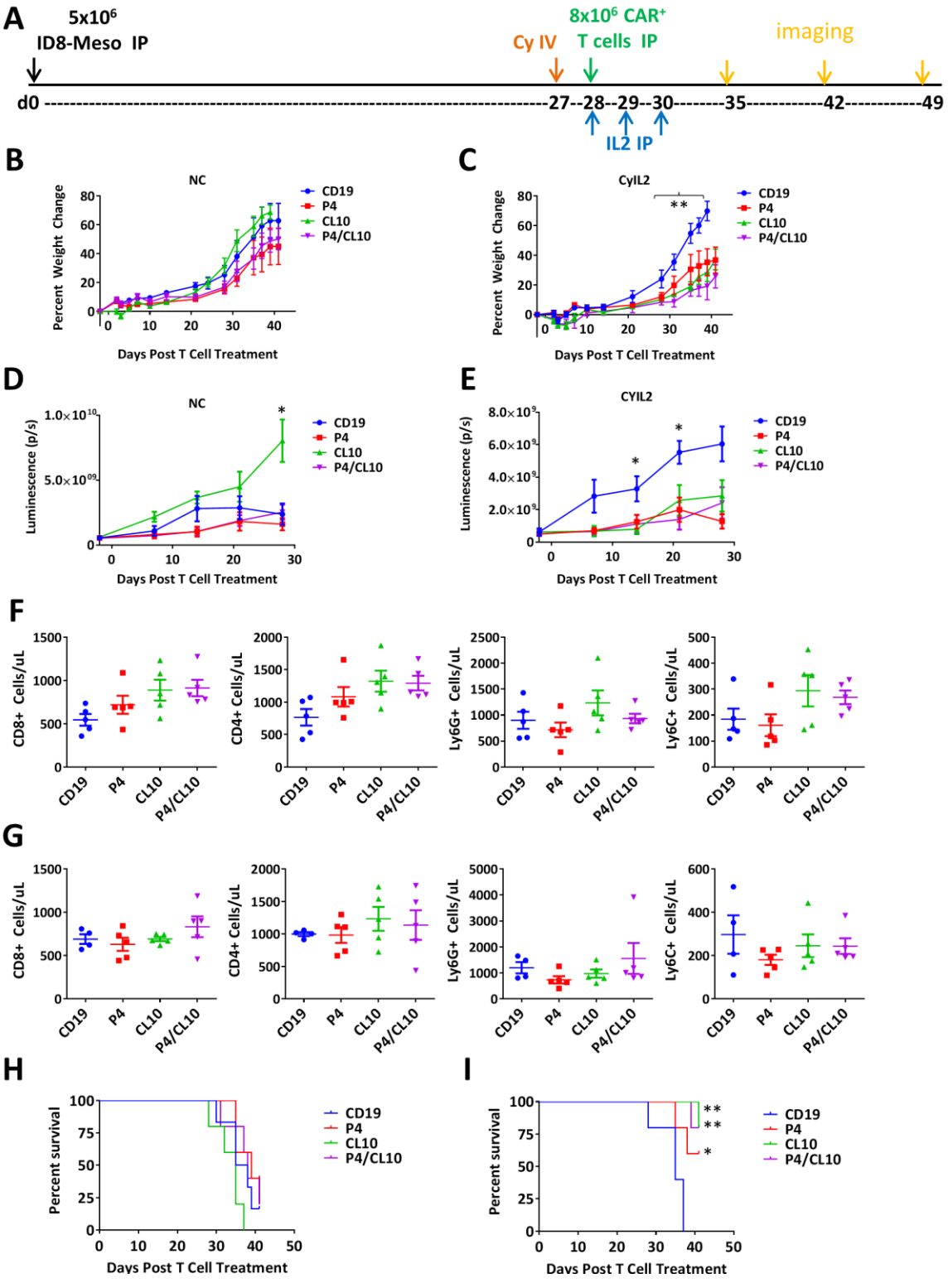

Figure 4.12 CL10 CAR T cells enhances tumor progression in NC mice and inhibits tumor growth in CyIL2 conditioned mice

(A) Treatment schedule of C57BL/6 mice implanted IP with $5x10^6$ $fLuc^+$ ID8-Meso and $8x10^6$ CAR^+ T cells on day 28 following tumor injection. P4 CAR T cells are specific for ID8-Meso and CD19 CAR T cells serve as a negative control. P4/CL10 groups received $4x10^6$ each of P4 and CL10 CAR^+ T cells. In CyIL2 conditioned mice, 150mg/kg cyclophosphamide (Cy) was given IV on day 27 and 15μg IL2 was given IP on days 28, 29, and 30. Non-conditioned (NC) mice were treated in the absence of Cy or IL2. Mice were monitored long term for tumor progression. Weight changes in **(B)** NC and **(C)** CyIL2 conditioned mice following transfer of CAR T cells. Tumor luminescence in **(D)** NC and **(E)** CyIL2 conditioned mice following T cell transfer. Peripheral blood cell counts on day 31 following T cell transfer in **(F)** NC and **(G)** CyIL2 conditioned mice. Survival in **(H)** NC and **(I)** CyIL2 conditioned mice following T cell transfer. Error bars represent mean ± SEM of n=5 mice per group.

Figure 4.13

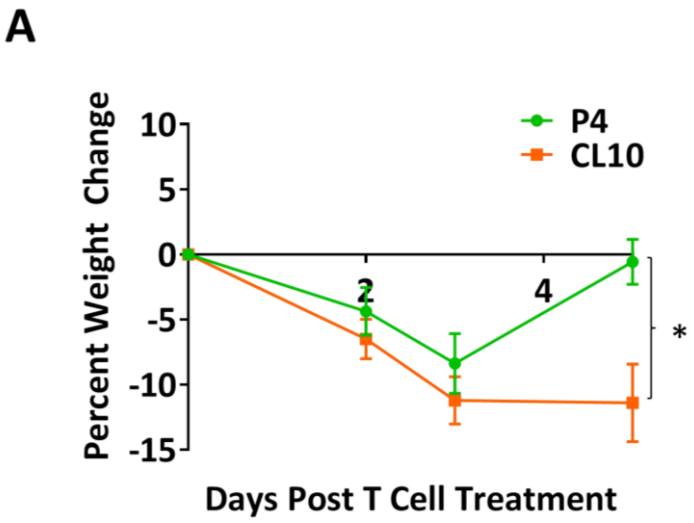

Figure 4.13 CL10 CAR T cells produce toxicity in non-tumor bearing mice

(A) Increased weight loss in 6-week old non-tumor bearing C57BL/6 mice treated according to the CyIL2 protocol with $8x10^6$ CL10 or control P4 CAR^+ T cells. Error bars represent mean ± SEM of n=5 mice per group. (* $P < .05$).

Figure 4.14

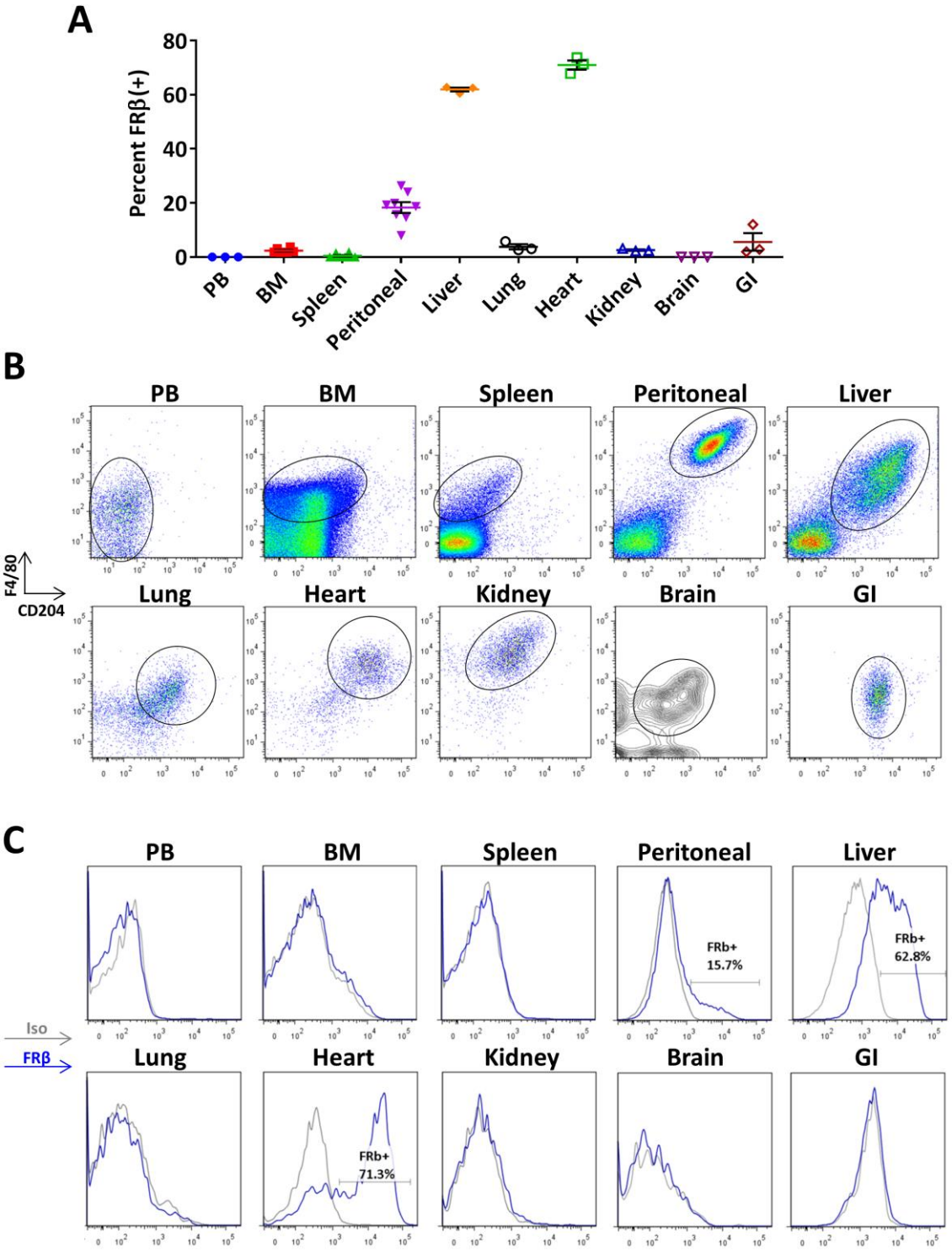

Figure 4.14 Expression of FRβ in healthy mouse tissue macrophages

(A) FRβ expression in tissue macrophages from different organs in healthy untreated C57BL/6 mice. At least 3 mice were analyzed for each tissue. Error bars represent mean ± SEM of n=3 to 8 mice per tissue. **(B)** F4/80 and CD204 expression of tissue resident myeloid ($CD45^+CD11b^+Ly6G^-$) cells in the indicated organs. The F4/80 vs CD204 gates shown were used to assess FRβ expression. **(C)** Representative macrophage FRβ expression histograms for each tissue. Frequency of $FR\beta^+$ cells is indicated in tissues with significant expression compared to isotype. Blue – CL10 IgG. Gray – rat IgG2a isotype. PB – peripheral blood, BM – bone marrow, GI – gastrointestinal tract.

Figure 4.15

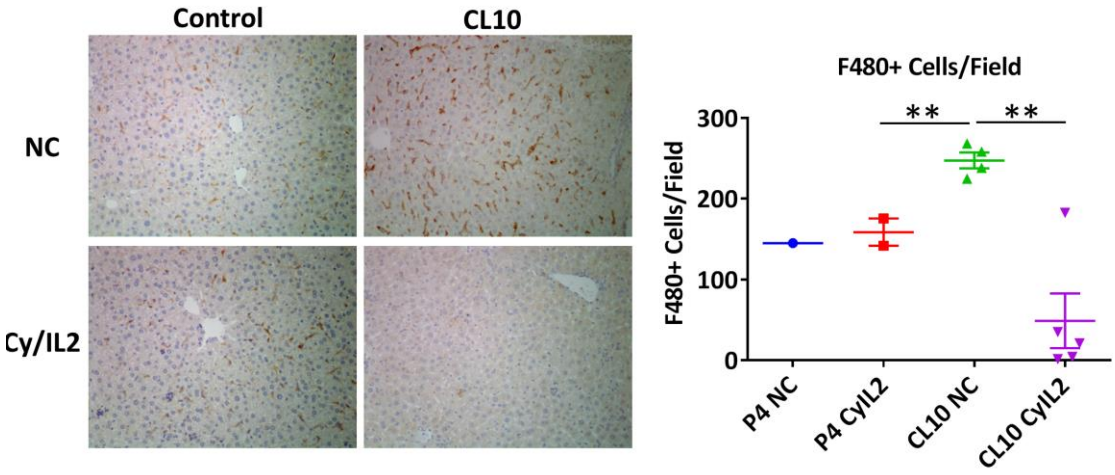

Figure 4.15 Liver Kupffer cells are depleted in CL10 CyIL2 treated mice

Kupffer cell depletion in CyIL2 CL10 treated mice as indicated by depletion of $F4/80^{+}$ cells. Left – representative 20X images of F4/80 IHC. Right – $F4/80^{+}$ cell quantification. n=1 to 5 mice per group. (** $P < .01$)

Figure 4.16

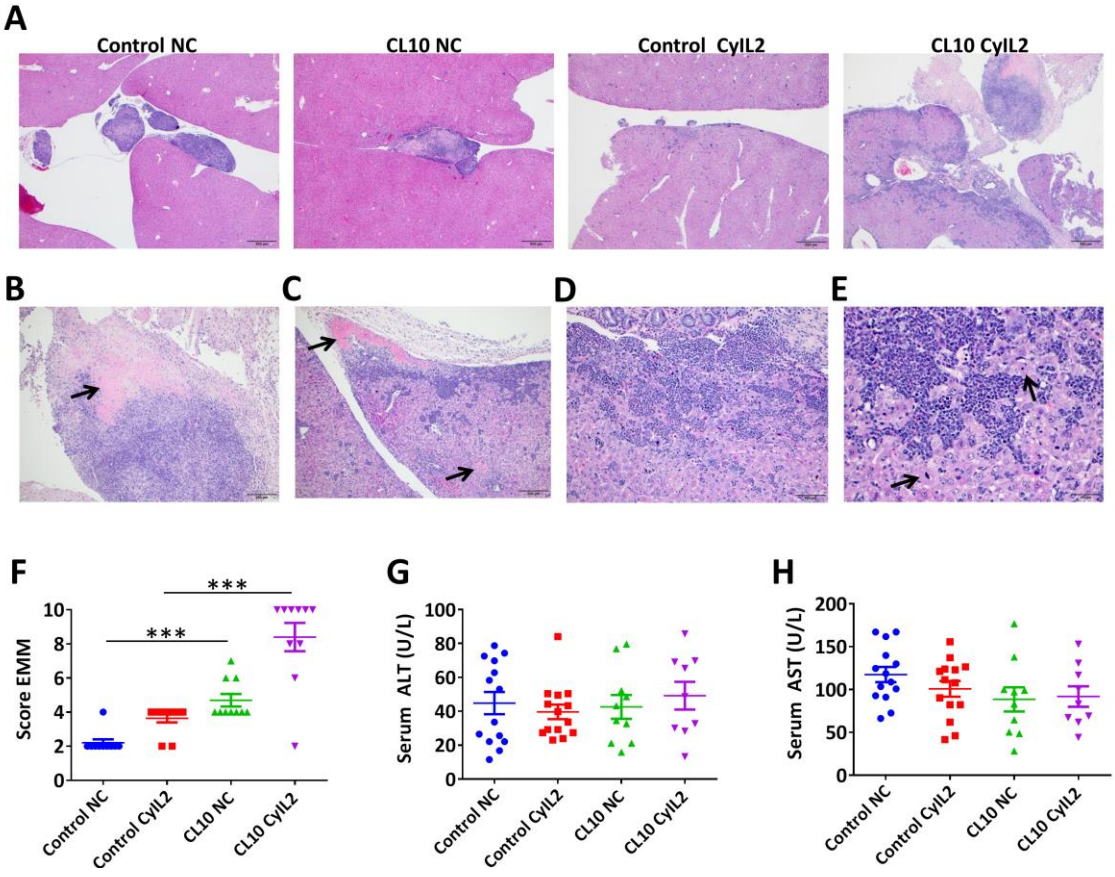

Figure 4.16 CL10 CAR T cell treatment leads to significant liver inflammation and necrosis

Fixed liver samples and serum from mice treated in experiments outlined in Figures 4.8, 4.9, and 4.10 were further analyzed for liver pathology. **(A)** Representative 4X H&E liver images from treated mice highlighting areas of carcinomatosis. **(B)** 10X image highlighting carcinomatosis with areas of tumor necrosis in CL10 CyIL2 treated mice. **(C)** 10X image highlighting liver necrosis in CL10 CyIL2 treated mice. **(D)** 10X image highlighting severe EMM in CL10 CyIL2 treated mice. **(E)** 40X image highlighting areas of hepatocyte regeneration (arrows point to multiple mitotic figures) surrounding severe EMM in CL10 CyIL2 treated mice. **(F)** EMM score (0=normal to 10=marked) from n=9-14 mice per treatment group. Error bars represent mean ± SEM. (*** P < .001) **(G)** Serum ALT 6-7 days post T cell transfer. **(H)** Serum AST 6-7 days post T cell transfer. Error bars represent mean ± SEM of n=9-14 mice per group. Control groups incorporate both CD19 and P4 CAR T cell treated mice from both ID8 and ID8-Meso tumor models.

Figure 4.17

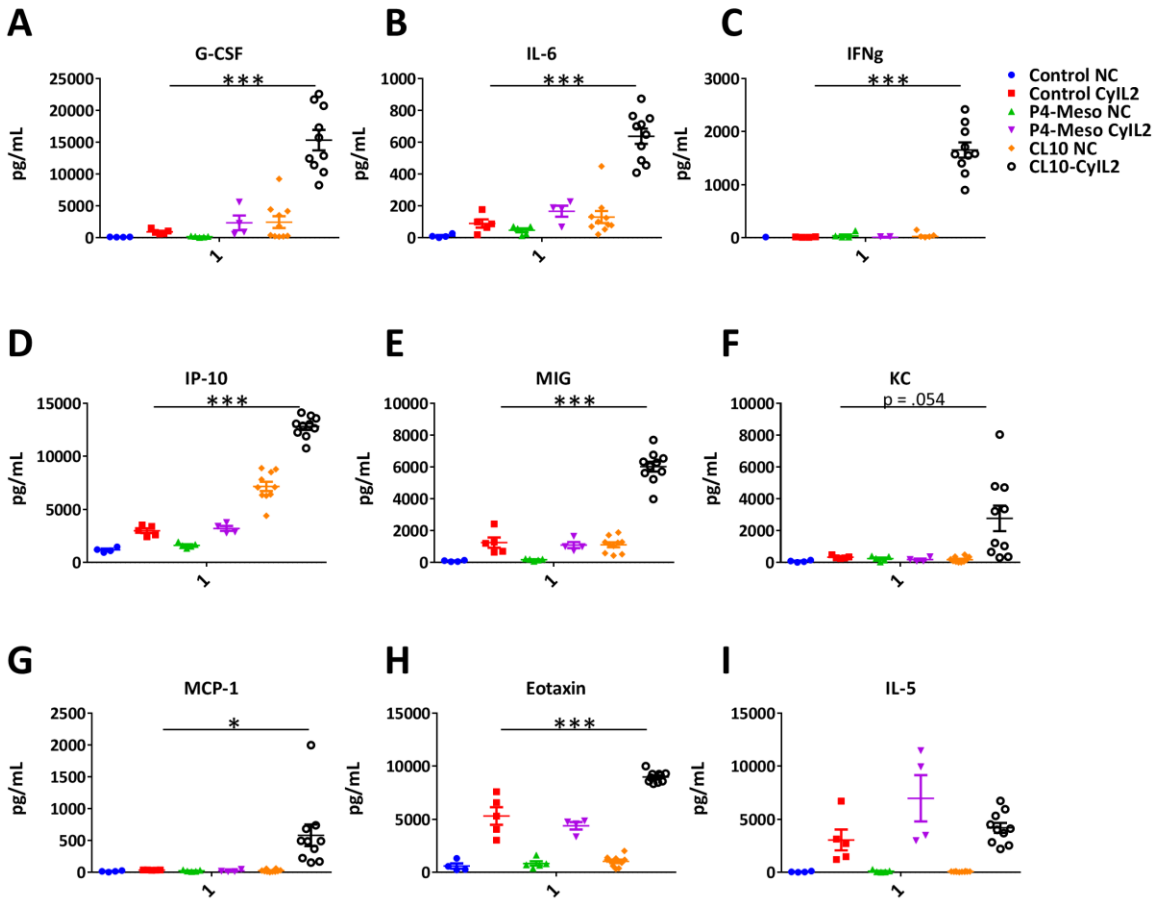

Figure 4.17 Chemokines and cytokines highly increased in CL10 CyIL2 treated mice

Luminex analysis of serum cytokine and chemokine levels were evaluated on day 3 following T cell transfer from mice treated in experiments outlined in Figures 4.8, 4.9, and 4.10. Cytokines that were substantially increased in CyIL2 conditioned CL10 CAR T cell treated mice include **(A)** G-CSF, **(B)** IL6, **(C)** IFNg, **(D)** IP-10, **(E)** MIG, **(F)** KC, **(G)** MCP-1, and **(H)** Eotaxin. **(I)** Serum IL-5 is highly increased likely due to cyclophosphamide/IL2 conditioning (CyIL2). Error bars represent mean ± SEM of n=5 to 10 mice per group. (* $P < .05$, ** $P < .01$, *** $P < .001$). P values were calculated to compare CyIL2 Control to CyIL2 CL10 CAR T cell treated groups. Control mice incorporate both CD19 in ID8-Meso and P4 in ID8 tumor models. P4-Meso designates P4 CAR T cell treated ID8-Meso tumor bearing mice.

Figure 4.18

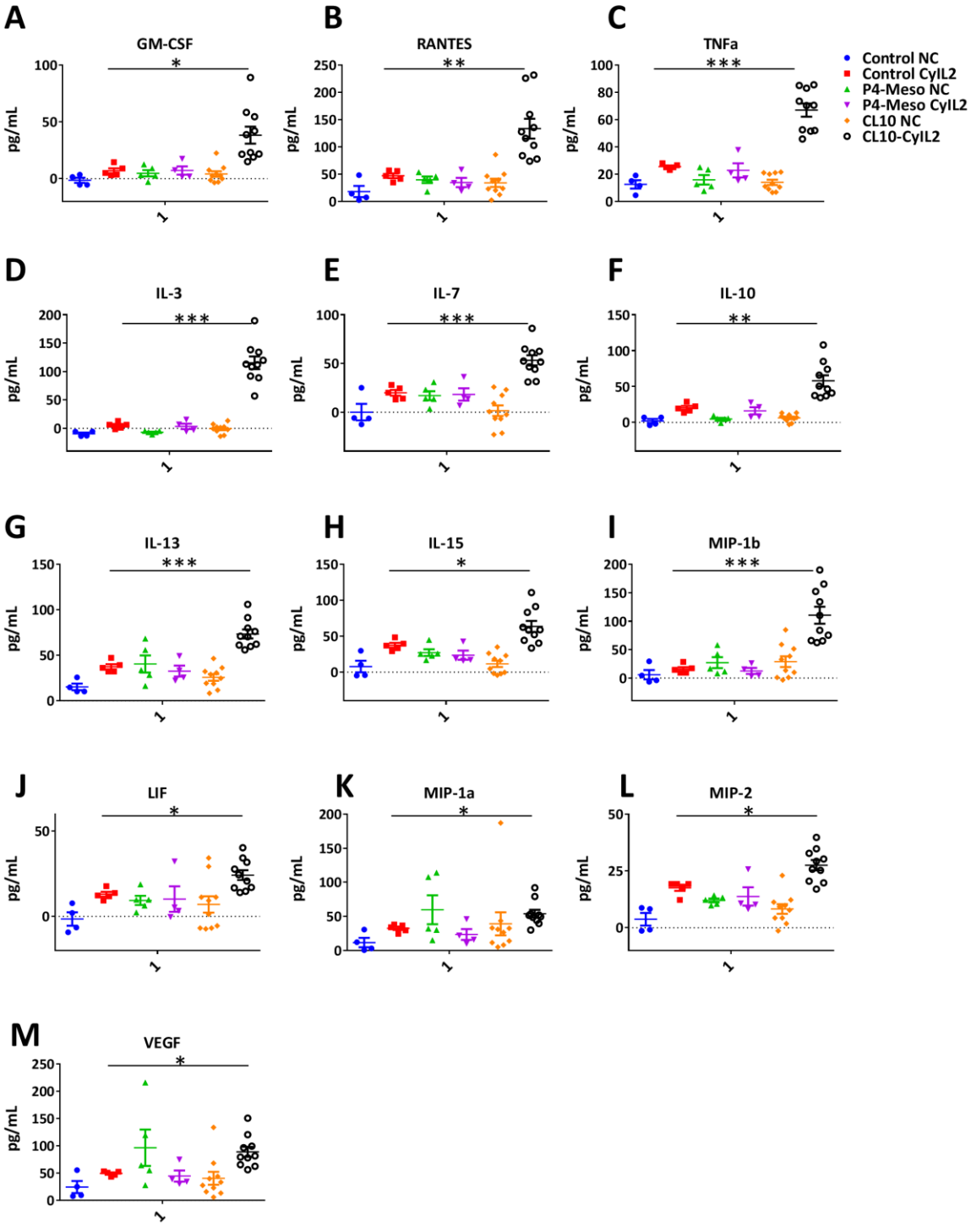

Figure 4.18 Chemokines and cytokines low/moderately increased in CL10 CyIL2 treated mice

Luminex analysis of serum cytokine and chemokine levels were evaluated on day 3 following T cell transfer from mice treated in experiments outlined in Figures 4.8, 4.9, and 4.10. Cytokines that were significantly but moderately (range < 200pg/mL) increased in CyIL2 conditioned CL10 CAR T cell treated mice include **(A)** GM-CSF, **(B)** RANTES, **(C)** TNFα, **(D)** IL-3, **(E)** IL-7, **(F)** IL-10, **(G)** IL-13, **(H)** IL-15, **(I)** MIP-1β, **(J)** LIF, **(K)** MIP-1α, **(L)** MIP-2, and **(M)** VEGF. Error bars represent mean ± SEM of n=5 to 10 mice per group. (* P < .05, ** P < .01, *** P < .001). P values were calculated to compare CyIL2 Control to CyIL2 CL10 CAR T cell treated groups. Control mice incorporate both CD19 in ID8-Meso and P4 in ID8 tumor models. P4-Meso designates P4 CAR T cell treated ID8-Meso tumor bearing mice.

Figure 4.19

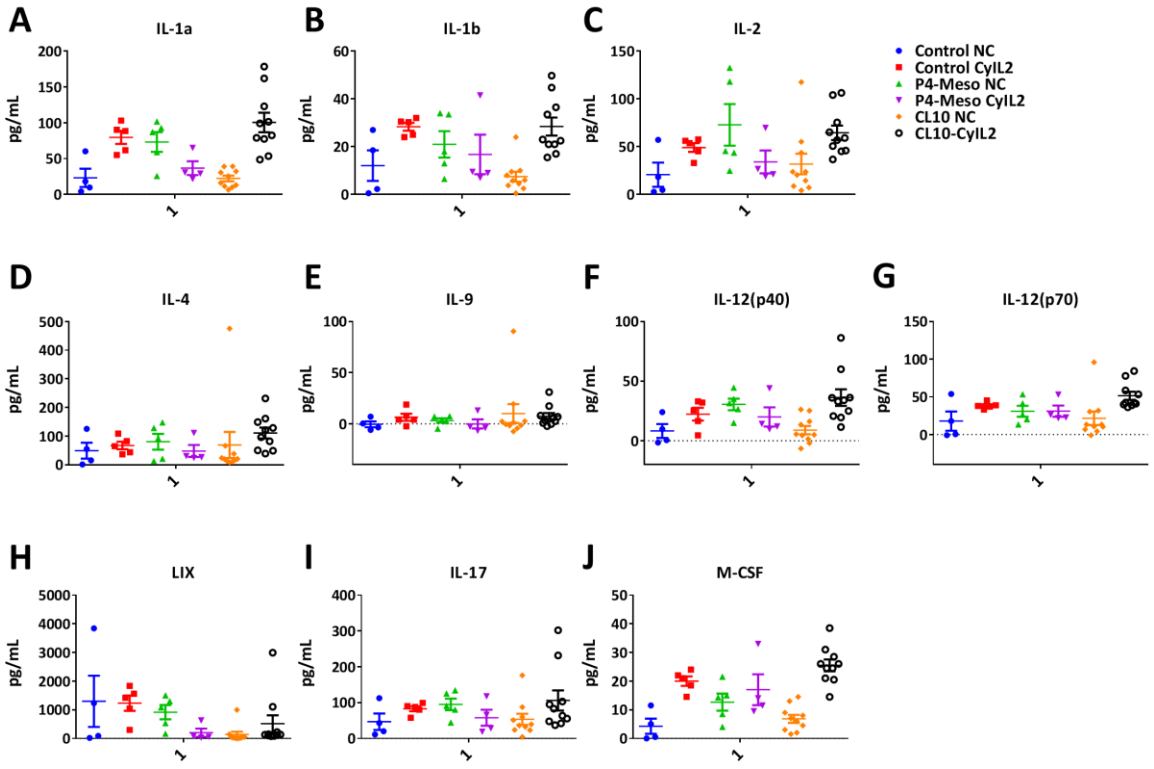

Figure 4.19 Chemokines and cytokines not changed in CL10 CyIL2 treated mice

Luminex analysis of serum cytokine and chemokine levels were evaluated on day 3 following T cell transfer from mice treated in experiments outlined in Figures 4.8, 4.9, and 4.10. Cytokines that were mostly unchanged between all groups include **(A)** IL-1a, **(B)** IL-1b, **(C)** IL-2, **(D)** IL-4, **(E)** IL-9, **(F)** IL-12p40, **(G)** IL-12p70, **(H)** LIX, **(I)** IL-17, **(J)** M-CSF. Error bars represent mean ± SEM of n=5 to 10 mice per group. Control mice incorporate both CD19 in ID8-Meso and P4 in ID8 tumor models. P4-Meso designates P4 CAR T cell treated ID8-Meso tumor bearing mice.

CHAPTER 5: FRβ CAR T cells: The Road Ahead

Other CAR T cells for AML

Since the inception of this thesis work, other CAR targets for AML have been evaluated and are currently in clinical development. To compare the potential benefits and limitations of FRβ CAR T cell therapy for AML, we will briefly summarize preclinical and clinical experience with other CARs currently in development to treat AML.

Expression of the carbohydrate tumor antigen, Lewis Y (LeY), has been reported in many types of cancer, and in 2010, Peinert and colleagues assessed its expression in AML and myeloma[250]. 46% of AML and 52% of MM patients expressed LeY. LeY CAR T cells were able to significantly lyse LeY^+ AML and MM cells. This group has previously published that although neutrophils express low levels of LeY, they were not significantly targeted by LeY CAR T cells, suggesting a favorable safety profile against normal tissues[251]. These findings led to the first CAR T cell trial for AML patients utilizing LeY CAR T cells[252]. Of the 4 patients treated, 3 had minimal residual disease (MRD) and one had active detectable disease in blood and BM before treatment. Infusions were well tolerated without high grade toxicity or cytokine storm. Transient decreases in blasts of the patient with detectable disease were observed. Trafficking to the BM and spleen and persistence of CAR T cells by PCR were also observed, however, all four patients relapsed with LeY^+ AML. These findings suggest that LeY CAR T cell therapy is feasible in AML patients, however, due to other contributing factors, possible suppression of T cells in patients, clinical efficacy is limited.

CD33 (or Siglec-3) is a sialic acid binding surface antigen of the myelomonocytic lineage[253]. It is expressed throughout myeloid differentiation, including in some $CD34^+$ HSCs. CD33 is widely

and highly expressed in the vast majority of AML patient tumors, and gemtuzumab ozogamicin, a toxin linked to a CD33-specific monoclonal antibody, was given accelerated FDA approval for use in AML patients in 2000. Unfortunately, after 9 years of experience with demonstrated suboptimal efficacy and the incidence of hepatotoxicity in a large percentage of patients[254], gemtuzumab ozogamicin was discontinued in 2010. Hepatotoxicity was likely related to the targeting of $CD33^+$ cells in the liver, such as liver Kupffer cells. Nevertheless, CD33 remained a target of interest for developing other immunotherapies for AML. In the first report of CD33-directed CARs, CD33 CARs were introduced into cytokine-induced killer (CIK) cells enriched for $CD3^+CD56^+CD8^+$ cells[188]. Addition of CD33 CAR significantly enhanced the anti-leukemic activity of CIK cells *in vitro*, however, increased cytotoxicity of CD33 CAR^+ CIKs was also noted against healthy $CD34^+$ HSCs. Follow-up experiments showed that CD33 CAR transduced EBV-specific T cells also displayed anti-leukemic activity *in vitro* and *in vivo*, however, colony formation following culture with $CD34^+$ HSCs was still impaired[189]. O'Hear and colleagues recently reported the use of a different CD33 CAR construct[255]. These CAR T cells also showed efficacy against primary AML and AML cell lines *in vitro*, and greatly improved survival of Molm13 xenograft tumor bearing mice *in vivo*. Again, CD33 CAR T cells significantly inhibited HSC colony formation *in vitro*. Kenderian et al created a CD33 CAR using the scFv from gemtuzumab and evaluated *in vivo* efficacy against primary AML and healthy human BM xenografts in mice[208]. CD33 CAR T cells display potent antitumor activity *in vivo* against AML cell line Molm14 and primary AML xenografts. In addition, the authors confirm the CD33 CAR-specific bone marrow toxicity suggested in the other studies with an *in vivo* model using human HSC xenografts. Despite the toxicity with gemtuzumab and preclinical evidence for normal HSC recognition *in vitro* and in mouse models, the Chinese PLA General Hospital is currently conducting a CD33 CAR trial for AML patients (NCT01864902). Results have been reported from one patient[256] with relapsed, refractory AML and pancytopenia. The patient experienced a

significant but transient decrease in $CD33^+$ blasts which was accompanied by fever and cytokine spikes that were manageable. Although CAR^+ T cells were still detectable by PCR, the disease rapidly progressed. Of interest, no hepatotoxic effects were observed. Although the antitumor effects were mild, the infusion of CD33 CAR T cells was reasonably well tolerated in this patient. More patients will need to be evaluated before safety concerns about CD33 targeting by CAR T cells can be alleviated.

CD123, the IL3 receptor α chain, is also highly expressed in AML and HSCs but has decreased expression in mature myeloid lineage cells. CD123 antibody-based therapies have not resulted in BM suppression, but efficacy against AML has been limited[257]. Like CD33, many groups have now evaluated CD123 CAR T cells in preclinical models. Tettamanti and colleagues found that CD123 CAR CIK cells showed comparable antitumor activity to CD33 but had a somewhat decreased inhibition of HSC colony formation[207]. CD123 CIK cells also targeted $CD14^+$ monocytes at roughly the same level as CD33. Mardiros *et al* compared the activity of two different anti-CD123 scFvs in CAR T cells[190]. Both CARs displayed potent anti-leukemic effects *in vitro* and *in vivo* and were capable of eliminating $CD123^+CD34^+$ cells from both leukemic and normal BM. Pizzitola also compared CD33 to CD123 CAR CIKs *in vivo* using primary AML and healthy $CD34^+$ HSCs in mouse models[258]. CD123 CAR T cells displayed comparable anti-leukemia activity and improved safety profile compared to CD33 against healthy $CD34^+$ cells *in vitro* and *in vivo*. On the other hand, Gill and colleagues described $CD34^+$ bone marrow destruction in humanized mice using CD123 CAR T cells[191]. Differences in these outcomes may be the result of the different CAR T cell constructs used (including scFv and costimulation), transduction and expansion methods, and T cell doses used for *in vivo* models. While some studies showed an improved safety profile for CD123 compared to CD33 in terms of the potential for healthy BM HSC elimination, this is still a major concern in applying CD123 CAR T cells in

the clinic. CD123 may have a better safety profile when considering expression in mature myeloid cells, like liver Kupffer cells. In a setting where BM transplant is available, CD123 CAR T cells may be a safer alternative to CD33. A clinical trial (NCT02159495) is planned, but not yet recruiting patients, to evaluate CD123 CAR T cells in AML.

CAR T cells specific for CD44v6, an isoform of the cell adhesion molecule CD44, have also been evaluated in preclinical models of AML and MM[259]. This target is particularly intriguing because it was demonstrated to be necessary for tumor growth and engraftment *in vivo*, minimizing the chance of tumor escape due to antigen loss. In addition CD44v6 is not expressed in hematopoietic progenitors and colony formation was not inhibited *in vitro* or *in vivo*. If successfully applied without toxicity, CD44v6 could be a promising CAR target for many indications including hematological and solid tumors. However, a large percentage of patients treated with bivatuzumab, a CD44v6-specific monoclonal antibody tested in clinical trials for head and neck squamous cell carcinoma[260] and metastatic breast cancer[261], experienced skin disorders including one fatal report of epidermal necrolysis[260]. These off-tumor effects, likely due to expression of CD44v6 in keratinocytes, resulted in discontinuation of clinical development of bivatuzumab. Interestingly, Casucci and colleagues report that while CD44v6 CAR T cells show high activity against AML, MM, and healthy monocytes, they were not reactive against primary human keratinocytes *in vitro*. While this finding is encouraging, it is unknown whether the low toxicity profile against keratinocytes *in vitro* will hold up during clinical use of CD44v6 CAR T cells in patients.

FRβ CAR T cells show a reduced likelihood to produce BM HSC toxicity

Although LeY and CD44v6 CAR T cells have been evaluated for AML, they are not myeloid restricted and their respective toxicities would likely result from recognition of antigen in non-

myeloid tissues. CD123, CD33, and FRβ have all been described as nearly exclusive to the myeloid lineage. However, there are noteworthy distinctions in expression of these molecules during myeloid lineage differentiation. CD123 is highly expressed on $CD34^+$ HSCs and myeloid progenitors in the bone marrow with reduced expression on mature monocytes and macrophages. CD33 is expressed on some $CD34^+$ HSCs, myeloid progenitors, peripheral monocytes and some tissue macrophages, including liver Kupffer cells and lung alveolar macrophages[208]. FRβ is not co-expressed with CD34 or CD123 in bone marrow HSCs and myeloid progenitors but shows high expression in $CD33^+$ and $CD14^+$ monocytes (**Figure 5.1**).

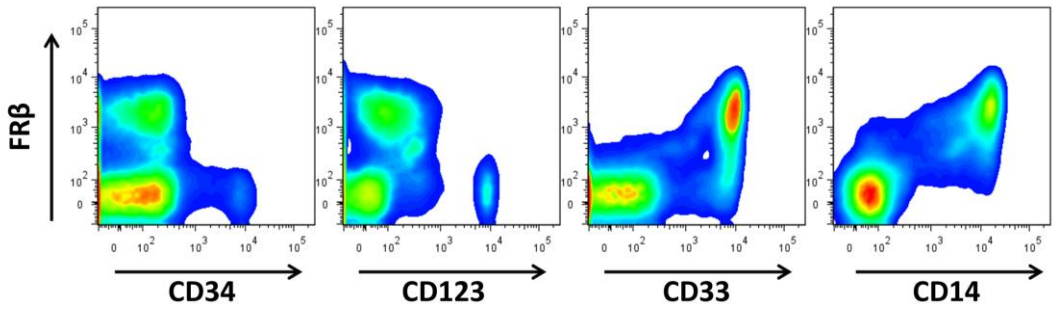

Figure 5.1 Co-expression of FRβ and CD34, CD123, CD33, and CD14 in healthy donor bone marrow

Due to demonstrated expression in HSCs, both CD33 and CD123 CAR T cells show the potential to eliminate healthy $CD34^+$ HSCs in the bone marrow microenvironment. Our experiments with FRβ reveal its expression is induced at a later phase of myeloid differentiation. These findings, coupled with our *in vivo* model using humanized mice engrafted with human $CD34^+$ BM, highly suggest a decreased risk of BM HSC toxicity in AML patients treated with FRβ CAR T cells compared to CD123 or CD33. CD123 and CD33 CAR T cells could potentially be safely applied in patients who are eligible for BM transplant following CAR T cell therapy. However, many patients are not eligible due to age[262] or lack of an appropriate donor.

FRβ CAR T cells recognize healthy monocytes

Like CD33 and CD44v6, FRβ is highly expressed in healthy peripheral monocytes. Monocytopenia would be an expected dose limiting toxicity in patients treated with CAR T cells targeting these antigens. We and Kenderian[208] have demonstrated the efficacy of transient mRNA CAR T cells for FRβ$^+$ and CD33$^+$ AML, and Casucci[259] showed that incorporation of an inducible caspase 9 suicide gene allowed for the return of monocytes *in vivo* following selective elimination of CD44v6 CAR T cells. These preclinical models suggest that transient CAR expression could be applied to eliminate tumor cells in the short term, following which CAR T cell deletion could allow for repopulation of peripheral monocytes.

Another consideration is that high levels of antigen positive monocytes in patients would provide an alternative source for T cell activation, which could contribute to cytokine release syndrome observed in some CAR T cell treated patients. A higher tumor burden seemed to correlate with the severity of cytokine storm in at least one study[263]. Therefore, pre-conditioning with myeloablative regimens could be added to clinical protocols to essentially "de-bulk" the patient of antigen positive target cells before CAR T cell transfer. These considerations could increase the chances for safe application of FRβ and other myeloid-directed CAR T cells.

Combination therapy with FRβ CAR T cells: couldn't we all work together?

A growing array of potential CAR T cell targets in AML will likely benefit patients in the future as we learn to safely implement CAR T cells. Not all patients' tumors will express any one antigen, and heterogeneity within a given patient increases the likelihood that someone treated with one CAR T cell specificity could relapse with antigen-negative disease. CD19 is one of the most ubiquitously expressed antigens in ALL, and CD19-negative disease relapse has been

observed following CAR therapy[122]. While the safety profiles of each CAR target antigen must be thoroughly investigated individually, parallel or sequential treatment could eventually be applied to target multiple AML tumor antigens in the same patient. Combined therapy of safe and effective CAR T cells of multiple specificities will likely improve CAR T cell efficacy and long term survival of patients in the future.

FRβ CAR T cells could also be beneficial in combination with other types of AML therapy. Already noted, myeloablative therapy and FRβ CAR T cells could be applied before stem cell transplant to increase the safety of FRβ CAR T cells and promote longer remissions following BM transplant. As highlighted in Chapter 2, combination with ATRA (already FDA approved for use in AML patients) would likely provide augmented activity of FRβ CAR T cells through antigen upregulation on AML blasts.

FRβ CAR T cells: what about tissue macrophages?

While FRβ has been observed on mature macrophages at sites of inflammation and tumor growth, expression in healthy tissue macrophages is not well characterized. We attempted to optimize our high affinity m923-IgG for use in IHC to evaluate FRβ expression in tissue sections from healthy organs, however, we were unable to achieve consistent staining. Another group recently published FRβ IHC expression in over 900 sections from human malignancies[168], but unfortunately, this did not include any non-tumor tissue sections. While this study supports the rationale for applying FRβ-directed therapy to eliminate tumor associated macrophages (TAMs), expression in healthy tissue macrophages should be investigated more thoroughly to evaluate the relative specificity of FRβ to tumor localized macrophages. This question will need to be more adequately addressed in order to accurately predict off-tumor toxicity in patients treated with FRβ CAR T cells. Although no hepatotoxicity was observed in one patient treated with CD33 CAR T

cells, the high liver toxicity in patients treated with gemtuzumab was attributed to destruction of $CD33^+$ cells (most likely Kupffer cells) in the liver. The strong correlation between CD33 and FRβ in bone marrow and peripheral blood monocytes suggests that tissue macrophage expression of these antigens may overlap as well.

FRβ CAR T cells: Lessons from mouse models

Our mouse model of FRβ-directed CAR T cell therapy also highlights the potential for toxicity associated with recognition of macrophages in otherwise healthy organs. In the setting of CyIL2 preconditioning, CL10 CAR T cells caused systemic aberrant myelopoiesis and on-target depletion of liver Kupffer cells. Although inflammation and toxicity ultimately resolved in CL10 treated C57BL/6 mice, even transient elimination of mature macrophages elicited a dramatic and potentially dangerous degree of systemic immune activation. It is possible that longer survival of CL10 CAR T cells would have ultimately led to mortality of the animals. As discussed in Chapter 4, future experiments will be needed to fully understand the nature of the toxicity produced using CL10 CAR T cells. We could then utilize the phenotype in our mouse model to evaluate which potential intervening therapies, such as neutralizing systemic cytokines IL6 or TNFα, are likely to improve the safety profile of macrophage-specific CAR T cells.

Our experiments with CL10 CAR T cells warrant caution for clinical development of FRβ CAR T cells in patients, particularly in the setting of non-myeloablative lymphodepletion and IL2. However, the relevance of FRβ-directed CAR T cells in mice to their application in humans is difficult to gauge because of the disparate distribution of FRβ during myeloid differentiation in mice and humans (**Figure 5.2**).

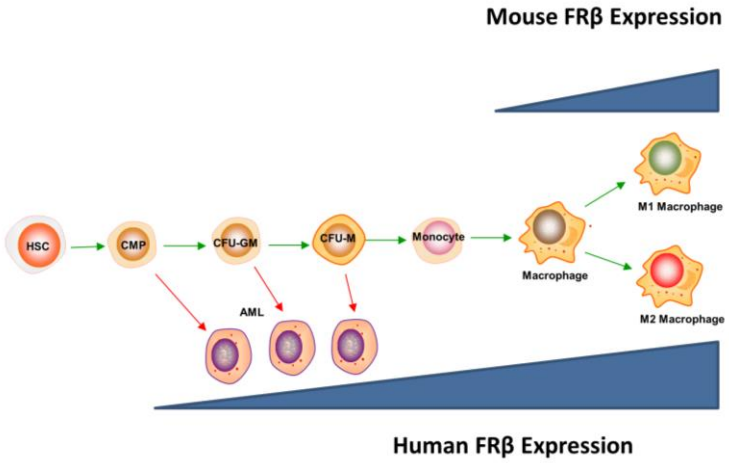

Figure 5.2 Expression of mouse and human FRβ during myeloid differentiation

Expression of FRβ in humans begins at the myeloid progenitor cell stage, with increasing expression along differentiation to monocytes. AML derived from these myeloid progenitor cells also expresses FRβ in humans. As discussed above, evidence for high expression in mature macrophages has also been suggested, however, the tissue distribution of macrophage FRβ expression in healthy individuals is not well characterized. In C57BL/6 mice, FRβ expression is absent in bone marrow myeloid progenitor cells, Trib2 induced AML (data not shown), bone marrow and peripheral blood monocytes, and most tissue macrophages. Therefore, the potential for bone marrow and monocyte toxicity could not be assessed using FRβ CAR T cells in mice. Like in humans, mouse and rat macrophages in models of inflammation and tumor growth show increased expression of FRβ. We also confirmed high expression of FRβ in liver and cardiac macrophages in healthy mice that was absent in macrophages from many other tissues. These findings suggest distinct control of FRβ expression in different tissue microenvironments. Future experiments will be needed to understand how the different tissue environments mediate macrophage phenotype. Again, in-depth analyses of tissue macrophages in humans are needed to evaluate whether differential FRβ tissue macrophage expression is reproducible in humans and

whether liver and cardiac macrophages show similarly high FRβ expression. An understanding of the potential sources of off-tumor CAR T cell attack will be invaluable for designing safe and effective FRβ CAR T cell therapies. For example, myeloablation or macrophage-specific elimination could be used in preconditioning therapies to decrease off-tumor T cell activation in healthy organs.

For consideration of CAR T cell therapy for TAM elimination in solid tumors, our experiments in the ID8 tumor model suggest that CL10 CAR T cells can eliminate FRβ^{+} TAMs in the tumor microenvironment and provide a significant but short survival benefit. However, due to the combination of short term persistence of CAR T cells in our mouse model and increased recruitment of Ly6C^{HI} monocytes we were unable to fulfill our goal of modeling long term depletion of TAMs with CAR T cells for the duration of tumor growth. Human peripheral blood monocytes, unlike in mice, highly express FRβ. The limitations associated with modeling FRβ in mice would not apply. Since FRβ is expressed earlier in myeloid differentiation, FRβ-specific CAR T cells would eliminate both mature TAMs and TAM precursor monocytes in humans. Therefore, long term depletion of human TAMs would likely be possible. Another population of immunosuppressive tumor associated myeloid cells known as MDSCs have been described in mouse tumor models and human patients. They resemble immature myeloid cells of either granulocytic (Ly6G^{+}) or monocytic (Ly6C^{+}) origin in mice, and both granulocytic (CD66b^{+}) and monocytic (CD14^{+}) MDSCs have been described in human cancer patients. Since FRβ is not expressed in immature Ly6C^{+} myeloid cells in mice, we would not be able to assess CAR-mediated MDSC elimination in our mouse model. However, in humans, CD14^{+} monocytic MDSCs would likely express FRβ. We hypothesize that FRβ-targeted CAR T cells have the potential to disrupt the tumor-myeloid cell axis of immunosuppression in human cancer patients with the potential to eliminate FRβ^{+} TAMs, systemic and tumor-localized MDSCs, and inhibit

repopulation of TAMs by elimination of peripheral monocytes. Unfortunately we are unable to model these aspects of FRβ CAR T cells in mouse models due to the differences in FRβ expression along myeloid-lineage differentiation. In addition, the major safety concerns for CAR T cells redirected against myeloid antigens would need to be addressed before clinical application for solid tumors.

With the excitement and potential of CAR T cells in cancer therapy, the field is constantly innovating new ideas for finer control of CAR T cell activity. Drug-inducible suicide genes[200] and newly described "ON-switches" for CAR induction[264] are likely only the beginning in the modern era of genome engineering, which will soon allow for precision network control and fine-tuned manipulation of engineered T cells.

REFERENCES

1. Heron M. Deaths: Leading Causes for 2011. *Natl Vital Stat Rep*. 2015;64(7):1-96.
2. Statistics at a Glance: The Burden of Cancer in the United States. Vol. 2015.
3. Hanahan D, Weinberg RA. The hallmarks of cancer. *Cell*. 2000;100(1):57-70.
4. Society AC. The History of Cancer; 2014.
5. Dvorak HF. Tumors: wounds that do not heal. Similarities between tumor stroma generation and wound healing. *N Engl J Med*. 1986;315(26):1650-1659.
6. Hanahan D, Weinberg RA. Hallmarks of cancer: the next generation. *Cell*. 2011;144(5):646-674.
7. McCarthy EF. The toxins of William B. Coley and the treatment of bone and soft-tissue sarcomas. *Iowa Orthop J*. 2006;26:154-158.
8. Kaplan DH, Shankaran V, Dighe AS, et al. Demonstration of an interferon gamma-dependent tumor surveillance system in immunocompetent mice. *Proc Natl Acad Sci U S A*. 1998;95(13):7556-7561.
9. Shankaran V, Ikeda H, Bruce AT, et al. IFNgamma and lymphocytes prevent primary tumour development and shape tumour immunogenicity. *Nature*. 2001;410(6832):1107-1111.
10. Dunn GP, Old LJ, Schreiber RD. The three Es of cancer immunoediting. *Annu Rev Immunol*. 2004;22:329-360.
11. Clemente CG, Mihm MC, Jr., Bufalino R, Zurrida S, Collini P, Cascinelli N. Prognostic value of tumor infiltrating lymphocytes in the vertical growth phase of primary cutaneous melanoma. *Cancer*. 1996;77(7):1303-1310.
12. Mahmoud SM, Paish EC, Powe DG, et al. Tumor-infiltrating CD8+ lymphocytes predict clinical outcome in breast cancer. *J Clin Oncol*. 2011;29(15):1949-1955.
13. Zhang L, Conejo-Garcia JR, Katsaros D, et al. Intratumoral T cells, recurrence, and survival in epithelial ovarian cancer. *N Engl J Med*. 2003;348(3):203-213.
14. Shibuya TY, Nugyen N, McLaren CE, et al. Clinical significance of poor CD3 response in head and neck cancer. *Clin Cancer Res*. 2002;8(3):745-751.
15. Dieu-Nosjean MC, Antoine M, Danel C, et al. Long-term survival for patients with non-small-cell lung cancer with intratumoral lymphoid structures. *J Clin Oncol*. 2008;26(27):4410-4417.
16. Al-Shibli KI, Donnem T, Al-Saad S, Persson M, Bremnes RM, Busund LT. Prognostic effect of epithelial and stromal lymphocyte infiltration in non-small cell lung cancer. *Clin Cancer Res*. 2008;14(16):5220-5227.
17. Nakakubo Y, Miyamoto M, Cho Y, et al. Clinical significance of immune cell infiltration within gallbladder cancer. *Br J Cancer*. 2003;89(9):1736-1742.
18. Mills CD, Kincaid K, Alt JM, Heilman MJ, Hill AM. M-1/M-2 macrophages and the Th1/Th2 paradigm. *J Immunol*. 2000;164(12):6166-6173.
19. Mantovani A, Sozzani S, Locati M, Allavena P, Sica A. Macrophage polarization: tumor-associated macrophages as a paradigm for polarized M2 mononuclear phagocytes. *Trends Immunol*. 2002;23(11):549-555.
20. Zhang QW, Liu L, Gong CY, et al. Prognostic significance of tumor-associated macrophages in solid tumor: a meta-analysis of the literature. *PLoS One*. 2012;7(12):e50946.

21. Gazzaniga S, Bravo AI, Guglielmotti A, et al. Targeting tumor-associated macrophages and inhibition of MCP-1 reduce angiogenesis and tumor growth in a human melanoma xenograft. *J Invest Dermatol*. 2007;127(8):2031-2041.
22. Popivanova BK, Kostadinova FI, Furuichi K, et al. Blockade of a chemokine, CCL2, reduces chronic colitis-associated carcinogenesis in mice. *Cancer Res*. 2009;69(19):7884-7892.
23. Zhu X, Fujita M, Snyder LA, Okada H. Systemic delivery of neutralizing antibody targeting CCL2 for glioma therapy. *J Neurooncol*. 2011;104(1):83-92.
24. Paulus P, Stanley ER, Schafer R, Abraham D, Aharinejad S. Colony-stimulating factor-1 antibody reverses chemoresistance in human MCF-7 breast cancer xenografts. *Cancer Res*. 2006;66(8):4349-4356.
25. Zeisberger SM, Odermatt B, Marty C, Zehnder-Fjallman AH, Ballmer-Hofer K, Schwendener RA. Clodronate-liposome-mediated depletion of tumour-associated macrophages: a new and highly effective antiangiogenic therapy approach. *Br J Cancer*. 2006;95(3):272-281.
26. Pulaski HL, Spahlinger G, Silva IA, et al. Identifying alemtuzumab as an anti-myeloid cell antiangiogenic therapy for the treatment of ovarian cancer. *J Transl Med*. 2009;7:49.
27. Bak SP, Walters JJ, Takeya M, Conejo-Garcia JR, Berwin BL. Scavenger receptor-A-targeted leukocyte depletion inhibits peritoneal ovarian tumor progression. *Cancer Res*. 2007;67(10):4783-4789.
28. Buhtoiarov IN, Lum H, Berke G, Paulnock DM, Sondel PM, Rakhmilevich AL. CD40 ligation activates murine macrophages via an IFN-gamma-dependent mechanism resulting in tumor cell destruction in vitro. *J Immunol*. 2005;174(10):6013-6022.
29. Beatty GL, Chiorean EG, Fishman MP, et al. CD40 agonists alter tumor stroma and show efficacy against pancreatic carcinoma in mice and humans. *Science*. 2011;331(6024):1612-1616.
30. Kerkar SP, Leonardi AJ, van Panhuys N, et al. Collapse of the tumor stroma is triggered by IL-12 induction of Fas. *Mol Ther*. 2013;21(7):1369-1377.
31. Pyonteck SM, Akkari L, Schuhmacher AJ, et al. CSF-1R inhibition alters macrophage polarization and blocks glioma progression. *Nat Med*. 2013;19(10):1264-1272.
32. Stockwin LH, McGonagle D, Martin IG, Blair GE. Dendritic cells: immunological sentinels with a central role in health and disease. *Immunol Cell Biol*. 2000;78(2):91-102.
33. Lotze MT. Getting to the source: dendritic cells as therapeutic reagents for the treatment of patients with cancer. *Ann Surg*. 1997;226(1):1-5.
34. Enk AH, Jonuleit H, Saloga J, Knop J. Dendritic cells as mediators of tumor-induced tolerance in metastatic melanoma. *Int J Cancer*. 1997;73(3):309-316.
35. Stoitzner P, Green LK, Jung JY, et al. Inefficient presentation of tumor-derived antigen by tumor-infiltrating dendritic cells. *Cancer Immunol Immunother*. 2008;57(11):1665-1673.
36. Piccard H, Muschel RJ, Opdenakker G. On the dual roles and polarized phenotypes of neutrophils in tumor development and progression. *Crit Rev Oncol Hematol*. 2012;82(3):296-309.
37. Fridlender ZG, Sun J, Kim S, et al. Polarization of tumor-associated neutrophil phenotype by TGF-beta: "N1" versus "N2" TAN. *Cancer Cell*. 2009;16(3):183-194.
38. Rodriguez PC, Quiceno DG, Zabaleta J, et al. Arginase I production in the tumor microenvironment by mature myeloid cells inhibits T-cell receptor expression and antigen-specific T-cell responses. *Cancer Res*. 2004;64(16):5839-5849.
39. Rodriguez PC, Hernandez CP, Quiceno D, et al. Arginase I in myeloid suppressor cells is induced by COX-2 in lung carcinoma. *J Exp Med*. 2005;202(7):931-939.

40. Kusmartsev S, Nagaraj S, Gabrilovich DI. Tumor-associated CD8+ T cell tolerance induced by bone marrow-derived immature myeloid cells. *J Immunol*. 2005;175(7):4583-4592.
41. Nelson BH. CD20+ B cells: the other tumor-infiltrating lymphocytes. *J Immunol*. 2010;185(9):4977-4982.
42. Beyer M, Schultze JL. Regulatory T cells in cancer. *Blood*. 2006;108(3):804-811.
43. Mocellin S, Pasquali S, Rossi CR, Nitti D. Interferon alpha adjuvant therapy in patients with high-risk melanoma: a systematic review and meta-analysis. *J Natl Cancer Inst*. 2010;102(7):493-501.
44. Gleave ME, Elhilali M, Fradet Y, et al. Interferon gamma-1b compared with placebo in metastatic renal-cell carcinoma. Canadian Urologic Oncology Group. *N Engl J Med*. 1998;338(18):1265-1271.
45. Gollob JA, Mier JW, Veenstra K, et al. Phase I trial of twice-weekly intravenous interleukin 12 in patients with metastatic renal cell cancer or malignant melanoma: ability to maintain IFN-gamma induction is associated with clinical response. *Clin Cancer Res*. 2000;6(5):1678-1692.
46. Schwartzentruber DJ. Guidelines for the safe administration of high-dose interleukin-2. *J Immunother*. 2001;24(4):287-293.
47. Kirkwood JM, Bender C, Agarwala S, et al. Mechanisms and management of toxicities associated with high-dose interferon alfa-2b therapy. *J Clin Oncol*. 2002;20(17):3703-3718.
48. Fisher RI, Rosenberg SA, Fyfe G. Long-term survival update for high-dose recombinant interleukin-2 in patients with renal cell carcinoma. *Cancer J Sci Am*. 2000;6 Suppl 1:S55-57.
49. Zhang L, Morgan RA, Beane JD, et al. Tumor-infiltrating lymphocytes genetically engineered with an inducible gene encoding interleukin-12 for the immunotherapy of metastatic melanoma. *Clin Cancer Res*. 2015;21(10):2278-2288.
50. Daud AI, DeConti RC, Andrews S, et al. Phase I trial of interleukin-12 plasmid electroporation in patients with metastatic melanoma. *J Clin Oncol*. 2008;26(36):5896-5903.
51. Gupta R, Emens LA. GM-CSF-secreting vaccines for solid tumors: moving forward. *Discov Med*. 2010;10(50):52-60.
52. Neller MA, Lopez JA, Schmidt CW. Antigens for cancer immunotherapy. *Semin Immunol*. 2008;20(5):286-295.
53. Suntharalingam G, Perry MR, Ward S, et al. Cytokine storm in a phase 1 trial of the anti-CD28 monoclonal antibody TGN1412. *N Engl J Med*. 2006;355(10):1018-1028.
54. Sznol M HF, Margolin K, McDermott DF, Ernstoff MS, Kirkwood JM,. Phase I study of BMS-663513, a fully human anti-CD137 agonist monoclonal

antibody, in patients (pts) with advanced cancer (CA). *Journal of Clinical Oncology*. 2008;26(15):Suppl 3007.
55. Yonezawa A, Dutt S, Chester C, Kim J, Kohrt HE. Boosting Cancer Immunotherapy with Anti-CD137 Antibody Therapy. *Clin Cancer Res*. 2015;21(14):3113-3120.
56. Curti BD, Kovacsovics-Bankowski M, Morris N, et al. OX40 is a potent immune-stimulating target in late-stage cancer patients. *Cancer Res*. 2013;73(24):7189-7198.
57. Stephen Maxted Ansell DWN, Ian Flinn, Howard A. Burris, Shira Naomi Dinner, Victor Manuel Villalobos, Branimir I. Sikic, Matthew Hiram Taylor, Lana Pilja, Thomas R. Hawthorne, Michael Jay Yellin, Tibor Keler, Thomas A. Davis. Phase I evaluation of an agonist anti-CD27 human antibody (CDX-1127) in patients with advanced hematologic malignancies. *Journal of Clinical Oncology*. 2014;32(5):Suppl 3024.

58. Carreno BM, Bennett F, Chau TA, et al. CTLA-4 (CD152) can inhibit T cell activation by two different mechanisms depending on its level of cell surface expression. *J Immunol*. 2000;165(3):1352-1356.
59. Chemnitz JM, Parry RV, Nichols KE, June CH, Riley JL. SHP-1 and SHP-2 associate with immunoreceptor tyrosine-based switch motif of programmed death 1 upon primary human T cell stimulation, but only receptor ligation prevents T cell activation. *J Immunol*. 2004;173(2):945-954.
60. Zhang X, Schwartz JC, Guo X, et al. Structural and functional analysis of the costimulatory receptor programmed death-1. *Immunity*. 2004;20(3):337-347.
61. Wu P, Wu D, Li L, Chai Y, Huang J. PD-L1 and Survival in Solid Tumors: A Meta-Analysis. *PLoS One*. 2015;10(6):e0131403.
62. Hodi FS, O'Day SJ, McDermott DF, et al. Improved survival with ipilimumab in patients with metastatic melanoma. *N Engl J Med*. 2010;363(8):711-723.
63. Topalian SL, Hodi FS, Brahmer JR, et al. Safety, activity, and immune correlates of anti-PD-1 antibody in cancer. *N Engl J Med*. 2012;366(26):2443-2454.
64. Hamid O, Robert C, Daud A, et al. Safety and tumor responses with lambrolizumab (anti-PD-1) in melanoma. *N Engl J Med*. 2013;369(2):134-144.
65. Brahmer JR, Tykodi SS, Chow LQ, et al. Safety and activity of anti-PD-L1 antibody in patients with advanced cancer. *N Engl J Med*. 2012;366(26):2455-2465.
66. Larkin J, Chiarion-Sileni V, Gonzalez R, et al. Combined Nivolumab and Ipilimumab or Monotherapy in Untreated Melanoma. *N Engl J Med*. 2015;373(1):23-34.
67. Rosenberg SA, Packard BS, Aebersold PM, et al. Use of tumor-infiltrating lymphocytes and interleukin-2 in the immunotherapy of patients with metastatic melanoma. A preliminary report. *N Engl J Med*. 1988;319(25):1676-1680.
68. Rosenberg SA, Yang JC, Sherry RM, et al. Durable complete responses in heavily pretreated patients with metastatic melanoma using T-cell transfer immunotherapy. *Clin Cancer Res*. 2011;17(13):4550-4557.
69. Robbins PF, Dudley ME, Wunderlich J, et al. Cutting edge: persistence of transferred lymphocyte clonotypes correlates with cancer regression in patients receiving cell transfer therapy. *J Immunol*. 2004;173(12):7125-7130.
70. Gattinoni L, Finkelstein SE, Klebanoff CA, et al. Removal of homeostatic cytokine sinks by lymphodepletion enhances the efficacy of adoptively transferred tumor-specific CD8+ T cells. *J Exp Med*. 2005;202(7):907-912.
71. Klebanoff CA, Khong HT, Antony PA, Palmer DC, Restifo NP. Sinks, suppressors and antigen presenters: how lymphodepletion enhances T cell-mediated tumor immunotherapy. *Trends Immunol*. 2005;26(2):111-117.
72. Stevanovic S, Draper LM, Langhan MM, et al. Complete regression of metastatic cervical cancer after treatment with human papillomavirus-targeted tumor-infiltrating T cells. *J Clin Oncol*. 2015;33(14):1543-1550.
73. Erdag G, Schaefer JT, Smolkin ME, et al. Immunotype and immunohistologic characteristics of tumor-infiltrating immune cells are associated with clinical outcome in metastatic melanoma. *Cancer Res*. 2012;72(5):1070-1080.
74. Lawrence MS, Stojanov P, Polak P, et al. Mutational heterogeneity in cancer and the search for new cancer-associated genes. *Nature*. 2013;499(7457):214-218.

75. Lu YC, Yao X, Li YF, et al. Mutated PPP1R3B is recognized by T cells used to treat a melanoma patient who experienced a durable complete tumor regression. *J Immunol*. 2013;190(12):6034-6042.
76. Lu YC, Yao X, Crystal JS, et al. Efficient identification of mutated cancer antigens recognized by T cells associated with durable tumor regressions. *Clin Cancer Res*. 2014;20(13):3401-3410.
77. Morgan RA, Dudley ME, Wunderlich JR, et al. Cancer regression in patients after transfer of genetically engineered lymphocytes. *Science*. 2006;314(5796):126-129.
78. Johnson LA, Morgan RA, Dudley ME, et al. Gene therapy with human and mouse T-cell receptors mediates cancer regression and targets normal tissues expressing cognate antigen. *Blood*. 2009;114(3):535-546.
79. Chen YT, Boyer AD, Viars CS, Tsang S, Old LJ, Arden KC. Genomic cloning and localization of CTAG, a gene encoding an autoimmunogenic cancer-testis antigen NY-ESO-1, to human chromosome Xq28. *Cytogenet Cell Genet*. 1997;79(3-4):237-240.
80. Zhao Y, Zheng Z, Robbins PF, Khong HT, Rosenberg SA, Morgan RA. Primary human lymphocytes transduced with NY-ESO-1 antigen-specific TCR genes recognize and kill diverse human tumor cell lines. *J Immunol*. 2005;174(7):4415-4423.
81. Robbins PF, Morgan RA, Feldman SA, et al. Tumor regression in patients with metastatic synovial cell sarcoma and melanoma using genetically engineered lymphocytes reactive with NY-ESO-1. *J Clin Oncol*. 2011;29(7):917-924.
82. Robbins PF, Kassim SH, Tran TL, et al. A pilot trial using lymphocytes genetically engineered with an NY-ESO-1-reactive T-cell receptor: long-term follow-up and correlates with response. *Clin Cancer Res*. 2015;21(5):1019-1027.
83. Rapoport AP, Stadtmauer EA, Binder-Scholl GK, et al. NY-ESO-1-specific TCR-engineered T cells mediate sustained antigen-specific antitumor effects in myeloma. *Nat Med*. 2015;21(8):914-921.
84. Ellis JM, Henson V, Slack R, Ng J, Hartzman RJ, Katovich Hurley C. Frequencies of HLA-A2 alleles in five U.S. population groups. Predominance Of A*02011 and identification of HLA-A*0231. *Hum Immunol*. 2000;61(3):334-340.
85. Hicklin DJ, Marincola FM, Ferrone S. HLA class I antigen downregulation in human cancers: T-cell immunotherapy revives an old story. *Mol Med Today*. 1999;5(4):178-186.
86. Gross G, Gorochov G, Waks T, Eshhar Z. Generation of effector T cells expressing chimeric T cell receptor with antibody type-specificity. *Transplant Proc*. 1989;21(1 Pt 1):127-130.
87. Gross G, Waks T, Eshhar Z. Expression of immunoglobulin-T-cell receptor chimeric molecules as functional receptors with antibody-type specificity. *Proc Natl Acad Sci U S A*. 1989;86(24):10024-10028.
88. Shaffer DR, Savoldo B, Yi Z, et al. T cells redirected against CD70 for the immunotherapy of CD70-positive malignancies. *Blood*. 2011;117(16):4304-4314.
89. Lehner M, Gotz G, Proff J, et al. Redirecting T cells to Ewing's sarcoma family of tumors by a chimeric NKG2D receptor expressed by lentiviral transduction or mRNA transfection. *PLoS One*. 2012;7(2):e31210.
90. Song DG, Ye Q, Santoro S, Fang C, Best A, Powell DJ, Jr. Chimeric NKG2D CAR-expressing T cell-mediated attack of human ovarian cancer is enhanced by histone deacetylase inhibition. *Hum Gene Ther*. 2013;24(3):295-305.

91. Kahlon KS, Brown C, Cooper LJ, Raubitschek A, Forman SJ, Jensen MC. Specific recognition and killing of glioblastoma multiforme by interleukin 13-zetakine redirected cytolytic T cells. *Cancer Res*. 2004;64(24):9160-9166.
92. Urbanska K, Stashwick C, Poussin M, Powell DJ, Jr. Follicle-Stimulating Hormone Receptor as a Target in the Redirected T-cell Therapy for Cancer. *Cancer Immunol Res*. 2015.
93. Hwu P, Shafer GE, Treisman J, et al. Lysis of ovarian cancer cells by human lymphocytes redirected with a chimeric gene composed of an antibody variable region and the Fc receptor gamma chain. *J Exp Med*. 1993;178(1):361-366.
94. Hwu P, Yang JC, Cowherd R, et al. In vivo antitumor activity of T cells redirected with chimeric antibody/T-cell receptor genes. *Cancer Res*. 1995;55(15):3369-3373.
95. Kershaw MH, Westwood JA, Parker LL, et al. A phase I study on adoptive immunotherapy using gene-modified T cells for ovarian cancer. *Clin Cancer Res*. 2006;12(20 Pt 1):6106-6115.
96. Park JR, Digiusto DL, Slovak M, et al. Adoptive transfer of chimeric antigen receptor re-directed cytolytic T lymphocyte clones in patients with neuroblastoma. *Mol Ther*. 2007;15(4):825-833.
97. Till BG, Jensen MC, Wang J, et al. Adoptive immunotherapy for indolent non-Hodgkin lymphoma and mantle cell lymphoma using genetically modified autologous CD20-specific T cells. *Blood*. 2008;112(6):2261-2271.
98. Finney HM, Lawson AD, Bebbington CR, Weir AN. Chimeric receptors providing both primary and costimulatory signaling in T cells from a single gene product. *J Immunol*. 1998;161(6):2791-2797.
99. Haynes NM, Trapani JA, Teng MW, et al. Single-chain antigen recognition receptors that costimulate potent rejection of established experimental tumors. *Blood*. 2002;100(9):3155-3163.
100. Haynes NM, Trapani JA, Teng MW, et al. Rejection of syngeneic colon carcinoma by CTLs expressing single-chain antibody receptors codelivering CD28 costimulation. *J Immunol*. 2002;169(10):5780-5786.
101. Maher J, Brentjens RJ, Gunset G, Riviere I, Sadelain M. Human T-lymphocyte cytotoxicity and proliferation directed by a single chimeric TCRzeta /CD28 receptor. *Nat Biotechnol*. 2002;20(1):70-75.
102. Finney HM, Akbar AN, Lawson AD. Activation of resting human primary T cells with chimeric receptors: costimulation from CD28, inducible costimulator, CD134, and CD137 in series with signals from the TCR zeta chain. *J Immunol*. 2004;172(1):104-113.
103. Imai C, Mihara K, Andreansky M, et al. Chimeric receptors with 4-1BB signaling capacity provoke potent cytotoxicity against acute lymphoblastic leukemia. *Leukemia*. 2004;18(4):676-684.
104. Pule MA, Straathof KC, Dotti G, Heslop HE, Rooney CM, Brenner MK. A chimeric T cell antigen receptor that augments cytokine release and supports clonal expansion of primary human T cells. *Mol Ther*. 2005;12(5):933-941.
105. Wang J, Jensen M, Lin Y, et al. Optimizing adoptive polyclonal T cell immunotherapy of lymphomas, using a chimeric T cell receptor possessing CD28 and CD137 costimulatory domains. *Hum Gene Ther*. 2007;18(8):712-725.
106. Milone MC, Fish JD, Carpenito C, et al. Chimeric receptors containing CD137 signal transduction domains mediate enhanced survival of T cells and increased antileukemic efficacy in vivo. *Mol Ther*. 2009;17(8):1453-1464.

107. Carpenito C, Milone MC, Hassan R, et al. Control of large, established tumor xenografts with genetically retargeted human T cells containing CD28 and CD137 domains. *Proc Natl Acad Sci U S A*. 2009;106(9):3360-3365.
108. Zhong XS, Matsushita M, Plotkin J, Riviere I, Sadelain M. Chimeric antigen receptors combining 4-1BB and CD28 signaling domains augment PI3kinase/AKT/Bcl-XL activation and CD8+ T cell-mediated tumor eradication. *Mol Ther*. 2010;18(2):413-420.
109. Song DG, Ye Q, Carpenito C, et al. In vivo persistence, tumor localization, and antitumor activity of CAR-engineered T cells is enhanced by costimulatory signaling through CD137 (4-1BB). *Cancer Res*. 2011;71(13):4617-4627.
110. Song DG, Ye Q, Poussin M, Harms GM, Figini M, Powell DJ, Jr. CD27 costimulation augments the survival and antitumor activity of redirected human T cells in vivo. *Blood*. 2012;119(3):696-706.
111. Brown CE, Badie B, Barish ME, et al. Bioactivity and Safety of IL13Ralpha2-Redirected Chimeric Antigen Receptor CD8+ T Cells in Patients with Recurrent Glioblastoma. *Clin Cancer Res*. 2015;21(18):4062-4072.
112. Richard P. Junghans QM, Ritesh Rathore, Robin Davies, Anthony Bais, Erica Gomes, Ryan Harvey, and Steven I. Cohen. Abstract C13: Phase I trial of anti-PSMA designer T cells in advanced prostate cancer. *Cancer Research*. 2012;72.
113. Ma Q, Gomes EM, Lo AS, Junghans RP. Advanced generation anti-prostate specific membrane antigen designer T cells for prostate cancer immunotherapy. *Prostate*. 2014;74(3):286-296.
114. Louis CU, Savoldo B, Dotti G, et al. Antitumor activity and long-term fate of chimeric antigen receptor-positive T cells in patients with neuroblastoma. *Blood*. 2011;118(23):6050-6056.
115. Beatty GL, Haas AR, Maus MV, et al. Mesothelin-specific chimeric antigen receptor mRNA-engineered T cells induce anti-tumor activity in solid malignancies. *Cancer Immunol Res*. 2014;2(2):112-120.
116. Janos L. Tanyi ARH, Gregory L. Beatty, Mark A. Morgan, Caitlin J. Stashwick, Mark H. O'Hara, David L. Porter, Marcela V. Maus, Bruce L. Levine, Simon F. Lacey, Anne Marie Nelson, Maureen McGarvey, Naseem DS Kerr, Gabriela Plesa, Carl H. June. Safety and feasibility of chimeric antigen receptor modified T cells directed against mesothelin (CART-meso) in patients with mesothelin expressing cancers. Proceedings of the 106th Annual Meeting of the American Association for Cancer Research. Philadelphia, PA; 2015:Abstract CT105.
117. Lamers CH, Sleijfer S, van Steenbergen S, et al. Treatment of metastatic renal cell carcinoma with CAIX CAR-engineered T cells: clinical evaluation and management of on-target toxicity. *Mol Ther*. 2013;21(4):904-912.
118. Porter DL, Levine BL, Kalos M, Bagg A, June CH. Chimeric antigen receptor-modified T cells in chronic lymphoid leukemia. *N Engl J Med*. 2011;365(8):725-733.
119. Kalos M, Levine BL, Porter DL, et al. T cells with chimeric antigen receptors have potent antitumor effects and can establish memory in patients with advanced leukemia. *Sci Transl Med*. 2011;3(95):95ra73.
120. Brentjens RJ, Riviere I, Park JH, et al. Safety and persistence of adoptively transferred autologous CD19-targeted T cells in patients with relapsed or chemotherapy refractory B-cell leukemias. *Blood*. 2011;118(18):4817-4828.

121. Kochenderfer JN, Dudley ME, Feldman SA, et al. B-cell depletion and remissions of malignancy along with cytokine-associated toxicity in a clinical trial of anti-CD19 chimeric-antigen-receptor-transduced T cells. *Blood*. 2012;119(12):2709-2720.
122. Grupp SA, Kalos M, Barrett D, et al. Chimeric antigen receptor-modified T cells for acute lymphoid leukemia. *N Engl J Med*. 2013;368(16):1509-1518.
123. Brentjens RJ, Davila ML, Riviere I, et al. CD19-targeted T cells rapidly induce molecular remissions in adults with chemotherapy-refractory acute lymphoblastic leukemia. *Sci Transl Med*. 2013;5(177):177ra138.
124. Lee DW, Kochenderfer JN, Stetler-Stevenson M, et al. T cells expressing CD19 chimeric antigen receptors for acute lymphoblastic leukaemia in children and young adults: a phase 1 dose-escalation trial. *Lancet*. 2015;385(9967):517-528.
125. Uckun FM, Jaszcz W, Ambrus JL, et al. Detailed studies on expression and function of CD19 surface determinant by using B43 monoclonal antibody and the clinical potential of anti-CD19 immunotoxins. *Blood.* 1988;71(1):13-29.
126. Morgan RA, Yang JC, Kitano M, Dudley ME, Laurencot CM, Rosenberg SA. Case report of a serious adverse event following the administration of T cells transduced with a chimeric antigen receptor recognizing ERBB2. *Mol Ther*. 2010;18(4):843-851.
127. Parkhurst MR, Yang JC, Langan RC, et al. T cells targeting carcinoembryonic antigen can mediate regression of metastatic colorectal cancer but induce severe transient colitis. *Mol Ther*. 2011;19(3):620-626.
128. Lamers CH, Willemsen R, van Elzakker P, et al. Immune responses to transgene and retroviral vector in patients treated with ex vivo-engineered T cells. *Blood*. 2011;117(1):72-82.
129. Maus MV, Haas AR, Beatty GL, et al. T cells expressing chimeric antigen receptors can cause anaphylaxis in humans. *Cancer Immunol Res*. 2013;1(1):26-31.
130. Maude SL, Frey N, Shaw PA, et al. Chimeric antigen receptor T cells for sustained remissions in leukemia. *N Engl J Med*. 2014;371(16):1507-1517.
131. Howlader N NA, Krapcho M, Garshell J, Miller D, Altekruse SF, Kosary CL, Yu M, Ruhl J, Tatalovich Z,Mariotto A, Lewis DR, Chen HS, Feuer EJ, Cronin KA (eds). SEER Cancer Statistics Review (CSR) 1975-2012. National Cancer Institute. http://seer.cancer.gov/csr/1975_2012/

1975-2012:based on November 2014 SEER data submission, posted to the SEER web site, April 2015.
132. Robak T, Wierzbowska A. Current and emerging therapies for acute myeloid leukemia. *Clin Ther*. 2009;31 Pt 2:2349-2370.
133. Burnett AK, Wheatley K, Goldstone AH, et al. The value of allogeneic bone marrow transplant in patients with acute myeloid leukaemia at differing risk of relapse: results of the UK MRC AML 10 trial. *Br J Haematol*. 2002;118(2):385-400.
134. Sadasivan E, Rothenberg SP. The complete amino acid sequence of a human folate binding protein from KB cells determined from the cDNA. *J Biol Chem*. 1989;264(10):5806-5811.
135. Elwood PC. Molecular cloning and characterization of the human folate-binding protein cDNA from placenta and malignant tissue culture (KB) cells. *J Biol Chem*. 1989;264(25):14893-14901.
136. Ratnam M, Marquardt H, Duhring JL, Freisheim JH. Homologous membrane folate binding proteins in human placenta: cloning and sequence of a cDNA. *Biochemistry*. 1989;28(20):8249-8254.

137. Shen F, Wu M, Ross JF, Miller D, Ratnam M. Folate receptor type gamma is primarily a secretory protein due to lack of an efficient signal for glycosylphosphatidylinositol modification: protein characterization and cell type specificity. *Biochemistry*. 1995;34(16):5660-5665.
138. Kamen B. Folate and antifolate pharmacology. *Semin Oncol*. 1997;24(5 Suppl 18):S18-30-S18-39.
139. Ross JF, Chaudhuri PK, Ratnam M. Differential regulation of folate receptor isoforms in normal and malignant tissues in vivo and in established cell lines. Physiologic and clinical implications. *Cancer*. 1994;73(9):2432-2443.
140. Campbell IG, Jones TA, Foulkes WD, Trowsdale J. Folate-binding protein is a marker for ovarian cancer. *Cancer Res*. 1991;51(19):5329-5338.
141. Coney LR, Tomassetti A, Carayannopoulos L, et al. Cloning of a tumor-associated antigen: MOv18 and MOv19 antibodies recognize a folate-binding protein. *Cancer Res*. 1991;51(22):6125-6132.
142. Weitman SD, Lark RH, Coney LR, et al. Distribution of the folate receptor GP38 in normal and malignant cell lines and tissues. *Cancer Res*. 1992;52(12):3396-3401.
143. Leamon CP, Low PS. Delivery of macromolecules into living cells: a method that exploits folate receptor endocytosis. *Proc Natl Acad Sci U S A*. 1991;88(13):5572-5576.
144. Leamon CP, Pastan I, Low PS. Cytotoxicity of folate-Pseudomonas exotoxin conjugates toward tumor cells. Contribution of translocation domain. *J Biol Chem*. 1993;268(33):24847-24854.
145. Lee RJ, Low PS. Folate-mediated tumor cell targeting of liposome-entrapped doxorubicin in vitro. *Biochim Biophys Acta*. 1995;1233(2):134-144.
146. Lu Y, Low PS. Folate targeting of haptens to cancer cell surfaces mediates immunotherapy of syngeneic murine tumors. *Cancer Immunol Immunother*. 2002;51(3):153-162.
147. Shen F, Ross JF, Wang X, Ratnam M. Identification of a novel folate receptor, a truncated receptor, and receptor type beta in hematopoietic cells: cDNA cloning, expression, immunoreactivity, and tissue specificity. *Biochemistry*. 1994;33(5):1209-1215.
148. Ross JF, Wang H, Behm FG, et al. Folate receptor type beta is a neutrophilic lineage marker and is differentially expressed in myeloid leukemia. *Cancer*. 1999;85(2):348-357.
149. Pan XQ. Strategy for the treatment of acute myelogenous leukemia based on folate receptor beta -targeted liposomal doxorubicin combined with receptor induction using all-trans retinoic acid. *Blood*. 2002;100(2):594-602.
150. Wang H, Zheng X, Behm FG, Ratnam M. Differentiation-independent retinoid induction of folate receptor type beta, a potential tumor target in myeloid leukemia. *Blood*. 2000;96(10):3529-3536.
151. Hao H, Qi H, Ratnam M. Modulation of the folate receptor type beta gene by coordinate actions of retinoic acid receptors at activator Sp1/ets and repressor AP-1 sites. *Blood*. 2003;101(11):4551-4560.
152. Qi H, Ratnam M. Synergistic induction of folate receptor beta by all-trans retinoic acid and histone deacetylase inhibitors in acute myelogenous leukemia cells: mechanism and utility in enhancing selective growth inhibition by antifolates. *Cancer Res*. 2006;66(11):5875-5882.
153. Mathias CJ, Wang S, Waters DJ, Turek JJ, Low PS, Green MA. Indium-111-DTPA-folate as a potential folate-receptor-targeted radiopharmaceutical. *J Nucl Med*. 1998;39(9):1579-1585.

154. Mathias CJ, Hubers D, Low PS, Green MA. Synthesis of [(99m)Tc]DTPA-folate and its evaluation as a folate-receptor-targeted radiopharmaceutical. *Bioconjug Chem*. 2000;11(2):253-257.
155. Mathias CJ, Lewis MR, Reichert DE, et al. Preparation of 66Ga- and 68Ga-labeled Ga(III)-deferoxamine-folate as potential folate-receptor-targeted PET radiopharmaceuticals. *Nucl Med Biol*. 2003;30(7):725-731.
156. Leamon CP, Parker MA, Vlahov IR, et al. Synthesis and biological evaluation of EC20: a new folate-derived, (99m)Tc-based radiopharmaceutical. *Bioconjug Chem*. 2002;13(6):1200-1210.
157. Fisher RE, Siegel BA, Edell SL, et al. Exploratory study of 99mTc-EC20 imaging for identifying patients with folate receptor-positive solid tumors. *J Nucl Med*. 2008;49(6):899-906.
158. Reddy JA, Xu LC, Parker N, Vetzel M, Leamon CP. Preclinical evaluation of (99m)Tc-EC20 for imaging folate receptor-positive tumors. *J Nucl Med*. 2004;45(5):857-866.
159. Nakashima-Matsushita N, Homma T, Yu S, et al. Selective expression of folate receptor beta and its possible role in methotrexate transport in synovial macrophages from patients with rheumatoid arthritis. *Arthritis Rheum*. 1999;42(8):1609-1616.
160. Turk MJ, Breur GJ, Widmer WR, et al. Folate-targeted imaging of activated macrophages in rats with adjuvant-induced arthritis. *Arthritis Rheum*. 2002;46(7):1947-1955.
161. Paulos CM, Turk MJ, Breur GJ, Low PS. Folate receptor-mediated targeting of therapeutic and imaging agents to activated macrophages in rheumatoid arthritis. *Adv Drug Deliv Rev*. 2004;56(8):1205-1217.
162. Paulos CM, Varghese B, Widmer WR, Breur GJ, Vlashi E, Low PS. Folate-targeted immunotherapy effectively treats established adjuvant and collagen-induced arthritis. *Arthritis Res Ther*. 2006;8(3):R77.
163. Nagayoshi R, Nagai T, Matsushita K, et al. Effectiveness of anti-folate receptor beta antibody conjugated with truncated Pseudomonas exotoxin in the targeting of rheumatoid arthritis synovial macrophages. *Arthritis Rheum*. 2005;52(9):2666-2675.
164. Nagai T, Tanaka M, Tsuneyoshi Y, et al. In vitro and in vivo efficacy of a recombinant immunotoxin against folate receptor beta on the activation and proliferation of rheumatoid arthritis synovial cells. *Arthritis Rheum*. 2006;54(10):3126-3134.
165. Nagai T, Kyo A, Hasui K, Takao S, Matsuyama T. Efficacy of an immunotoxin to folate receptor beta in the intra-articular treatment of antigen-induced arthritis. *Arthritis Res Ther*. 2012;14(3):R106.
166. Puig-Kroger A, Sierra-Filardi E, Dominguez-Soto A, et al. Folate receptor beta is expressed by tumor-associated macrophages and constitutes a marker for M2 anti-inflammatory/regulatory macrophages. *Cancer Res*. 2009;69(24):9395-9403.
167. Kurahara H, Takao S, Kuwahata T, et al. Clinical significance of folate receptor beta-expressing tumor-associated macrophages in pancreatic cancer. *Ann Surg Oncol*. 2012;19(7):2264-2271.
168. Shen J, Putt KS, Visscher DW, et al. Assessment of folate receptor-beta expression in human neoplastic tissues. *Oncotarget*. 2015;6(16):14700-14709.
169. Sun JY, Shen J, Thibodeaux J, et al. In vivo optical imaging of folate receptor-beta in head and neck squamous cell carcinoma. *Laryngoscope*. 2014;124(8):E312-319.
170. Turk MJ, Waters DJ, Low PS. Folate-conjugated liposomes preferentially target macrophages associated with ovarian carcinoma. *Cancer Lett*. 2004;213(2):165-172.

171. Nagai T, Tanaka M, Tsuneyoshi Y, et al. Targeting tumor-associated macrophages in an experimental glioma model with a recombinant immunotoxin to folate receptor beta. *Cancer Immunol Immunother*. 2009;58(10):1577-1586.
172. Roboz GJ. Current treatment of acute myeloid leukemia. *Curr Opin Oncol*. 2012;24(6):711-719.
173. Kandalaft LE, Powell DJ, Jr., Coukos G. A phase I clinical trial of adoptive transfer of folate receptor-alpha redirected autologous T cells for recurrent ovarian cancer. *J Transl Med*. 2012;10:157.
174. Pan XQ, Zheng X, Shi G, Wang H, Ratnam M, Lee RJ. Strategy for the treatment of acute myelogenous leukemia based on folate receptor beta-targeted liposomal doxorubicin combined with receptor induction using all-trans retinoic acid. *Blood*. 2002;100(2):594-602.
175. Feng Y, Shen J, Streaker ED, et al. A folate receptor beta-specific human monoclonal antibody recognizes activated macrophage of rheumatoid patients and mediates antibody-dependent cell-mediated cytotoxicity. *Arthritis Res Ther*. 2011;13(2):R59.
176. Lanitis E, Poussin M, Hagemann IS, et al. Redirected antitumor activity of primary human lymphocytes transduced with a fully human anti-mesothelin chimeric receptor. *Mol Ther*. 2012;20(3):633-643.
177. Godwin AK, Meister A, O'Dwyer PJ, Huang CS, Hamilton TC, Anderson ME. High resistance to cisplatin in human ovarian cancer cell lines is associated with marked increase of glutathione synthesis. *Proc Natl Acad Sci U S A*. 1992;89(7):3070-3074.
178. Zhang L, Yang N, Conejo-Garcia JR, et al. Expression of endocrine gland-derived vascular endothelial growth factor in ovarian carcinoma. *Clin Cancer Res*. 2003;9(1):264-272.
179. Betts MR, Brenchley JM, Price DA, et al. Sensitive and viable identification of antigen-specific CD8+ T cells by a flow cytometric assay for degranulation. *J Immunol Methods*. 2003;281(1-2):65-78.
180. Cantorna MT, Nashold FE, Hayes CE. In vitamin A deficiency multiple mechanisms establish a regulatory T helper cell imbalance with excess Th1 and insufficient Th2 function. *J Immunol*. 1994;152(4):1515-1522.
181. Frankenburg S, Wang X, Milner Y. Vitamin A inhibits cytokines produced by type 1 lymphocytes in vitro. *Cell Immunol*. 1998;185(1):75-81.
182. Cippitelli M, Ye J, Viggiano V, et al. Retinoic acid-induced transcriptional modulation of the human interferon-gamma promoter. *J Biol Chem*. 1996;271(43):26783-26793.
183. Ertesvag A, Engedal N, Naderi S, Blomhoff HK. Retinoic acid stimulates the cell cycle machinery in normal T cells: involvement of retinoic acid receptor-mediated IL-2 secretion. *J Immunol*. 2002;169(10):5555-5563.
184. Engedal N, Ertesvag A, Blomhoff HK. Survival of activated human T lymphocytes is promoted by retinoic acid via induction of IL-2. *Int Immunol*. 2004;16(3):443-453.
185. Allende LM, Corell A, Madrono A, et al. Retinol (vitamin A) is a cofactor in CD3-induced human T-lymphocyte activation. *Immunology*. 1997;90(3):388-396.
186. Kowolik CM, Topp MS, Gonzalez S, et al. CD28 costimulation provided through a CD19-specific chimeric antigen receptor enhances in vivo persistence and antitumor efficacy of adoptively transferred T cells. *Cancer Res*. 2006;66(22):10995-11004.
187. Savoldo B, Ramos CA, Liu E, et al. CD28 costimulation improves expansion and persistence of chimeric antigen receptor-modified T cells in lymphoma patients. *J Clin Invest*. 2011;121(5):1822-1826.

188. Marin V, Pizzitola I, Agostoni V, et al. Cytokine-induced killer cells for cell therapy of acute myeloid leukemia: improvement of their immune activity by expression of CD33-specific chimeric receptors. *Haematologica*. 2010;95(12):2144-2152.
189. Dutour A, Marin V, Pizzitola I, et al. In Vitro and In Vivo Antitumor Effect of Anti-CD33 Chimeric Receptor-Expressing EBV-CTL against CD33 Acute Myeloid Leukemia. *Adv Hematol*. 2012;2012:683065.
190. Mardiros A, Dos Santos C, McDonald T, et al. T cells expressing CD123-specific chimeric antigen receptors exhibit specific cytolytic effector functions and antitumor effects against human acute myeloid leukemia. *Blood*. 2013;122(18):3138-3148.
191. Gill S, Tasian SK, Ruella M, et al. Preclinical targeting of human acute myeloid leukemia and myeloablation using chimeric antigen receptor-modified T cells. *Blood*. 2014;123(15):2343-2354.
192. Reddy JA, Haneline LS, Srour EF, Antony AC, Clapp DW, Low PS. Expression and functional characterization of the beta-isoform of the folate receptor on CD34(+) cells. *Blood*. 1999;93(11):3940-3948.
193. Shen J, Hilgenbrink AR, Xia W, et al. Folate receptor-beta constitutes a marker for human proinflammatory monocytes. *J Leukoc Biol*. 2014;96(4):563-570.
194. Breitman TR, Selonick SE, Collins SJ. Induction of differentiation of the human promyelocytic leukemia cell line (HL-60) by retinoic acid. *Proc Natl Acad Sci U S A*. 1980;77(5):2936-2940.
195. Drach J, Lopez-Berestein G, McQueen T, Andreeff M, Mehta K. Induction of differentiation in myeloid leukemia cell lines and acute promyelocytic leukemia cells by liposomal all-trans-retinoic acid. *Cancer Res*. 1993;53(9):2100-2104.
196. Cho HY, Choi EK, Lee SW, et al. All-trans retinoic acid induces TLR-5 expression and cell differentiation and promotes flagellin-mediated cell functions in human THP-1 cells. *Immunol Lett*. 2011;136(1):97-107.
197. Hudecek M, Lupo-Stanghellini MT, Kosasih PL, et al. Receptor affinity and extracellular domain modifications affect tumor recognition by ROR1-specific chimeric antigen receptor T cells. *Clin Cancer Res*. 2013;19(12):3153-3164.
198. Xia W, Hilgenbrink AR, Matteson EL, Lockwood MB, Cheng JX, Low PS. A functional folate receptor is induced during macrophage activation and can be used to target drugs to activated macrophages. *Blood*. 2009;113(2):438-446.
199. Zhao Y, Moon E, Carpenito C, et al. Multiple injections of electroporated autologous T cells expressing a chimeric antigen receptor mediate regression of human disseminated tumor. *Cancer Res*. 2010;70(22):9053-9061.
200. Straathof KC, Pule MA, Yotnda P, et al. An inducible caspase 9 safety switch for T-cell therapy. *Blood*. 2005;105(11):4247-4254.
201. Ayala-Lopez W, Xia W, Varghese B, Low PS. Imaging of atherosclerosis in apoliprotein e knockout mice: targeting of a folate-conjugated radiopharmaceutical to activated macrophages. *J Nucl Med*. 2010;51(5):768-774.
202. Furusho Y, Miyata M, Matsuyama T, et al. Novel Therapy for Atherosclerosis Using Recombinant Immunotoxin Against Folate Receptor beta-Expressing Macrophages. *J Am Heart Assoc*. 2012;1(4):e003079.
203. Li H, Nagai T, Hasui K, Matsuyama T. Depletion of folate receptor beta-expressing macrophages alleviates bleomycin-induced experimental skin fibrosis. *Mod Rheumatol*. 2014;24(5):816-822.

204. Kanate AS, Pasquini MC, Hari PN, Hamadani M. Allogeneic hematopoietic cell transplant for acute myeloid leukemia: Current state in 2013 and future directions. *World J Stem Cells*. 2014;6(2):69-81.
205. Jacobsohn DA, Vogelsang GB. Acute graft versus host disease. *Orphanet J Rare Dis*. 2007;2:35.
206. Hahn T, McCarthy PL, Jr., Zhang MJ, et al. Risk factors for acute graft-versus-host disease after human leukocyte antigen-identical sibling transplants for adults with leukemia. *J Clin Oncol*. 2008;26(35):5728-5734.
207. Tettamanti S, Marin V, Pizzitola I, et al. Targeting of acute myeloid leukaemia by cytokine-induced killer cells redirected with a novel CD123-specific chimeric antigen receptor. *Br J Haematol*. 2013;161(3):389-401.
208. Kenderian SS, Ruella M, Shestova O, et al. CD33 Specific Chimeric Antigen Receptor T Cells Exhibit Potent Preclinical Activity against Human Acute Myeloid Leukemia. *Leukemia*. 2015.
209. Lynn RC, Poussin M, Kalota A, et al. Targeting of folate receptor-beta on acute myeloid leukemia blasts with chimeric antigen receptor expressing T cells. *Blood*. 2015.
210. Chmielewski M, Hombach A, Heuser C, Adams GP, Abken H. T cell activation by antibody-like immunoreceptors: increase in affinity of the single-chain fragment domain above threshold does not increase T cell activation against antigen-positive target cells but decreases selectivity. *J Immunol*. 2004;173(12):7647-7653.
211. Lamers CH, Sleijfer S, Vulto AG, et al. Treatment of metastatic renal cell carcinoma with autologous T-lymphocytes genetically retargeted against carbonic anhydrase IX: first clinical experience. *J Clin Oncol*. 2006;24(13):e20-22.
212. Hinrichs CS, Restifo NP. Reassessing target antigens for adoptive T-cell therapy. *Nat Biotechnol*. 2013;31(11):999-1008.
213. Feng Y, Zhu Z, Xiao X, Choudhry V, Barrett JC, Dimitrov DS. Novel human monoclonal antibodies to insulin-like growth factor (IGF)-II that potently inhibit the IGF receptor type I signal transduction function. *Mol Cancer Ther*. 2006;5(1):114-120.
214. Hombach AA, Schildgen V, Heuser C, Finnern R, Gilham DE, Abken H. T cell activation by antibody-like immunoreceptors: the position of the binding epitope within the target molecule determines the efficiency of activation of redirected T cells. *J Immunol*. 2007;178(7):4650-4657.
215. James SE, Greenberg PD, Jensen MC, et al. Antigen sensitivity of CD22-specific chimeric TCR is modulated by target epitope distance from the cell membrane. *J Immunol*. 2008;180(10):7028-7038.
216. Chinnasamy D, Yu Z, Theoret MR, et al. Gene therapy using genetically modified lymphocytes targeting VEGFR-2 inhibits the growth of vascularized syngenic tumors in mice. *J Clin Invest*. 2010;120(11):3953-3968.
217. Kakarla S, Chow KK, Mata M, et al. Antitumor effects of chimeric receptor engineered human T cells directed to tumor stroma. *Mol Ther*. 2013;21(8):1611-1620.
218. Wang LC, Lo A, Scholler J, et al. Targeting fibroblast activation protein in tumor stroma with chimeric antigen receptor T cells can inhibit tumor growth and augment host immunity without severe toxicity. *Cancer Immunol Res*. 2014;2(2):154-166.
219. Chinnasamy D, Tran E, Yu Z, Morgan RA, Restifo NP, Rosenberg SA. Simultaneous targeting of tumor antigens and the tumor vasculature using T lymphocyte transfer synergize to induce regression of established tumors in mice. *Cancer Res*. 2013;73(11):3371-3380.
220. Caruana I, Savoldo B, Hoyos V, et al. Heparanase promotes tumor infiltration and antitumor activity of CAR-redirected T lymphocytes. *Nat Med*. 2015;21(5):524-529.

221. Mhawech-Fauceglia P, Wang D, Ali L, et al. Intraepithelial T cells and tumor-associated macrophages in ovarian cancer patients. *Cancer Immun*. 2013;13:1.
222. Kawamura K, Komohara Y, Takaishi K, Katabuchi H, Takeya M. Detection of M2 macrophages and colony-stimulating factor 1 expression in serous and mucinous ovarian epithelial tumors. *Pathol Int*. 2009;59(5):300-305.
223. Wan T, Liu JH, Zheng LM, Cai MY, Ding T. [Prognostic significance of tumor-associated macrophage infiltration in advanced epithelial ovarian carcinoma]. *Ai Zheng*. 2009;28(3):323-327.
224. Zhang M, He Y, Sun X, et al. A high M1/M2 ratio of tumor-associated macrophages is associated with extended survival in ovarian cancer patients. *J Ovarian Res*. 2014;7:19.
225. Busuttil RA, George J, Tothill RW, et al. A signature predicting poor prognosis in gastric and ovarian cancer represents a coordinated macrophage and stromal response. *Clin Cancer Res*. 2014;20(10):2761-2772.
226. Lan C, Huang X, Lin S, et al. Expression of M2-polarized macrophages is associated with poor prognosis for advanced epithelial ovarian cancer. *Technol Cancer Res Treat*. 2013;12(3):259-267.
227. Tran E, Chinnasamy D, Yu Z, et al. Immune targeting of fibroblast activation protein triggers recognition of multipotent bone marrow stromal cells and cachexia. *J Exp Med*. 2013;210(6):1125-1135.
228. Cheadle EJ, Hawkins RE, Batha H, O'Neill AL, Dovedi SJ, Gilham DE. Natural expression of the CD19 antigen impacts the long-term engraftment but not antitumor activity of CD19-specific engineered T cells. *J Immunol*. 2010;184(4):1885-1896.
229. Kochenderfer JN, Yu Z, Frasheri D, Restifo NP, Rosenberg SA. Adoptive transfer of syngeneic T cells transduced with a chimeric antigen receptor that recognizes murine CD19 can eradicate lymphoma and normal B cells. *Blood*. 2010;116(19):3875-3886.
230. Davila ML, Kloss CC, Gunset G, Sadelain M. CD19 CAR-targeted T cells induce long-term remission and B Cell Aplasia in an immunocompetent mouse model of B cell acute lymphoblastic leukemia. *PLoS One*. 2013;8(4):e61338.
231. Cheadle EJ, Sheard V, Rothwell DG, et al. Differential role of Th1 and Th2 cytokines in autotoxicity driven by CD19-specific second-generation chimeric antigen receptor T cells in a mouse model. *J Immunol*. 2014;192(8):3654-3665.
232. Zhang T, Lemoi BA, Sentman CL. Chimeric NK-receptor-bearing T cells mediate antitumor immunotherapy. *Blood*. 2005;106(5):1544-1551.
233. Barber A, Rynda A, Sentman CL. Chimeric NKG2D expressing T cells eliminate immunosuppression and activate immunity within the ovarian tumor microenvironment. *J Immunol*. 2009;183(11):6939-6947.
234. VanSeggelen H, Hammill JA, Dvorkin-Gheva A, et al. T Cells Engineered With Chimeric Antigen Receptors Targeting NKG2D Ligands Display Lethal Toxicity in Mice. *Mol Ther*. 2015.
235. Sampson JH, Choi BD, Sanchez-Perez L, et al. EGFRvIII mCAR-modified T-cell therapy cures mice with established intracerebral glioma and generates host immunity against tumor-antigen loss. *Clin Cancer Res*. 2014;20(4):972-984.
236. Wang LX, Westwood JA, Moeller M, et al. Tumor ablation by gene-modified T cells in the absence of autoimmunity. *Cancer Res*. 2010;70(23):9591-9598.
237. Globerson-Levin A, Waks T, Eshhar Z. Elimination of progressive mammary cancer by repeated administrations of chimeric antigen receptor-modified T cells. *Mol Ther*. 2014;22(5):1029-1038.

238. Chmielewski M, Hahn O, Rappl G, et al. T cells that target carcinoembryonic antigen eradicate orthotopic pancreatic carcinomas without inducing autoimmune colitis in mice. *Gastroenterology*. 2012;143(4):1095-1107 e1092.
239. Furze RC, Rankin SM. Neutrophil mobilization and clearance in the bone marrow. *Immunology*. 2008;125(3):281-288.
240. Bendall LJ, Bradstock KF. G-CSF: From granulopoietic stimulant to bone marrow stem cell mobilizing agent. *Cytokine Growth Factor Rev*. 2014;25(4):355-367.
241. Demetri GD, Griffin JD. Granulocyte colony-stimulating factor and its receptor. *Blood*. 1991;78(11):2791-2808.
242. Liu M, Guo S, Hibbert JM, et al. CXCL10/IP-10 in infectious diseases pathogenesis and potential therapeutic implications. *Cytokine Growth Factor Rev*. 2011;22(3):121-130.
243. Farber JM. Mig and IP-10: CXC chemokines that target lymphocytes. *J Leukoc Biol*. 1997;61(3):246-257.
244. Deshmane SL, Kremlev S, Amini S, Sawaya BE. Monocyte chemoattractant protein-1 (MCP-1): an overview. *J Interferon Cytokine Res*. 2009;29(6):313-326.
245. Qian BZ, Li J, Zhang H, et al. CCL2 recruits inflammatory monocytes to facilitate breast-tumour metastasis. *Nature*. 2011;475(7355):222-225.
246. Li M, Knight DA, L AS, Smyth MJ, Stewart TJ. A role for CCL2 in both tumor progression and immunosurveillance. *Oncoimmunology*. 2013;2(7):e25474.
247. Lee DW, Gardner R, Porter DL, et al. Current concepts in the diagnosis and management of cytokine release syndrome. *Blood*. 2014;124(2):188-195.
248. Maude SL, Barrett D, Teachey DT, Grupp SA. Managing cytokine release syndrome associated with novel T cell-engaging therapies. *Cancer J*. 2014;20(2):119-122.
249. van der Stegen SJ, Davies DM, Wilkie S, et al. Preclinical in vivo modeling of cytokine release syndrome induced by ErbB-retargeted human T cells: identifying a window of therapeutic opportunity? *J Immunol*. 2013;191(9):4589-4598.
250. Peinert S, Prince HM, Guru PM, et al. Gene-modified T cells as immunotherapy for multiple myeloma and acute myeloid leukemia expressing the Lewis Y antigen. *Gene Ther*. 2010;17(5):678-686.
251. Westwood JA, Smyth MJ, Teng MW, et al. Adoptive transfer of T cells modified with a humanized chimeric receptor gene inhibits growth of Lewis-Y-expressing tumors in mice. *Proc Natl Acad Sci U S A*. 2005;102(52):19051-19056.
252. Ritchie DS, Neeson PJ, Khot A, et al. Persistence and efficacy of second generation CAR T cell against the LeY antigen in acute myeloid leukemia. *Mol Ther*. 2013;21(11):2122-2129.
253. Crocker PR, Varki A. Siglecs, sialic acids and innate immunity. *Trends Immunol*. 2001;22(6):337-342.
254. Rajvanshi P, Shulman HM, Sievers EL, McDonald GB. Hepatic sinusoidal obstruction after gemtuzumab ozogamicin (Mylotarg) therapy. *Blood*. 2002;99(7):2310-2314.
255. O'Hear C, Heiber JF, Schubert I, Fey G, Geiger TL. Anti-CD33 chimeric antigen receptor targeting of acute myeloid leukemia. *Haematologica*. 2015;100(3):336-344.
256. Wang QS, Wang Y, Lv HY, et al. Treatment of CD33-directed chimeric antigen receptor-modified T cells in one patient with relapsed and refractory acute myeloid leukemia. *Mol Ther*. 2015;23(1):184-191.
257. Frankel A, Liu JS, Rizzieri D, Hogge D. Phase I clinical study of diphtheria toxin-interleukin 3 fusion protein in patients with acute myeloid leukemia and myelodysplasia. *Leuk Lymphoma*. 2008;49(3):543-553.

258. Pizzitola I, Anjos-Afonso F, Rouault-Pierre K, et al. Chimeric antigen receptors against CD33/CD123 antigens efficiently target primary acute myeloid leukemia cells in vivo. *Leukemia*. 2014;28(8):1596-1605.
259. Casucci M, Nicolis di Robilant B, Falcone L, et al. CD44v6-targeted T cells mediate potent antitumor effects against acute myeloid leukemia and multiple myeloma. *Blood*. 2013;122(20):3461-3472.
260. Tijink BM, Buter J, de Bree R, et al. A phase I dose escalation study with anti-CD44v6 bivatuzumab mertansine in patients with incurable squamous cell carcinoma of the head and neck or esophagus. *Clin Cancer Res*. 2006;12(20 Pt 1):6064-6072.
261. Rupp U, Schoendorf-Holland E, Eichbaum M, et al. Safety and pharmacokinetics of bivatuzumab mertansine in patients with CD44v6-positive metastatic breast cancer: final results of a phase I study. *Anticancer Drugs*. 2007;18(4):477-485.
262. Luger SM. Treating the elderly patient with acute myelogenous leukemia. *Hematology Am Soc Hematol Educ Program*. 2010;2010:62-69.
263. Davila ML, Riviere I, Wang X, et al. Efficacy and toxicity management of 19-28z CAR T cell therapy in B cell acute lymphoblastic leukemia. *Sci Transl Med*. 2014;6(224):224ra225.
264. Wu CY, Roybal KT, Puchner EM, Onuffer J, Lim WA. Remote control of therapeutic T cells through a small molecule-gated chimeric receptor. *Science*. 2015.